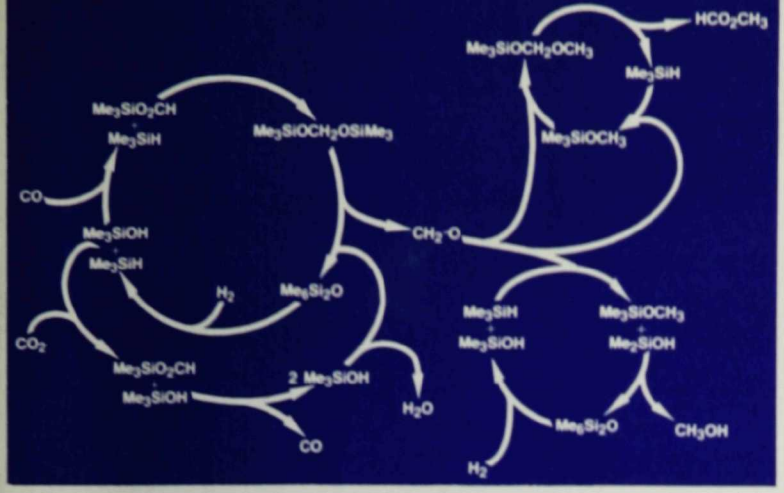

ANL-87-19

Chemical Technology Division

Annual Technical Report 1986

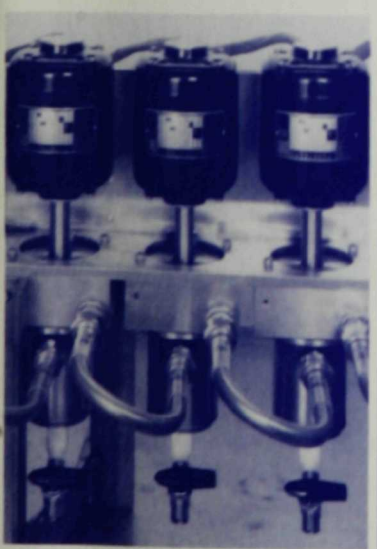

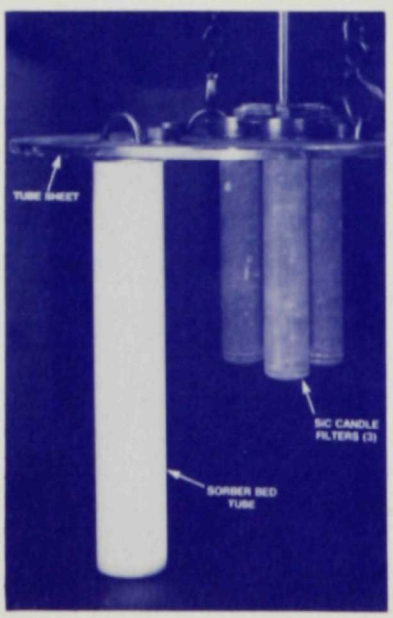

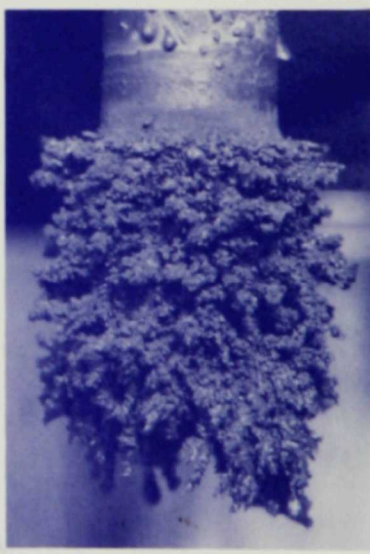

Argonne National Laboratory
Operated by The University of Chicago for the U. S. Department of Energy under Contract W-31-109-Eng-38

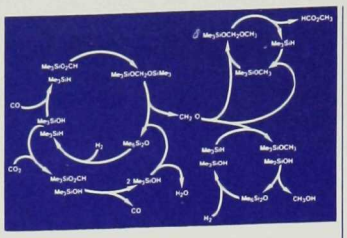

1.

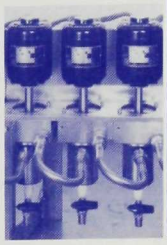

2.

3.

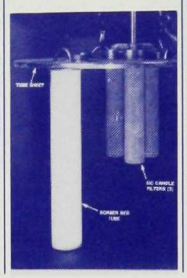

4.

5.

Cover Description

1. Proposed mechanism for catalysis of carbon monoxide hydrogenation by hexamethyldisiloxane.
2. Centrifugal contactors used in a solvent extraction process for removing transuranic elements from waste streams.
3. Testing of a lithium/iron sulfide battery designed for electric-van application.
4. Activated-bauxite sorber (left) and SiC candle filters (right) used for cleanup of alkali vapor and particulate in hot flue gas.
5. Uranium deposit formed in electrorefining simulated fuel for the Integral Fast Reactor.

Disclaimer

Printed in the United States of America

Available from
National Technical Information Center
U. S. Department of Commerce
5285 Port Royal Road
Springfield, VA 22161

NTIS price codes
Printed copy: A10
Microfiche copy: A01

Cover design by Argonne Graphic Arts Department

Distribution Category:
General, Miscellaneous, and Progress Reports (Nuclear) (UC-2)
General, Miscellaneous, and Progress Reports (Nonnuclear) (UC-13)

ANL-87-19

ARGONNE NATIONAL LABORATORY
9700 South Cass Avenue
Argonne, IL 60439

CHEMICAL TECHNOLOGY DIVISION ANNUAL TECHNICAL REPORT 1986

M. J. Steindler — Division Director
P. A. Nelson — Deputy Division Director
C. E. Johnson — Associate Division Director

June 1987

Previous reports in this series

ANL-86-14	January-December 1985
ANL-85-9	January-December 1984
ANL-84-26	January-December 1983
ANL-83-55	January-December 1982

TABLE OF CONTENTS

TABLE OF CONTENTS (contd)

TABLE OF CONTENTS (contd)

TABLE OF CONTENTS (contd)

CHEMICAL TECHNOLOGY DIVISION
ANNUAL TECHNICAL REPORT
1986

ABSTRACT

Highlights of the Chemical Technology (CMT) Division's activities during 1986 are presented. In this period, CMT conducted research and development in areas that include the following: (1) high-performance batteries--mainly lithium-alloy/metal sulfide and sodium/sulfur; (2) aqueous batteries (lead-acid, nickel/iron, etc.); (3) advanced fuel cells with molten carbonate or solid oxide electrolytes; (4) coal utilization, including the heat and seed recovery technology for coal-fired magnetohydrodynamics plants, the technology for fluidized-bed combustion, and a novel concept for CO_2 recovery from fossil fuel combustion; (5) methods for recovery of energy from municipal waste; (6) methods for the electromagnetic continuous casting of steel sheet; (7) techniques for treatment of hazardous waste such as reactive metals and trichloroethylenes; (8) nuclear technology related to waste management, a process for separating and recovering transuranic elements from nuclear waste, and the recovery processes for discharged fuel and the uranium blanket in a sodium-cooled fast reactor; and (9) physical chemistry of selected materials in environments simulating those of fission and fusion energy systems. The Division also has a program in basic chemistry research in the areas of catalytic hydrogenation and catalytic oxidation; materials chemistry for associated and ordered solutions at high temperatures; interfacial processes of importance to corrosion science, surface science, and catalysis; the thermochemistry of zeolites and related silicates; and the geochemical processes responsible for trace-element migration within the earth's crust. The Division continued to be the major user of the technical support provided by the Analytical Chemistry Laboratory at ANL.

SUMMARY

Current programs within CMT are briefly summarized below. These programs are discussed in greater detail in the remainder of the report.

1. *Battery Research and Development*

The Division is engaged in a variety of activities related to the development of high-performance secondary batteries (lithium/metal sulfide with molten-salt electrolyte and sodium/sulfur with glass electrolyte) and aqueous-electrolyte batteries (lead-acid, nickel/iron, etc.). These activities include research, performance and lifetime testing, post-test examination, modeling, and test data analysis of battery systems. In addition, the Division provides technical management of industrial contracts from the Department of Energy (DOE) for aqueous-battery R&D. The batteries being developed by CMT are primarily intended for electric-vehicle propulsion, with secondary consideration given to utility energy storage and military uses.

The research effort was centered on the Li-Al/FeS_2 and Na/S systems. During the past year, testing was completed on a 24-Ah prismatic cell having a LiCl-LiBr-KBr electrolyte. With the discharge limited to the upper voltage plateau, this cell exhibited no degradation in cell capacity during more than 400 charge/discharge cycles. Previous cells would have lost 30% of their capacity in the first 200 cycles. Development of a new cylindrical cell design for the Li-Al/FeS_2 system has been initiated. The research on sodium-ion conducting glasses for use as an electrolyte in Na/S batteries has resulted in the definition of a glass composition that provides the chemical stability and high conductivity needed. Calculations indicate that this glass could permit development of secondary batteries having high specific energy and specific power. This novel glass has also permitted the development of novel, miniature reference electrode systems that can be used to measure either sodium or sodium/polysulfide activity.

A joint program between ANL and the Gould Research Laboratory is underway to develop the lithium-alloy/FeS battery for testing in an electric van. During 1986, a 36-V battery design for a van was completed. The battery design is based on previously tested 12-V modules fabricated by Gould and incorporates all necessary components needed for thermal management, charging, performance monitoring, and data collection. A 36-V battery has been constructed by Gould and delivered to ANL for test in 1987.

The Analysis and Diagnostics (A&D) Laboratory in CMT continues to play a leading role in the testing and evaluation of various battery technologies (Na/S, Zn/Br, Zn/Cl, advanced lead-acid, etc.) fabricated by both domestic and foreign battery developers for electric-vehicle and load-leveling applications. The experimental results in combination with post-test examinations and battery modeling provide insight into technology deficiencies and aid in establishing the most-promising R&D approaches. The test results for advanced lead-acid modules from Exide Management and Technology Co. provided Southern California Edison with sufficient confidence to initiate construction of a large load-leveling plant.

Physical and chemical analyses of batteries are performed after termination of testing at the A&D Laboratory or at other facilities. In 1986, post-test analyses were conducted on Na/S cells, lead-acid modules, and Ni/Fe modules. Examination of cells from a Na/S battery led to the identification of the failure mode (fracture of an electrolyte tube) and its propagation during cool down of the battery. Post-test analyses of lead-acid modules led to the establishment of a relationship between capacity, pore volume, and degree of grid corrosion. For the Ni/Fe modules, capacity decline was found to be related to a reduction in the contact area between the current collector and the active material, plus contamination of the nickel-active material with iron.

Measurements were made of arsine and stibine emissions from a lead-acid load-leveling cell. The results indicated that hydride abatement equipment and adequate air ventilation will be needed to keep arsine and stibine levels to safe limits in a utility load-leveling plant with this technology.

An electrochemical model was used to predict energy and power capabilities of various cell design alternatives for Na/S cells utilizing glass electrolyte. In addition, a multiple regression analysis was performed with capacity and peak power data obtained from six lead-acid electric-vehicle modules (six cells each) tested at ANL. The analysis showed that the most important factors affecting

performance degradation were the levels of peak power demand for the driving profile and the location of a cell within each six-cell module.

A study of the corrosion behavior of 32 metals and alloys in sulfur and sodium polysulfides at 350°C was completed. It was concluded that molybdenum is the only metal or alloy that can be recommended as a positive current collector/container material for the Na/S cell.

2. *Advanced Fuel Cell Development*

The advanced fuel cells under development at ANL have electrolytes of molten carbonate and solid oxide.

The major technical problems in development of the molten carbonate cell are electrolyte management, cathode degradation, anode creep, corrosion of the bipolar separator sheet used to connect adjacent cells, and cross-leakage of electrode gases. The CMT research emphasizes the development of an alternative cathode material to NiO, which had been found to have a long-term stability problem. The activities during 1986 were concentrated on improving our understanding of the conduction mechanisms in doped $LiFeO_2$ and doped Li_2MnO_3 and in developing procedures for fabricating cathodes of tailored microstructure from these materials. Calculations indicate that our present alternative cathode materials will give adequate performance, and the optimum cathode microstructure was calculated to guide the cathode fabrication effort. Cells will be run to test the performance of the new cathode materials.

During 1986, ANL continued to provide technical support for the molten carbonate fuel cell program of the DOE Morgantown Energy Technology Center. This support took the form of program planning, systems analysis, technical monitoring of contractors efforts, and preparation of work statements. New contracts were initiated for developing base-technology support for the major stack development effort, and a procurement for a follow-on stack development is nearing completion.

The work on solid oxide fuel cells is concentrated on development of the monolithic fuel cell. This new design, which ANL is developing for the Department of Defense, employs the same thin, ceramic layer components of existing solid oxide fuel cells in a strong, lightweight honeycomb structure of small cells and is expected to yield much higher power per unit mass or volume. The design takes advantage of the ability to fabricate the solid electrolyte and other fuel cell components in shapes that cannot be achieved in liquid electrolyte systems. In 1986, arrays with monolithic fuel cells in electrical series were fabricated and operated. Fabrication involved tape casting of the thin-layer ceramic components (anode, cathode, electrolyte, and interconnection), assembling of the desired configuration, and firing of the configuration in one high-temperature operation. An array of monolithic fuel cells was operated for 700 h. Successful operation demonstrated the feasibility of the monolithic fuel cell concept.

The Division also performs systems analysis and cost assessment in support of the DOE fuel cell program. The purpose is to assess the economic viability of fuel cell systems and to define R&D priorities. In 1986, an analysis

was completed for cogeneration applications of fuel cell systems operated with natural gas. Three types of fuel cell plants (phosphoric acid, molten carbonate, and solid oxide) were compared to a gas-turbine/combined cycle system. The comparisons were made using the net present value of all future revenues as the measure of economic merit. The results indicated that fuel cells have potential in cogeneration applications.

3. *Fossil Fuel and Municipal Waste Utilization*

The program in municipal solid waste (MSW) utilization centers on the pyrolysis of MSW to form fuel-like liquid and gaseous products that are storable and transportable. The basic mechanisms of the thermokinetic degradation of MSW are being investigated with a thermogravimetric analyzer (TGA) and a bench-scale reactor. The data obtained from these experiments will be used to derive a kinetic model of the pyrolysis mechanisms associated with gasification, liquefaction, and charring of MSW components. Under subcontract with ANL, the Solar Energy Research Institute is using a flame pyrolyzer with a molecular-beam mass spectrometer sampling device to determine the influence of sample properties and reaction conditions on the solid-phase and gas-phase processes of MSW pyrolysis to oils.

The CMT program in coal utilization is focused on developing the hot-gas cleanup technology for pressurized fluidized-bed combustors (FBC), assessing materials for air heat exchangers in atmospheric FBCs, and developing the heat and seed recovery technology for coal-fired magnetohydrodynamics (MHD).

When gas turbines are directly operated with hot flue gas from the fluidized-bed combustion of coal, particulates of ash and condensed alkali metal compounds in the flue gas cause erosion, corrosion, and fouling of the gas turbine blades and hardware. For several years, CMT has investigated the use of sorbents for the removal of alkali vapor from the hot flue gas. A granular-bed sorber was designed and fabricated, and its effectiveness will soon be tested on the pressurized fluidized-bed combustor in CMT. Laboratory studies confirmed that activated bauxite would be an effective sorbent.

In the assessment of materials for air heat exchangers in atmospheric FBCs, a materials data base was established by collecting and assessing technical information on the performance of heat exchanger materials, particularly materials that have been exposed at temperatures greater than 650°C. The data were collected from 13 sources and generated in 16 different experimental FBCs. Materials tests are now being performed at CMT to provide corrosion information on a variety of structural materials, coatings, claddings, and weldments under conditions that simulate the FBC atmosphere.

The CMT Division is the lead ANL division in a multidivisional effort that is directed toward developing the technology required for the design of components in the MHD bottoming cycle. Over the past few years, the Fossil Energy Users Laboratory (FEUL) has been utilized to conduct fouling tests in which tube banks were exposed to simulated MHD combustion gases and the deposited seed and ash material was studied. The factors primarily responsible for sintering and densification of the deposits and their tenacity have been identified. Calculated data derived from a theoretical model have shown that potassium atoms and slag particles increase the gas emissivity, especially at high

gas temperatures. This effect is being experimentally studied in FEUL. Work is continuing on the severity of potential problems related to back-wall burnout of the radiant boiler caused by the high-velocity, high-temperature gas jet from the diffuser. Model calculations indicated that large slag particles (>10 μm) shed by the MHD diffuser will have a high impact velocity on the boiler backwall. Preliminary tests have shown that SO_x-NO_x emissions from an MHD plant can be controlled by use of a staged-cyclone coal combustor with limestone injection.

In other work, CMT is participating in efforts (1) to characterize, on a chemical and molecular basis, polyethylene pipe, resins, and materials and to relate this characterization with mechanical properties of the pipe and (2) to develop a novel concept for the recovery of CO_2 from fossil fuel combustion. With regard to the latter effort, staff from CMT participated in a successful test of this concept for CO_2 recovery at the Black Hills Power Company's Service Center.

4. *Electromagnetic Continuous Casting of Steel Sheet*

Argonne National Laboratory has recently started a cooperative R&D program with the steel industry. The overall objective is to improve the competitiveness of the domestic steel industry through the development of advanced technology that substantially reduces equipment, operating, and energy costs. The primary purpose of the CMT effort is to develop an electromagnetic process for the continuous casting of various grades of steel in large-aspect-ratio shapes such as steel strip. In 1986, efforts were directed toward a review of the current status of electromagnetic technologies in casting metals; an analysis of the electromagnetic, thermal-hydraulic, and fluid-dynamic requirements for a continuous casting operation; and a preliminary design for a bench-top electromagnetic caster for the initial casting studies. In addition, an experimental magnet was designed and fabricated, and experiments were initiated to establish the boundary conditions for liquid-metal stability in a high-velocity coolant system and to confirm theoretical predictions concerning the extent of suppression of these instabilities in the presence of a high-frequency magnetic field.

5. *Hazardous Waste Treatment Research*

The research on hazardous waste treatment includes an investigation of a process for the conversion of reactive metal (primarily sodium) to a glass for disposal. A high-soda silicate glass was selected as the most desirable glass form for sodium disposal; however, it was found that small quantities of other additives would be necessary to impart acceptable resistance to leaching by groundwaters and other environmental stresses. Differential thermal analyses with varying compositions of sodium oxide, silicon dioxide, calcium oxide, and magnesium oxide showed that the primary glass-forming reactions occur at less than 300°C. The absence of additional thermal effects as the temperature was raised to 1250°C indicated that no other glass-forming reactions were active. A conceptual process for sodium conversion to a soda-silica-lime glass form was designed.

In another effort, the technical feasibility of using a microwave-assisted chemical process for the detoxification of trichloroethylene (TCE) was demonstrated. The TCE detoxification was completed in a two-step process: (1) TCE was sorbed onto an activated carbon bed (with and without metal catalyst), and (2) the carbon bed was heated by microwave radiation to ~350°C while a

stream of moist air was passed over it. Principal detoxification products observed were CO_2, CO, and HCl. The TCE conversions achieved by this method with a metal catalyst were greater than 80%, much better than the 12% achieved by conventional heating under similar conditions.

Finally, the effect of the U.S. Army decontamination agent C-8 (a mixture of calcium hypochlorite, perchloroethylene, water, and nonionic detergents) on populations of normal soil microorganisms was investigated. Although the agent is diluted 30/1 with water for normal use, both the concentrated and diluted mixtures were used in our studies. Analyses of soil cores used to investigate the agent's effects on soil bacteria indicated that many bacteria, such as those that required only minimal nutrients or those that degrade pectin, are not significantly harmed by the components of the decontamination mixture, even in those regions of soil that contained high concentrations of calcium hypochlorite. These results suggest that much of the hypochlorite is still emulsified and is thus not available to the cells. Hypochlorite that is released from the emulsion appears rapidly neutralized by soil components. An unexpected result was that the growth of a few species of bacteria was actually enhanced by exposure to the decontamination agent.

6. *Nuclear Waste Management and Fuel Reprocessing*

High-Level Waste/Repository Interactions. Laser Photoacoustic Spectroscopy (LPAS) is being developed as a method for trace-level detection and speciation of actinides in groundwater near high-level nuclear waste repositories, specifically the Basalt Waste Isolation Project (BWIP). In preliminary experiments with Ho^{3+} and uranyl ion, the sensitivity that was achieved with a single-beam, dual-channel, laser photoacoustic spectrometer was essentially identical to that reported in the literature. Future LPAS work will emphasize measurements of transuranic elements in synthetic groundwater typical of the environment of the BWIP repository.

In a nuclear waste repository, the predominant type of radiation outside the container is gamma radiation. Tests are being performed to measure the effects of irradiating low-carbon steel coupons, basalt, packing (75% basalt, 25% sodium bentonite), and synthetic groundwater containing small amounts of CH_4 at a dose ratio of $\leq 10^4$ rad/h and temperature of 200°C. The results to date indicate that radiation at a dose rate of 10^4 rad/h alters the gas, liquid, and solid phases in tests which contain various combinations of the waste package components.

Separation Science and Technology. The Division's work in Separation Science and Technology consists of four projects. Three of these projects are concerned with removing and concentrating actinide elements from transuranic (TRU) contaminated waste streams, thus recovering valuable TRU elements and lowering waste disposal costs. The major project in this area involves development of a generic data base and modeling capability for the TRUEX (TRansUranic EXtraction) process. This capability will allow us to design flowsheets for specific waste streams and to predict the cost and space requirements for implementing a site- and feed-specific TRUEX process. It will also be useful as a tool for plant operators to vary, monitor, and control the

process once it is in place. Work in 1986 led to (1) collection of extraction-behavior data for a variety of important aqueous phase species and (2) modeling of the concentration profiles for nitric acid and americium in a 14-stage countercurrent demonstration of the TRUEX process. The second project, supported by Rockwell Hanford Operations, entails development of the TRUEX process for removing americium and plutonium from waste generated by the Hanford Plutonium Finishing Plant (PFP) while recovering a purified plutonium stream. A flowsheet for this process was completed and will be demonstrated in the Hanford PFP during 1987. Design of a plant-size centrifugal contactor for this process was also completed. The third project entails developing a PUREX/TRUEX flowsheet for removing plutonium from concentrated HCl/brine waste streams. Distribution ratios of important feed components were measured for this flowsheet.

The fourth project, which is unrelated to the first three, is concerned with the feasibility of substituting low enriched uranium (LEU) for the high enriched uranium (HEU) currently used in the production of fission product ^{99}Mo. Technetium-99m, the daughter of ^{99}Mo, is widely used in medical diagnosis. Results obtained thus far indicate that substitution of LEU for HEU is technically feasible with fairly minor variations in current processes.

The Integral Fast Reactor Pyrochemical Process. The Integral Fast Reactor (IFR) is an advanced reactor concept proposed by, and under development at, Argonne. Its distinguishing features are that it is a sodium-cooled, pool-type reactor; employs a metallic fuel (U-Pu-Zr alloy); and has an integral fuel cycle (discharged core and blanket materials are reprocessed and refabricated in an on-site facility). The advantages of this concept are an exceptionally high degree of inherent safety, resulting from use of a metallic fuel with a sodium coolant, and competitive economics, resulting from low costs for reactor construction and fuel recycle. The CMT Division has the responsibility of developing the on-site process for recovering plutonium and uranium from the core and blanket, removing fission products from them, and reenriching the core alloy with plutonium bred in the blanket.

Pyrochemical-type processes are under development for processing core and blanket fuel materials because metal products can be produced directly. The current reference flowsheet employs (1) electrorefining to separate fission products and the fuel cladding from uranium and plutonium and (2) halide slagging to enrich plutonium bred in the blanket to a concentration high enough (from about 3 wt % to 30-40 wt % plutonium) to reenrich the core. The feasibility of these steps has been demonstrated, but, in the course of this work, the possibility of eliminating halide slagging and relying solely on electrorefining was revealed. This is achievable through the use of a cadmium cathode as well as a cadmium anode (in conjunction with a molten chloride electrolyte). Current work is being directed to demonstration of this advanced process.

The chemical basis of the electrorefining step has been fairly well established. Equipment and facilities built for large-scale processing (approximately 20 kg of uranium) are nearly ready to operate. Work is also underway on processing the two major fission product waste streams--small fractions of the electrolyte salt and cadmium from the anode--to produce acceptable waste forms.

7. *Applied Physical Chemistry*

LWR Fission Product Chemistry. The Division is engaged in five experimental efforts to investigate fission product release and transport under accident-like conditions.

In the first effort, the chemical form and rate of release from an irradiated fuel pin are being determined. In the past year, our experimental apparatus was modified so that condensable gaseous species released from the fuel sample could be collected on a cold plate. Condensed samples were collected in which the maximum sample temperature reached was 1187, 1563, and 1668 K. The cooled samples were leached with water and analyzed for cesium and iodine as iodide ion. Only the first sample, collected at the lowest temperature, was found to contain a significant amount of iodine as the iodide ion. The results from this experiment also indicated that the rates of release for cesium and xenon are not the same as had been previously assumed in degraded-core accident analysis.

During a loss-of-coolant accident, fission products released from defected fuel pins are likely to form aerosols and be transported out of the reactor. The second experimental effort involves study of the action caused by a flow of gas over a deposit, i.e., revaporization. Our results suggest that the amount converted to aerosol depends on the rate of cooling of the gas: the greater the rate of cooling, the more likely that aerosols would be formed. Such deposits could heat up because of radioactive decay. If there is a flow of gas over the self-heated deposits, material could be vaporized, converted to aerosols, and carried further downstream. Depending on the integrity of the downstream components, outside release could occur.

In the third experimental effort, a transpiration technique is being used to study the release of three volatile fission products (La_2O_3, BaO, and SrO) from a core-concrete melt. Material loss by vaporization was by far the most important route; loss by entrainment made only a less than 10% contribution. The trend in the release of refractory fission products followed the sequence: Ba>Sr>La.

The fourth experimental effort focused on the collection of thermodynamic and vapor pressure data of the more-abundant species in the Cs-I-O-H system. This study was stimulated by the suggestion that the previously uncharacterized species, CsI•CsOH(g), contributed to iodine transport in our earlier experiments. The experimental effort utilized both transpiration and Knudsen effusion mass spectrometry for analysis of the vapor phase. Results to date strongly support a stable CsI•CsOH complex molecule. Further, our studies of the CsOH system indicate that the total pressure of CsOH vapor species (monomer and dimer) above condensed CsOH is a factor of 10 lower than previously reported.

In the fifth effort, laboratory studies were conducted on selected fission products in support of the Source Term Experiments Program (STEP) conducted in the Transient Reactor Test during 1984-1985. In these in-pile simulations, fission products were released from irradiated UO_2 fuel rods (overheated in flowing steam) and were then collected on various coupons and wires. The compound CsI could not be identified in any collected deposits. Long needles containing Ag,

Cs, and I were seen on many coupons. X-ray diffraction identified metallic silver in these deposits; we had anticipated finding one or more of the $Cs_{1-x}Ag_xI$ compounds. Further studies are needed to explain the transport mechanism for getting natural silver in these downstream deposits. Inconclusive results were obtained for delineating the stoichiometry of Cs and Te deposits among the possible compounds CsTe, Cs_2Te, Cs_2TeO_3, and Cs_2TeO_4. The rate of vaporization of selected fission products, control rod, and structural materials is being studied to provide data for modeling the transport of such materials during a nuclear accident.

Metal Fuels Properties. An assessment of the data available on the thermophysical properties of metal fuel and blanket materials for the Integral Fast Reactor revealed some important gaps. Our ongoing program is designed to correct the most important of these deficiencies by performing selected experiments. Currently, progress has been made on determining the thermal expansion of U-8.4 wt% Pu-1.3 wt% Zr alloys, the thermal conductivity of U-11.4 wt% Zr alloy, the solidus and liquidus temperatures for the U-Pu-Zr system, and the fuel-cladding compatibility in a nitrogen-helium environment.

Fusion-Related Research. A critical element in the development of the fusion reactor is the blanket for breeding tritium fuel. Several studies are in progress with the objective of determining the feasibility of using lithium-containing ceramics as the breeder material.

Our ongoing thermodynamic and kinetic studies of tritium breeder materials are focused on surface adsorption/desorption, the solubility of hydroxide in $LiAlO_2$, and gas-phase chemical control of the breeder surface. Calculations were made of the thermodynamic relationships among the gaseous and condensed phases and the breeder surface at temperatures of 700-1300 K and oxygen activities of 10^{-25} to 10^{-5}. The results indicated that surface adsorption can be expected to make its greatest contribution to inventory under conditions of low temperatures and high oxygen activities. An experimental effort using frontal gas chromatography has been started to measure the uptake of water vapor by $LiAlO_2$. These data will yield adsorption isotherms to describe the thermodynamics of the adsorption of water vapor and the dissolution of hydroxide. Data have been obtained for a gas mixture of 550 ppm H_2O in helium to temperatures of 891 K. Adsorption/desorption and dissolution were observed.

The lithium ceramics may be used in the blanket in several different forms, one of which is the sphere-pac configuration. For this configuration, an important material parameter is its thermal conductivity, improvements in which would lead to better mechanical and thermal performance. Further, for tritium self-sufficiency, most lithium ceramics require the presence of a neutron multiplier, e.g., beryllium. A sphere-pac bed in the mixed-sphere configuration and the coated-sphere configuration has been analyzed in detail. The latter configuration has touching spheres of $LiAlO_2$ coated with BeO, and the former has randomly mixed, similar-sized spheres of both $LiAlO_2$ and BeO. The coated-sphere configuration showed better thermal-conduction behavior, close to that of 100% dense $LiAlO_2$.

A computer model is being developed to depict tritium transport and release from ceramic breeder materials. This model will include diffusion in the solid, desorption from the solid surface, and transport through a porous medium.

The model is based on a differential equation that predicts heat transfer in a solid sphere at constant heat generation and heat radiation at the surface. The tritium release over time calculated with our model was compared with measured release for samples of Li_2SiO_3. Overall, agreement between the model and experiment was good. Improvements in the model to handle samples with a large distribution of grain sizes are now being considered.

For fusion to be attractive as an alternative energy source, the direct capital cost of the reactor per kilowatt-hour and the bus-bar cost of electricity have to be significantly reduced. A goal of our current design study is to evaluate the economic impact of innovative design concepts on capital costs and operating costs for a tokamak-based reactor. The cost for a recent fusion reactor design, the tokamak power systems reactor plant, was found to compare favorably with current 1000 MW fission and fossil power plants.

In neutron dosimetry and damage analysis, neutron facilities are being characterized in terms of neutron flux and energy spectrum, which can be used to calculate atomic displacements and transmutations. These damage parameters can also be used to correlate properties changes and to predict materials performance in fusion reactors. Recent research has focused on measuring production rates for long-lived isotopes in order to assess potential waste-handling problems. Attention has also been given to improving our capability for doing damage calculations in compounds such as $LiAlO_2$, Li_2O, and stainless steel. For these materials, the general trend indicates that the damage calculated will be larger than the linear combination of elemental sums when there is significant difference in the atomic masses involved in the compound.

8. *Basic Chemistry Research*

Fluid Catalysis. This research is designed to determine reaction mechanisms and to explore new catalytic chemistry involving small molecules (e.g., CO, CO_2, O_2). Research is being done on carbon monoxide hydrogenation catalyzed by soluble oxides. Activation of hydrogen by the oxide was identified as the rate-determining step in the reaction catalyzed by hexamethyldisiloxane. Based on the premise that this activation step involves nucleophilic attack on the hydrogen molecule, nucleophilic siloxide catalysts, exemplified by $NaOSiMe_3$, were tested and found to greatly enhance both the rate of hydrogen activation and carbon monoxide hydrogenation.

Research is also underway to explore the concept of utilizing catalytically activated organic bases as oxygen carriers to reversibly bind O_2 and thereby separate it from air. Mechanistic studies were recently completed on the oxidation of tertiary amines containing α hydrogen atoms. Rate-limiting electron transfer from amine to the oxygen molecule accompanied by sacrificial loss of an alpha proton was found to be characteristic of this system.

Multinuclear NMR spectroscopy has been the single most useful spectroscopic tool in our studies. To obtain full advantage of the NMR method, efforts have been initiated to design and construct an NMR probe for use with *in situ* kinetic and thermochemical studies at high pressures and temperatures. An NMR test probe was fabricated and used to identify a copper-aluminum alloy (CDA-642) which is superior for our purposes when compared with others currently used in NMR pressure vessels.

High-Temperature Materials Chemistry. Quantum mechanical calculations were performed for oxide, fluoride, and sulfide complexes in an ionic medium with Al^{3+} and Mg^{2+} cations to determine their structures, energies of formation, and vibrational frequencies. The few available experimental measurements are consistent with our results.

Measurements were made of the thermodynamic properties of molten K-Pb alloys. Plotting of the heat capacities for this alloy as a function of composition revealed an unexpected large, temperature-dependent peak near the $X_K = 0.5$ composition. This anomalous behavior is indicative of long-range ordering or clustering.

A method that leads to accurate predictions of sulfide capacities for binary slags (i.e., the ability of a slag to extract sulfur from liquid alloys) was developed. Knowledge of these values is important in pyrometallurgy and steelmaking. Extension of our calculational method to more complex slags will be based on concepts developed earlier for reciprocal systems.

A general computer program has been developed for the calculation of gas/condensed-phase equilibria in multicomponent-multiphase systems. The program has been tested on several problems concerned with the combustion of coal.

Interfacial Materials Chemistry. Significant advances have been made in the research on aqueous corrosion at elevated temperature and pressure. The Fe^{2+}/Fe^{3+} redox reaction was studied as a function of temperature; from room temperature (25°C) to 150°C, the overall rate of reaction increased by a factor of four—a level of increase that is typical of diffusion-controlled reactions. Two electrochemical techniques were developed to eliminate the interferences in electrochemical kinetics measurements that result from the presence of trace amounts of certain anionic impurities (such as Cl^-). The phase chemistry of lead(II) in aqueous sulfate media from room temperature to 280°C was investigated using a combination of Raman spectroscopic and electrochemical techniques. The results of this work permitted the construction of a temperature-dependent Pourbaix diagram for the $Pb/H_2O/H_2SO_4$ system. A systematic study of the corrosion products of nickel in aqueous media was completed; long-standing uncertainties concerning the valence of nickel in its higher oxide forms were resolved by this work. *Ab Initio* molecular orbital techniques were used to develop potential energy functions for hydrated transition metal cations. These functions are being employed in molecular dynamics studies of electron transfer reactions at metal/water interfaces. The aim of this research is to provide first-principle calculations of electron transfer rates against which comparisons with paralleling experimental measurements can be made.

Zeolite catalysis is being studied by a combination of infrared spectroscopy and gas chromatography. The results to date have shed new light on the temperature dependence of mechanisms for carbon-carbon bond formation and carbon-hydrogen bond scission in the catalytic conversion of alcohols to gasoline-range hydrocarbons using the synthetic zeolite H-ZSM-5. The vibrational dynamics of zeolite framework structures was explored by group theoretical and empirical methods. Potential energy functions suitable for use in lattice dynamics analyses of zeolites were developed and tested on a model system. *Ab initio*

molecular orbital theory was employed to investigate rotational barriers and vibrational frequencies of organic templating cations used in the crystallization of synthetic zeolites. The torsional modes of occluded templates were found to be a sensitive indicator of the interaction between the template cation and the surrounding zeolite cage structure.

Thermochemistry. Thermochemical studies of zeolite faujasites with different Si-to-Al ratios are in progress. The information from this work is intended to give a quantitative measure of the influence of this ratio on the standard molar enthalpy of formation and other thermodynamic properties. This will have likely application in future modeling studies of rock-water interactions.

Fluorine-bomb calorimetric measurements on "high-tech" materials, primarily chalcogenides, are also underway. Current studies deal with the crystalline and vitreous forms of $GeSe_2$, $MoSe_2$, and the newly synthesized Mo_6Se_6.

Geochemistry of Natural Hydrothermal Systems. An effort is underway to study the geochemical processes involved in water/rock interactions that occur in active hydrothermal systems in the Earth's crust. The time scale of hydrothermal activity in several active systems under study as part of the Continental Scientific Drilling Program is being determined with U-series methods. Also underway is analysis of oxygen and carbon isotope ratios in minerals from drill core samples. To date, ~50 samples of hydrothermal silica and carbonate minerals from drill cores in Yellowstone National Park have been analyzed. In another effort, the hydrothermal system of Nevado del Ruiz volcano, which erupted in 1985, is under investigation. A wide variety of data have been collected from chemical and isotopic analyses of thermal wastes and gases, cold surface waters, and the lava ejected during the eruption.

9. *Analytical Chemistry Laboratory*

The Analytical Chemistry Laboratory (ACL) is administratively within CMT, the principal user, but collaborates with most of the technical divisions and many of the programs at ANL as a full-cost-recovery service center. In addition, the ACL conducts a research program in analytical chemistry and provides analytical services for governmental, educational, and industrial organizations.

In 1986, the ACL provided analytical support to a wide variety of programs, including efforts (1) to develop the Integral Fast Reactor, (2) to identify areas of environmental risk at DOE facilities, (3) to monitor the emissions from municipal waste incinerators, (4) to gain a better understanding of degradation mechanisms for historical monuments and buildings, (5) to investigate the commercial production and separation of ^{99}Mo from low-enriched uranium, (6) to characterize the organics in solid and sludge wastes from new energy technologies such as coal gasification and liquefaction, (7) to provide the coal community with well-characterized and stabilized samples of coal, (8) to determine the source term associated with a postulated light water reactor accident, (9) to study the degradation of toluene in an Organic Rankine cycle engine, (10) to characterize the chemical and molecular properties of polyethylene (PE) resins and to determine the effect of these properties on the mechanical strength of PE pipe, and (11) to assess the environmental implications of neutralizing spills of hydrazine fuels with hypochlorite. In addition, the ACL developed a laser Raman

microprobe that is capable of resolving areas on solids of ~1 μm^2 and developed a cleanup technique that will remove unwanted coextractives that interfere with measurements of targeted compounds from a soil extract.

Increased analytical capabilities were established in 1986 by the addition of an inductively coupled plasma/atomic emission spectrometry system for analysis of radioactive samples, a sample receiving room, a containment room, and a liquid scintillation counter. Several analytical instruments were automated.

10. *Computer Applications*

The Computer Applications Group assists CMT staff in many aspects of computer-related activities, including laboratory data acquisition and control, computer modeling and simulation studies, analysis of experimental results, graphics, information management and data-base development, computer networking, procurement of automatic data processing equipment, and advisory and consulting services. In 1986, the Division upgraded its VAX computer from a model 11/780 to 11/785, which increased capacity by 50-70% and better accommodated its increased usage. In addition, the disk storage capacity was increased from 2000 to 2500 megabytes, and memory was increased from 16 to 32 megabytes. The VAX 11/785 is being used for a wide variety of applications, including post-analysis of experimental data, theoretical calculations in basic energy science, graphics applications, electronic mail and other office automation and management functions.

I. BATTERY RESEARCH AND DEVELOPMENT

The battery program at ANL involves a variety of activities with high-performance rechargeable batteries (lithium/metal sulfide and sodium/sulfur) and aqueous batteries (lead-acid, nickel/iron, etc.). These activities involve battery research, technical management of DOE contracts to industry, performance and lifetime tests, post-test analysis, and battery modeling and analysis of test data. The batteries being developed by ANL are primarily intended for electric-vehicle application, with secondary consideration given to utility energy storage and military uses.

A. *Molten-Electrolyte Cell Research*

Research is being conducted to attain major improvements in the performance of secondary batteries having molten-salt electrolyte, lithium alloy negative electrodes, and metal disulfide positive electrodes. To maintain the electrolyte in the molten state, cells are operated at temperatures of 350-450°C. The objective of this task is to bring about innovations in the current technology that will yield a specific energy of 175-200 Wh/kg at a 4-h discharge rate, a specific power of 200-300 W/kg, and a cycle life of 1000 cycles. A lithium-alloy/FeS_2 cell with LiCl-LiBr-KBr electrolyte has shown promise of achieving these performance and cycle-life goals.

Our 1986 efforts included (1) experiments to determine the influence of physical electrode parameters on cell performance, (2) examination of electrochemical electrode processes with candidate active materials that provide effective overcharge protection for lithium/metal sulfide cells, (3) demonstration of long life and ultra-high pulse power capability for a Li-Al/FeS_2 cell couple, and (4) modeling studies of cylindrical electrodes that are simpler and less costly than flat-plate designs.

The electrochemical characteristics of the Li-Si/FeS_2 cell and its electrodes were examined using a set of five voltage sensors inserted at different locations within the cell to find relationships between various physical parameters of the electrodes and cell performance. The potential changes measured by the voltage sensors during galvanostatic discharge, current interruptions, and current pulses were converted into values that described electrode impedance as a function of the depth of discharge and changes in cell-component composition. Electrode impedance values were used to calculate specific energy and specific power of cells under various conditions of cell discharge. Analysis of the digitally stored data to date indicated that the positive electrode develops high impedance that limits cell power, capacity, and energy. High temperatures (>400°C) and fine FeS_2 particle size significantly reduce the impedance of the positive electrode.

A special test cell was designed and assembled to investigate the thermodynamic, kinetic, and thermal properties of active materials under conditions relevant to advanced battery operations. Cyclic voltammetry with the special test cell is being used to obtain information about the kinetics of metal disulfides and to study a newly discovered overcharge-protection mechanism for the Li-alloy/metal disulfide cell.

Cell tests were conducted to examine active material processes that offer overcharge protection for both the negative and the positive electrodes. Active materials and proper operating conditions that assure overcharge tolerance at high charge rates were identified. The basic principles of the overcharge tolerance were verified in small Li-Al-Si/(Fe-Ni)S_x test cells (0.5-2.0 Ah capacity) using an intermittent galvanostatic cycling technique. Figure I-1 shows a section of a cycling diagram as an example for one of the overcharge tests. This cell was overcharged with a current density of 50 mA/cm^2 to approximately 2.5 times the theoretical capacity in charge cycle 21, when the voltage-limiter relay was inactivated. The plots of the following cycles indicated that no damage occurred in the electrodes. The cell performed many more cycles with several overcharges and showed good capacity retention.

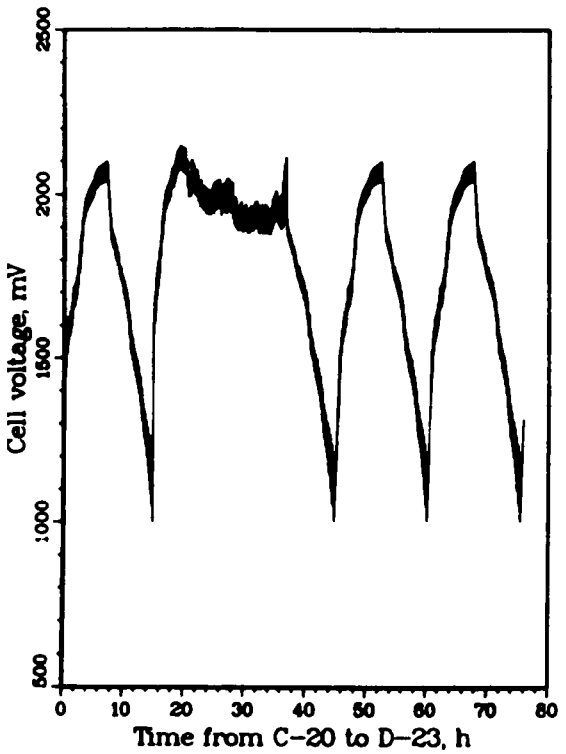

Fig. I-1.

Voltage Curve of Li-Al-Si/(Fe-Ni)S_2 Cell from 21st Charge to 23rd Discharge

Tests with experimental Li-Si/FeS_2 cells were also conducted to explore options in separator materials and wetting procedures. The options examined included pressed pellets of LiCl-KCl-MgO, tape-cast and salt-impregnated MgO powder, salt-impregnated yttria cloth, and salt-impregnated BN-MgO felt separator layers. A cell with a 0.7-mm thick separator of pressed LiCl-KCl-MgO achieved the best performance, with a peak power density of 8.8 W/cm^2.

An apparatus was developed to conduct high-intensity current pulse tests that would relate electrode potential, current density, and time and to study cell/electrode performance as a function of component fabrication parameters such as particle size of the active materials, loading density, electrolyte volume fraction, separator properties, and electrical conductivity. The pulse response of the Li-alloy/FeS_2 system is illustrated in Fig. I-2 with data plots of cell current

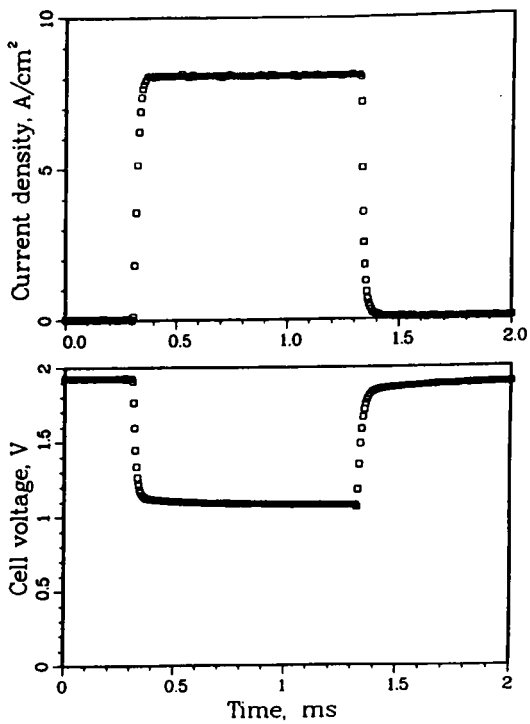

Fig. I-2.

Voltage Trace Measured in 1-ms Discharge Pulse of Li-Si/FeS_2 Cell. The upper plot shows the current density applied during the pulse.

and voltage as a function of time. The cell was at full charge and subjected to an intense current pulse of 8.04 A/cm^2 and 1-ms duration. The current pulse caused a drop in cell voltage of about 0.84 V (from 1.93 V before the pulse to 1.09 V at the end of the pulse) because of an internal cell resistance of ~0.1045 Ω cm^2 ($R_t = \Delta V/\Delta I = 0.84/8.04$). With this R_t (t = 1 ms), a peak power density of 8.91 W/cm^2 (volumetric power density of 32.8 W/cm^3) was available. A specific peak power of 17.6 kW/kg for the cell is projected based on its size (7.91-cm^2 area, 2.72-mm thickness) and weight (4 g). Full cell capacity was obtained with high-intensity pulses having durations of more than 250 ms and rates of more than 20 pulses a second. Because of the endothermic nature of the electrochemical discharge reaction, calculations showed that the usual heat generated by internal power (I^2R) losses is cancelled in the lithium-disulfide system for output pulse power levels as high as 165 kW/kg. This self-cooling feature allows very compact packaging of the cells in a battery. As a result, a rechargeable bipolar cell battery incorporating newly developed active materials and molten-salt electrolytes is projected to have a specific power of 150-300 kW/kg in 1- to 1000-ms pulses. This durable electrochemical system provides very high power in a compact, self-cooling package that is ideally suited for new demanding applications such as powering electromagnetic launchers that require short but extremely energetic pulses.

An intermediate-size "bicell" (i.e., central positive electrode and two facing negative electrodes) of about 24-Ah capacity was employed in evaluating the lifetime of the Li-Al/LiCl-LiBr-KBr/FeS_2 cell. In this test, the cell was charged at an 8-h rate (25 mA/cm^2) and discharged at a 4-h rate (50 mA/cm^2) between voltage cutoffs of 2.05 and 1.25 V, respectively. This maintained discharge on the upper of the two voltage plateaus for the FeS_2 cell. The cell operating temperature was 388-427°C. A Ni/Ni_2S_3 reference electrode was used to determine working-electrode potentials during the deep-discharge cycling. The

curve for capacity utilization vs. cycle number for this FeS_2 cell is shown in Fig. I-3 (the coulombic efficiency of the cell is >99%), and its utilization is 89% at a current density of 50 mA/cm^2. Cell capacity was nearly constant through more than 400 cycles and 5400 h, and the cell voltage vs. capacity curve was little changed during this time. With LiCl-KCl electrolyte, the Li-Al/FeS_2 cell would have lost 50% of its upper-plateau FeS_2 capacity in the first 200 cycles.

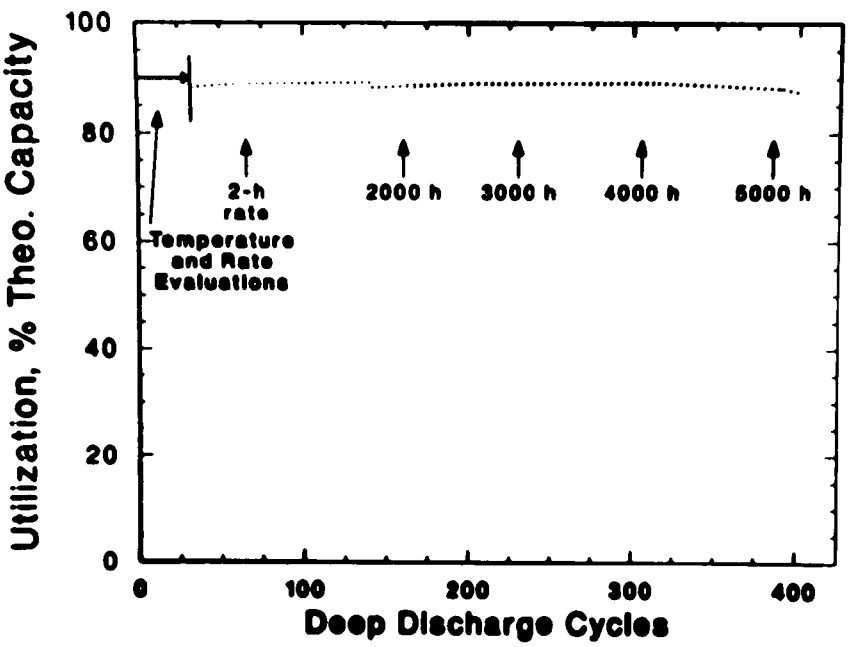

Fig. I-3. Cell Discharge Capacity as Function of Cycle Life

A post-test analysis of the upper-plateau FeS_2 cell revealed the presence of a much smaller amount of Li_2S + Fe in the separator area than that of earlier (LiCl-KCl electrolyte) cells. The high, stable capacity through 400 cycles supports this finding. The absence of capacity decline in this cell suggests that an event in testing or a peculiarity in design is responsible for the presence of the Li_2S + Fe. We suspect the following as causes: (1) impure CoS_2 additive in the positive electrode, (2) short-term high temperature (427°C) operation, and (3) increased positive-electrode polarization during charge due to negative-electrode oxidation. Barring mechanical short circuits, the upper-plateau FeS_2 cell has the potential for 1000 cycles of high-performance operation. Efforts in 1987 will be directed at substantiating the stability and high performance of this system.

Simplified current collector shapes are needed to facilitate the fabrication and reduce the cost of molten-salt cells that use molybdenum current collectors. Modeling and cell fabrication studies were initiated to investigate alternative electrode designs. A model was developed for a cylindrical cell with the positive electrode in the shape of a rod having an outer annulus of separator material (MgO powder). The positive current collector is in the shape of a molybdenum wire at the center of the electrode. This electrode shape affords simpler and less costly fabrication than that of flat-plate designs. The model was used to evaluate

various design options and identify key components for further study. Calculations for a cylindrical cell design (5-cm OD and 19.5-cm length) containing seven positive electrodes (~150-Ah capacity) showed an achievable specific energy of 190 Wh/kg and a specific power of 185 W/kg. Improvement in the electronic conductivity of the positive electrode would result in a significant increase in cell power capability.

B. *Glass-Electrolyte Sodium/Sulfur Cell Research*

Glass electrolytes for Na/S cells are promising alternatives to employing the ceramic electrolyte, sodium β"-alumina, that is being used currently. The objective of our research is the development of a glass that will be highly conductive for Na^+ ions, will be chemically stable in the hostile Na/S cell environment, and can be easily fabricated at low cost. Soda-rich glasses in the soda-alumina-zirconia-silica system were selected for in-depth study based on our earlier experiments, thermodynamic calculations, and review of the literature.

After we characterized 25 glass compositions that span the soda-alumina-zirconia-silica system, we selected a glass composition for further development (in mol %) 42 Na_2O, 8 Al_2O_3, 5 ZrO_2, and 45 SiO_2. This composition (designated ANL glass) met our initial acceptance criteria: high Na^+-ion conductivity (resistivity of 221 Ω cm at 300°C) and good chemical stability in accelerated screening tests (immersion in Na, Na_2S_4, Na_2S_3, and S at 400°C for 1000 h).

By using a stainless steel blowpipe, we could easily draw (by hand) tubes of sufficient dimension from the ANL glass melt at about 1000°C. Further experimentation with the hand-drawn glass tubes showed that metal-to-glass seals could be made using thin-walled Types 304 and 316 stainless steel tubing (3.2-mm OD, 0.25-mm wall thickness). The coefficients of thermal expansion for these metals and ANL glass are reasonably well matched; in fact, the glass-to-metal seals have been thermally cycled from ambient to 450°C at least twice. Metallographic examination of a Type 316 stainless steel-to-glass seal showed the glass to be chemically bonded to the steel (reaction zone was 1- to 2-μm thick) and bonding present over 85% of available surface area.

We assembled eight sealed Na/S cells, each of which had a single hand-drawn glass electrolyte tube with the above metal-to-glass seal. After conditioning, the cell was cycled at a 6- to 10-h rate. Unfortunately, the cells routinely failed after about three cycles. The most likely causes of failure were ambient moisture or nonuniformities within the tube from the fabrication process.

The first attempt to fabricate a large quantity of ANL glass tubes for proof-of-materials testing was not successful. Under the conditions used, there was no problem producing uniform glass billets (500-1000 g) from high-purity reagents. However, the glass was not amenable to redrawing from the billet. The usual procedure is to heat a billet from room temperature to its softening point (~850°C), a process that takes about 3 h. We found that ANL glass crystallized during the heat up.

The facilities and process now under development for fabrication of glass tubes will take into account the physical and chemical properties of ANL glass. Because of the high soda concentration of ANL glass, fabrication will most likely be performed under anhydrous conditions. Further studies have shown that the

minimum temperature for glass-melt stability is approximately 1350°C. At lower temperatures, Na_2ZrSiO_5 precipitates as prismatic crystals within an hour. It was found that the temperature range for tube drawing was 850-1000°C, with a cooling rate of 200-300°C/min.

Sealed, small-scale Na/S cells (2-mm^2 active area; 1- to 3-mAh capacity) were fabricated and gave an indication of the electrochemical life of ANL glass. These small cells consisted of a membrane of ANL glass attached to an α-Al_2O_3 tube and were prepared with minimum air exposure. In these tests, cells achieved 36-40 cycles at 4-h discharge and 8-h charge rates. Problems not necessarily related to the chemistry of the glass caused cells to fail. These included detachment of the membrane because of thermal expansion mismatch and redistribution of the positive electrode within the cell body.

The electrochemical life of ANL glass was also investigated in cells using other materials as positive electrodes (or sodium-ion sinks). To eliminate the containment problem associated with sulfur, NiS was used for the positive electrode. In the course of experimentation, it was found that sodium from the sodium-pool electrode crept along and darkened the ANL glass disk. Because it was thought that capillary action would help hold the sodium in place, we built and tested an electrode of sodium in iron Retimet for a sodium/sodium cell. All Na^+-ions in the glass were exchanged on the order of 200 times before the test was stopped. Examination of the glass disk showed much less darkening of the glass in the area outside of the electrode than previously found. This demonstration illustrates that there are no first-order problems with Na^+-ion transport in the glass.

Novel, miniature reference electrode systems are being developed to measure either sodium or sodium polysulfide activity. The reference electrode is a spin-off from the Na^+-ion-conducting glass technology. The reference electrodes use small (2-mm^2 active area), thin membranes of ANL glass. The small, electrochemically active area of the reference electrode makes precise positioning possible in an electrochemical system of interest. For example, in the sulfur electrode of Na/S cells, precise positioning of the reference electrode would allow satisfactory spatial resolution of activity gradients in cells at operating temperature (300-350°C).

Typically, the reference electrode is made in an analogous fashion to the small-capacity cells described above. Once a reference material is sealed within the reference electrode, the small active area performs electrochemically like a Luggin capillary tip. However, instead of diffusion-limited mixing of system components, the new reference electrode completely isolates the reference material from the rest of the system.

A reference electrode containing sodium was tested in a Na_2S_4 melt[1] to determine emf stability and the thermal coefficient of the emf in the range of 300-400°C (573-673 K). The stability of the electrode was good. Over the course of 99 h at 350°C (623 K), a small potential drift of -0.13 mV/h was observed, which was accountable as the slow evaporation of sulfur from the Na_2S_4 melt. The temperature was inversely related to the measured emf. The thermal coefficient of the emf of the Na|ANL Glass|Na_2S_4 cell, -0.70 mV/K, was calculated

[1]A. P. Brown and J. E. Battles, Synth. React. Inorg. Met. Org. Chem. **14**, 945 (1984).

from the slope of the best-fit line to these values (Fig. I-4). From the measured emf values, the calculated free energy changes agreed quite well with previously obtained values from open-circuit measurements on a Na/β"-alumina/S cell.[2] We will continue to develop the reference electrode to fully explore its operating temperature range and utility.

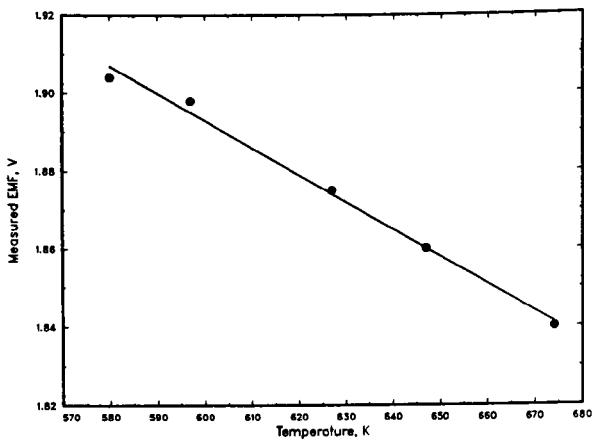

Fig. I-4.

Plot of emf for (Mo)Na|ANL Glass|Na_2S_4(Mo) Cell vs. Temperature

C. *Engineering Development of Lithium-Alloy/Iron Sulfide Batteries*

A program is underway at ANL and Gould Inc. (Cleveland, OH) to develop the Li-alloy/FeS battery for electric-van propulsion. The program is funded by the Electric Power Research Institute (EPRI), the U.S. Department of Energy (DOE), and the Tennessee Valley Authority (TVA).

We completed a 36-V battery design based on the 12-V Li-alloy/FeS module that was fabricated by Gould Inc. and successfully tested last year.[3] The design provides all the necessary components needed for thermal management, charging, and performance monitoring and data collection.

A heat exchanger designed by ANL was fabricated by Gould Inc. for the 36-V battery. The design integrates the functions of heating and cooling and supports three 12-V modules in a single, lightweight unit. Electrical resistance heaters heat the battery, and once-through ambient air is used for cooling.

A new approach to high-efficiency, lightweight insulation is being examined by CMT working in collaboration with Meyer Tool & Manufacturing, Inc. (Oak Lawn, IL). Compressed layers of aluminum foil and fiberglass paper in a vacuum annulus are being assessed as the insulating medium. Laboratory tests at the Linde Division of Union Carbide suggest that an insulating medium having a thermal conductivity of 0.0011 W $m^{-1}K^{-1}$ and a specific gravity of 0.43 can be

[2]J. L. Sudworth, "The Sulfur Electrode," Chap. 5 in *The Sodium-Sulfur Battery*, J. L. Sudworth and A. R. Tilley, Eds., Chapman and Hall Ltd., New York (1985).

[3]M. J. Steindler et al., *Chemical Technology Division Annual Technical Report, 1985*, Argonne National Laboratory Report ANL-86-14, p. 21 (1986).

obtained. This insulation will reduce the volume and weight of the battery case and is expected to be less expensive to manufacture than the presently available "board" insulation produced by the Linde Division of Union Carbide. A contract has been awarded to Meyer Tool & Manufacturing for the fabrication of a 36-V battery case using the new insulation.

Two 36-V batteries are scheduled to be tested during 1987. The first, funded by EPRI, has been fabricated by Gould and was delivered to ANL in December 1986. This battery will be tested in ANL's Analysis and Diagnostics (A&D) Laboratory on an SAE J227 a/C driving schedule (a computer-driven simulation of a stop-go driving pattern for a van battery). The second battery, funded by TVA, will be assembled at ANL from components supplied by Gould and others. This battery is being designed to be tested both in the A&D Laboratory and in a van at the TVA Test Facility in Chattanooga, TN.

D. *Electric- and Hybrid-Vehicle Battery R&D Support*

1. Aqueous Electric-Vehicle Batteries

The Division provides technical support to DOE for the development of aqueous battery technology for electric vehicles. The technical support includes assistance in program planning, preparation of work statements, technical assessments, and system analyses. In this capacity, CMT continued to provide technical management of two major industrial contracts: one with Johnson Controls, Inc., for the development of advanced lead-acid batteries, and the other with Eagle-Picher Industries, Inc., for development of nickel/iron batteries.

The work at Johnson Controls is focused on research and development of an advanced lead-acid battery based on the forced flow of electrolyte through the porous lead and lead dioxide electrodes--an innovative design approach that yields better utilization of the active materials. An improved full-size cell with flow-through electrolyte was fabricated in 1986 and delivered to the A&D Laboratory for testing and evaluation. This experimental cell achieved very high levels of active-material utilization (85% greater than that obtained in commercially available lead-acid batteries); this dramatic increase in utilization should yield a 40% increase in the specific energy of lead-acid batteries. This effort will be continued in 1987, with emphasis on obtaining cycle lifetimes of up to 200 charge/discharge cycles for this technology.

The effort at Eagle-Picher is directed toward reducing the cost of advanced nickel/iron batteries. The work is focused on the development of nickel electrodes up to twice as thick as in prior technology and having the desired porosity and strength required for good performance and long life. Cell designs based upon thick-electrode technology are projected to significantly reduce battery costs and to improve battery specific energy. Nickel electrodes of 3-mm thickness were fabricated successfully and tested for the first time during 1986. Meanwhile, laboratory and in-vehicle field tests continued to confirm the ruggedness and long life of nickel/iron batteries developed under this effort. A complete nickel/iron battery system has powered an electric vehicle for over 30,000 actual miles of operation to date at the TVA Electric Vehicle Test Facility. Nickel/iron batteries also continue to perform well after five years in commercial fleet operations at industrial sites. Efforts to reduce the cost of this performance-proven technology will be continued in 1987.

2. Hybrid-Vehicle Batteries

As part of DOE's Hybrid Vehicle Propulsion Technology Program, CMT completed a study which identified the most promising battery designs for application in hybrid vehicles. One conclusion from this study was that, as compared with the electric-vehicle battery, the hybrid-vehicle battery must be smaller, have higher power capability per unit weight, and be discharged at higher rates. The analysis showed that several battery types are good candidates for meeting the hybrid vehicle requirements, including bipolar designs (lead-acid and Li/FeS), alkaline batteries (Ni/Fe, Ni/Cd), and high-temperature batteries (Na/S, Li/FeS). A report that presents conclusions resulting from the study and identifies battery development needs for hybrid propulsion was prepared and submitted to DOE in 1986; no further work on this effort is planned in 1987.

E. *Performance and Life Evaluation*

We are evaluating cells, multicell modules, and full-scale batteries fabricated by industrial firms in the A&D Laboratory to determine their performance and life characteristics. These evaluations provide an interim measure of the progress being made in battery R&D programs, as well as basic data needed for modeling and continuing R&D. The experimental results and analysis of data, in combination with post-test examination (Sec. I.F) and modeling (Sec. I.G) of advanced battery technologies, provide insight into their deficiencies and help identify the most-promising R&D approaches for overcoming these deficiencies. The battery technology being evaluated is primarily applicable to utility load-leveling (LL) and electric-vehicle (EV) application.

During 1986, technology evaluation was completed on 200 cells and was continued on 295 others. These cells are mostly in the form of three- to six-cell modules, but also in the form of full-sized 30- to 50-kWh batteries with up to 140 cells, and are primarily Na/S, Zn/Br, Zn/Cl, lead-acid, Ni/Fe, and Ni/Cd technologies from a variety of battery manufacturers. Highlights of these evaluations are given below.

1. Na/S Technology

Performance and lifetime characterization testing was completed on four Na/S LL cells, five EV cells, and an EV battery (87 cells) fabricated by Ford Aerospace & Communication Corp. (FACC).

Testing of the four LL cells was initiated in 1984 and terminated in 1986. Three of the four LL cells completed 1241 to 1366 cycles, equivalent to about 5 years service in a utility application of 250 cycles/year. The fourth cell completed 659 cycles. One cell (1350 cycles) had 105% of rated capacity when testing was terminated. The test results indicated that this technology is capable of efficient electrical storage but still requires R&D in design and materials to improve reliability sufficiently that this technology would be of economic interest for utility application. Of particular concern for Na/S cells is their potential for failure caused by inadvertent cooling and fracture of the solid electrolyte when the molten electrodes solidify and their sensitivity to slight overdischarge.

Testing of the five EV cells was initiated in 1985. Of the five, four were still on test in 1986, and two were operational with 96% of rated capacity

when testing was terminated in November 1986. The EV cells accrued up to 560 cycles during performance and life evaluations, and simulated driving profile tests indicated that a Na/S battery for an advanced passenger vehicle (the IETV-1 design) made up of these cells would power this vehicle for a range of 240 to 248 miles (384-397 km) following the SAE J227a/D driving cycle. The results of this technology evaluation demonstrated that the EV cells from FACC yield very long vehicle range but have the same reliability constraints as the LL cells.

A sub-battery for the EV application, previously tested by Ford Research and made up of 87 FACC Na/S cells, was tested at the A&D Laboratory. Results of these tests indicated that one of the cell failure modes presented an additional problem with regard to the vehicle design. It was discovered that a modification of the charge/discharge control algorithm or battery instrumentation would be needed to assure proper battery charge/discharge with partial cell failure. A cell can exhibit a partial failure that makes it appear as a good cell on charge and a failed cell on discharge. This complicates the ability to predict the number of failed cells and, hence, the ability to determine the necessary charge and discharge limits.

2. Zn/Br Technology

Testing of a 124-cell (30-kWh) Zn/Br EV battery from Exxon was initiated in 1985. The experience gained has confirmed that battery performance is near the state of the art for Ni/Fe technology, with a specific energy of 45 Wh/kg at a 3-h discharge rate. However, the present design has several areas where significant improvement could be made. The system reliability is low primarily because (1) electrolyte leaks cause corrosion of the electrical controls and instruments in the area of the leaks, and (2) motor repair for the electrolyte pump is required after each 60 h of pump operation. In addition, the specific energy of the battery appears to be somewhat power limited above about 25 W/kg (see Fig. I-5). This may be a limitation due to catholyte pump capacity or other flow design problems. Since the catholyte pump is operating at its maximum capacity, investigation of this problem is hampered.

3. Zn/Cl Technology

Testing was completed on a 50-kWh Zn/Cl LL battery fabricated by Energy Development Associates (EDA). The final testing provided two principal results: (1) an additional 10% capacity could be achieved from the same battery configuration by adding 10% more electrolyte and charging to a 10% higher value, and (2) the battery maintained its voltage by periodically pulsing the electrolyte pumps, thereby showing its potential usefulness in supplying power for utilities on short notice.

4. Advanced Lead-Acid Technology

Evaluation was completed on the advanced 3100-Ah lead-acid LL technology developed by Exide Management and Technology Co. under subcontract to CMT. The objective of this program was to develop and test low-cost cells with a battery life of 4000 cycles to 80% depth-of-discharge. Two three-cell and one six-cell module were cycled to 80% depth-of-discharge at 50°C and 60°C from April 1982 to 1986. The results of the testing indicated that this

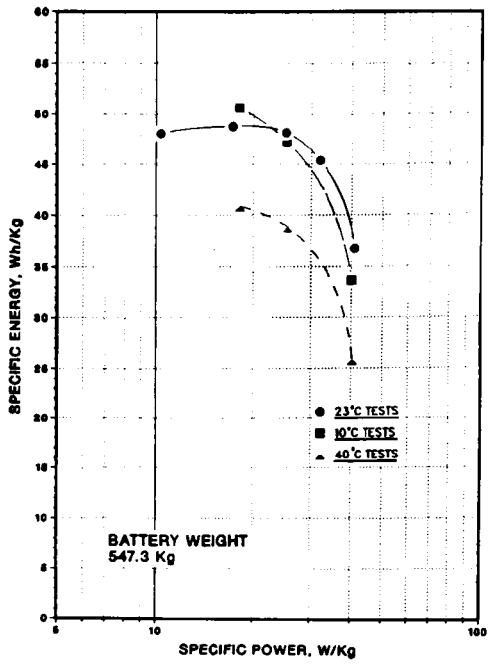

Fig. I-5.

Ragone Plot for 30-kWh Zn/Br Battery of Exxon

technology should provide adequate life to make the use of the lead-acid LL cell economic on a utility grid. In fact, Southern California Edison is designing and installing a 10-MW (40-MWh) plant based on this technology. In the CMT testing, these LL cells achieved over 1000 cycles at 60°C (equivalent to over 3240 cycles at 25°C) and 2300 cycles at 50°C (equivalent to over 6400 cycles at 25°C). Although all modules had over 100% of rated capacity when testing was stopped, two of the plastic cases on the cells in one of the 60°C-tested modules had failed. This temperature-related failure mode is not considered a problem since other case materials are available or operation can be restricted to temperatures where this failure mode is not significant.

The first of a series of advanced lead-acid flow-through EV cells from Johnson Controls (see Sec. I.D.1) was evaluated. This cell was subjected to 26 charge/discharge cycles made up of 80% and 100% depth-of-discharge cycles under a simulated driving profile (a simplified version of the Federal Urban Driving Schedule for a van) as well as constant current cycles. The capacity fell from 173 Ah and 337 Wh to 133 Ah and 259 Wh. The range under the driving profile to 100% discharge was determined to be 62 miles (100 km). The results of this cell evaluation will be used as a performance baseline for comparison of later advanced lead-acid cells.

5. Advanced Ni/Fe Technology

Nickel/iron EV modules from the Societe des Accumulateurs Fixe et de Traction (SAFT), Eagle-Picher Industries (EPI), and the Dual Shaft Electric Propulsion (DSEP) program of Eaton Corp./EPI were evaluated to obtain the performance and life characteristics of this technology. The specific energy as a function of specific power and the peak power output of the different Ni/Fe technologies are plotted in Figs. I-6 and -7. The life of two five-cell modules

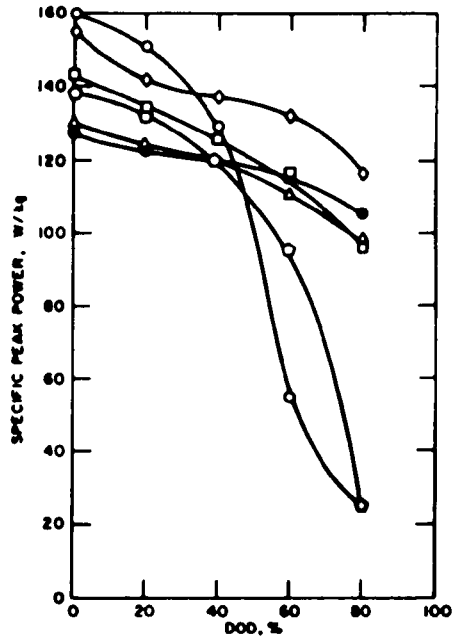

Fig. I-6.

Specific Peak Power as Function of Depth-of-Discharge (DOD) for Ni/Fe and Ni/Cd Battery Technologies

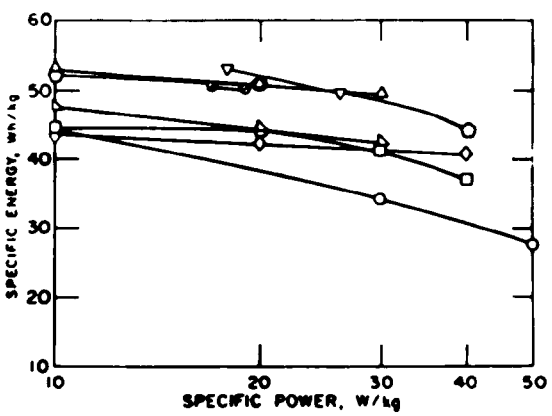

▽ EPI(Ni/Fe) 1986 TECHNOLOGY EPO5FN30
△ EPI(Ni/Fe) 1985 TECHNOLOGY EPO5FN27
○ SAFT(Ni/Fe) 1985 TECHNOLOGY STO5FN01-FN02
⊕ EPI(Ni/Fe) 1986 TECHNOLOGY EPO5FN29
◺ EPI(Ni/Fe) 1984 TECHNOLOGY
□ ERC(Ni/Cd) 1985 TECHNOLOGY ERO5CN01-CN02
◇ EATON/EPI/DSEP(Ni/Fe) 1986 TECHNOLOGY
○ ERC(Ni/Cd) 1986 TECHNOLOGY ERO5CN06-CN07

Fig. I-7.

Ragone Plot for Ni/Fe and Ni/Cd Battery Technologies

(210 Ah) from SAFT, operated at the 120-A rate to 80% depth-of-discharge, was 238 cycles before the capacity degraded to 75% (of rated). The modules have not yet received a post-test analysis to determine the reason for this premature capacity degradation. The lifetime test of the EPI and Eaton/EPI/DSEP technology has not been completed.

6. Advanced Ni/Cd Technology

An advanced Ni/Cd module has been under development by Energy Research Corp. (ERC) since March 1985. Advancements are being sought to improve performance and reduce costs of batteries built with this technology. The R&D effort is focused on using low-cost polymer-bonded electrodes and optimizing the design for vehicle use. Electric-vehicle modules based on 1985 and 1986 technologies have been evaluated in performance characterization tests in the A&D Laboratory. The test results indicate that the specific energy of this technology at a given specific power is comparable to the lower range of the Ni/Fe technology (see Fig. I-6); however, for vehicular application, the range for a vehicle powered by Ni/Cd technology may be limited by the available acceleration (peak power) at high depths-of-discharge (see Fig. I-7). In addition, lack of cell integrity, as exhibited by electrolyte seepage at cell-top joints, became evident early in cycle life on both the 1985 and 1986 technology, indicating that hydrogen leakage may be a problem.

F. *Post-Test Analyses of Battery Cells*

The Division maintains specialized facilities for the examination of aqueous and high-temperature battery cells. These examinations serve to identify existing and potential failure mechanisms, to assess the reliability of hardware components, and to characterize changes in electrode morphology as a function of a cell's operational history. Analysis of the cell data provides a measure of the technical progress made by battery developers and an indication of needed design and/or material changes.

1. Na/S Cells

This project supports DOE's contracts for the development of sodium/β"-alumina/sulfur cells. In 1986, we concluded our studies of Na/S cells built by FACC. Of the nine cells examined, three were EV cells from the ETX-1 sub-battery, and the rest were tested individually.

a. Cells from ETX Sub-Battery

The ETX-1 sub-battery was initially composed of four strings of 29 cells. The fracture of a single electrolyte tube during cool down of the sub-battery prior to its shipment to CMT for testing was responsible for loss of voltage from one of the four strings and subsequent string failure. The well-charged sub-battery had cooled to about 160°C when the electrolyte fractured in the fifth cell in the string. Different sodium polysulfides then formed from the still-molten sodium and sulfur. As shown in Fig. I-8, most of this reaction occurred in the lower half of the cell where the fracture originated and included the formation of solid sodium monosulfide and sodium disulfide. Over time, the continuing formation of solid polysulfides caused expansion of the cell container until it ruptured longitudinally near the base. The heat of reaction was sufficient to maintain higher sodium polysulfides in the molten state. The higher

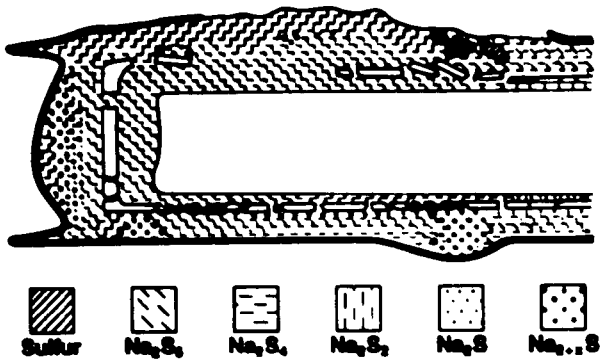

Fig. I-8.

Schematic of Lower Half of the Sodium/Sulfur Cell Responsible for String Failure in the ETX-1 Module. (The different shade patterns indicate the location of various positive electrode phases that formed subsequent to failure of the electrolyte.)

polysulfides seeped out of this rupture and contacted the 25th cell in this two-row string. This pathway formed about four hours after the failure of the fifth cell and had sufficient conductivity to induce a partial discharge of the 25th cell and the intervening 19 cells in the string.

Further studies of cells in the affected string indicated that all cells but one are probably recoverable. The affected cells did have low cold voltages (0.2 to 0.7 V) but were not discharged significantly. Deep discharge was prevented because the sodium polysulfide film normally present on electrolyte tubes (even in charged cells) had solidified during the reduced module temperature. The unrecoverable cell in the string underwent electrolyte failure during this time period. The uncontrolled formation of solid polysulfides in this cell breached the container along the end-cap weld seam. Leakage was minimal and did not propagate the short circuit.

Two other failures, which occurred elsewhere in the sub-battery and independently from this event, demonstrated that electrolyte fractures do not necessarily lead to cell swelling. This condition can be prevented by design improvements that limit the quantity of sodium supplied to any one section of a cell after a fracture has occurred.

b. Individual Cells

Examinations were conducted on three LL cells from FACC, including a cell that operated for more than five years at rated capacity. Information obtained from these cells further enhanced our understanding of (1) the compositional gradients that develop in the sulfur electrode during cycling and (2) the cumulative effects of hardware corrosion on the morphology of this electrode. In addition, these examinations established that the protective chromium plating used in the present cell design is capable of providing a container lifetime of more than five years.

Two EV cells revealed a previously unseen cause for cell failure. Both cells experienced an inadvertent overdischarge and failed to regain their former capacities. Analysis of the positive electrodes revealed high concentrations of iron near the electrolytes. The probable source of iron was the safety tube on the anode side of the electrolyte. The iron was transferred while sodium was depleted from the anode during the overdischarge. During the subsequent cycles aimed at recovering the capacity, the iron adversely affected the charging kinetics at the interface between the electrolyte and the positive electrode.

An examination was also conducted on one cell designed for baseload power applications on orbiting satellites. The satellite cell failed during heat-up because of an electrical short circuit. A defective aluminum compression seal permitted sodium to leak over the external surface of an alumina insulating collar and into contact with the container.

2. Aqueous Batteries

In 1986, we also completed examinations of eight lead-acid modules and one Ni/Fe module after testing at the A&D Laboratory. Most of this work was funded by EPRI and DOE. A related activity, measurement of hydride generation from lead-acid modules for LL applications, was also conducted under EPRI sponsorship.

a. Capacity Decline in Lead-Acid Modules

We examined seven lead-acid EV modules from Johnson Controls (JCI EV-2300). Three of these modules were expressly tested to study the causes of capacity decline, with operation being terminated when capacity fell below 95, 85, and 75% of rated capacity. The other JCI EV-2300 modules were operated as part of a 12-module battery tested under a driving profile.

The post-test findings identified key correlations among pore volume, grid corrosion, and capacity. As shown in Fig. I-9, a decline of 0.01 cm^3/g in positive-electrode pore volume accounted for a ~14% loss in capacity. (It should be noted, however, that nonlinear curves can also be fitted to this porosimetry data.) A decrease in pore volume implies a loss in capacity

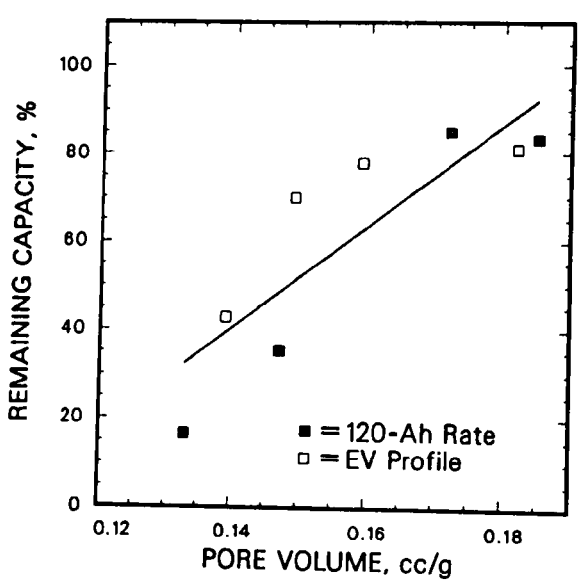

Fig. I-9.

Relationship Between Positive-Electrode Pore Volume and Remaining Cell Capacity for JCI EV-2300 Modules. (The open squares are for JCI EV-2300 modules from an earlier EPRI sponsored study.[4])

[4]C. C. Christianson et al., *Testing and Development of Electric Vehicle Batteries for EPRI Electric Transportation Program: Technical Report for November 1982 Through December 1984*, Argonne National Laboratory Report ANL/OEPM-85-4 (November 1985).

because of concentration polarization of electrolyte within the pores. A relationship between positive-grid corrosion and capacity was also established. As Fig. I-10 illustrates, the remaining cross-sectional area of the grid wires was less in cells with lower capacities. In addition to capacity loss caused by increased IR losses within the positive electrodes, grid corrosion could also contribute to reduced pore volume because the formation of the more-voluminous corrosion scale would occur at the expense of pore volume in a well-contained cell.

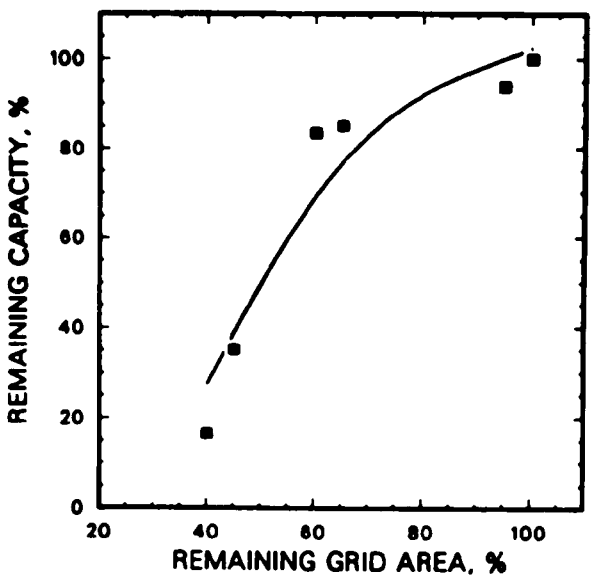

Fig. I-10.

Relationship Between Grid Corrosion and Remaining Cell Capacity for JCI EV-2300 Modules

b. Failure of Ni/Fe Module

We analyzed a ten-cell Ni/Fe module (160 Ah) fabricated by Eagle-Picher to determine the causes for its failure to deliver rated capacity after 1050 cycles of operation. Reference electrode measurements determined that the iron electrodes were limiting performance. Studies on three cells from the module revealed that part of the performance loss was strictly related to increased electrical resistivity. Contact between the current collector and active material mass had deteriorated and the electrodes were severely blistered. Contamination of the nickel electrodes with iron also affected performance. Iron-rich particulate migrated through the porous separator and became incorporated into the nickel electrode as a mixed oxide compound. Self-discharge of the cells occurred because the iron remaining in the separator formed a conductive particulate bridge.

c. Hydride Generation in Lead-Acid Modules

The evolution of toxic hydrides from arrays of lead-acid batteries could pose a potential health hazard in future utility load-leveling facilities. To determine the severity of this potential problem, the generation rates were measured for three of the six cells in a prototypic 36-kWh module built by Exide. A specially prepared gas collection apparatus enabled us to determine the maximum and average rates for evolution of both toxic hydrides. As typified by Fig. I-11, hydride generation began once the cell voltage exceeded 2.4 V. The maximum rate for arsine occurred just above 2.5 V and consistently preceded the

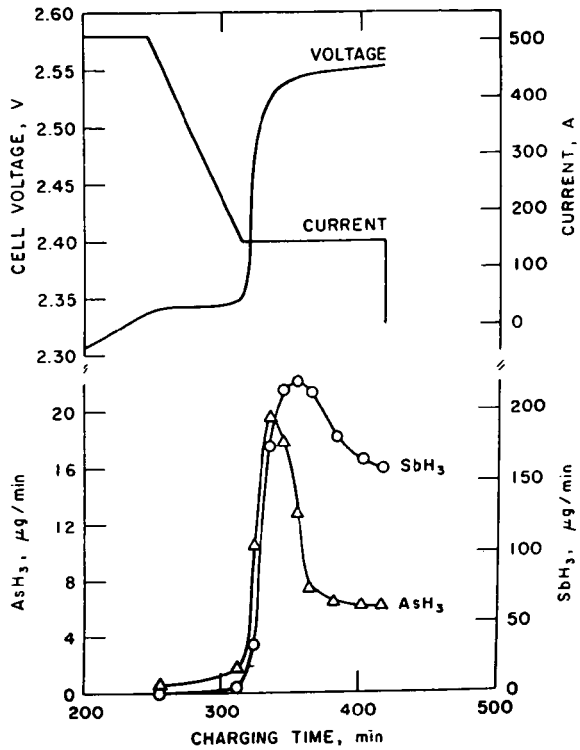

Fig. I-11.

Typical Curves of Stibine and Arsine Generation for One Cell During Charging of Exide Load-Leveling Module

peak rate for stibine for each sampled cell. Both peaks then decayed and began to approach steady-state values by the end on the charge cycle.

The average rates of hydride evolution, as determined by dividing the total quantity of arsine or stibine by the duration of the final constant current portion of the charge cycle, were 12.6 μg/min for arsine and 175 μg/min for stibine. Based on the latter rate and a 0.1 ppm exposure limit for stibine, the minimum air flow requirement (exclusive of a safety factor) is 340 L/min per cell. This air flow is over 12 times greater than the air flow required for safe ventilation of the hydrogen evolved during charging. The information from this study is providing guidance in determining ventilation and abatement requirements for the load-leveling plant being constructed by Southern California Edison.

G. *Modeling and Analyses*

To assist battery developers, we are undertaking electrochemical and thermal modeling of battery systems and statistical analysis of test results.

1. Electrochemical Modeling

A mathematical model was developed for Na/S cells with conductive glass electrolyte. The model calculates current, potential, composition, and temperature distributions based on the cell geometry, sulfur polarization, and the resistances of the current collector, glass electrolyte, graphite matrix, and polysulfide melt. The model was used to evaluate various cell design alternatives and to predict energy and power capabilities of the cell under different design and operating conditions.

Model calculations for the power of the Na/S cell as a function of glass thickness are plotted in Fig. I-12. The results indicate that the specific power of the cell is strongly affected by the thickness of the glass electrolyte, and that a cell with 0.1-mm-thick glass will achieve a peak power of ~900 W/kg at the 6.2-A discharge rate. This information is useful in selecting cell designs to meet the energy and power requirements for various applications. The model can also be used to study the degradation mechanism of the battery under various operating conditions. In the future, the electrochemical model will be extended to include other electrolyte materials and to compare the performance of Na/S batteries made by different battery developers. Other electrochemical models will also be developed for advanced battery systems such as tubular Li/FeS_2 cells.

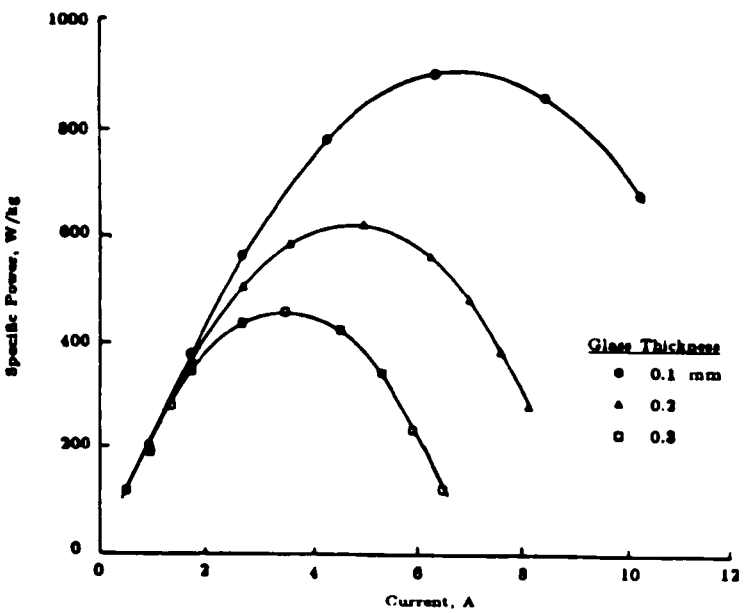

Fig. I-12. Calculations of Specific Power for Na/S Cell with Glass Electrolyte of Varying Thickness

2. Thermal Modeling

The three-dimensional battery thermal model developed at ANL[5] was transferred to several industrial users in 1986. The model was also used at CMT to evaluate the thermal behavior of an advanced lead-acid module built by the Jet Propulsion Laboratory (JPL) for EPRI. It was found that this advanced module (thin-electrode horizontal plates) is capable of delivering ~30% higher specific energy than the Gould GC2-EV200 lead-acid battery (conventional plates), while having about the same degree of temperature rise. The maximum temperature rise of the JPL battery under the SAE J227a/C driving profile was found to be 15.5°C for a Volkswagen van and 9.5°C for a Bedford van (a larger

[5]J. Lee, K. W. Choi, N. P. Yao, and C. C. Christianson, J. Electrochem. Soc. 133, 1286-1291 (1986).

vehicle with lower specific-power demand). Therefore, one would not anticipate any excessive heating problem for the JPL battery in van applications.

3. Statistical Analysis of Test Data

Multiple regression analysis was performed using the capacity and peak power data obtained from six EV-2300 lead-acid modules (six-cells each) tested earlier in the A&D Laboratory. The purpose of the analysis was to verify the statistical significance of the test results and to separate and quantify the effects of various operating parameters on the performance variation and degradation of the modules.

The results of the analysis[6] showed that the most important factors causing performance variation were the levels of peak power demand by the vehicle and the cell location within the six-cell module. The effects of charge methods and rest times were found to be small. As the level of peak power demand was increased, the degradation of battery capacity and specific peak power was accelerated. For example, the rate of capacity degradation increased from 0.230 to 0.317 Ah/cycle as the peak power level of the driving profile (SAE J227a/C for Volkswagen van) was increased from 35 to 57 W/kg. For the same change in the level of power demand, the degradation rate in specific peak power of the battery increased from 0.112 to 0.191 W/kg per cycle.

Analysis of the test data also indicated that the two end cells in each six-cell module had consistently higher rate of capacity degradation than the middle four cells. On average, the difference in capacity degradation rates between middle cells and end cells was about 0.11 Ah/cycle. In most cases, the module capacities were eventually limited by these end cells. The causes of the poorer performance of the end cells are being further investigated.

H. *Polysulfide Containment Materials*

During the past 2-3 years, we have examined the corrosion behavior of six metals (Al, Cr, Fe, Mo, Ni, and Ti), ten aluminum-based alloys, and sixteen iron- and/or nickel-based alloys in sulfur and sodium polysulfides at 350°C. The objectives of these studies were to obtain a basic understanding of the corrosion reactions and to develop an alloy for use as a positive current collector/container in the Na/S cell. Work on this project has now been completed. It was concluded that the continued development of new alloys will probably not result in a material of sufficiently low cost, low density, and low corrosion rate to be useful as a positive current collector/container material for the Na/S cell. The summary below presents the principal findings of this project.

In general, a remarkable difference was found in the corrosion behavior of the metals and alloys in pure sulfur as opposed to a polysulfide composition of Na_2S_3. For most of the metals and alloys studied, corrosion rates were higher in the polysulfide than in sulfur. Chromium and nickel were the only exceptions,

---

[6]J. Lee, A. F. Tummillo, J. F. Miller, F. Hornstra, and C. C. Christianson, "Capacity and Peak Power Degradation of Lead-Acid Battery under Simulated EV Operations," Proc. of Eighth Int. Electric Vehicle Symp., Washington, DC, October 20-23, 1986, pp. 151-156 (November 1986).

and only with chromium was the corrosion rate markedly lower in the Na_2S_3 than in the sulfur. Corrosion penetrations of the metals and alloys after up to 2500 h of exposure varied by as much as two orders of magnitude between sulfur and Na_2S_3, as indicated in Fig. I-13.

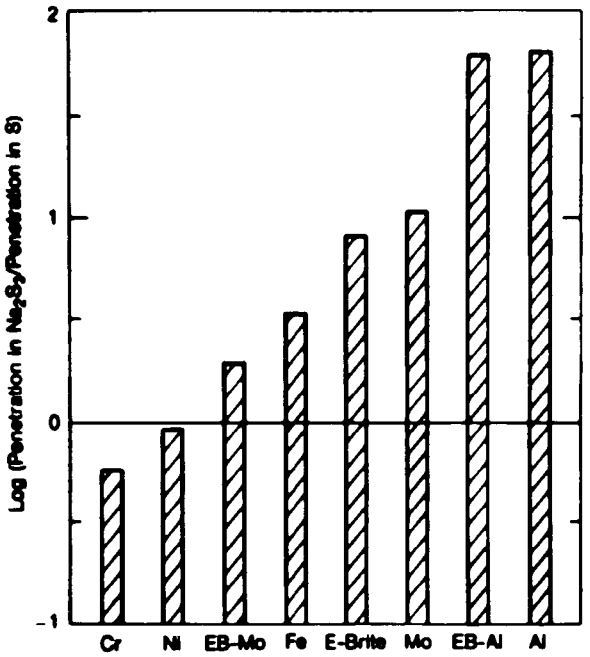

Fig. I-13.

Comparison of the Relative Corrosion Penetration in Sulfur and Na_2S_3 at 350°C for Various Metal Alloys. Corrosion times were 25 h for the Ni and Fe, 900 h for the Al, and 2500 h for the others. EB-Mo = E-Brite + 3 wt % Mo; EB-Al = E-Brite + 3 wt % Al.

The principal cause for the higher corrosion rates in Na_2S_3 is related to the corrosion scale composition and morphology. The high basicity of the Na_2S_3 results in the formation of ternary sodium metal sulfides, which are partially soluble in the corrosion medium; for example, iron forms Na_3FeS_3, chromium forms $NaCrS_2$, and aluminum forms several different phases depending on the polysulfide composition (Table I-1). Even when a ternary sulfide phase is not formed, the binary metal sulfides often exhibit sufficient solubility in the Na_2S_3 to modify the scale morphology; for example, NiS_2 forms with nickel-based alloys of high chromium content, and MgS forms with aluminum-magnesium alloys.

The principal findings for the various metals and alloys can be summarized as follows. Molybdenum has excellent corrosion resistance to Na_2S_3, with corrosion rates being almost zero after the first 100 h of exposure. However, it is not effective as an alloying element in arresting the rapid corrosion observed for iron and nickel. Chromium corrodes relatively slowly and appears useful as a coating material for Na/S cells with lifetimes of less than five years. It is moderately successful in reducing corrosion rates when used as the primary alloying element in iron- and nickel-based alloys. Chromium concentrations in the alloys need to be about 25 wt % because, although a higher chromium concentration decreases the corrosion rate in Na_2S_3, it increases the corrosion rate in sulfur. With these chromium-containing alloys, molybdenum and yttrium are useful as secondary alloying elements for improving the corrosion scale morphology (by reducing spalling) and for reducing the corrosion rates in Na_2S_3. Aluminum corrodes relatively quickly in Na_2S_3. Magnesium alloyed to aluminum, however, reduces the corrosion rate in Na_2S_3 and, at a 9.6 wt % Mg concentration, the

Table I-1. Corrosion Product Phases Formed when Aluminum Is Corroded in Various Polysulfides

Polysulfide Stoichiometry	Temperature, °C	Corrosion Product
S	350	Al_2S_3
Na_2S_5	350	D[a]
Na_2S_4	350	$NaAlS_2$
Na_2S_3	350	α-Na_3AlS_3[b]
Na_2S_3	550	β-Na_3AlS_3[b]
Na_2S_2	550	Na_5AlS_4[b]

[a]Unidentified phase.

[b]Previously unknown compounds.

corrosion rate becomes effectively zero after 1000 h of exposure. However, when subjected to electrochemical polarization in the form of a continuous constant-current square wave ($\pm$ 10 mA/cm^2 with pulse lengths of 5 h), 0.05-cm thick coupon of the same alloy is completely corroded within 350 h.

In conclusion, based solely on consideration of corrosion resistance, molybdenum is the only material that can be recommended as a positive current collector/container for the Na/S cell. If a metal or alloy were to be used as a substrate for a corrosion-resistant coating, then the best metal or alloy to provide adequate protection against coating defects would be a stainless steel with a composition near to Fe-26Cr-3Mo, such as Ferralium 255.

Promising materials to investigate as candidate current collector/container materials are composites based on known corrosion-resistant inorganics. Some of the new fiber-reinforced ceramics and glasses might be modified to induce electronic conductivity but still retain adequate mechanical integrity and ease of fabrication so that they would be superior to present positive electrode containers for the Na/S cell.

II. ADVANCED FUEL CELL DEVELOPMENT

Fuel cell power plants are one of the more-attractive energy technologies under development. Argonne is predominant among the national laboratories in advanced fuel cell technology, which includes both molten carbonate (MCFC) and solid oxide (SOFC) fuel cells. The ANL fuel cell programs are led and mostly executed by CMT, but there are other important contributions, primarily from the Materials and Components Technology (MCT) Division, but also from the Engineering (ENG) and the Energy and Environmental Systems (EES) Divisions. The ANL effort provides the DOE programs in advanced fuel cell technology with research, testing, modeling, systems analysis, and technical management assistance; however, since the primary development effort of the DOE program is by industrial contractors, ANL does not carry out design and development of stacks of fuel cells for DOE.

For the Department of Defense, ANL is developing a high-power fuel cell--the monolithic oxide fuel cell. The monolith concept originated at CMT and is being developed exclusively by ANL. The most difficult of the many challenges in this effort is simply fabrication of the necessary ceramic structure. There is considerable industrial interest; joint development programs with industry are expected in the coming year.

A. *Molten Carbonate Cell Development*

Present-day MCFCs consist of a porous nickel alloy anode, a porous metal oxide cathode, an electrolyte structure separating the anode and cathode, and appropriate metal separator sheets. A schematic of a single cell and its electrochemical reactions is shown in Fig. II-1. Separator sheets isolate reactant gases in adjacent cells of a stack, electronically join these cells, and bear upon the electrolyte structure to form a "wet" seal that separates the cell interior from the surroundings. The electrolyte structure is a composite of discrete submicron $LiAlO_2$ particles and a mixture of lithium and potassium carbonates that is liquid at the cell operating temperature of about 650°C. In a power plant, many cells (50-1000) with parallel gas flows will be assembled in a series electrical connection to form a stack. Each cell adds about 0.8 V to the stack voltage at a current density of 200 mA/cm^2; tens or hundreds of stacks will be used, depending on the plant size. In practical cell stacks, CO_2 for the cathode will probably be obtained from the anode exhaust. An economic advantage exists for large plants to run at pressures of 6-10 atm.

1. Research on Cathode Materials

In earlier work,[1] we found that the NiO cathode undergoes continuous migration of material toward the anode, which limits cell lifetime. We, therefore, searched for stable ceramic materials that met known requirements for cathode materials. The materials $LiFeO_2$ and Li_2MnO_3 were chosen from a large number of compounds that were identified as being thermodynamically stable in the

[1] L. Burris et al., *Chemical Engineering Division Annual Technical Report, 1980*, Argonne National Laboratory report ANL-81-38, p. 64 (1981).

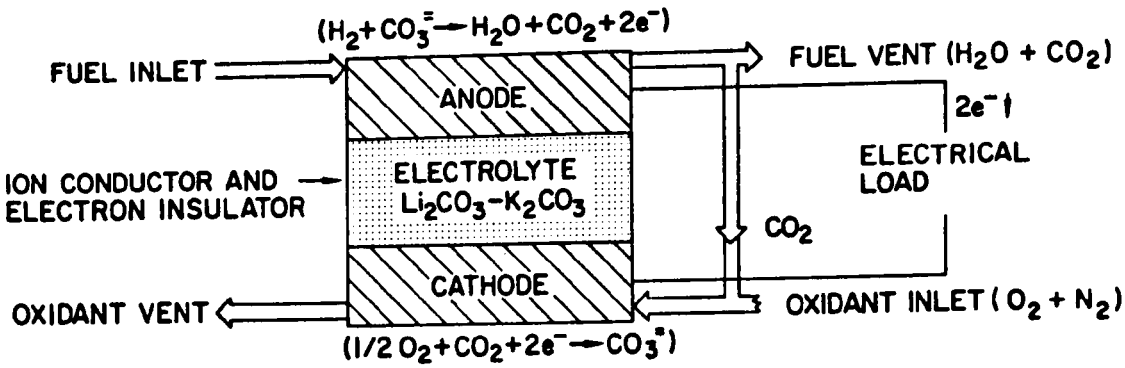

Fig. II-1. Schematic of Molten Carbonate Fuel Cell

cathode environment. The undoped forms were extensively tested and found to meet the requirements of low solubility, non-migration, and stability.[2,3] Doping has been done to enhance the conductivity of these two materials.

The conductivities for $LiFeO_2$ and Li_2MnO_3 are dependent on stoichiometry and, therefore, on cell environment. In typical cell environments, the undoped materials have resistivities of from a few hundred to about one thousand ohm-centimeters. Resistivities as low as ~10 Ω-cm can be achieved with doped materials. As yet, the precise requirement for cathode use has not been clearly defined because of the incomplete understanding of cathode operation.

The material development effort at CMT is continuing, but priority is now being placed on developing the complex cathode microstructure required for in-cell use. In addition, cell testing is being done to examine the relationship between material properties and microstructure in determining cell performance, as well as to improve our understanding of cathode-material behavior.

a. Testing of Doped Materials

Our earlier studies indicated that $LiFeO_2$ in the undoped state is a good conductor (~3 Ω-cm resistivity at 650°C) when synthesized in air but is about two orders of magnitude more resistive when synthesized in higher partial

[2]J. L. Smith, T. D. Kaun, N. Q. Minh, and R. D. Pierce, "Stable Materials for Molten Carbonate Fuel Cell Cathodes," 1983 National Fuel Cell Seminar Abstracts, Orlando, FL, November 13-16, 1983, p. 65 (1983).

[3]G. H. Kucera, N. Q. Minh, J. L. Smith, and F. C. Mrazek, "Molten Carbonate Fuel Cell Cathode Development," 1985 National Fuel Cell Seminar Abstracts, Tucson, AZ, May 19-22, 1985, p. 158 (1985).

pressures of CO_2.[4] The objective of doping this material was to reduce the resistivity to the levels of air-prepared material and to eliminate the CO_2 sensitivity.

We have doped $LiFeO_2$ and then evaluated the resultant materials in laboratory tests. Use of the dopants manganese, copper, and cobalt can produce $LiFeO_2$ with potentially useful resistivity. The manganese-doped material has been the most extensively tested. Samples of this material were prepared by three different procedures for mixing the dopant and $LiFeO_2$ (co-precipitation of hydroxides, co-precipitation of carbonates, and a gel process[5]). Under realistic cell operating conditions (10 atm), the optimum dopant concentration resulted in a resistivity of ~25 Ω-cm at 650°C. There was excellent correlation between dopant level and resistivity (Fig. II-2) and lattice parameter (Fig. II-3). The excellent agreement also indicates that all three procedures are effective for preparing the doped material. The material is a p-type conductor in cathode conditions, as indicated by its conductivity behavior and by Seebeck measurements. Any simple substitution of an Mn^{3+} or Mn^{4+} would result in an n-type conductor; thus it is probable that a more-complex defect structure in the $LiFeO_2$ material is occurring (for example, formation of oxygen interstitials).

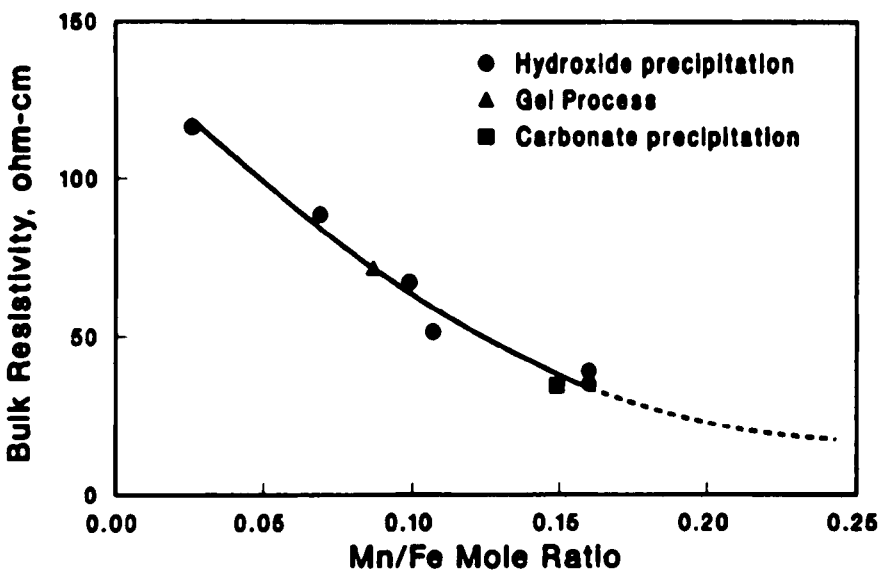

Fig. II-2. Resistivity of Mn-Doped $LiFeO_2$ as Function of Dopant Level

[4]N. Q. Minh, G. H. Kucera, and J. L. Smith, "The Influence of Preparation Conditions on Electronic Resistivity of $LiFeO_2$ Synthesized in Molten Carbonates," Proc. of Fifth Int. Symp. on Molten Salts, Las Vegas, NV, October 13-18, 1985, Vol. 86-1, The Electrochemical Society, pp. 597-603 (1986).

[5]Carried out by Harlan Anderson, University of Missouri.

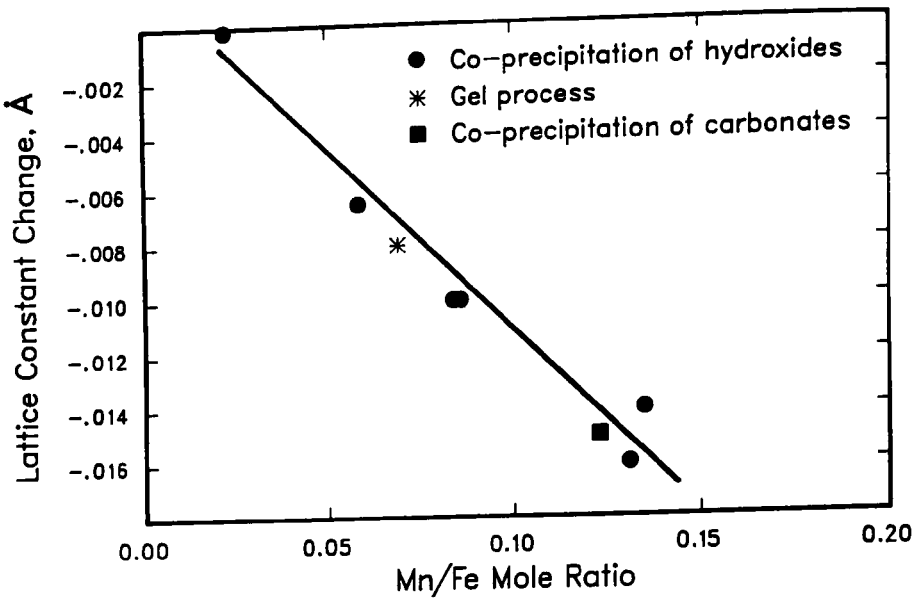

Fig. II-3. Lattice Constant of Mn-Doped $LiFeO_2$ as Function of Dopant Level

When doped with copper, $LiFeO_2$ yielded a resistivity of ~10 Ω-cm under high partial pressures of CO_2. This conductivity should be adequate for cell testing. Of concern are the migration and subsequent precipitation of copper; these will be studied further through cell testing. The material is a p-type conductor and, therefore, improves in conductivity with increasing partial pressures of O_2.

Cobalt-doped $LiFeO_2$ had resistivity in the 10 Ω-cm range at 650°C (Fig. II-4). Although the optimum dopant concentration has not been determined for this material, up to the 0.125 Co/Fe ratio in Fig. II-4, the resistivity is still improving. It is thus probable that further improvements will be attained. (The datum at the far right is for a sample with two phases present. This amount of cobalt is in excess of that which can be accommodated by the $LiFeO_2$ lattice.)

In the undoped state, Li_2MnO_3 is a poorer conductor in realistic cell environments than $LiFeO_2$. It is an n-type rather than a p-type conductor and has very low solubility, and cell tests suggest that it has no migration tendencies in the cell environment. The doping of this material has received less attention than that of $LiFeO_2$ but has resulted in resistivities of ~20 Ω-cm in realistic cell environments. Further investigation of doped Li_2MnO_3 is planned.

b. Cell Testing

We have now entered a second phase of the MCFC program, directed toward fabricating cathode materials, then testing them in cells.

The cell testing began with 25-cm^2 boiler-plate cells having nickel anodes. A problem in cell testing was in achieving an acceptable cathode microstructure. Our analyses with a model developed by Physical Sciences, Inc.,

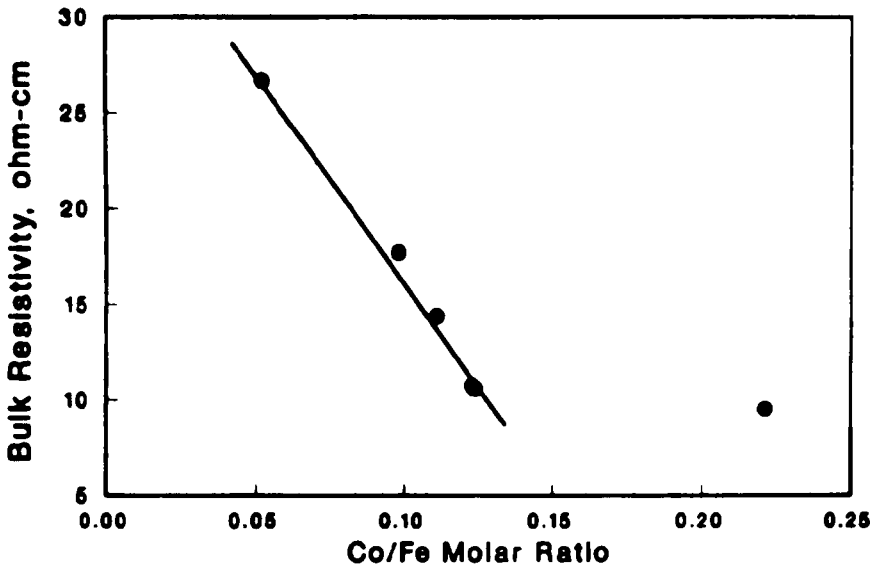

Fig. II-4. Resistivity of Cobalt-Doped $LiFeO_2$ Prepared under High CO_2 Pressure and Tested in Air at 650°C

indicated that resistivities of alternative cathode materials of up to about 20 Ω-cm should give comparable performance to nickel-oxide cathodes (far right side of solid line in Fig. II-5), if care is taken to achieve the correct microstructure (dotted line in Fig. II-5).

The particles from which the cathode is to be fabricated must be of submicron size to obtain adequate catalytic surface area and to form agglomerates flooded with molten electrolyte. The agglomerate size is of importance because the reactants must diffuse to the reaction site through the liquid phase in the agglomerate. The path length can be minimized by keeping the agglomerate size small: 3-8 μm typical diameter. There must also be the usual large gas passages, ~10 μm diameter, between agglomerates; this requirement is determined by the pore characteristics of other components. Finally, a cathode porosity of ~45-55% is being sought.

Spherical agglomerates alone cannot be used to achieve the desired structure because it is impossible to obtain the combination of small agglomerates and large pores. Consequently, pores are being made using a variety of pore formers, and agglomerates are being made in nonspherical geometries.

Pore formers, such as starches, cellulose, flours, etc., generally do not produce the desired interconnected pores without a very high porosity. With fibrous pore formers, conventional fabrication techniques do not readily yield the desired fiber orientation normal to the surface of the thin planar body. The fibers tend to lie along the fluid's streamlines in a tape casting or similar process and, therefore, will not penetrate the cathode-material face in sufficient numbers.

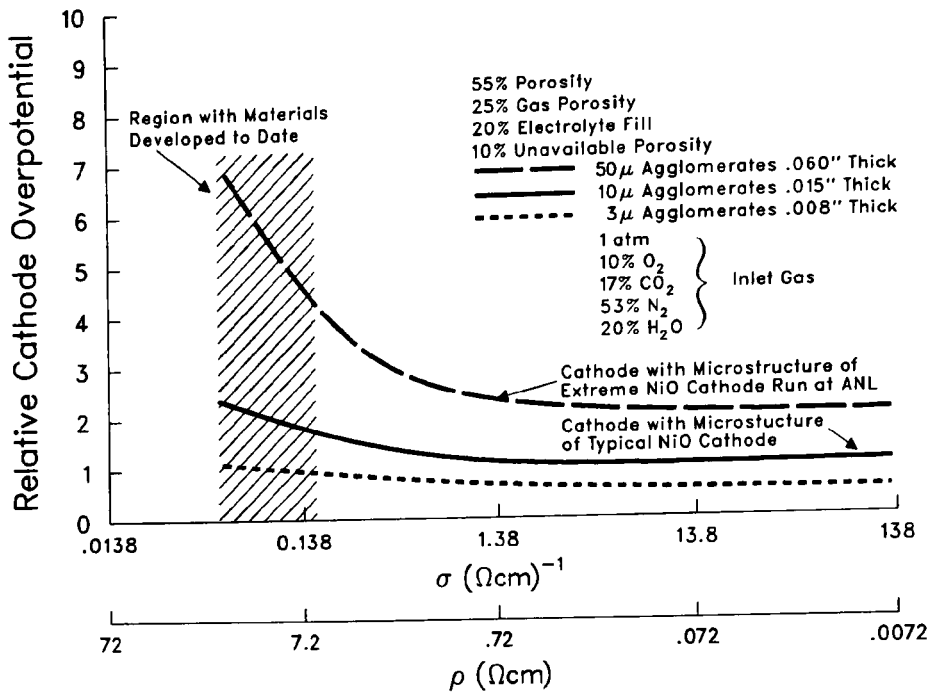

Fig. II-5. Calculated Relative Cathode Overpotential as Function of Resistivity (ρ), Conductivity (σ), and Microstructure. (The shaded region is a conservative estimate of the resistivity range attainable by alternative cathode materials to NiO at their present stage of development.)

We have developed a process to provide holes of 10-15 μm dia through the plane of such a cathode, but the number density is such that lateral channels will be required for sufficient gas access. These may best be formed by fabricating the structure with preformed agglomerates. The agglomerates can be formed by several methods. One is to fill a foam or other porous organic body with a ceramic slip, burn off the organics, and sinter. Depending on the degree of fill, this procedure can result in a replica of the foam (Fig. II-6) or of the voids in the foam. This then can be crushed to obtain nonspherical agglomerates. In a similar process, organic fibers can be mixed with a ceramic slurry and sintered. This process will yield small ceramic tubes (Fig. II-7), which can be crushed to provide the agglomerates. Many other organics could be used to produce such agglomerates.

The cell-testing effort will be designed to acquire some of the much-needed information on cathode behavior. By running cells with variables of cathode microstructure and conductivity and using cathode models to interpret the test results, we expect to gain insight into cathode behavior.

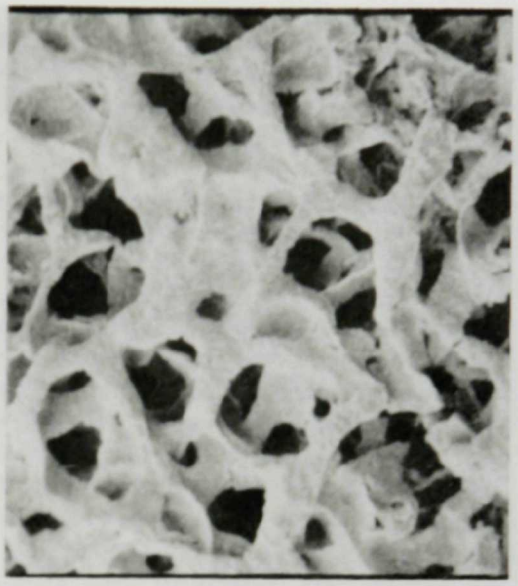

Fig. II-6.

Structure of $LiFeO_2$ Prepared by Impregnating Foam with Slip and Sintering

Fig. II-7.

"Tubes" Prepared by Sintering $LiFeO_2$ with Pore Formers

2. Technical Support

The Advanced Fuel Cell Program Office at CMT provides technical support to the Morgantown Energy Technology Center (METC), which has programmatic responsibility for the MCFC program for DOE. Technical support includes assistance in program planning, systems analysis, technical monitoring of the contracts, and preparation of work statements for new work. In 1986, International Fuel Cells (IFC), formerly the Power Systems Division of United Technologies Corp., continued to be a major DOE contractor for development of MCFCs. During 1986, direction of the work at Energy Research Corp. (ERC) was modified to prepare for stack fabrication and testing. Research also was sponsored by DOE at the Institute of Gas Technology (IGT) and Physical Sciences, Inc. (PSI).

The technical approach of this DOE program is to integrate the development of a fundamental understanding of fuel cell behavior with cell and stack engineering. The DOE goal is to be in a position to construct and operate a full-scale stack, capable of operation on gases from a coal-based system, with a projected life of 40,000 h in the 1990s. With ANL assistance, DOE/METC

planned and prepared Program Research Development Announcements (PRDAs), which solicited proposals for (1) base technology studies addressing areas of concern and (2) follow-on contract(s) to promote stack development efforts to meet the DOE goal.

In the past year, IFC operated a scaled-up version of the 20-cell stacks (area, 710 cm^2; power, 3 kW) they had been testing. This stack was intended to evaluate the effects on performance of scale-up of area to the size proposed for large plants (0.7 m^2). The stack, which was tested for 800 h, operated at about 30 kW and had good initial performance, but several problems affecting performance were observed later in the test. Fuel distribution seems to have been one source of difficulty; test-stand problems also resulted in subsequent lower performance. The cause of individual cell performance problems has not yet been identified by post-test examination. This stack had the same compaction of cell components as its subscale precursor, indicating that scale-up did not worsen the earlier problem of electrode compaction.

As stated in Sec. II.A.1, ANL is searching for an alternative cathode; in the meantime, however, both IFC and ERC are attempting to extend the life of NiO cathodes. To address this acid/base dissolution problem, both contractors have accepted some performance loss from the NiO cathode and lowered the nickel solubility by reducing the CO_2 partial pressure in the cathode gas. The performance loss is a result of both decreased Nernst potential and increased polarization. Another approach being examined by ERC is to make the electrolyte more basic and decrease nickel solubility by the addition of selected cations (e.g., barium) to the melt.

Energy Research Corp. is also developing cell and stack components and a reference MCFC plant design and testing cells and stacks with reforming catalysts in the anode region that convert methane to carbon monoxide and hydrogen. During this year, a 2-MW plant design was completed, and the stack and cell requirements from this design formed the focus for development efforts at ERC. A subscale (~0.1 m^2) stack of four cells is being tested and has shown good performance on simulated gases. In development work on the reformer design, ERC is striving to mitigate the effects of electrolyte transfer to that section on performance of the catalyst.

The Institute of Gas Technology has completed a study of the sulfur reactions leading to poisoning of MCFCs. This work indicated that a fuel cell operating on medium-Btu fuel gas at atmospheric pressure can tolerate about 1 ppm of total sulfur (from H_2S, COS, SO_2, etc.) without suffering any performance loss. In other work, IGT completed a study on nickel migration mechanisms in the electrolyte following cathode dissolution. Tests verified nickel migration via the electrolyte through the matrix and into the anode (IGT had substituted cobalt for the standard nickel anode). Two transport mechanisms were hypothesized. The first is slow chemical diffusion after acidic dissolution as nickel ions, and the other is Faradaic transport of nickelate ions. The IGT study also demonstrated that the rate of attrition of the cathode can be reduced by increasing the basicity of the melt.

Under a subcontract to ANL, PSI completed work to upgrade its performance model for the MCFC. This model, based on fundamental properties of a fuel cell and its components, was modified to reflect changes in components

and new information about reaction mechanisms, electrode structures, electrolyte distribution, etc. The model was verified against the best available experimental data. We are using this model to assess contractor-cell performance, perform systems studies, and plan research.

Our efforts in 1986 included preparation of statements of work for seven PRDAs for base technology studies and a PRDA for stack development and testing. We reviewed and commented on the technical segments of the proposals received by DOE in response to these PRDAs. The base technology areas covered were (1) cathode dissolution, (2) component deformation, (3) alternative electrolyte compositions, (4) corrosion, (5) electrode reaction mechanisms, (6) electrolyte wetting, and (7) sulfur-tolerant anode materials. A contract has been awarded in five of these areas. The Source Evaluation Board of DOE is completing its review of the proposals in response to the stack PRDA.

We will continue our technical monitoring of contractor efforts in 1987. This will cover the base technology contracts, interim stack development contracts, and any new stack contracts.

B. *Solid Oxide Cell Development*

The SOFC consists of a lanthanum manganite cathode, a zirconium dioxide (yttria-stabilized) electrolyte, a cermet (Ni or Co with ZrO_2) anode, and lanthanum chromite for electronic cell-to-cell interconnections. These components are all ceramic materials. At the anode, hydrogen and carbon monoxide in the fuel gas react with oxide ions from the electrolyte to form carbon dioxide and water, giving up electrons to the external circuit. At the cathode, oxygen in the air accepts electrons from the external circuit to form oxide ions, which are conducted through the electrolyte to the anode. These cells operate at temperatures of 800-1000°C. In a power plant, cells (approximately 100) will be connected in electrical series with parallel gas flows to form a module; depending on desired plant size, hundreds or thousands of modules will be used.

We are investigating a new concept for a compact solid oxide cell that promises to deliver very high power density. This concept is based on the premise that the thin solid components of oxide cells can be fabricated into compact shapes having power-to-weight ratios that are a factor of 100 higher than those of conventional fuel cells. Work on this concept began in 1983 with support from DOE. Beginning in mid-1983, support from the Defense Advanced Research Projects Agency (DARPA) made this development effort a major program.

The "monolithic fuel cell" is being developed in a joint program between the CMT and MCT Divisions. The monolithic design employs the same thin ceramic components used in other oxide fuel cells in a strong, lightweight honeycomb structure of small cells, and thus can achieve very high power per unit mass or volume. A monolithic fuel cell would convert hydrocarbon fuel to DC power at 50% efficiency, which is higher than any non-fuel-cell technologies that use this fuel.

In the monolithic concept, fuel and air are combined electrochemically in a ceramic cell at an operating temperature of 800-1000°C. Cell components are fabricated as one piece, much like a block of corrugated paperboard. Fuel

and oxidant are conducted through alternating passages in the stack, as shown in Fig. II-8. These passages are formed from thin (0.025 to 0.100 mm) layers of the active cell components: the anode, cathode, electrolyte, and the interconnection material that connects cells in electrical series (bipolar plate). The corrugations also form the gas seal at the edges of the structure. Advantage is taken of the ability to fabricate the solid electrolyte and other solid cell components into shapes that cannot be achieved in liquid electrolyte systems, for which much of the mass and volume goes into building the inert container for the liquid. Eliminating this unnecessary material gives the monolithic fuel cell a significant advantage in performance.

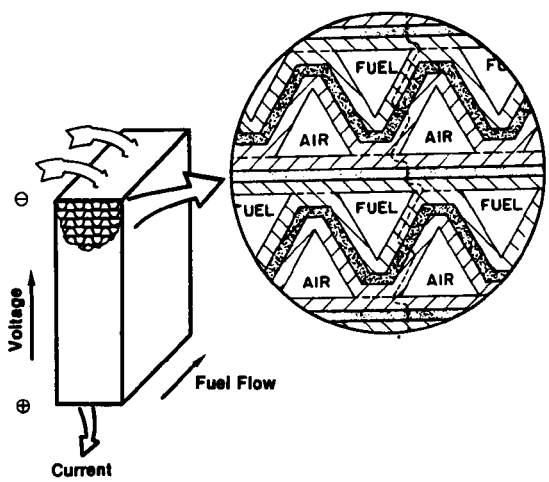

Fig. II-8.

Monolithic Fuel Cell

The potential for the high power density of the monolithic fuel cell results from the small cell size. Cells with gas passages 1 to 2 mm in diameter or smaller are achievable when the inert container for electrolyte and the inert support for the thin active layers are eliminated. The small cell size increases the active surface area per unit volume of the cell. More important, the small cell size in the monolithic design reduces the voltage losses caused by internal electrical resistance. This reduction is a significant consideration, because internal resistance is the principal dissipative loss for the ceramic materials and temperatures of interest. Decreasing the cell size decreases the current path length because current is carried "in-plane" by the electrodes in the monolithic design.

The principal challenge for the development of the monolithic fuel cell is fabrication of the intricate structures. Well-developed ceramic fabrication techniques are being employed. A tape casting methodology used in the ceramic capacitor industry is being optimized to fabricate thin, high-density layers of electrolyte and interconnection material. Tape casting is also being used to form the thin porous layers of the anode and cathode. Alternative thin-layer fabrication techniques, such as spraying, curtain coating, and hot roll milling, are also being considered.

The fabrication effort focuses on the critical three-layer composites: cathode-electrolyte-anode and cathode-interconnection-anode. These are the fundamental building blocks of the array. Considerable attention is given to achieving adequate bonding between the layers. In addition, methods have been developed to produce the desired corrugated structure. Thermosetting resins make the structure sufficiently rigid so that the corrugated tapes can be stacked in the unfired state.

All layers of the array are co-fired in air under the same conditions. The principal challenge for co-firing is to match the shrinkage rates of all four materials by tailoring the particle size and the binder content in each layer. Gas manifolding is added after the array is fired. At present, cross-flow gas passages are used to reduce the complexity of manifolding.

In 1986, the first arrays (stacks) of the monolithic design were built and operated. An array of two cells in series, each with an active area of 9 cm^2, has been operated for more than 700 hours, as shown in Fig. II-9. The operating conditions were a temperature of 1000°C, a current density of 50 mA/cm^2, hydrogen as the fuel, and air as the oxidant. The performance demonstrates the feasibility of the monolithic fuel cell concept.

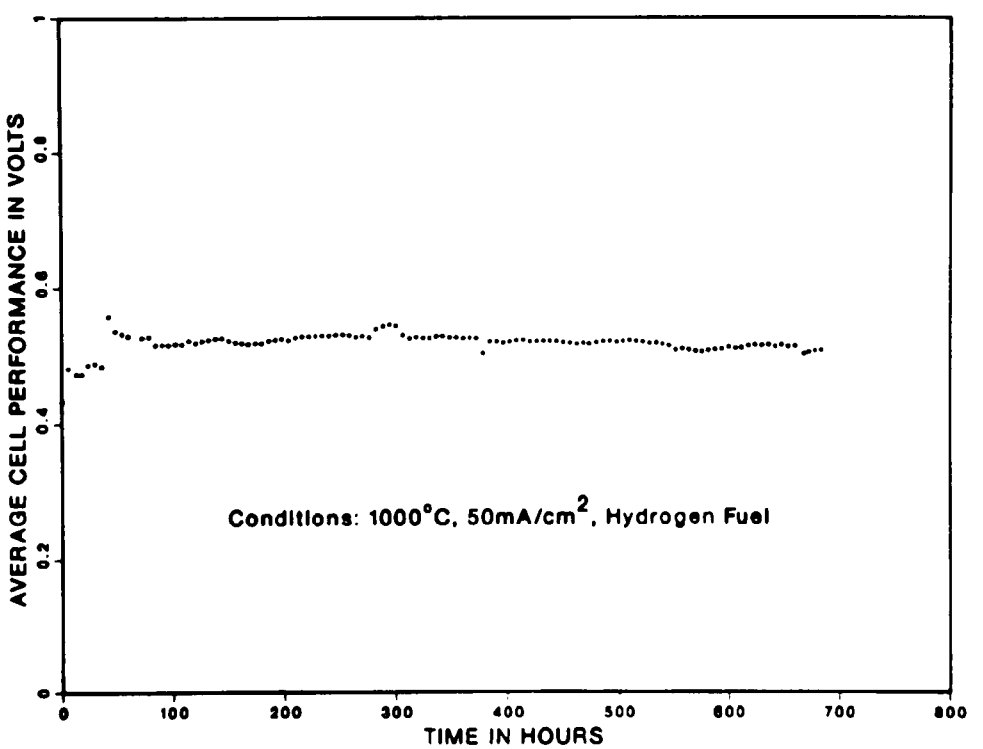

Fig. II-9. Voltage during Monolithic Fuel Cell Array Test

Operation of a fuel cell array on hydrocarbon fuels was also demonstrated. The hydrocarbons were mixed with steam and introduced directly into the array. The fuels include methane, propane, octane, ethanol, and natural gas. The array performance was similar to operation on hydrogen. Since the natural gas contained about 5 ppm sulfur in the form of an odor-producing mercaptan, this test also demonstrated operation with a sulfur-containing fuel.

The array, shown in Fig. II-10, incorporated a cross-flow pattern of gas channels. The electrochemically active region was a three-layer composite of cathode/electrolyte/anode. A corrugated anode layer formed the fuel gas channels on one side of the three-layer composite. Similarly, a corrugated cathode layer formed the oxidant gas channels on the other side of the three-layer composite. The oxidant channels in the cathode were at right angles to the fuel channels in the anode. An interconnection layer separated the fuel and oxidant channels and linked the layers in electrical series.

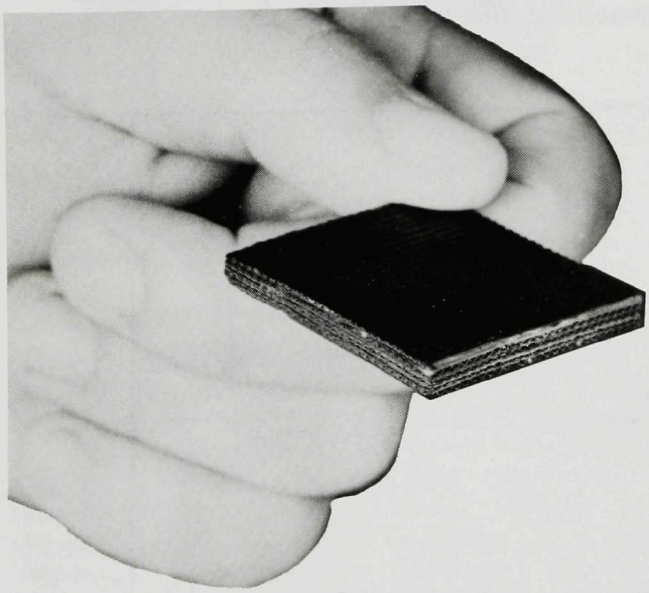

Fig. II-10.

Sintered Four-Cell Stack (flat, well-bonded structure free from visible cracks)

The emphasis of future research will be on improving performance and scaling up the size of the arrays. Improvements are desired in matching the firing shrinkage in order to reduce the incidence of cracks in the electrolyte and interconnection layers. The cracks allow fuel and oxidant to mix. Such mixing is the principal limitation on open-circuit performance of the array. Improvement is also needed in the internal resistance of the array. The height of the arrays will be increased by linking more cells in electrical series to produce greater voltage, and the active area will be increased so that more current can be produced. During the scale-up effort, industrial participation will be sought so that commercially viable fabrication methodology is incorporated.

C. *Analysis of Fuel Cell Systems*

In a joint effort with the EES and ENG Divisions, we are analyzing, for DOE, the major fuel cell applications to assess their economic viability and to make recommendations for future R&D. Initially, the effort was concentrated on utility base-load power plants. Fuel cells were found to be competitive with other technologies if the power density was doubled and the utilization of fuel was substantially decreased compared with state-of-the-art technology. Both recommendations have been incorporated into the industrial contracts by DOE.

More recently, we analyzed cogeneration applications of fuel cells operated with natural gas. The three types of fuel cells being sponsored by DOE for power plant applications (phosphoric acid, molten carbonate, and solid oxide) were compared to a gas-turbine/combined-cycle system in a generic cogeneration application. The application was defined as a process consuming 20 MW of electricity and 20 MW of steam at 0.5 MPa (75 psi) pressure. These values were based on a survey of electrical and thermal requirements of the U.S. manufacturing industry. The comparison was made using net present value (NPV) of all future revenues from each of the power plants as the measure of economic merit. The NPV is calculated by cash flow analysis relative to the "default option" of buying the electricity from the grid and generating the steam in a boiler. Utility rates of 70 and 54 mills/kWh for sale and buy-back of power, a fuel cost of $\$2.50/10^6$ Btu, and a discount rate of 15% in inflation-free dollars were assumed.

Five types of power plants were compared:

(1) A gas-turbine/combined-cycle plant with a waste-heat boiler having an electrical efficiency of 31.7% higher heating value (HHV), a power-to-heat ratio of 0.96, and a total installed cost of $685/kW.

(2) A plant having phosphoric acid fuel cells (PAFCs) with an electrical efficiency of 31.1% HHV, a power-to-heat ratio of 1.10, and an installed cost of $1026/kW.

(3) A plant using internally reforming molten carbonate fuel cells with a waste-heat boiler. The electrical efficiency is 43.2% HHV, the power-to-heat ratio is 2.03, and the installed cost is $867/kW.

(4) A plant integrating solid oxide fuel cells and a combustion turbine. The electrical efficiency is 36.6% HHV, the power-to-heat ratio is 1.33, and the installed cost is $590/kW.

(5) A plant consisting of internally reforming molten carbonate fuel cells operating under high pressure and integrated with a combustion turbine. The efficiency is 45.6% HHV, the power-to-heat ratio is 1.92, and the installed cost is $614/kW.

Estimates of NPV and rates of return for the five systems are as follows:

	Net Present Value, $M	Rate of Return, %
Gas-Turbine/Combined-Cycle	10.8	25.6
PAFC	3.6	17.3
Internally Reforming MCFC	3.2	16.3
SOFC/Combined Cycle	13.2	25.5
MCFC/Combined Cycle	15.3	23.1

The sensitivity of the NPV was evaluated for a range of discount rates, electric rates, fuel prices, the ratio of electric rates to fuel prices, and plant size. The relative ranking of the five systems remained the same over a $\pm 50\%$ range of these variables. Also, the issue of whether the plant should be sized for optimal electric or thermal match was analyzed. High electric rates relative to fuel prices, as are characteristic for the present U.S. market, favor electric matches.

Following suggestions by utility executives, we also considered the effects of utility demand charges and off-design operating modes on the plants. By virtue of the modularity of fuel cell plants, their economics was found to improve relative to the gas-turbine/combined-cycle system in these modes of operation.

The results of our economic comparisons indicated that the greatest potential gain from additional R&D would be for SOFCs. A cell with a simpler geometry and lower operating temperature than the 1000°C of the current SOFCs could enhance their economic advantage. In comparison to the SOFC, the MCFC and PAFC hold less promise for the medium-size cogeneration application. However, at the 1-5 MW power level, the internally reforming MCFC appears promising in locations with high electric rates.

Future systems analysis will explore how coal gasification and gas cleanup can be tailored for fuel cells so that the overall system costs are lower than state-of-the-art technology.

III. COAL AND MUNICIPAL WASTE UTILIZATION

This CMT program is focused on furthering the development of thermal-conversion processes that hold promise for having efficiencies that are dramatically higher than those of current technologies. The impetus for this effort stems from the fact that, in spite of significant technical progress, very few of the processes that have been developed thus far have been commercialized because the energy produced is not competitive with that of conventional fossil fuels. So great is the economic disparity that small incremental improvements in the processes will not, in general, alter the situation.

The CMT effort on municipal waste utilization centers on the pyrolysis of this solid waste to form liquid or gaseous fuels that are storable and transportable. The effort in fossil fuel utilization has several thrusts: cleanup of the hot off-gas streams from coal combustion and conversion systems, assessment of materials for air heat exchangers in the cogeneration of electricity and process steam from atmospheric fluidized-bed combustors, recovery of heat and seed from the bottoming cycle of a magnetohydrodynamics power plant, and recovery and recycle of CO_2 during coal combustion. Another effort entails investigation into the degradation of natural-gas transport pipe. Two new efforts are the development of a verified, in-depth description of the role that fouling deposits play in the corrosion of boiler heat-transfer surfaces and investigations into the combustion of char to optimize the utilization of hydrogen.

A. *Energy from Municipal Waste*

To date, the pyrolysis of municipal solid waste (MSW) to produce a storable, transportable, gaseous or liquid fuel has not been commercially successful. Several unsuccessful demonstration facilities have been built, and many additional processes have been proposed. Before a useful engineering design can be developed, however, the basic mechanisms of MSW thermal degradation must be better understood.

The objective of this CMT project is to create a data base for future MSW conversion technologies that can be developed by private industry. The technical approach is to undertake long-range research to expand the data base and thereby increase the understanding of the thermokinetic mechanisms associated with MSW pyrolysis. We will attempt (1) to define the primary and secondary chemical reactions involved in the pyrolysis, (2) to identify the important operating parameters and determine their influence on the reactions, and (3) to produce a useful kinetic model that describes decomposition of cellulosic material.

In 1986 data collection for pyrolysis in the low-temperature range (<500°C) was continued with a bench-scale reactor that consists of a fixed bed within a quartz tube (70-mm ID) enclosed in a furnace. The gases generated as the tube is heated are analyzed by mass spectrometry (MS), and the liquid samples are analyzed by gas chromatography (GC) and gas chromatography/mass spectrometry (GC/MS). The experimental parameters being varied are feedstocks (Whatman No. 1 filter paper, newsprint, Kraft paper, and cardboard), sample size (5-50 g), heat-up rate (5-75°C/min), and final temperature (200-750°C). Other than the feedstock, we found that the most important parameter in determining the product yields (tars, chars, and gases) is the final temperature.

Figure III-1 summarizes the product yields for 5 g of Whatman No. 1 filter paper pyrolyzed in the bench-scale unit at a heating rate of 5°C/min. This figure indicates that the cellulose started to decompose at about 280°C and was complete at about 380°C. Tar formation is observed at temperatures above 300°C. Similar curves have been obtained for other components of the MSW (e.g., newsprint, Kraft paper, wood).

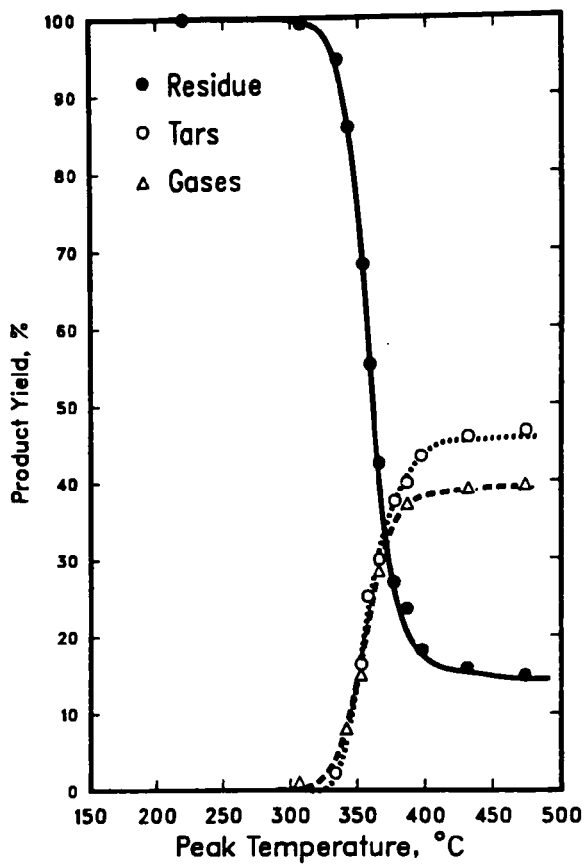

Fig. III-1.

Product Yields (dry, ash-free basis) from Pyrolysis of Whatman No. 1 Paper at Heating Rate of 5°C/min

Table III-1 summarizes the atomic ratios and heating values of some selected fuels and MSW materials. As shown in Table III-1, the atomic ratios and the heating value of cellulose are comparable to those of MSW and the ECO fuels, a dry powdered fuel produced from MSW by Combustion Engineering Associates. This finding is not surprising, especially since it is well established that cellulosic materials constitute a major portion of MSW. The atomic ratios and the heating value of cellulosic chars indicate that they are very similar to coal. The H/C ratio of cellulose tars is comparable to that of No. 2 fuel oil. Unfortunately, the high oxygen content indicated by the O/C ratio significantly reduces the heating value of the tars.

Data from the bench-scale experiments are also being analyzed to determine the influence of experimental parameters on the product mix from pyrolysis. The results in Table III-2 illustrate the influence of sample weight and heating rate on

Table III-1. Atomic Ratios and Heating Values of Some Fuels and MSW Materials

Substrate	Atomic Ratio H/C	Atomic Ratio O/C	Heating Value, cal/g
Cellulose[a]	1.58	0.83	4170
Wood	1.44	0.56	5000
MSW	1.51	0.52	4565
ECO I	1.61	0.61	3679
ECO II	1.55	0.49	5303
Cellulose chars	0.53	0.14	7566
Utah bituminous coal	0.92	0.09	7872
Lignite	0.79	0.23	5710
Cellulose tars	1.73	0.91	4330
No. 2 fuel	1.84	0.01	10,917
No. 6 fuel	1.47	0.02	10,105
Benzene	1.00	–	9589
n-Octane	1.00	–	10,611

[a]Whatman No. 1 paper.

Table III-2. Effect of Sample Weight and Heating Rate on Product Yields from Whatman No. 1 Paper

Sample No.	Pyrolysis Sample Weight, g	Heating Rate, °C/min	Yields,[a] wt % Tar[b]	Yields,[a] wt % Char	Char, wt % C	Char, wt % H	Char, wt % O[c]
FPL08	5	5	46.14	14.55	82.80	3.75	13.45
FPL15	10	5	42.13	15.26	81.00	3.55	15.45
FPL13	15	5	38.54	15.66	81.90	3.45	14.65
FPM03	5	20	47.18	12.65	81.30	3.45	15.15
FPH05	5	30	47.76	11.93	80.30	3.55	16.15

[a]Product yields are given for a peak temperature of 475°C.

[b]Based on weight percent Whatman No. 1 paper (dry basis).

[c]Derived by adding together C and H contents and subtracting from 100%.

tar and char yields. The data suggest that increasing sample size reduces the tar yields and increases the char yields. The drastic decrease in tar yields is primarily due to increased vapor residence time in the reaction bed. If the vapor residence time is reduced in the reaction bed by using a fluidized bed or an entrained flow reactor, then secondary decomposition can be significantly reduced, and the effects of sample weight will not be as drastic. Thus, data collected in the loosely packed fixed-bed reactor of the present study may represent an extreme for an operating industrial reactor.

Increasing the heating rate appears to decrease the char yields but has little influence on tar yields. This implies that gas yields increase at the expense of char yields, and that chars and gases may be formed from different reaction mechanisms. Elemental analyses of chars formed by pyrolysis (see Table III-2) indicated that the composition of chars is not strongly influenced by either the heating rate or sample weight. The observation that tar yields are independent of heating rates is strengthened by our earlier work,[1] which showed that the apparent activation energy for cellulose decomposition is similar to that for tar formation.

The liquid mixtures are too complex to allow rapid identification. However, various samples from the bench-scale runs were analyzed with GC and GC/MS. Preliminary analysis of tars produced from a newsprint feedstock allowed identifications of some components. In general, the classes of compounds included furfurals (9.4%), phenols (2.5%), methoxyphenols (16.9%), cyclic compounds such as methyl cyclopentanones (10.8%), methoxy benzenes (3.8%), and substituted propane (36.8%).

Solar Energy Research Institute (SERI) continues to work as a subcontractor on the MSW effort. A flame pyrolyzer with a molecular-beam mass spectrometer sampling device is being used to perform quantitative studies on the influence of sample properties and reaction conditions on the solid-phase and gas-phase processes of low-temperature MSW pyrolysis (<500°C) to oils. In addition, SERI is working on a rapid characterization technique for waste-derived pyrolysis oils that will index oils to include all of the products, including those that cannot be successfully chromatographed.

High-temperature gasification studies at ANL (>500°C) have been started on single components of MSW. In both the high- and low-temperature ranges, product distributions, product quality, and the effects of operating parameters are being determined.

Future work includes continued bench-scale experiments (isothermal and nonisothermal) to determine the mechanisms and reaction kinetics for both individual components and mixtures of MSW. An important related effort is the characterization of the tars produced. To completely understand the reaction pathways, we must analyze what is being produced. This difficult analysis is being attempted with tools such as GC, GC/MS, high pressure liquid

---

[1]M. J. Steindler et al., *Chemical Technology Division Annual Technical Report, 1985*, Argonne National Laboratory Report ANL-86-14, p. 64 (1986).

chromatography, and Fourier transform infrared spectroscopy. Also, as the data base on the chemistry of MSW pyrolysis is expanded, heat and mass transfer studies will be combined with the chemical decomposition work for reactor design analyses.

B. *Cleanup of Hot Flue Gas*

Experience in operating gas turbines with hot flue gas from the direct combustion of liquid fuel and pulverized coal indicates a potential problem in application of the pressurized fluidized-bed combustion (PFBC) of coal for power generation. Hot corrosion of the gas turbines could occur, owing to the presence of alkali metal compounds (such as chlorides and sulfates of sodium and potassium) in the flue gas. A fixed, granular-bed sorber is being developed at CMT to clean up these alkali corrodents from the flue gas. In our earlier laboratory tests under a simulated PFBC flue gas environment, activated bauxite was found to be a very effective sorbent, and we also demonstrated its regenerability by a simple water-leaching process. Because of the promising results obtained from laboratory studies, a laboratory-scale alkali sorber was designed, fabricated, and installed and is being operated with a pressurized fluidized-bed combustor (PFBC/alkali sorber) at CMT to (1) measure the alkali-vapor (sodium and potassium) concentration in PFBC flue gas on a real-time, on-line basis and (2) demonstrate the fixed, granular-bed sorber for the control of alkali vapors from the actual PFBC flue gas.

In the PFBC/alkali sorber, the flue gas from the combustor exits through a horizontal port located in the middle of the freeboard section and enters a primary hot cyclone, on top of which is installed the alkali sorber vessel. A fraction of the flue gas is directed into secondary and tertiary cyclones contained inside the vessel for further separation of the entrained particulates in the flue gas. The gas exiting the tertiary cyclone enters a head space and then flows into an activated-bauxite sorbent bed. The sorber-inlet and -outlet gas streams are continuously sampled through an electrically heated stainless steel line maintained in the temperature range of 850-900°C. Alkalis in the gas stream are analyzed by an Ames on-line alkali analyzer through a filtered or an unfiltered sampling line. A batch-type alkali and particulate sampling train (APST) is also installed as a back-up for the analysis of both alkali vapor and particulate in the gas stream.

During 1986, three tests (Nos. 4, 5, and 6) with the PFBC/alkali sorber were conducted (1) to investigate the possible source of discrepancy between the two analytical techniques observed in the previous three tests (Nos. 1-3, results of which were discussed in last year's report[2]) and (2) to evaluate the performance of the activated bauxite for the removal of alkali vapor. In these tests, Sewickley coal (Pittsburgh, PA) and Tymochtee dolomite (Huntsville, OH) were combusted at an average bed temperature ranging from 900 to 925°C and a system pressure of 9 atm absolute. Also, a controlled amount of NaCl vapor was injected through a pressurized NaCl-vapor generation unit into either the head space of the sorber (for Tests 4 and 5) or the sorber-inlet sampling gas stream (for Test 6). The purpose of this additional NaCl-vapor injection was to provide

---

[2]M. J. Steindler et al., *Chemical Technology Division Annual Technical Report, 1985*, Argonne National Laboratory Report ANL-86-14, pp. 65-67 (1986).

sufficient NaCl vapor in the flue gas for assisting in the quantification of the alkali measurement by both analytical techniques and also for evaluating the activated-bauxite sorber for the removal of NaCl vapor.

1. Alkali Measurement

The alkali measurement in the flue gas was made both with and without NaCl-vapor injection. The NaCl vapor was injected at the target NaCl-vapor concentration in the flue gas of 0.58 ppmW for Tests 4 and 5 and 0.44, 1.7, and 3.0 ppmW for Test 6.

For all three tests, the range of alkali-vapor concentration in the sorber-inlet filtered stream with no NaCl-vapor injection is plotted in Fig. III-2. Both sodium and potassium vapor concentrations measured in Test 4 were up to five times greater than the <10 ppbW sodium and 20-30 ppbW potassium measured in an earlier test (No. 3, where no NaCl was injected). For Test 5, the sodium and potassium vapor concentrations were in the range of 2.5-7.5 and 25-75 ppbW, respectively, which are similar to the results of Test 3. However, in Test 6, the vapor concentrations showed much higher levels: 20-62 and 300-520 ppbW for sodium and potassium, respectively.

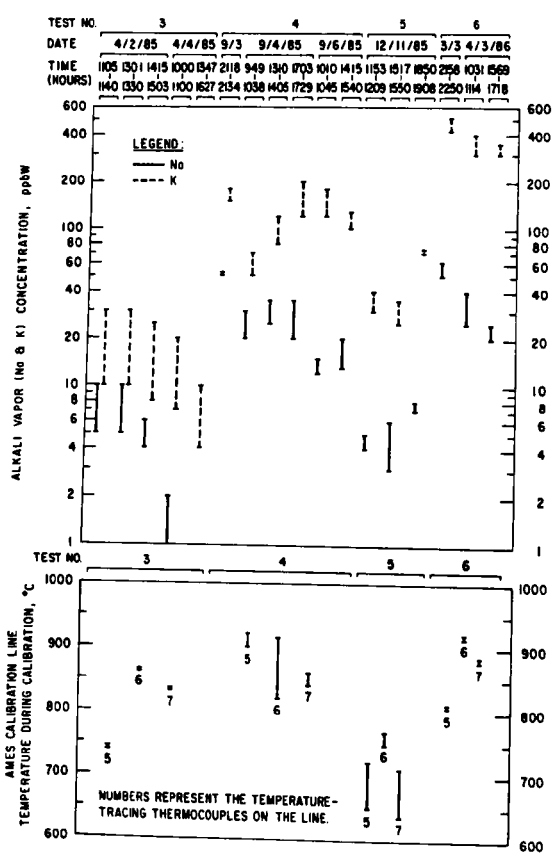

Fig. III-2.

Alkali Vapor Concentrations Measured in the Sorber-Inlet Filtered Stream by Ames Alkali Analyzer and Temperatures of Calibration Line Measured during Calibration of Ames Alkali Analyzer

A possible explanation for these variations is that the high concentrations measured in Tests 4 and 6 are contributed by the evolution of alkalis from the section of the sampling line that had been shared for use with the

calibration of the Ames analyzer before each test. As shown in Fig. III-2, the temperatures for the Ames calibration line in Tests 4 and 6 were much higher than those of Tests 3 and 5. Under such a high temperature, Na_2SO_4 aerosols generated from the calibration solution during the calibration could have been melted (the melting point of Na_2SO_4 is 884°C). Low-melting-point eutectic compounds of Na_2SO_4 and K_2SO_4 could also have been formed and stuck on the wall of the calibration line. Several times during Test 6, the alkali-vapor concentration immediately dropped to <1 ppbW once the Ames calibration line had been cooled by turning off its heater, and this value returned to the earlier alkali level after the line had been heated to its previous temperature range.

On the basis of results in Fig. III-2 and melting-point data for the Na_2SO_4-K_2SO_4 solid solutions, 800°C is probably a reasonable temperature limit to prevent the alkali compounds in the calibration solution from being retained on the wall of the calibration line.

In all three tests, the alkali concentration in the sorber-inlet unfiltered stream, which contains the entrained fly ash, showed a continuous decrease with time. This decrease, plotted in Fig. III-3 for Test 4, is attributed to the continuous capture of the fly ash by the Ames needle valve used to control the stream flow. This capture resulted in the continuous loss of the gas flow, as well as loss of the ash particles being carried from the stream into the flame for alkali analysis.

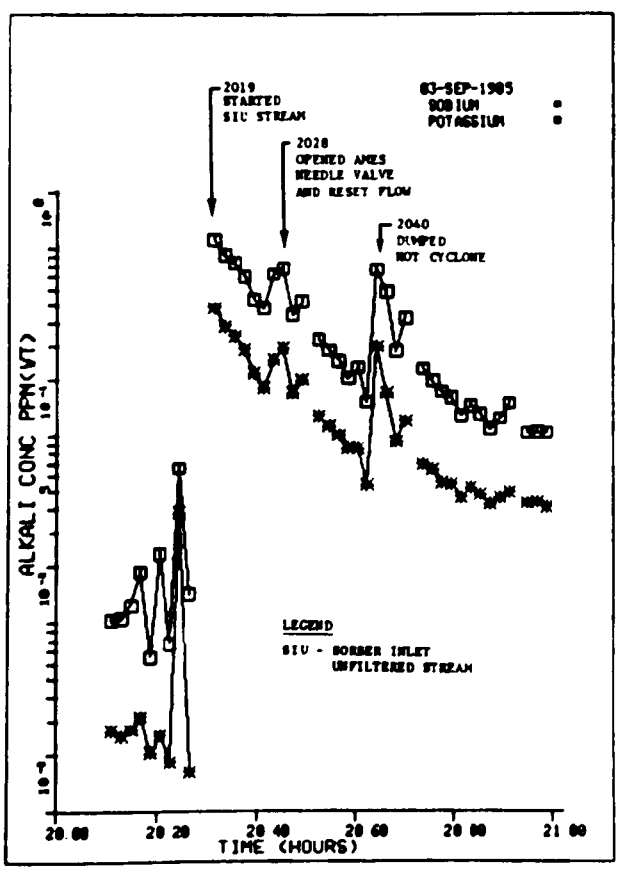

Fig. III-3.

Alkali Concentrations in Sorber-Inlet Unfiltered Gas Stream Measured by Ames Alkali Analyzer (Test 4)

The injection of NaCl vapor into the head space and the sorber-inlet sampling line did not produce any detectable sodium increase in either the filtered or unfiltered sorber-inlet stream measured by the Ames alkali analyzer. The analyses of fly ash samples indicated that the injected NaCl vapor was essentially retained by the fly ash at the injection point in Test 4. For Test 5, the injected NaCl vapor was essentially carried by the flue gas downward into the activated-bauxite sorbent bed. In Test 6, where the NaCl vapor was injected directly into the sorber-inlet sampling stream, the vapor was effectively captured by the fly ash retained in the fiber filter that had been installed in the Ames alkali analyzer.

In agreement with the Ames results, the alkali-vapor concentrations measured by the batch-type APST did not show any increase in sodium during the period when the NaCl vapor was injected. However, the average alkali-vapor concentrations measured by the APST were 1-2 orders of magnitude greater than those measured by the Ames analyzer. To resolve the analytical discrepancy between the Ames alkali analyzer and the batch-type APST, we will set up a laboratory-scale test rig that will generate a simulated PFBC flue gas containing a controlled amount of NaCl and KCl vapors, and then will run a series of tests with both the Ames alkali analyzer and the APST on stream simultaneously to determine the accuracy of the alkali measurement by each technique. In parallel to this, laboratory testing will also be initiated to obtain a better understanding of alkali-vapor capture by the heated stainless steel.

2. NaCl-Vapor Sorption Performance of Activated Bauxite

In Test 5, a 7.9-cm-dia, 25.4-cm-long activated bauxite bed divided into ten sections of equal length was tested at a bed temperature of 850°C, a system pressure of 9 atm absolute, a superficial gas velocity (of the flue gas passing through the bed) of 46 cm/s (1.5 ft/s), and a gas hourly space velocity* of 6480 h^{-1}. The bed was exposed to the flue gas containing an average fly ash loading of about 480 ppmW and an injected NaCl vapor of about 580 ppbW for 6 h. Under these test conditions, visual inspection showed that the fly ash did not penetrate through the first section of the bed. The sodium vapor concentration in the sorber-outlet flue gas, which was measured at the beginning and the end of the test by the Ames alkali analyzer, showed only 4-5 ppbW, suggesting that the injected NaCl vapor carried by the flue gas did not break through the activated bauxite. The effectiveness of activated bauxite as a sorbent was further confirmed by water-leaching studies in which the injected NaCl vapor was totally captured by the first two sections of the activated-bauxite bed.

3. Future Work

The three tests completed in 1986 demonstrated that the fly ash present in the flue gas of the current PFBC/alkali sorber captures the NaCl vapor and plugs the Ames needle valve, thereby impeding acquisition of a

*The volumetric flow of flue gas per hour per sorbent volume. The reciprocal of this value is related to the contact time of flue gas with the sorbent bed.

representative sampling of the flue gas for alkali analysis. Therefore, a method of extensively reducing the fly ash loading is deemed necessary. To achieve this reduction, the alkali sorber vessel will be modified by replacing the existing secondary and tertiary high-temperature cyclones with high-efficiency, high-temperature candle filters, which should remove greater than 99% of the particulates from simulated flue gas. With this modification, along with the establishment of the accurate analytical techniques and a better understanding of the alkali-vapor capture by the heated stainless steel, a reliable PFBC/alkali sorber can be counted on to achieve the objective of this research project.

C. *Atmospheric Fluidized-Bed Combustion*

1. Atmospheric Fluidized-Bed Cogeneration Air Heater Experiment

Argonne is managing the Atmospheric Fluidized-Bed Cogeneration Air Heater (ACAH) Experiment for DOE. The objective of this effort is to assess materials and process performance of in-bed air heaters for cogeneration of electricity and process steam in an atmospheric fluidized-bed combustor (AFBC). The effort is expected to be about four years in duration, with the start of air-heater testing at Rockwell International scheduled for the fall of 1987. The experiment is being done in cooperation with Westinghouse Corp. and several boiler vendors under subcontract to Westinghouse. The ANL involvement in this effort includes three tasks, described below.

a. Materials Data Base

The first task, which is completed, was to establish a materials data base by collecting and assessing current technical information on the performance of heat exchanger materials, particularly materials that have been exposed at temperatures of 650°C or higher. The data discussed in the report[3] on this data base were collected from 13 sources and were generated in 16 different experimental fluidized-bed combustors (four pressurized, the others atmospheric). The plan sections ranged from a 152-mm dia circle to a 3.7-m by 5.5-m rectangle. Seventy-seven alloys or coating/cladding combinations of alloys were tested. Besides ANL, the investigating organizations were Oak Ridge National Laboratory (assisted by FluiDyne Engineering Corp.); Rocketdyne Division of Rockwell International Corp.; the UK Coal Utilization Research Laboratory; the Coal Research Establishment of the UK National Coal Board; Exxon Research and Engineering Co. (assisted by the Westinghouse Electric Corp.); Babcock & Wilcox Co.; Tennessee Valley Authority; Battelle Columbus Laboratories; the International Energy Agency (assisted by the UK National Coal Board); the Netherlands Organization for Applied Scientific Research; and Nova Scotia Power Corp. The 19 research campaigns that produced the data were carried out between 1969 and 1986 (some are still ongoing).

In our report, data are tabulated for exposures of 10 to 10,000 h (few were shorter than 240 h) at temperatures between 572 and 900°C; but data analysis was normally limited to tests for temperatures no lower than 650°C

---

[3]K. Natesan, S. A. Miller, and W. F. Podolski, *An Assessment of the Performance of Heat Exchanger Materials in Fluidized-Bed Combustors*, Argonne National Laboratory Report ANL-86-42 (1986)

and exposures no shorter than about 500 h. Corrosion rates were calculated by assuming parabolic kinetics for scale formation, penetration, and total metal loss. For each alloy, rates so computed from the data from all sources are plotted against temperature. In general, these graphs can be interpreted as linear relationships, although the scatter is large.

The data analysis confirmed that austenitic stainless steels (notably types 304 and 310) and cobalt-base alloys (notably Haynes Alloy 188) are clearly superior to nickel-base alloys. Of the nickel-base alloys, Hastelloy X and the Inconels 601, 617, and 671 performed particularly badly, experiencing breakaway corrosion. Of the austenitics, Type 347 and Incoloy 800 H are questionable: both are subject to greater penetration than Types 304 and 310, and the penetration appears to increase dramatically with time of exposure, suggesting unsatisfactory long-time performance. Few data are available for claddings and coatings. Although these few data are quite scattered, they indicate that alloys with relatively high chromium content and with added yttrium are better than others at resisting oxidation-sulfidation attack.

We also reviewed hypotheses about the mechanisms of metal degradations and recent research contributing to the understanding of degradation phenomena. Owing to the development of sensitive electrochemical probes, the oxygen concentration and its variation, both spatially and temporally, in a fluidized bed now can be mapped with a precision of 10^{-15} atm and 0.1 second. This technique has enabled investigators to demonstrate that in-bed metal wastage is aggravated by the sustained exposure of the metal to an atmosphere very low in oxygen partial pressure ($<10^{-12}$ atm). It also has permitted experimental confirmation that, in beds in which the average oxygen partial pressure is reasonably high (around 0.01 atm), frequent local cycling in partial pressure can occur to values smaller than 10^{-12} atm. Although the partial pressures of SO_2 and sulfur cannot be measured, the equilibria of systems of sulfur, SO_2, oxygen, $CaSO_4$, CaO, and the oxides and sulfides of the alloy metals of interest are sufficiently well known to permit the confident calculation of these concentrations. The results shed light on the probable mechanisms of the oxidation-sulfidation process, including the phenomena of breakaway corrosion (i.e., the onset of rapid, catastrophic degradation, sometimes in less than 500 h). They support the recent demonstration that, at 600°C and above, $CaSO_4$ alone deposited on iron-base and nickel-base alloys can initiate sulfidation, presumably because of dissociation.

Erosion wastage of tube-bundle components has occurred unexpectedly in several fluidized-bed combustors. The cause is obvious--the impact of high-velocity, abrasive particles against the metal surface--but how to anticipate and avoid this problem is not known, nor is there a clear rationale for eroding potential and erosive action in a fluidized bed. Although no really satisfactory explanation for the observation has been offered, it is notable that all of the reported incidents of severe erosion included cooled components with surface temperatures below 600°C.

From the correlations of the corrosion-rate data compiled for several of the more-promising alloy candidates for ACAH application, we were able to define guidelines for the selection of materials for which one can be reasonably assured that the corrosion resistance will be adequate for more or less

"standard" designs. (The term "standard" has no precise definition: it means designs that involve combustor proportions, dimensions, and operating conditions that fall within the boundaries characterizing the tests in which satisfactory performance of specimens was observed.)

b. Laboratory Materials Tests

The second task is to conduct materials tests in the laboratory that will complement tests in an actual AFBC unit and to fill in data gaps noted in the literature review discussed above. Westinghouse has designated materials for laboratory testing at ANL, in addition to those that will be exposed in the AFBC unit.

The purpose of the laboratory materials tests is to provide corrosion information on a variety of ASME-coded and noncoded structural materials, coatings, claddings, and weldments under a well-characterized test environment that simulates an FBC atmosphere. A series of six laboratory tests will be performed at CMT in support of the data needs by Babcock & Wilcox, Foster Wheeler Development Corp., and Combustion Engineering, Inc. These firms are involved in the tube-bundle materials selection and design.

Results are available from the first 1000-h test (test A), which was conducted in support of Babcock & Wilcox and Foster Wheeler. In this test, 11 ring specimens were used to simulate the heat exchanger tubes exposed to an environment arising from the combustion of coal. In addition, 13 experimental alloys were exposed in flat-form coupons to evaluate their corrosion resistance. A schematic of the experimental setup is shown in Fig. III-4. The ring specimens of different alloys were attached to a corrosion probe, approximately 0.4 m in length, with a specially designed head that incorporated the cooling fluid path and thermocouples. A photograph of the fully assembled corrosion probe is shown in Fig. III-5. The entire probe was inserted in a reaction chamber constructed of aluminized Type 310 stainless steel. The heating of the specimens (to ~870°C) and the gases (to ~900°C) was accomplished by resistance-wound heating elements surrounding the reaction chamber. The alloy coupons were placed in the annular region between the probe and furnace wall.

In the present test, the outer surfaces of the ring specimens and one surface of the flat coupons were coated with reagent grade $CaSO_4$. The deposit material was made into a water-based paste and applied onto the alloy specimens. The thickness of the deposit layer was in the range 0.25 to 0.50 mm. The corrosion test probes were cooled to room temperature after 500 h of exposure at the test temperature. During the cool-down period, the specimens were recoated with the deposit material to ensure that there was no starvation of reactant for the next corrosion exposures.

Upon completion of two 500-h exposures, we performed macroscopic and microscopic examinations of various specimens. Cross sections of the ring specimens were examined using a scanning electron microscope (SEM) equipped with an energy dispersive X-ray analyzer (EDAX) and an electron microprobe to identify the morphological features of corrosion-product phases in the scale layers. In addition, SEM and optical metallography were used to determine the thickness of scale layers and depth of intergranular penetration in the substrate material. Surface recession in various specimens was calculated from measurements on the exposed specimens and the initial wall thickness.

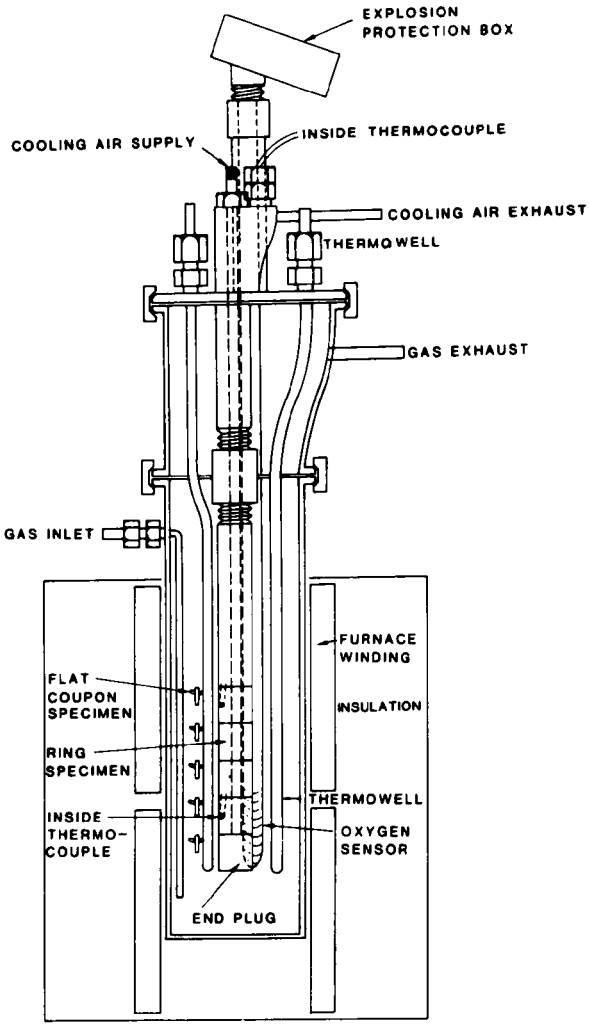

Fig. III-4.

Experimental Setup for AFBC Materials Tests

Based on the Test A data, the following conclusions were drawn:

1. Austenitic stainless steels such as Types 304, 316, and 310 showed acceptable corrosion behavior, even in the presence of simulated sulfur sorbent.

2. Alloys such as Incoloy 800 and Haynes 188 and, to a lesser extent, RA330 were susceptible to catastrophic attack, especially in the presence of $CaSO_4$ deposit.

3. A CoCrAlY-coated 800 specimen exhibited a low rate of scaling, but the stability of the coating under thermal cycling needs to be established since the underlying base metal is susceptible to catastrophic corrosion.

4. Alloys 304 and 800 with chromized surface treatments exhibited low-to-moderate attack of the coating layers.

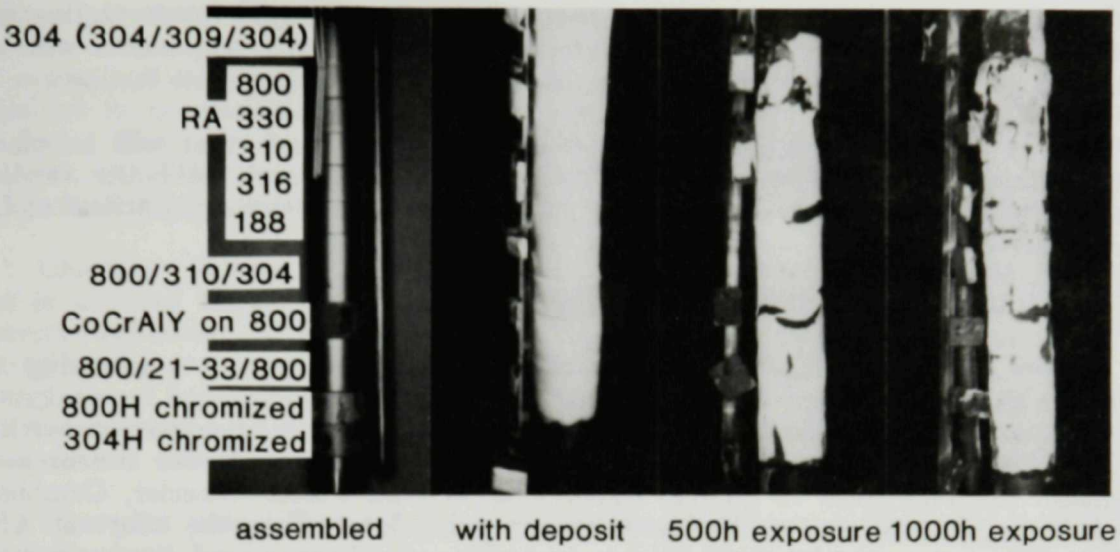

Fig. III-5. Corrosion Probe Used in AFBC Materials Tests

5. All the three weldment specimens (304/309/304, 800/310/340H, 800/21-33/800) exhibited minimal attack on both the deposit- and air-exposed surfaces; however, the susceptibility of the alloy 800 base metal to corrosion in regions unaffected by welding was very evident.

6. Among the coupon specimens, alloy 556, HK40, Mn-Nb modified 800H, and 54E exhibited significant corrosive attack both under the deposit and on the bare side exposed only to the simulated combustion atmosphere. Alloys such as 253MA, FW-4C, HR-3C, and RV 8413 exhibited minimal attack in these conditions. In particular, the alumina-forming alloy RV 8413 looked superior in its corrosion resistance.

7. Among the aluminide materials, nickel aluminide (IC-50) was found to corrode owing to formation of nickel sulfide in the presence of deposit and in the gas-phase environment. Iron aluminide (FA41) had the least attack, and preoxidized nickel-base alloy (IC-266) exhibited intergranular penetration in the substrate material.

c. AFBC Test

The third task is to subcontract with Rockwell International for the required modification, installation, and experimental testing of heat-exchanger tube bundles in the DOE-owned AFBC unit (1.8 by 1.8 m) located at Rockwell International. Argonne will also provide an independent data reduction and assessment of the heat-exchanger performance. Two tests of 1000-h duration each are planned. The first test will emphasize performance of air-cooled heat exchangers in a bubbling fluidized bed, while the second test will be configured to

assess materials and components for air-cooled heat exchangers in circulating or fast fluidized-bed combustors. The materials and other test components will be delivered to ANL by Westinghouse for installation at the Rockwell facility.

Currently, Rockwell is designing modifications that will be made to the facility for these tests. In addition, Westinghouse and the boiler vendors are preparing a test plan document to specify the experimental conditions and equipment configuration.

2. Erosion in Fluidized-Bed Combustors

Metal loss from in-bed heat transfer tubes in FBCs is a recurring problem that is impeding the commercialization of FBC technology for coal combustion. To address this problem, we are initiating a cooperative research and development venture with the following groups: Electric Power Research Institute (EPRI), State of Illinois, Babcock & Wilcox, Foster Wheeler, Combustion Engineering, and Tennessee Valley Authority. Involvement in the effort at ANL will include not only the CMT Division but also the Energy and Environmental Systems and Materials and Components Technology Divisions.

The goal will be to produce guidelines for the design and operation of FBCs to minimize metal loss. Tasks include (1) experiments to determine the relationship between particle size and particle velocity at the limits of detectable erosion and the effects of temperature and particle characteristics at conditions similar to those in FBCs; (2) cold- and hot-fluidized-bed experiments to determine such information as void fraction and pressure distribution fluctuations, solids and bubble motions, and erosion of immersed tubes for model refinement and validation; (3) mechanistic computer modeling of the fluidized-bed hydrodynamic and erosion processes, with validation from the above experiments; and (4) development of improved *in situ* erosion monitoring techniques for application in FBCs based on a previously successful development at Argonne.

Some of the R&D will be carried out at ANL, but experimental work will also be carried out at the University of Illinois, Illinois Institute of Technology, and at one or more of the industrial organizations mentioned above.

D. *Magnetohydrodynamic Heat and Seed Recovery*

Open-cycle magnetohydrodynamics (MHD) is a developing technology with the potential to improve substantially the electrical efficiency of coal-fired power plants and to reduce their environmental impact. In the coal-fired concept of MHD, an easily ionized seed material (usually a potassium salt) is injected into a high-temperature, slag-rejecting coal combustor. The resulting electrically conductive fuel-rich combustion gas then flows through a high-velocity channel in the presence of a strong magnetic field. An electrical potential is developed across electrodes in contact with the gas stream in the channel walls and an electrical current is produced. In this manner, up to 25% of the gas enthalphy can be converted into electrical energy.

The fuel-rich combustion gas leaves the MHD topping cycle at 1 atm and approximately 2300 K and enters a bottoming cycle that is somewhat similar to the steam bottoming cycle of a conventional power plant. However, the MHD

steam plant must not only extract heat from the combustion gas to produce high-pressure steam, but also separate the seed from the ash, recover the seed material for reuse, preheat the primary combustion air to at least 1000 K, lower NO_x emissions to acceptable levels, and inject secondary air to complete combustion of the fuel. Moreover, because the combustion gas contains a large amount of seed material, the MHD steam plant must operate under conditions that are more highly fouling and corrosive than those of conventional coal-fired power plants.

Chemical Technology is the lead ANL division in a multidivisional project that is directed toward developing the technology required for the heat and seed recovery technology in the MHD plant. Much of the CMT effort, in addition to managing the program, involves experiments that are performed in the Fossil Energy Users Laboratory (FEUL), an ANL combustion test facility that includes two test trains: one equipped with a 2-MW slagging coal combustor and the other with a 3-MW combustor for burning liquid fuels, including slurries.

This past year, effort has been focused on investigations into the fouling of the boiler tube banks, the enhancement of radiant heat transfer caused by potassium atoms and solid ash particles in the combustion gases, the interface between the MHD topping cycle and the bottoming cycle, and the corrosion of materials for superheater and air-heater service.

1. Fouling of Steam Heaters by Seed and Ash

Over the past few years, fouling tests in which tube banks were exposed to simulated MHD combustion gases have been conducted at ANL in the oil-fired test leg of FEUL.[4] These tests demonstrated that the character of the tube deposits depended primarily on whether the gas temperature was above or below the melting temperature of the seed material. At gas temperatures below about 1340 K, the entrained seed and ash formed a low-density, loosely adhering deposit that was readily removed by sootblowing. At temperatures above about 1600 K, the outer surface of the growing deposit layer reached the melting temperature. Depositing seed and ash material then flowed off the tubes, resulting in a stable deposit thickness. At gas temperatures between about 1400 and 1600 K, however, the deposition of liquid seed and solid ash particles resulted in the formation of dense, adherent deposits that occasionally proved difficult to remove by sootblowing.

During 1986, a series of short-duration fouling tests (generally 6 to 8 h) was completed, along with one of 30-h duration. The primary objective of the tests was to identify the parameters primarily responsible for sintering and densification of the deposits and their increasing tenacity. Secondary objectives were to continue (1) acquiring data on deposition rates and heat transfer characteristics of the deposits and (2) improving the ANL heat and mass transfer model for use in the scale up and design of MHD plants.

---

[4]M. J. Steindler et al., *Chemical Technology Division Annual Technical Report, 1985*, Argonne National Laboratory Report ANL-86-14, p. 70 (1986).

The parameters investigated in the fouling tests were gas temperature (1200 to 1800 K) and the chemistry of the depositing species. In some tests, the depositing species was pure K_2SO_4. Tests were also performed with fly ash and K_2SO_4 in the combustion gas simulating both 50% and 80% slag rejection during combustion. In two tests, K_2CO_3 was added to the K_2SO_4 and fly ash in the combustion gas to simulate excess K_2CO_3 (for SO_2 control) in the seed material injected into the MHD coal combustor.

The key findings from the completed fouling tests with respect to deposit characteristics and tenacity can be summarized as follows:

1. Ash-free deposits of K_2SO_4 formed at gas temperatures above the melting temperature of the salt were very hard and dense and could prove troublesome (as reportedly have ash-free MHD deposits of K_2CO_3 in the Soviet U-25 facility).

2. Deposits containing ash were noticeably more porous than seed-only deposits. The deposits that formed during the tests simulating 50% ash carryover were observed to be very chalky, light, and fluffy and could be easily removed by sootblowing, even after 6 h.

3. Small amounts of K_2CO_3 mixed with the K_2SO_4 (ratio of 1:4) in the seed added to the combustion gas did not noticeably alter the characteristics or the tenacity of the deposits formed.

4. At high gas temperatures (>1600 K), liquid deposits readily formed, but they had marginal effects on the heat transfer coefficient to the clean tubes.

5. The characteristics of the deposits in the 30-h test (at low heat flux) were similar to those formed during the 6- to 8-h tests under similar operating conditions. The tubes were successfully cleaned by operating the sootblowers every 6 h.

In addition to the above tests, a special series of six fouling tests was completed with the assistance of Mississippi State University. The purpose of these tests was to experimentally determine the thermal conductivity of fouling deposits formed at gas temperatures of 1200 to 1800 K and test durations of 2 to 6 h. These tests were performed to obtain a better understanding of the deposit physical properties that influence heat transfer to fouled tubes and deposit hardness and tenacity. The thermal conductivity of the seed and slag deposit was calculated directly from the measured data on deposit thickness, wall temperature, deposit surface temperature, and average heat transfer rate. The measured thermal conductivities of the deposit for these tests ranged from 0.20 to 0.35 W $m^{-1}K^{-1}$. The data are being analyzed to determine if the changes in deposit thermal conductivity can be correlated with operating conditions and the observed characteristics of the fouling deposits.

2. Thermal Radiation in MHD Systems

Coal slags absorb, emit, and scatter thermal radiation because they are electrically conductive. Potassium atoms also absorb and emit thermal radiation similar to carbon dioxide and water vapor. Thus, in a combustion gas where

potassium atoms and submicron slag particles are also present, radiation heat transfer from the gas stream to the surrounding environments should include contributions from potassium atoms and slag particles, as well as from carbon dioxide and water vapor. Earlier theoretical studies[5,6] at ANL had indicated that, at high gas temperatures, the portion of the total radiation heat transfer from the combustion gas attributable to potassium atoms and slag particles could exceed the portion attributable to CO_2 and H_2O by a factor of two or more.

The purpose of the present work is to use a modified theoretical model to generate scale-up data on the effective emissivity of a gas containing carbon dioxide, water vapor, potassium atoms, and submicron slag particles for the design of MHD components. The radiant heat transfer model had been partially validated experimentally for combustion gases with and without potassium atoms in a gas temperature range from 1850 to 1950 K and a mean beam length of 0.6 m.[7,8] Comparisons between calculated and measured heat transfer data were in good agreement. Although the model was not validated experimentally for the effects of particle radiation on total gas emissivity, model predictions compared favorably with existing computational results in the literature.[9,10]

We used this model to generate scale-up data on total gas emissivity and absorptivity for the case of combustion of Illinois No. 6 coal, 1 wt % potassium in the combustion gas, combustion stoichiometric ratios ranging from 0.75 to 1.05, and slag carryover rates ranging from 10 to 100%. The scale-up data have been assembled in the format of standard Hottel charts (gas emissivity as a function of gas temperature for different mean beam lengths), which can be directly used by a design engineer. Calculations from these data (Fig. III-6) showed a significant effect of potassium atoms and slag particles on total gas emissivity, especially at high gas temperatures. This work also resulted in the development of a correlation to calculate the total gas absorptivity from the computed total gas emissivity.

---

[5]K. H. Im, R. K. Ahluwalia, and G. F. Berry, "Heat Transfer in Slagging MHD Radiant Boilers," Am. Inst. of Aeronautics and Astronautics, 19th Meeting, St. Louis, MO, Paper No. 81-0316 (1981).

[6]K. H. Im and R. K. Ahluwalia, "Nucleation of Slag and Seed in MHD Plants," paper presented to the 20th Symp. on Engineering Aspects of MHD, Irvine, CA (1982).

[7]C. S. Wang, L. S. H. Chow, and E. B. Smyk, "Thermal Radiation from Potassium Atoms in MHD Systems," 23rd Symp. on Engineering Aspects of MHD, Somerset, PA, June 24-27, 1986, pp. 686-700 (1986).

[8]S. S. Wang, L. S. H. Chow, and E. B. Smyk, "Experimental Investigations on Thermal Radiation from Potassium Atoms and Design Applications," *Radiation Heat Transfer*, B. F. Armaly and A. F. Emergy, eds., ASME HTD-Vol. 49, 23rd National Heat Transfer Conf., Denver, CO (1985).

[9]N. L. Krascella, *Theoretical Investigation of the Absorption and Scattering Characteristics of Small Particles*, National Aeronautics and Space Administration Report NASA CR-210 (1965).

[10]Van de Hulst, *Light Scattering by Small Particles*, John Wiley & Sons, Inc., New York, pp. 404-407 (1957).

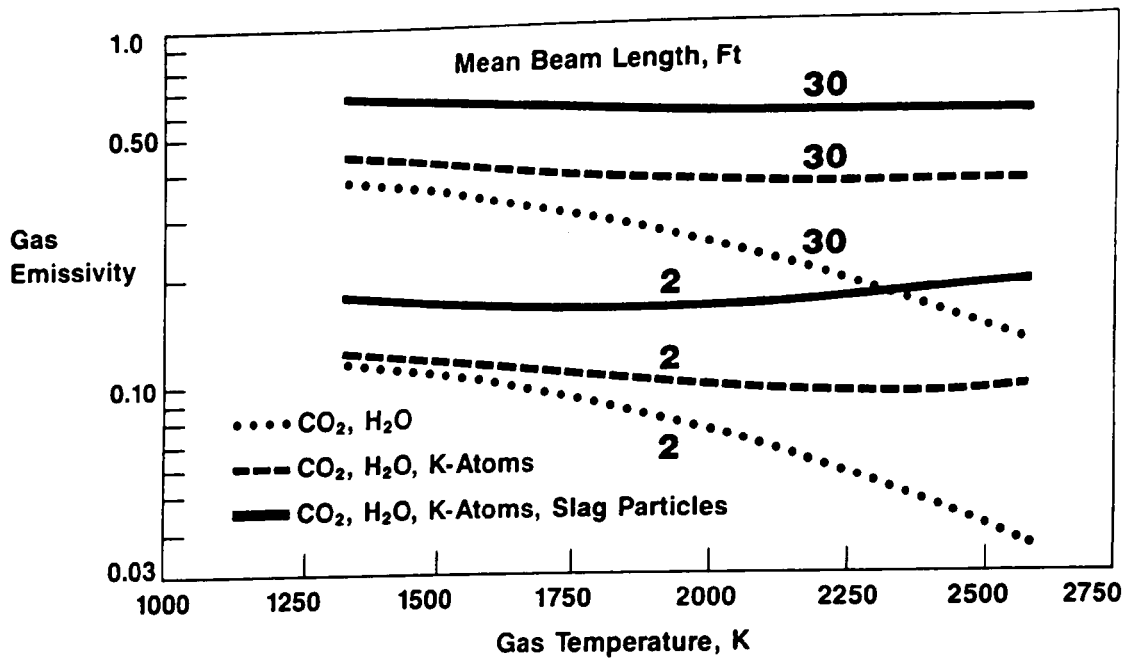

Fig. III-6. Total Gas Emissivity Chart Showing the Enhancement Effects of Potassium Atoms and Slag Particles

Additional tests in FEUL are planned to obtain experimental data on the enhancement in radiation heat transfer caused by potassium atoms and slag particles.

3. Interface Analysis

The objective of this work is to analyze the effect of the diffuser/boiler interface design on the potential for erosion and burnout of the back wall of the radiant boiler. As generally configured, gases flow through the MHD diffuser in the horizontal direction, whereas the flow is essentially vertical in the radiant boiler. In this design concept, the potential exists for severe damage to the boiler back wall because the gas jet from the diffuser strikes the back wall at high velocity and temperature.

The effects of the gas jet on the potential for burnout of the boiler back wall have been previously investigated.[11,12] An important parameter in these

[11]G. F. Berry, C. S. Wang, and U. S. Choi, *Analysis of Backwall Burnout in MHD Radiant Boilers*, Argonne National Laboratory Report ANL/MHD-86-1 (1986).

[12]G. F. Berry, C. S. Wang, and U.S. Choi, "The Effect of Impinging Particle-Laden Gas Jets on the Potential for Burnout in an MHD Radiant Boiler," in Proc. 24th Symp. on the Engineering, Butte, MT, June 24-27, 1986, pp. 169-174 (1986).

studies was refractory thickness, which is altered by both the high temperature at the back wall and erosion damage caused by ash and slag particles carried by the gas impacting the back wall. In the present work, the influence of diffuser design and interface conditions on the gas-velocity distribution and the velocity of the impinging particles is being investigated.

Fluid flow in MHD diffusers and radiant boilers is being simulated numerically using COMMIX-1B, a computer program developed at ANL for the analysis of three-dimensional incompressible fluid flows in nuclear reactors and validated against a variety of experimental data. The results are in reasonable agreement with the jet-flow calculations done in earlier ANL investigations of heat transfer to the back wall.[11,12]

To help determine erosion potential, we developed a simple one-dimensional particle transport code that assumes spherically shaped slag or ash particles in the gas stream. The centerline gas velocity in the diffuser and the calculated gas velocity in the radiant boiler are being used to calculate the impact velocity of the particles as a function of their radius. For small ash particles leaving the combustor (<10 μm), impact velocities are negligible; however, for larger slag particles that are shed by the MHD diffuser, the impact velocity is high (see Fig. III-7). This latter result is valid even if the diffuser can reduce the exit velocity to less than 100 m/s.

In future work, we will calculate the gas velocities in a diffuser/radiant boiler for a reference MHD design and will model the size distribution for particles leaving the walls of an MHD channel and becoming entrained in the gas flow through the channel and diffuser.

4. Materials Studies

A program is being initiated to conduct laboratory autoclave corrosion studies of candidate superheater and air-heater alloys exposed to simulated MHD conditions of gas temperature and chemistry, deposit chemistry, and metal temperatures. A test plan that includes test durations covering the range 500 to 8000 h has been developed in cooperation with Babcock & Wilcox and the University of Tennessee Space Institute (UTSI). The results of the tests will be compared with the results of materials performance in shorter-duration tests at the Coal Fired Flow Facility (CFFF), a bottoming-cycle pilot plant located at UTSI.

The necessary equipment to do the tests has been assembled and the preparation of the test specimens has been initiated. Babcock & Wilcox is participating in the preparation of various weldment specimens that will also be investigated. A supply of seed/ash deposits from the convective sections of CFFF has been obtained and will be applied to the surface of the specimens for the exposure tests. Actual testing is scheduled to begin during March 1987.

5. Combustor Additives to Control Sulfurous Emissions

Slag-rejecting cyclone combustors are being considered for their potential application to coal-fired gas turbine systems and to retrofitting of existing gas- and oil-fired boilers without extensive plant modifications or significant derating (owing to increased fouling). Screening tests were completed to investigate

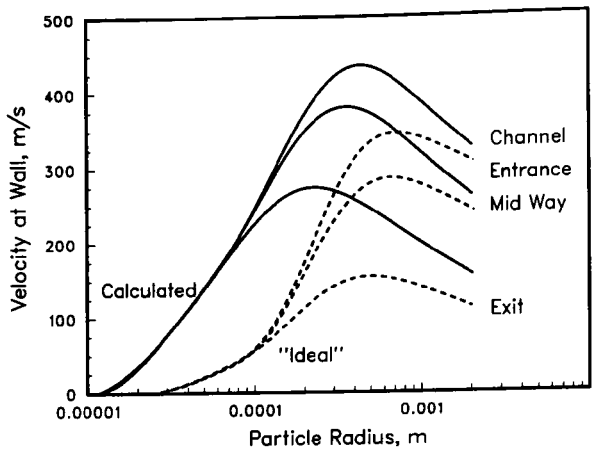

Fig. III-7.

Back-Wall Velocity of Particles (initially at rest) at Channel Entrance, Midpoint, and Exit for Calculated Centerline Gas Velocities and for Ideal Case of 100 m/s at Diffuser Exit

the potential for SO_x-NO_x control in a staged-cyclone coal combustor with limestone injection. These tests were performed in the FEUL coal-fired test leg, which consists of a primary combustion stage into which the coal and primary combustion air (axial and swirl) are injected, a secondary combustion stage, and a diagnostic section for gas sampling.

In work for DOE performed under a contract with Coal Tech Corp., tests were performed to investigate limestone injection into the first and/or second stages of the combustor for the control of SO_2 emissions. Primary air/fuel ratios were varied from 0.6 to 1.1; overall air/fuel ratios were from 1.2 to 1.8 during the tests; and Ca/S ratios were generally 1.5 to 3.5. Additional tests with pressure-hydrated limestone were performed under funding from the Illinois Coal Industry Committee through the Illinois Center for Research on Sulfur in Coal.

The coals used in the combustion tests were a finely pulverized West Virginia low-sulfur bituminous coal (0.8% S), an Illinois No. 6 medium-sulfur coal (1.5% S), and an Illinois No. 6 high-sulfur coal (3.0% S). With limestone injection in the first stage of the combustor and a separate injection in the second stage, SO_2 reductions of approximately 80% were obtained under several test conditions at Ca/S ratios of 2.5 to 3. Similar results were obtained during the injection of pressure-hydrated lime in the fuel-rich first combustion stage. Tests of sorbent injection indicated that the second-stage combustion temperature and Ca/S ratio are important factors in sulfur capture.

Nitrous oxide emissions measured at the exit of the second-stage combustor varied from 0.17 to 0.43 g NO_2/MJ (the current emission limit is 0.26 g NO_2/MJ). The benefits of a staged-cylone combustor for NO_x control were enhanced when the second-stage gas temperature was minimized, either through increasing second-stage air dilution or maximizing first-stage carbon conversion.

The results of the preliminary tests indicate that several factors control the sulfur capture process in the combustor, which are not as yet completely understood. The results indicate, however, that high sulfur capture meeting the

requirements of the New Source Performance Standards is feasible with direct sorbent injection in the cyclone combustor at conditions applicable to gas turbines. Further work is planned to investigate more fully the effect of second-stage combustor temperature on sulfur retention and the use of additives (such as $NaHCO_3$) to improve the performance of the limestone sorbents.

E. *Chemical Characterization of Polyethylene Pipe Materials*

United States gas utilities have been using polyethylene (PE) pipe for gas distribution systems for about the last 20 years. Utilization of plastic pipe offers a number of benefits to gas utilities and consumers through lower installation costs, reduced operating and maintenance costs, and possibly longer life because of the better corrosion resistance of polyethylene versus steel pipe. A minimum of 50-year service life is required for the PE pipe to achieve this potential. For the last three years, the Gas Research Institute (GRI) has funded this effort at Argonne for the purpose of characterization of PE resins and pipe materials on a chemical and molecular basis and correlation of these characterization data with mechanical properties and expected long-term performance.

To characterize the mechanical properties of the pipes, an extensive data base has been developed consisting primarily of results from constant tensile load (CTL) tests and ring tensile strength tests for 15 PE pipe samples. These experiments, carried out by ANL's Materials and Components Technology Division, provided measures of material resistance to stress rupture, stress relaxation, and crack growth. The chemical and molecular structures of the samples are being determined by the Analytical Chemistry Laboratory (Sec. IX). Coordination of this inter-divisional effort is being handled by the Coal and Municipal Waste Section of CMT.

The primary analytical techniques used for these chemical characterization studies include gas chromatography/mass spectrometry, ^{13}C nuclear magnetic resonance spectroscopy, gel permeation chromatography, differential scanning calorimetry, X-ray diffractometry, and inductively coupled plasma spectrometry. A large portion of the chemical-properties data base has been acquired, and efforts this year have been related to verification and improvement in the quality of certain aspects of the data base, as well as extensive statistical analysis of the chemical and mechanical data. The purpose of the statistical analysis is to identify correlations between the chemical and mechanical data that would permit specification of optimized chemical properties of the PE pipes during manufacture with respect to mechanical strength.

An example of the correlations found between certain chemical and mechanical properties of the pipes is shown in Fig. III-8, where the tensile strength of eight pipe samples is plotted versus the weight-average molecular weight (M_w) and the dispersivity (weight-average molecular weight/number-average molecular weight, M_w/M_n). Other molecular properties found to have strong correlation with mechanical strength of the pipe materials include crystallinity and preferred crystal orientation at the surface layers of the pipes.

During 1987, verification of the chemical properties studies and the statistical analyses will be completed. During 1988 and beyond, GRI is expected to fund a broader-based study in which pipe materials with optimized chemical properties are prepared and characterized.

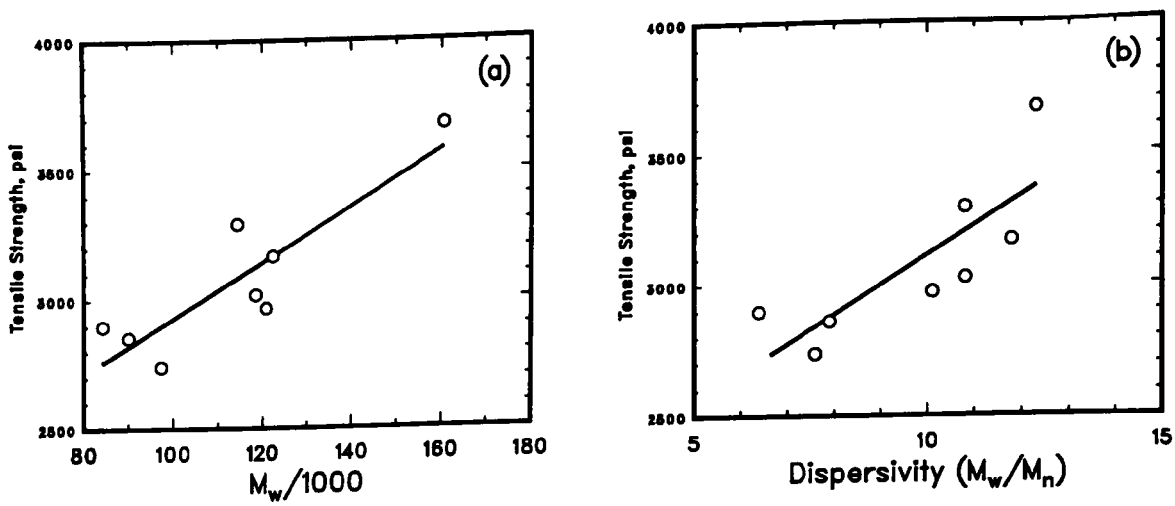

Fig. III-8. Tensile Strength as Function of Weight-Average Molecular Weight (a) and Dispersivity (b)

F. *CO_2 Recovery from Fossil Fuel Combustion*

Carbon dioxide has been proposed for use in enhanced oil recovery for certain types of oil fields. The CO_2 for this purpose would normally be derived from naturally occurring underground reservoirs. The Energy and Environmental Systems Division is involved in developing a novel concept for the economic and efficient recovery of CO_2 from fossil fuel combustion used in electric power or process steam generation. Under this concept, the fossil fuel would be burned in oxygen rather than in air; then, instead of separating CO_2 from the large quantity of nitrogen in flue gas, the CO_2 would be obtained as essentially the only noncondensable component of the flue gas. Part of the flue gas would be recycled back to the combustor to control the combustion temperature.

Staff from CMT were involved in the design, instrumentation, and coordination of a test of the Argonne concept at a small (2.2×10^6 Btu/h or 6.4×10^5 W) boiler located at the Black Hills Power Company's Service Center in Rapid City, South Dakota. The objective of the test was to demonstrate the concept in a utility setting, using the utility's own furnace operators and to determine if coal can be burned with oxygen and recycled flue gas without any deleterious effects on boiler operations.

A simple computer model of coal combustion under air-blown and oxygen-blown modes of operation was set up to calculate expected combustion and flue gas compositions as a function of recycle ratios and design purity of product CO_2. The results of one such set of calculations for an oxygen content of 5% and CO_2 purity of 95% (on a dry basis) in the product gas are shown in Fig. III-9; this figure shows the inlet (solid curves) and outlet (broken lines) gas compositions on a wet basis as a function of the recycle ratio. Also shown in Fig. III-9 is the calculated adiabatic flame temperature as a function of recycle ratio (dotted

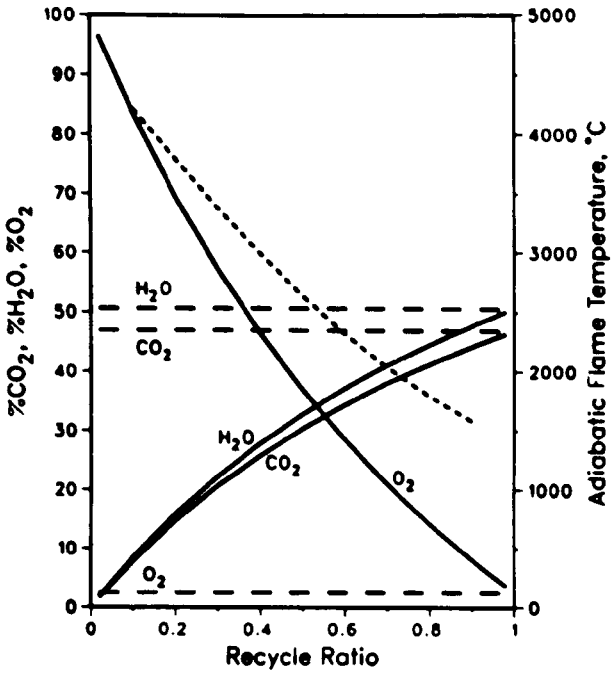

Fig. III-9.

The Effect of Recycle Ratio on the Wet-Basis Gas Compositions of the Furnace Inlet (solid curves) and Furnace Exhaust (broken lines) for an Idealized Furnace Producing 95% CO_2 and 5% O_2 on a Dry Basis. The dotted line shows the effect of the recycle ratio on the approximate adiabatic flame temperature.

curve). For Wyodak coal (4-5% ash, 30% water content) burned with 15% excess air, the adiabatic flame temperature is approximately 2000°C; to obtain a similar adiabatic flame temperature in the CO_2 production mode, Fig. III-9 shows that a recycle ratio of about 0.7 would be needed. Under these conditions, the furnace inlet gas would contain, on a wet basis, 38% CO_2, 41% H_2O, and 21% O_2 (assuming no inleakage of air into the system). For a specified concentration of CO_2 in the product gas, the concentrations of H_2O and O_2 in the flue gas are unaffected by the recycle ratio. Figure III-9 also shows that, under the recycle conditions, carbon dioxide and water vapor are present in approximately equal amounts for the entire range of recycle ratios. Thus, the combustion and flue gases have a relatively high water vapor content, which must be taken into account in designing the recirculation system.

For full-load operation with 0.7 recycle ratio, the overall material balance and the boiler's fuel, oxygen, and gas flow rates are shown in Fig. III-10. Thus, while the oxygen feed rate is 71.5 scfm (0.034 m^3/s), the combustion gas flow rate is more than five times that, 369 scfm (0.174 m^3s). The net flue gas production at full load (on a dry basis) is 64.8 scfm (0.030 m^3/s), 95% of which is CO_2.

The first tests of the concept were at least partially successful. Switching from the air-blown to the oxygen-blown mode could be carried out in a matter of minutes by the utility's operators. No significant operational problems were noted during the tests. However, because of inleakage of air at various points in the system, the nitrogen concentration in the flue gas could not be reduced below 54%. The major sources of air inleakage were identified to be the furnace brick-work, the induced draft fan, the ash handling system, and various penetrations into the furnace and gas supply and exhaust lines, including the coal feed hoppers.

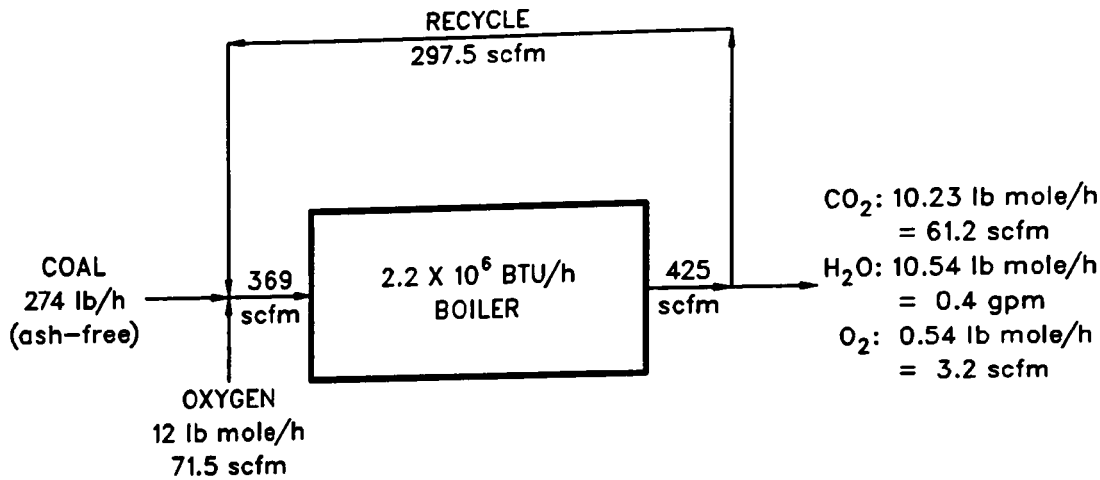

Fig. III-10. Coal, Oxygen Feed, Product and Recycle Gas Flow Rates for Test Boiler under Full Load with 70% Flue Gas Recycle

A second series of tests was conducted after attempts were made to seal up the furnace as much as possible to reduce the unwanted inleakage of air. The brickwork was patched up with a refractory cement, the induced draft fan was sealed to the extent possible, an isolation valve was installed in the ash disposal system, the furnace doors were re-gasketed, and the various penetrations were sealed. As a result, the highest concentration of CO_2 was increased from about 22% produced in the first series of tests to over 48% in the second series of tests. However, a stoker fired furnace has inherent limitations that prevent its being sealed up completely, and no further attempts are being made to tighten up the furnace.

These tests were valuable in several respects: they (1) showed that the Argonne concept of producing CO_2 from utility fossil fuel combustion for recovery and use is feasible, (2) demonstrated that there are no deleterious side effects of coal combustion with oxygen and recycled flue gas, (3) showed that such a process can be conducted in a utility setting and by the utility's own operators without special training, (4) identified strict sealing requirements for the process to work well, and (5) provided much needed information on furnace behavior when operated in the CO_2 production mode.

IV. ELECTROMAGNETIC CONTINUOUS CASTING OF STEEL SHEET

Argonne National Laboratory has recently started a cooperative R&D program with the steel industry. The overall objective is to improve the competitiveness of the domestic steel industry through the development of advanced technology that substantially reduces equipment, operating, and energy costs. The primary purpose of the CMT effort is to develop an electromagnetic process for the continuous casting of various grades of steel in large-aspect-ratio shapes such as steel strip. This electromagnetic continuous casting (EMCC) process should also be applicable to the casting of other shapes such as tubes, squares, slabs, and "dogbones"; however, the primary focus will be on the casting of thin strips or sheets. The application of electromagnetic technology to attain stable liquid-metal containment and control will be supported by development efforts on a heat transfer and cooling system and liquid-metal feed system. The cast product will be evaluated for quality. Additionally, efforts will be directed toward the development, as needed, of models and sensors for process control and innovative techniques for the removal of nonmetallic inclusions from molten steel.

This project consists of three phases, involving development and testing of (1) bench-scale electromagnetic casters, (2) a laboratory-scale electromagnetic caster, and (3) a pilot-scale demonstration plant. Phase 1 is expected to require about two years and Phase 2, about three years. Phase 3 will be the responsibility of the steel industry, with ANL providing technical support as appropriate.

A. *Background*

Electromagnetic fields, alone or in combination with mechanical systems, have potential for innovative application in the continuous casting of steel with large-aspect-ratio shapes. The success achieved with this technology by the aluminum industry provides confidence that electromagnetic technologies can be successfully developed for this purpose. The electromagnetic casting process presently used by the U.S. aluminum industry is based on developments in the USSR in the late sixties and subsequent refinement of the process by Alusuisse (Swiss Aluminum Ltd.). Since the present electromagnetic casting of aluminum uses a batch rather than a continuous casting system and is designed primarily for the casting of slabs or ingots, the Alusuisse method is unsuitable for EMCC of thin strips or sheets with large aspect ratios. Aluminum ingots produced by this process have very smooth surfaces, little liquation, uniform distribution of alloying elements, excellent microstructure (particularly on outer surfaces), and good workability. Economic benefits reported include elimination of scalping, less edge trim, increased rate of metal solidification, and good product consistency. Evaluation and assessment of the critical factors for this process (such as molten-metal treatment, molten-metal handling and distribution, inductor mold and bottom block design, power supply control, liquid-metal hydraulic head, and casting drop rate) are expected to be important for EMCC of steel. However, it should be noted that the goal of this project surpasses what has been achieved thus far by the aluminum industry. Specifically, this project is directed toward the development of an EMCC process for large-aspect-ratio shapes requiring a

minimum of additional thermal-mechanical treatment. Realization of this goal would result in a significant reduction in the equipment, manpower, and energy needed in the present processing of slabs and ingots. The application of electromagnetic technology to the casting of steel is expected to be more difficult than was the case for aluminum because of the higher temperature and density (ferrostatic head) of liquid steel.

B. *Recent Progress*

The work plan for this project was implemented on a small scale during FY 1985. In FY 1986, efforts were directed toward (1) a review of the current status of electromagnetic technologies in casting metals; (2) an analysis of the electromagnetic, thermal-hydraulic, and fluid-dynamic requirements for a continuous casting operation; and (3) a preliminary design for a bench-top electromagnetic caster for the initial casting studies.

We defined the electromagnetic requirements in terms of field strength, shape, spatial distribution, and frequency for casting large-aspect-ratio shapes. This analysis included both vertical and horizontal casting orientations and different casting speeds. In addition, we determined the heat transfer requirements in terms of melt superheat, mass flow rate, coolant designs, and induced heating from the electromagnet. Different coolant systems were considered.

Heat-transfer and fluid-dynamic analyses are underway to establish the boundary conditions and limitations with regard to coolant composition, flow rates, and coolant methodologies. The development of the liquid-metal feed system is also being addressed.

The design, fabrication, and setup of the "head-start" experimental magnet were completed and experimentation initiated. The major objective of this experiment is to establish the boundary conditions for liquid-metal stability in a high-velocity coolant system and to confirm theoretical predictions concerning the extent of suppression of these instabilities in the presence of a high-frequency magnetic field. Tests are being run with and without an electromagnetic field. The tests without an electromagnetic field are designed to establish the initiating conditions for surface disturbances. The tests with an electromagnetic field are aimed at determining the magnitude of the restoring forces at which the surface disturbances subside.

The preliminary results from the head-start magnet were useful in selecting the boundary and operating conditions for a test magnet and finalizing the design. The test magnet will be used to investigate magnetohydrodynamic stabilities in molten metals, to determine critical magnet design features, and to serve as a diagnostic tool for problems that may arise in the work with the bench-top caster.

C. *Future Work*

Instrumentation and testing of the test magnet will be completed to select the design parameters for the bench-top electromagnetic caster, and the electromagnetic requirements and limitations will be finalized. A bench-top

electromagnetic casting facility will be designed and constructed, and initial experiments to determine the process variables (e.g., liquid metal/magnetic field interaction under flow conditions) will be conducted. Also, efforts will continue on development of the liquid-metal feed system, a coolant system, sensors, and process control systems.

V. HAZARDOUS WASTE TREATMENT RESEARCH

Two efforts are underway in hazardous waste treatment research. The first addresses the problems associated with the disposal of reactive metals such as sodium; the second deals with the application of microwave energy to assist in the chemical conversion/detoxification of chlorinated hydrocarbons. The objective of these efforts is to develop processes for the conversion of hazardous waste material into forms that are nontoxic and suitable for disposal. A third effort is underway to determine the effects of a decontamination agent on soil bacteria.

A. *Improved Treatment/Disposal of Reactive Metal Wastes*

The objective of this effort is to develop an integrated process for the conversion of hazardous reactive metals into a stable waste form, such as a glass, for disposal. The process is "integrated" in that the reactive metal, along with its radioactive contaminants, is borne by an N_2 stream into a reactor at the same time as an air stream (which contains a glass-forming material, e.g., SiO_2) is introduced to oxidize the sodium. Thus, the conversion of the metal to the oxide occurs in the same step as the glass is formed.

For this study, sodium was selected as the reactive metal. The main consideration that determines the acceptability of a sodium waste form is its chemical reactivity with water (liquid or vapor), oxygen, and carbon dioxide. A secondary concern is the effect of groundwaters at the disposal site with regard to the solubility of the sodium waste and the leachability of its trace contaminants. Although relatively water-soluble but stable chemical forms of sodium (such as sodium carbonate) are considered acceptable, a low-solubility waste form, such as a glass, is considered more desirable.

Our effort to identify an appropriate glass for the process consists of three parts: (1) preparation of glass samples using various compositions of sodium carbonate, silicon dioxide, and other components such as calcium oxide, magnesium oxide, or alumina, (2) preliminary leaching studies of the sodium oxide/silica glass in deionized water, and (3) differential thermal analysis of sodium oxide/silica blends.

The composition of the glass waste form is an important consideration. Ideally, the glass should be low in cost and readily available and should have certain physical properties (e.g., low viscosity and low leachability). In addition, the volume of the final form should be as compact as possible to minimize cost and effort in its transport and storage. We prepared sodium-containing glasses in platinum crucibles, using accurate weights of the different glass components. After being heated overnight at 900°C to achieve the calculated weight loss from the decomposition of the carbonates, the blends were brought to the appropriate temperatures to convert the sintered material to glass. Several compositions of glass were made using this technique. These glasses were inspected visually for viscosity, and some were then measured for leachability.

Preliminary leaching studies of glass fibers with a sodium oxide/silica in the molar ratio of 1:2 were carried out using deionized water in Teflon containers at room temperature. The ratio of sample surface area to the volume of the

deionized water was maintained constant. Samples of the water were removed periodically and analyzed for sodium. Over a 10,000-min period, the leaching rate of the glass was 78 μg sodium per square millimeter of the glass surface.

Differential thermal analysis (DTA) of a series of sodium oxide-silica blends was carried out in a DTA furnace by heating the samples to 1250°C at a steady predetermined rate. Significant thermal events were recorded on a strip chart recorder as exothermic or endothermic signals. A typical DTA curve can be seen in Fig. V-1. The reaction temperature was usually around 275°C. Melting occurred at 1030°C, and a recrystallization step, which was endothermic, was evident at 835°C on cooling.

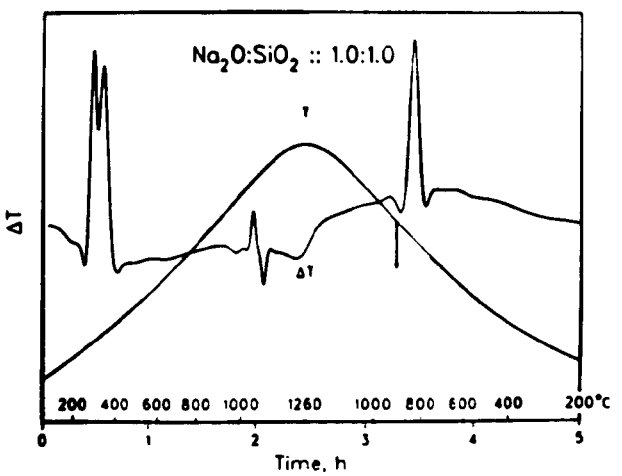

Fig. V-1.

Differential Thermal Analysis Curve for 1:1 $Na_2O:SiO_2$ Sample

A conceptual design was developed for an integrated process to convert sodium to a soda-silica-lime glass form. A low-g and low-pressure drop cyclone designed to withstand high operating temperatures is used as the reactor. The solid reactants are introduced to the reactor as a suspension in the combustion air for sodium. Liquid sodium is injected into the reactor using nitrogen as an aspirator and atomizer. The reactions occur primarily at the walls of the cyclone reactor, and the product glass is withdrawn from the bottom of the reactor. The metal containment of the reactor is lined with glass-type refractories. Because a protective layer of the product forms early in the reaction, no damage to the reactor is expected. Heater elements in the reactor are used as needed to keep the reaction temperature at an appropriate level to ensure that the product flows smoothly. Preliminary material and energy flows are shown in Fig. V-2.

Calculations indicate that the combined sodium oxidization and glass formation reaction may or may not be self-sufficient in energy, depending on the glass composition chosen. For two gram atoms of sodium reacting with one-half mole of oxygen and two moles of silica, the overall reaction to form the disilicate is exothermic. When the amount of silica is increased, the excess energy decreases, primarily because of the higher reaction temperature. If some of the reactants are provided as the carbonate, the additional energy needed to decompose the carbonates would make the process endothermic, and external energy would be required, probably in the form of a fuel gas. Detailed process material and energy balance calculations will be completed after an acceptable glass composition is more clearly defined.

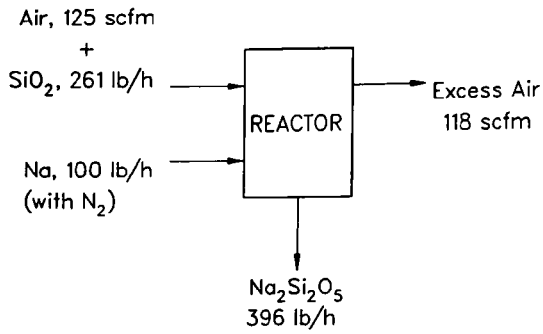

Fig. V-2.

Materials and Energy Flows for Integrated Process to Convert Sodium Waste to Glass

B. *Microwave-Assisted Chemical Process for Treatment of Hazardous Waste*

The objective of this effort is to determine the technical feasibility of using a microwave-assisted chemical process for detoxification (i.e., conversion into harmless products) of hazardous waste. Microwaves provide rapid and uniform heating in high-dielectric-loss materials. Since heat can be transferred to reactants *in situ*, chemical reactions can be conducted without heating the entire reaction vessel. Thus, energy use is expected to be more efficient with the microwave-assisted process than with traditional thermal-heating processes.

Trichloroethylene (TCE) is a major constituent of many of the waste streams documented in the waste data base of the Oak Ridge National Laboratory, Hazardous Defense Waste Program (ORNL-HDWP)[1]; for this reason, liquid TCE was selected for our detoxification study. To carry out this work, we modified a microwave oven (600-W output) to energize a flowthrough quartz-tube reactor (20-25 cm long and 12-mm ID). The TCE detoxification was completed in a two-step process: (1) TCE from a TCE-saturated nitrogen stream was adsorbed on active carbon beds (with and without Cr and Cu catalysts that have surface areas of ~1000 m^2/g) and packed inside the quartz-tube reactor at room temperature, and (2) the carbon bed was heated by microwave radiation to moderate temperatures (<400°C) while a stream of nitrogen or moist air was passed through it. The detoxification of TCE preadsorbed on active carbon and then exposed to a moist air stream under microwave heating can probably be described by the reaction

$$C_2HCl_3 + O_2 + H_2O \rightarrow 3HCl + CO + CO_2$$

This reaction is complex because it involves, in part, catalysis, hydrogen abstraction, and thermal decomposition.

As expected, when the carbon bed was heated, the TCE was readily detoxified (i.e., converted into HCl, CO_2, CO, and $C_2H_2Cl_2$). The fraction of TCE converted during oxidative degradation can be estimated in the following manner. Since the original TCE is converted into HCl gas and is also absorbed in carbon by reaction, the amount of TCE converted may be derived from the

[1]C. S. Fore, Oak Ridge National Laboratory, unpublished information.

sum of the original chlorine loadings retained in the carbon and the chloride loading in the gas phase. The total conversion of TCE into degradation products, on this basis, turned out to be greater than 80 wt %. The oxidative degradation of TCE observed was highest with catalyst-loaded active carbon and moist air rather than the nitrogen stream. Preliminary data obtained on an analogous process conducted with traditional thermal heating indicated much lower conversion of TCE (~12%), even at 600°C. By avoiding the high temperatures of traditional thermal-heating processes, microwave heating allows better detoxification of hazardous wastes.

In separate experiments, we found that used-carbon beds could be regenerated by microwave heating under a moist N_2 stream or, better still, a moist air stream. Several Japanese patents support our observed results on the regeneration of used carbon.

The research completed during this past year has laid the groundwork for the successful demonstration of new technologies for microwave-assisted detoxification of liquid hazardous organic wastes. For future experiments, a 6-kW microwave heating system has been designed and fabricated.

C. *Chemical Effects on Soil Bacteria*

The objective of this program is to measure the effect of a U.S. Army decontamination agent C-8 [a mixture of calcium hypochlorite (7-8%), perchloroethylene (15%), water (~76%), and nonionic detergents (1%)][a] on populations of normal soil microorganisms. The agent is presently used by the Army to treat surfaces that have been exposed to chemical or biological agents. The Army is interested in C-8's effect on soil microorganisms since C-8 is often spilled on the ground. Although the agent is diluted with water during normal use, we have employed both the concentrated and diluted mixture in our experiments because some of the concentrated mixture might be spilled accidently during dilution. This program is a joint effort with ANL's Energy and Environmental Systems Division.

To simulate the passage of C-8 down through the layers of normal soil, we prepared a number of relatively undisturbed soil cores, approximately four inches across and two feet deep. The cores were placed in glass columns, so that fluid passing through the soil could be collected from the bottom and analyzed. The decontamination agent, either concentrated or diluted with water, was placed on the surface of the soil and allowed to drain through. Some of the columns received additional liquid, in the form of a simulated acid rain, in order to dilute the agent and wash the components further into the soil. Fluid emerging from the bottom of the column was analyzed by gas chromatography. Finally, some of the columns were disassembled, and soil samples from several depths were removed for biological analysis.

[a] The values given are for the concentrated material; the dilute material is formed by diluting 30:1 with water.

Each sample was tested for the presence of different groups of soil microbes, such as filamentous fungi, sulfate-reducing bacteria, anaerobic bacteria, or enteric bacteria. Previous work had shown which general groups of soil microbes were present in the chosen soil area, and which of these might be suitable for this project. In this phase of the work, no attempt was made to classify individual bacteria or fungi. Each group of organisms contained several different, but related, species.

From each soil sample, individual microbes were encouraged to multiply and form many-cell colonies on a prepared growth medium. Each medium contained a different collection of growth-promoting substances and inhibitory chemicals. Occasionally, media were formulated to detect compounds produced by the colonies. Using this method, the number of successful colonies on a particular medium is an indication of the presence and viability of that selected group of organism. Although this technique is very sensitive, it does not detect cells that are alive but, for some reason, unable to multiply.

The results of our experiments indicate that many bacteria, such as those that required only minimal nutrients or those that degrade pectin, are not significantly harmed by the components of the decontamination mixture. Recovery of these types of bacteria matched the results of control columns, even in those regions of the soil that contained high concentrations of calcium hypochlorite. These results, although somewhat surprising, are thought to indicate that much of the hypochlorite is still emulsified, and thus is not available to the cells. Hypochlorite that is released from the emulsion may be rapidly neutralized by soil components. In fact, preliminary experiments have indicated that this soil has considerable ability to bind or chemically reduce the hypochlorite.

Organisms that were killed by the concentrated C-8 emulsion include gram-positive anaerobic bacteria, bacteria that produce hydrogen sulfide, most filamentous soil fungi, and several slow-growing bacteria grown on minimum nutrients. However, C-8 that had been diluted normally (termed "simulated waste water"), as it would be for use in surface decontamination, had no measurable effect on these groups. The effect of agent C-8 on the "minimum-nutrient" bacteria is shown in Fig. V-3.

An unexpected result of the studies was that the growth of a few species of bacteria was actually enhanced by exposure to the decontamination agent. It is not yet known if these bacteria represent helpful, or harmful, species.

Additional experiments in which a modified Ames test was used to indicate the presence of mutagenic chemicals determined that, within the sensitivity of the test, agent C-8 did not create or contain mutagenic compounds.

In general, the bacteria found in soil are poorly characterized. For many studies, it is therefore beneficial to include "tracer" bacteria, which are laboratory strains whose sensitivity and metabolic potential have been established. Information on the survival of tracers exposed to hazardous wastes would be very useful, for example, should it ever become possible to introduce special bacterial strains into the soil to decontaminate dump sites. Two varieties of tracer

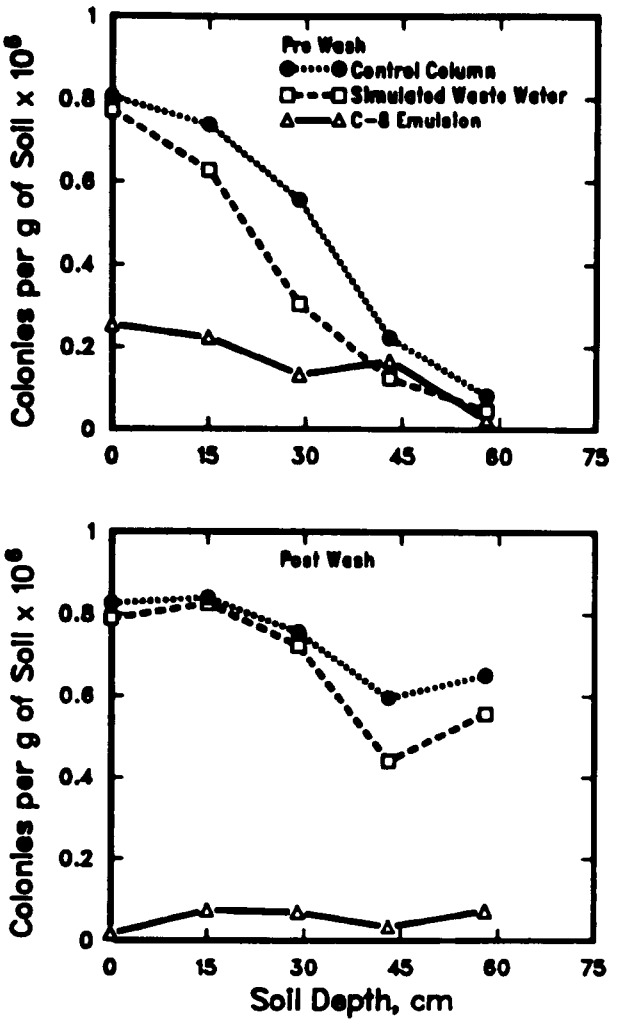

Fig. V-3.

Effect of Agent C-8 on "Minimum-Nutrient" Bacteria. Results are shown for both concentrated (C-8 emulsion) and dilute (simulated waste water) solutions.

bacteria were used in this study. The first, an antibiotic-resistant strain of *E. coli*, showed only limited recovery and was apparently effectively killed by concentrated decontamination agent. The second tracer, an azide-resistant streptococcus that was especially isolated for use in these experiments, was easily recovered and unharmed by any of the manipulations.

VI. NUCLEAR WASTE MANAGEMENT AND FUEL REPROCESSING

This CMT effort is (1) examining waste-package performance in potential high-level waste repositories located in tuff and basalt, (2) developing a process for the extraction, separation, and recovery of transuranic elements in a nuclear waste stream, and (3) developing a reprocessing method for the core fuel and blanket material of a sodium-cooled fast reactor.

A. *High-Level Waste/Repository Interactions*

For this effort, we are examining waste package performance for potential high-level waste repositories located in tuff and basalt. The potential repository in tuff is located at Yucca Mountain, Nevada, and the work is sponsored by the Nevada Nuclear Waste Storage Investigations (NNWSI) project. The potential basalt repository is located in the basalt flows of the Hanford Reservation, Washington, and the work is sponsored by the Basalt Waste Isolation Project (BWIP).

Work for NNWSI includes determination of waste form (glass and spent fuel) performance and repository analog test development, studies of glass reactions in saturated and unsaturated environments, and an examination of the effects of penetrating gamma radiation on the waste package environment. Emphasis of these activities has been to study materials interactions in a fashion which realistically reproduces conditions anticipated to exist in a high-level waste repository thousands of years after waste emplacement. This work is ongoing and has been described in previous CMT annual reports. (See, for example, Ref. 1.)

The work for the BWIP has centered in two areas: effects of radiation on the near-field waste package environment and development of sensitive laser-based techniques to study the behavior of actinide elements in basalt groundwater. Each of these activities is discussed below.

1. Laser Photoacoustic Spectroscopy for Trace-Level Detection of Actinides in Groundwater

a. Introduction

One aspect of the BWIP effort is to develop an understanding of the chemical behavior of radionuclides in the near-field environment of the waste container. Such information is needed to determine radionuclide release rates from the waste package and to make long-term projections of repository performance. To accomplish this, ultrasensitive laser-based techniques, such as laser photoacoustic spectroscopy (LPAS) and laser induced fluorescence (LIF), are being developed as analytical methods for the trace-level detection and speciation of actinides in solutions typical of those encountered in groundwaters near the BWIP repository.

---

[1]M. J. Steindler et al., *Chemical Technology Division Annual Technical Report, 1985*, Argonne National Laboratory Report ANL-86-14, pp. 75-78 (1986).

These sensitive spectroscopic methods are being developed because initial characterization of the repository environment has suggested that those actinide elements of greatest interest to long-term repository performance (Pu and Am) will be quite insoluble in the BWIP groundwater. These techniques will provide the most-refined data possible to be used as input for development and validation of codes that will be used to describe and project repository performance. The most-useful application of the techniques will be when applied directly to conditions anticipated to exist in the repository after containment failure. Such conditions include repository groundwater at elevated temperature in contact with waste package components. Studies done using *in situ* conditions will allow the qualitative aspects of actinide complexation to be examined as a function of the redox state of the experimental system and will provide data to support steady-state solubility studies being done in other parts of the BWIP program.

This work is being done as a joint effort by the High Level Waste/Repository Interactions Group (CMT), the Analytical Chemistry Laboratory (CMT), and the Heavy Metal Group (Chemistry Division).

b. Background

Optical absorption spectroscopy can be used to characterize actinide complexes in solution because the "fingerprint" of the observed f-f transitions allows identification of the element and oxidation state in favorable cases. Spectra are available for most of the oxidation states of actinide ions, generally in favorable acid solutions or solid phases, and they indicate that, while unique, such optical transitions are weak. As a consequence, conventional absorption spectrometers, which rely on pronounced differences in light absorption, are too insensitive for trace-level detection of actinides. Recently, LPAS was utilized for oxidation-state-specific detection and speciation of actinides in aqueous solution.[2] Using this technique, detection limits of 10^{-6} to 10^{-8}M were obtained for several actinides in acid media.[3]

The conditions of interest to BWIP (e.g., elevated temperature, groundwater samples, equilibration with waste package components such as mineral phases and carbon steel) are not those that have been routinely pursued by groups studying actinide chemistry. However, information and established descriptions of actinide speciation that have been collected under specialized conditions will be useful in guiding the development of the present experimental setup and in interpreting what likely will be complex spectra.

For example, groundwater samples are different from simple solutions because they will contain a variety of metal ions and complexing ligands. Basalt groundwater of interest to the BWIP effort contains carbonate, sulfate, fluoride, and other anions that are capable of complexing actinide ions. Since both the electronic structure and the transition intensities of actinide ions are influenced by ligand field effects, care will have to be exercised when applying the literature data for the acid solution and the solid to the interpretation of

---

[2]C. K. N. Patel and A. C. Tam, Rev. Mod. Phys. **53**, 517-550 (1981).

[3]R. Stumpe, J. I. Kim, and H. Walther, Appl. Phys. B, **34**, 203-206 (1984).

spectra collected for groundwater. However, we expect that complexed actinides in near-neutral pH solutions will exhibit "fingerprint" spectra involving 5f electronic states, and that selective modification of the groundwater chemistry will allow us to develop a working theory that describes the character of spectra under varying repository conditions.

The nature of the species formed will also likely depend on several parameters, including temperature. Maximum temperatures on the order of 150°C are anticipated during the isolation period. Oxidation state distributions, stability, and solubility constants are temperature dependent, and the temperature dependence of each of these factors will need to be incorporated into models describing repository performance. To date, few thermodynamic solution data concerning actinides at temperatures above 25°C are available, and common methods used to extrapolate these data to higher temperatures do not take into account the potential changes in complexation that may occur as the temperature is increased. This accentuates the importance in collecting spectra for conditions that are repository relevant.

c. Experimental

A schematic of the experimental arrangement is shown in Fig. VI-1. The excitation source is a dye laser (Molectron DL16) pumped by the third harmonic of a Nd^{3+}/YAG laser (Quanta-Ray DCR-2A). This laser system was operated at a maximum energy of 3 mJ at a frequency of 10 Hz, as determined by two energy monitors located downfield from the sample cells. The bandwidth of the laser was <1 cm^{-1} and its pulse width was ~5 ns.

The output of the laser was directed into the sample compartments of a single-beam, dual-channel, photoacoustic spectrometer. This arrangement allowed real-time subtraction of the photoacoustic signal due to optical absorbance of water. The blank (GR-4 water, which is a synthetic basaltic groundwater, or 0.1 M $HClO_4$) and sample solutions, contained in quartz cuvettes, were housed in aluminum blocks capable of heating the solutions to temperatures above 80°C. For experiments above ambient temperature, the cells were sealed under partial vacuum. To prevent condensation onto the upper surfaces, the portion of the sealed cell above the liquid/air interface was maintained at a temperature slightly greater than the solution. Acoustic contact to the cell was achieved by means of a quartz rod (1-cm dia by 10-cm long), which, in turn, was in contact with a silvered mirror. Contact with a piezoelectric transducer (PZT) (Transducer Products LTZ-2) was made through a thin, stainless steel membrane that was part of the housing which was in contact with the mirror. This combination eliminated problems associated with scattered light (with ~40% loss in acoustic signal) and isolated the transducer from the adverse effects of elevated temperature. To improve acoustic contact, a thin layer of chloro-fluorocarbon grease was applied to all appropriate surfaces.

d. Results and Discussion

Preliminary experiments to determine the overall sensitivity of the apparatus were performed by two different methods.

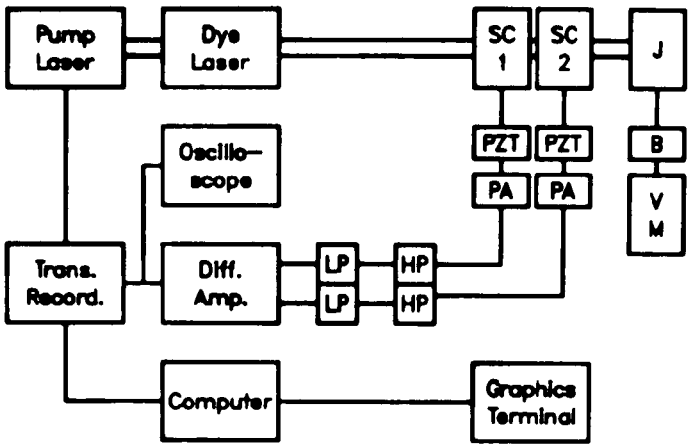

Fig. VI-1. Block Diagram of Single-Beam, Dual-Channel, Laser Photo-acoustic Spectrometer. The major components are as follows:

COMPUTER	Digital Equipment Corp. 11/23+.
DIFFERENTIAL AMPLIFIER	Tektronix AM502.
VM	Digital voltmeter.
DYE LASER	Molectron DL16 dye laser with home-built post amplifier. Typical output energy was a 3 mJ/pulse in a 5-ns pulse.
HP	High pass electrical filter, 10th order design, passive components.
J	Molectron Joulemeter.
LP	Low pass electrical filter, 1st order design, passive components.
PRE-AMP (PA)	Analog Devices 50K operational amplifier in a custom-designed, variable gain circuit.
PUMP LASER	Quanta Ray DCR-2A operated at 355 nm at 10 Hz rep. rate.
PZT	9-mm dia by 5-mm thick solid cylinder piezoelectric transducer (LTZ-5A material) in stainless steel housing.
SC	Sample cell, 1-cm long x 1-cm ID, quartz, polished five sides.
TRANSIENT RECORDER	LeCroy TR8818 (10 ns per channel best time resolution).
B	Brookdeal linear gate.

The first method was based on measurements of signal-to-noise ratio using a single PZT transducer in direct contact with the sample cell and a solute with an absorption band that was narrow compared with the rate of change of the absorbance of water. The solute that was selected was holmium perchlorate present at a concentration of 0.00487 M in perchloric acid. The molar absorptivity of the 450.7 nm band of Ho(III) is 3.90 M^{-1} cm^{-1}. Based on repeated signal averaging runs, the signal-to-noise ratio achieved with this solution was 700, averaged over 100 laser shots. This corresponds to a detection sensitivity (signal-to-noise ratio of 1) of about 2.8 x 10^{-5} absorbance units (a.u.) per centimeter of optical path through the sample solution. These results were confirmed by eliminating the contribution of water absorption in the excitation spectrum of 2 x 10^{-4} M Ho(III) in the 460-500 nm region, using the differential mode of operation (see Fig. VI-2). The peak at 486 nm has a molar extinction coefficient of 1.89 M^{-1} cm^{-1}. Averaging 100 laser shots for each resolution element, a signal-to-noise ratio of 15 was obtained. Thus, for a signal-to-noise ratio of 1, the limit of detection is 2 x 10^{-5} a.u. per cm of path length.

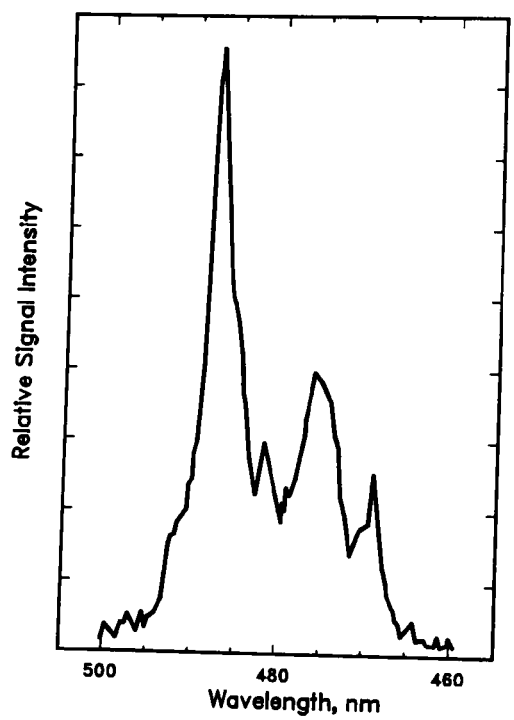

Fig. VI-2.

Differential Photoacoustic Spectrum of 2 x 10^{-4} M Ho^{3+} in Dilute $HClO_4$. Spectrum not corrected for dye laser intensity.

The second method was based on measured dilution curves using the difference photoacoustic signal between sample (anolyte and solvent) and reference channels (neat solvent). For this study, the uranyl ion in 0.1 M perchloric acid was selected. Using 427 nm excitation and interpolating between data points on the dilution curve, we found that a signal-to-noise ratio of 1 occurs at 7 x 10^{-6} M uranyl; the molar absorptivity of uranyl at 427 nm is 5.9 M^{-1} cm^{-1}. Thus, the sensitivity of the laser photoacoustic spectrometer used in the differential mode is equivalent to an absorbance of 4 x 10^{-5} a.u. per cm.

e. Conclusions

The sensitivity that we achieved using the single-beam, dual-channel, laser photoacoustic spectrometer is essentially identical to that reported by Kim et al.[3] for work at 22°C (~10^{-5} a.u. per cm). Minor differences are likely, due to the methods used for interpretation of data. The main difficulty encountered in the initial phases of our work was the lack of reproducibility. Subsequent developments, which minimized scattered laser light and the presence of suspended particulate matter, have largely eliminated this problem. The LPAS system has been tested in single and dual channel modes at 76°C using uranyl in GR-4 groundwater. In preliminary investigations, we observed an improved sensitivity in aqueous solution at high temperatures, as expected from photoacoustic theory. In the spectral range investigated, the absorption of water is not a significant limiting factor; however, the need for differential measurements increases [e.g., Pu(VI) absorption at 830 nm] where water absorption is significant. Based on the reported absorption spectra of uranyl carbonato complexes,[4] the observed photoacoustic spectra do not arise from a simple mixture of di- and tri-carbonato species.

The high sensitivity of the LPAS technique in aqueous solution at temperatures to 100°C and beyond recommends it for actinide speciation studies in basalt groundwater. Future LPAS work will emphasize transuranic elements of interest to the BWIP effort in synthetic groundwater solution.

2. Effects of Gamma Radiolysis on Waste Package Components

The emplacement of nuclear waste in a repository will increase the temperature of the waste package environment and subject the package to ionizing radiation. The predominant type of ionizing radiation, outside the container, during the "saturated post-closure period" (which begins at full saturation of the repository and ends at the time of container failure) is gamma radiation. Much of our effort has, therefore, been directed toward studying the effects of gamma radiation on the waste package components in a hydrothermal, basaltic environment. Some of the questions that are currently being addressed are:

1. What is the effect of repository conditions on the yield of the primary radiolytic species, H_2?

2. What effect will gamma radiation and hydrothermal conditions have on CH_4, which has been found in some sections of the proposed repository?

3. What are the long-term effects of gamma radiation on the environment of the waste package? Specifically, is there a radiolytic enhancement of container corrosion?

These questions have been examined previously but have not been answered completely.

---

[4]J. P. Scanlan, J. Inorg. Nucl. Chem. 39, 625-639 (1977).

The current group of experiments was designed to measure the effects of irradiating groundwater containing small amounts of CH_4 at a dose rate of $\leq 10^4$ rad/h. The design of these experiments should permit answers to be given to the questions posed.

The components of the waste package were exposed to a gamma radiation field of 10^4 rad/h while the following conditions were maintained in low-carbon steel pressure vessels: T = 200°C, P $\geq$ 70 bars (7 MPa) hydrostatic pressure, total dose = 7.4 x 10^6 and 15 x 10^6 rad. The test components were GR4 groundwater, basalt or packing material (75% basalt, 25% sodium bentonite), low-carbon steel in the form of coupons, and low-carbon steel pressure vessels. Each set of experiments consisted of three separate tests: two with irradiation and one without. The tests were run for periods of 1-2 months.

The tests were performed as follows. The coupon and the basalt or the packing were placed in the test vessel at room temperature. The vessel was then evacuated and flushed several times with argon or methane to assure that there were no impurities such as O_2. Methane was added (270 ppm) after the last evacuation for those tests that required methane. The vessel was then placed in an oven and connected to a water transfer line. With the oven temperature raised to 200°C, GR4 groundwater at the same temperature was transferred from a high-pressure autoclave to the test vessel. With the pressure in the vessel at ~150 bar (~15 MPa), the vessel was closed, disconnected from the water transfer line, and transferred (using a heated insulated container) to another oven maintained at 200°C for a hydrothermal test or to a specially modified oven in a gamma field, also at 200°C, for an irradiation-hydrothermal test. After testing, the liquid, gas, and solid components were analyzed. Liquid samples were obtained at two temperatures: 185-200°C or room temperature.

There were only a very limited number of tests so that these first results are considered a qualitative statement of what might occur in a basalt repository, if the repository conditions are similar to the test conditions.

The composition of the gas phase was altered by the irradiation. The H_2 yield increased by factors of 10 to 200, the amount of increase varying with the components of the test. The two mechanisms that contributed to the production of H_2 were the radiolysis of water and CH_4.

The liquid phase was not as sensitive to gamma radiation. The only change observed in the two-month irradiation tests was an increase in SO_4^{2-} concentration for tests containing basalt. The other changes observed in the solution chemistry were changes in pH and solution composition. These were controlled primarily by the components of the test (i.e., whether or not basalt or packing was present), by hydrothermal conditions, and by the sampling temperature. The effect of adding CH_4 to GR4 groundwater and irradiating the test solution was to increase the organic carbon concentration from about 8 ppm to about 33 ppm. This is believed to be due to the formation of more-soluble, higher-hydrocarbon homologs and possibly alcohol from the various radiolysis reactions of CH_4 and groundwater. However, when basalt or packing was added to the CH_4-groundwater in the low-carbon steel vessel, the effect of radiation as reflected in the organic carbon content of the water was less dramatic. There was only a slight increase in the organic carbon content, and the increase was similar in both the irradiated and non-irradiated tests.

Radiation appeared to increase the corrosion rate of the low carbon steel coupon significantly in tests that contained basalt or packing and, to a lesser extent, in tests that contained only GR4 or GR4 and CH_4.

Longer tests of three and six months have been initiated. These should clarify and strengthen many of the observations, but it is readily apparent that radiation at dose rates of 10^4 rad/h alters the gas, liquid, and solid phases in tests that contain various combinations of waste package components.

B. *Separation Science and Technology*

The Division's work in Separation Science and Technology consists of four projects. Three of these projects are concerned with removing and concentrating actinide elements from transuranic (TRU) contaminated waste streams, thus recovering valuable TRU elements and lowering waste disposal costs. The major project in this area involves development of a generic data base and modeling capability for the TRUEX (TRansUranic EXtraction) process. This capability will allow us to design flowsheets for specific waste streams and to predict the cost and space requirements for implementing a site- and feed-specific TRUEX process. It will also be useful as a tool for plant operators to vary, monitor, and control the process once it is in place. The second project, supported by Rockwell Hanford Operations, entails development of the TRUEX process for removing americium and plutonium from waste generated by the Hanford Plutonium Finishing Plant (PFP) while recovering a purified plutonium stream. The third project entails developing a PUREX/TRUEX flowsheet for removing plutonium from concentrated HCl/brine waste streams. The fourth project, which is unrelated to the first three, is concerned with the feasibility of substituting low enriched uranium for the high enriched uranium currently used in the production of fission product ^{99}Mo. Technetium-99m, the daughter of ^{99}Mo, is widely used in medical diagnosis.

1. TRUEX Process Development

The TRUEX process extracts, separates, and recovers TRU elements from solutions containing a wide range of nitric acid, fission product, and nitrate salt concentrations. It is also applicable in concentrated chloride media. These separating capabilities make TRUEX an important tool for converting a variety of TRU-containing waste streams to nonTRU waste. The application of the TRUEX process to nuclear wastes in the United States would (1) greatly lessen the bulk of waste that must be buried as TRU waste at the Waste Isolation Pilot Plant (WIPP) or as glass in a high-level nuclear waste repository; (2) recover substantial amounts of TRU elements (e.g., plutonium) that otherwise would be lost; and (3) alleviate long- and short-term waste storage problems that threaten to curtail production.

The TRUEX solvent extraction process was invented by members of the Chemical Separation Group (Chemistry Division, ANL) as a result of basic studies on a number of neutral, phosphorus-based, bifunctional extractants. Process application, flowsheet development and testing, and the use of centrifugal contactors for TRUEX processing have since become a cooperative effort between this group and CMT's Separation Science and Technology Group. The extractant found most satisfactory for the TRUEX process is CMPO, which has the

chemical structure shown in Fig. VI-3. This extractant is combined with tributyl phosphate (TBP) and a diluent to formulate the TRUEX process solvent. The diluent is typically a normal paraffinic hydrocarbon (NPH) or a nonflammable chlorocarbon such as carbon tetrachloride (CCl_4) or tetrachloroethylene (TCE).

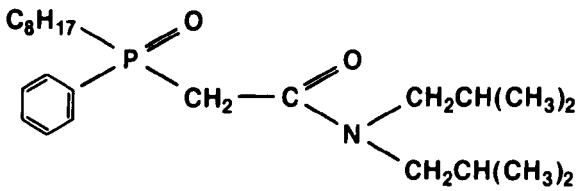

Fig. VI-3.

The Chemical Structure of CMPO

Because of their small size and high throughput, centrifugal contactors are an integral part of implementing TRUEX processing, allowing it to be installed in already available space in the production or processing plant. Development of the centrifugal contactor will be continued to increase its throughput efficiency and reliability.

Overall, the operation of the basic TRUEX flowsheet is as follows. The TRU waste is fed into a bank of centrifugal contactors, where the TRU elements are extracted by the TRUEX solvent, and the aqueous raffinate containing the bulk of the waste exits as a nonTRU waste. The loaded solvent is scrubbed to effect a cleaner separation; the solvent is then stripped with dilute acid to recover the TRU elements that are tripositive cations, e.g., americium and curium, as well as the rare-earth fission products. In a second strip, the plutonium is recovered by adding a small amount of complexant or reductant in the aqueous feed to this strip, e.g., HF or hydroxylammonium nitrate (HAN). Any uranium and technetium in the feed would be removed from the solvent in the solvent cleanup step.

a. TRUEX Technology-Base Development

A center for TRUEX technology development is being established at CMT to perform R&D that will broaden the applicability of TRUEX processing of high-level and TRU-containing waste streams. The overall purpose of this center is to facilitate the implementation of TRUEX solvent extraction processing in the DOE community. In general, the R&D is directed toward (1) gathering information pertinent to the whole range of predicted and unexpected (plant upset) processing conditions and (2) improving TRUEX processing by working on problems common to all sites. Our primary task is the creation of a generic TRUEX process data base and modeling capability that can be used to project process flowsheets based on site-specific criteria such as feed composition, feed volume/flow rate, time schedule for processing, available space for implementing the process, and projected fate of the TRU element streams. This capability could be used by DOE and facility management to decide between this and other options for handling specific waste streams. Once a TRUEX process is implemented, the TRUEX model can become a tool for operators to vary, monitor, and control the process.

The generic data base will include distribution ratios for extractable metals and inorganic acids, aqueous-phase acid dissociation constants and stability constants for aqueous-phase metal complexes, and activity coefficients for nitrate solutions of high ionic strength. It will also include models for predicting activity coefficients in mixed electrolyte systems.

Distribution ratios are being determined for the extraction of nitric acid and important metal-ion and acidic species present in high-level liquid waste and other TRU-containing nitric acid waste streams. These data will measure the effects of temperature, aqueous-phase compositional variation, TRUEX process solvent composition, and the chemical form of the extracting species.

The extraction behavior of nitric acid was modeled using batch distribution ratio measurements for the TRUEX process solvent of 0.25 M CMPO-0.75 M TBP in tetrachloroethylene. The algorithm developed from this model was combined with a stagewise solvent extraction model in an electronic spreadsheet. This combined model was used to predict the behavior of nitric acid in a 14-stage demonstration of the TRUEX process flowsheet for treating Hanford Plutonium Finishing Plant (PFP) waste using simulated feed. Model calculations gave an excellent fit to the measured nitric acid concentrations of steady-state samples from each stage in the bank of centrifugal contactors and from the effluent streams. Because the concentration of nitric acid affects the extraction behavior of all other species, this success is the first step in modeling the extraction behavior of all species. We have also successfully modeled the extraction behavior of americium and fit the stage-to-stage and effluent behavior of americium from an earlier demonstration of the PFP flowsheet with 0.25 M CMPO-0.75 M TBP in carbon tetrachloride. The good fit of the model to the measured nitric acid and americium profile is shown in Figs. VI-4 and VI-5, respectively.

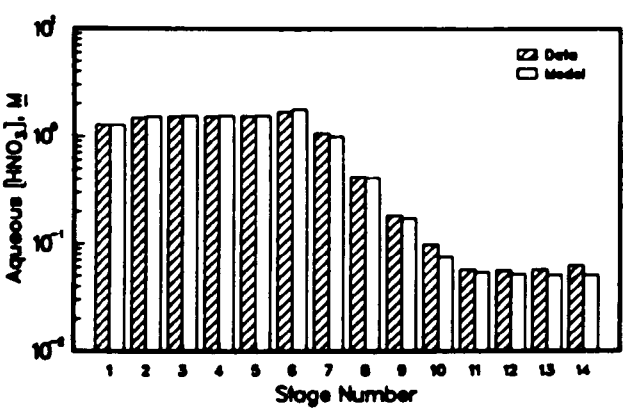

Fig. VI-4.

Experimental and Calculated Values for the Stage-to-Stage Concentrations of Nitric Acid in the Aqueous Phases of a 14-Stage Countercurrent Solvent Extraction Flowsheet

The effects of temperature, aqueous-phase complexation, activities of aqueous phase species, and solvent compositional variations on the extraction behavior of important species are being incorporated into more sophisticated algorithms. Using a mechanistic approach to the modeling of distribution ratio data, we have already been successful in predicting the influence of salting-out agents in nitric acid extraction. Nitric acid extraction by the TRUEX solvent was described by the following reactions:

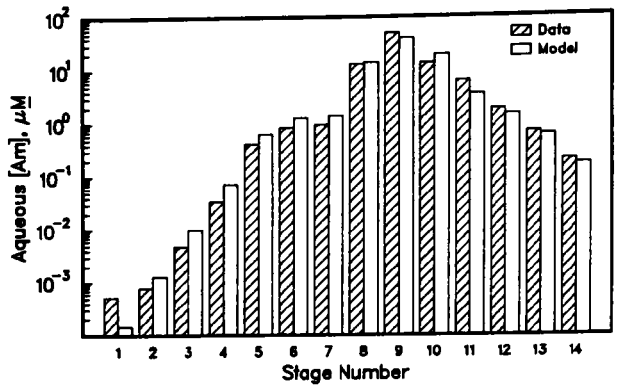

Fig. VI-5.

Experimental and Calculated Values for the Stage-to-Stage Concentrations of Americium in the Aqueous Phases of a 14-Stage Countercurrent Solvent Extraction Flowsheet

$$H^+ + NO_3^- + \overline{CMPO} \overset{KC1}{\rightleftharpoons} \overline{CMPO \cdot HNO_3} \quad (1)$$

$$2H^+ + 2NO_3^- + \overline{CMPO} \overset{KC2}{\rightleftharpoons} \overline{CMPO \cdot 2HNO_3} \quad (2)$$

$$H^+ + NO_3^- + \overline{TBP} \overset{KT1}{\rightleftharpoons} \overline{TBP \cdot HNO_3} \quad (3)$$

$$H^+ + NO_3^- + 2\overline{TBP} \overset{KT2}{\rightleftharpoons} \overline{(TBP)_2 \cdot HNO_3} \quad (4)$$

where the bar represents an organic-phase species. The first two reactions alone have been found to adequately describe nitric acid extraction by solutions of CMPO, while the second set of reactions describes the TBP-alone system. As shown in Fig. VI-6, model calculations (using the extraction equilibrium constants KT1 and KT2) fit nitric acid extraction data for a TBP concentration range of 5 to 30%.[5]

By combining the two separate sets of reactions for nitric acid extraction (Eqs. 1-4), behavior of the TRUEX process solvent can be described. Figure VI-7 shows the excellent agreement between the calculated and measured nitric-acid extraction for TRUEX (with NPH diluent) at 25°C.

[5]Data were taken from the literature, W. Davis, Jr., Nucl. Sci. Eng. **14**, 159 (1962).

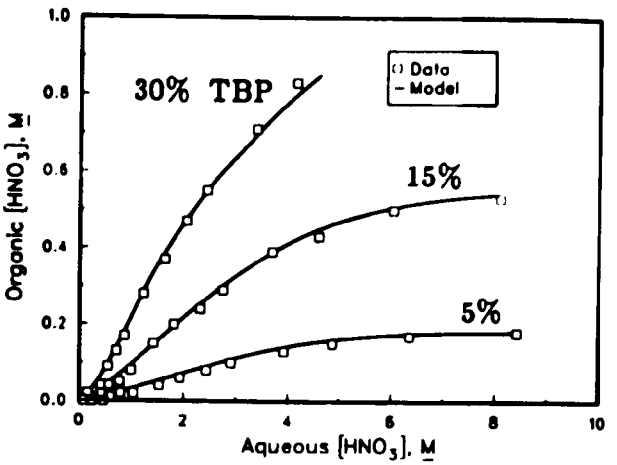

Fig. VI-6.

Nitric Acid Extraction by TBP in AMSCO 125-82 at 25°C

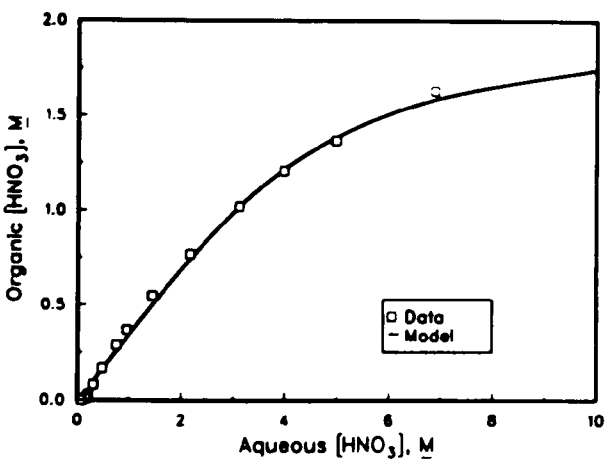

Fig. VI-7.

Nitric Acid Extraction by TRUEX-NPH at 25°C

The spreadsheet algorithm for stagewise solvent extraction (SASSE) will incorporate these mechanistic algorithms and will be further refined to easily permit the addition or subtraction of stages, feed ports, and exit ports. The SASSE code is now capable of measuring the effects of varying flow rates of all currently designated streams and varying the concentration of CMPO between 0.1 and 0.4 M.

b. TRUEX Processing of PFP Waste

In 1986, we continued the process development work directed toward a raffinate typical of that produced by the TBP-based solvent-extraction process used to remove uranium and plutonium from dissolved waste generated during the processing and production of plutonium. This waste stream is designated "PFP waste" because it is typical of that exiting the Hanford Plutonium Finishing Plant.

A cold (i.e., non-radioactive) demonstration of the PFP flowsheet was carried out using a bank of fourteen centrifugal contactors (five extraction stages, two scrub stages, four americium-strip stages, and three plutonium-strip stages) with a 4-cm dia rotor. The TRUEX process solvent chosen for this demonstration was 0.25 M CMPO and 0.75 M TBP with tetrachloroethylene (TCE) as the diluent.

In the demonstration, the evaporative loss for the solvent after one complete pass was reduced from 7% in an earlier test to less than 0.2% by modifying the contactor design, switching from CCl_4 to TCE diluent, and changing the operating procedure to account for heat generated by the contactor motor after shutdown. The switch in diluent had no significant effect on either contactor hydraulics or process chemistry. A set of operating conditions that optimizes the solvent composition and the scrubbing and stripping sections of the flowsheet was also developed and tested. Detailed results of these activities will be given in an ANL report to be issued in early 1987.

The first four-stage laboratory contactor built and tested at ANL has been started up at Rockwell Hanford and is now being used to familiarize Rockwell Hanford personnel with contactor operation. A prototype Argonne contactor has been designed for the PFP waste treatment facility at Rockwell Hanford. Blueprints are completed, and a four-stage unit is being fabricated in the ANL Shops.

The overall conclusion of this effort is that there are no foreseeable problems in implementing a TRUEX solvent extraction process on solutions having the general composition of a typical PFP waste. Future work will be directed toward assisting Rockwell Hanford in implementing the process in the PFP facility.

c. Solvent Extraction Processing of Chloride Salt Waste Solutions

In 1985 work was begun on the development of a solvent extraction process to remove Pu and Am from chloride salt wastes being stored at Los Alamos National Laboratory (LANL). These wastes are generated from the pyrometallurgical processing of plutonium, e.g., Direct Oxide Reduction (DOR), Electrorefining (ER), and Molten Salt Extraction (MSE). The goals of this process are three-fold: (1) to recover plutonium and remove other elements from these chloride salt wastes, which have a wide range of compositions, (2) to produce a plutonium product containing <100 ppm of any other metal and <1000 ppm total of all other metals, and (3) to produce an aqueous raffinate with <100 nCi of α-activity per gram of solid. A two-part flowsheet was

proposed in 1985 to meet these objectives. In this flowsheet, Pu(IV) would first be recovered in a PUREX-TCE cycle (25 vol % TBP in TCE), then the americium and other transuranic elements would be removed from the salt wastes in a TRUEX-TCE cycle (0.5 M CMPO in TCE), thereby leaving the raffinate as a discardable, nonTRU waste.

Since a 16-stage annular centrifugal contactor was in place at LANL, the work during FY 1986 focused on measuring the distribution ratios for use in the electronic spreadsheet, which will optimize the flowsheet parameters for specific plutonium-containing feed streams. To measure the Pu(IV) distribution ratios between PUREX-TCE and a chloride media, it was first necessary to develop a method of oxidizing the mixture of Pu(III/IV), which exists in the chloride media, to >99.99% Pu(IV) and maintaining the IV oxidation state. This oxidation was accomplished on a laboratory scale by the use of a ten-fold excess of sodium chlorite ($NaClO_2$); however, on a production scale, oxidation would be more controllable if a commercial chlorine dioxide (ClO_2) generator were used.

Distribution ratios were measured for Pu(IV) and co-extractable ions such as Fe, Mo, and Zn between 25, 35, and 40 vol % TBP in TCE and aqueous solutions containing 0.1 to 8 M HCl. The potential that these co-extractable ions would reduce the purity of the plutonium product prompted the initiation of plutonium loading studies, which indicated that at least zinc could be eliminated from the organic phase by loading the solvent with plutonium. Although the distribution ratios measured indicate that Pu(IV) can be extracted from aqueous phases containing $\geq$5 M HCl and stripped with $\leq$ 2 M HCl solutions, some interfering ions (e.g., Fe, Mo, Ga) may need to be dealt with by separating them from a Pu(III)-containing feed in a head-end process.

Planned work for FY 1987 includes distribution ratio measurements for Pu(IV), Fe, Mo, Zn, and other co-extractable metal ions as well as HCl between PUREX-TCE solvents and simulated chloride salt solutions. The measurements will be used to empirically model and thus predict distribution ratios for a wide range of chloride salt wastes. In addition, solvent treatment studies will be conducted to determine the effect of solvent degradation on stripping and to evaluate solvent cleanup procedures.

2. Production and Separation of ^{99}Mo from LEU Targets

Technetium-99m (used for medical purposes) is a decay product of ^{99}Mo, which is produced in nuclear reactors by the fissioning of ^{235}U or from the neutron capture of ^{98}Mo. Presently, most of the world's supply of fission-product ^{99}Mo is produced in targets of high enriched uranium (HEU, 93% ^{235}U). The United States is considering prohibiting the export and internal commercial use of HEU because of its potential use in nuclear weapons. The purpose of this study is to assess the technical feasibility of substituting LEU (<20% ^{235}U) for HEU in targets for production of fission-product ^{99}Mo.

Presently, ^{99}Mo is produced from a variety of target designs that contain HEU as either uranium aluminide in curved plates, uranium-aluminum alloy in modified fuel rods, or an electrodeposited film of UO_2 on the inside surface of enclosed cylinders. The main issues to be addressed in substituting

LEU for HEU for the production of ^{99}Mo are (1) attainment of purity and yield requirements of the $^{99}Mo/^{99m}Tc$ product, (2) fabrication of LEU targets and related concerns, (3) disposal of radioactive waste, and (4) overall safety and economics of irradiating and processing LEU targets. Thus far, our efforts have been concentrated on the first two issues. Work in FY 1986 was centered on ^{99}Mo separation and purification techniques that were patented by Union Carbide in the 1970s[6–8]; these techniques are presumed to be still employed today for separating ^{99}Mo from irradiated, electrodeposited UO_2 films.

In FY 1987, efforts were begun on ^{99}Mo separation and purification from targets containing uranium silicide fuel. Because of their higher densities, LEU silicides can be substituted for uranium aluminide and uranium-aluminum alloy fuel in present targets for the production of ^{99}Mo without affecting the fission yield. Our studies for processing silicide targets are also based on assumptions of what current industrial processing schemes are for uranium aluminides and uranium-aluminum alloy targets.

a. Purity and Yield of the $^{99}Mo/^{99m}Tc$ Product

The change in target material from HEU to LEU will affect the separation by increasing the amount of uranium to be dissolved and separated from ^{99}Mo by approximately five and increasing the amount of alpha-emitting isotopes (especially ^{239}Pu) in the irradiated targets. The greater amount of uranium would likely influence the purification of ^{99}Mo from other radionuclide impurities. With preliminary experiments using stable Mo, depleted U, ^{239}Pu, ^{237}Np, and three fission-product radioisotopes (^{110}Ag, ^{131}I, and ^{137}Cs), two methods of separating molybdenum have been studied thus far: (1) alpha-benzoinoxime precipitation and (2) adsorption by Ag-coated activated charcoal (ACAC) columns.

Conclusions drawn from the study with the first method were as follows:

- There is no significant penalty in yield of ^{99}Mo or in the purification of ^{99}Mo from U.
- The use of an ACAC polishing step following precipitation of ^{99}Mo can further reduce contamination by uranium.
- Neptunium and plutonium can be removed to prescribed limits by a combination of precipitation and an ACAC polishing step.
- Separation of fission-product Ag^+, Cs^+, and I^- will be as effective for LEU as for HEU targets.

---

[6]H. Arino, H. H. Kramer, J. J. McGovern, A. K. Thornton, "Production of High Purity Fission Product Molybdenum-99," U.S. Patent 3,799,883 (March 28, 1974.

[7]H. Arino, F. J. Cosolito, K. D. George, A. K. Thornton, "Preparation of a Primary Target for the Production of Fission Products in a Nuclear Reactor," U.S. Patent 3,940,318 (February 24, 1976).

[8]H. Arino and P. M. Madigan, "Production of High-Purity Molybdenum Using Silver-Coated Carbon as Adsorbent," U.S. Patent 3,745,119 (July 10, 1973).

For studies with the second method, molybdenum yields and separation from uranium were much lower than those by alpha-benzoinoxime precipitation (yields, 20-80% vs. >97%; separation from uranium, 10-300 vs. 5×10^4), although the column conditions were far from optimized. In addition, these values were inversely dependent on the amount of uranium in solution. However, ACAC purification of molybdenum from fission products was much better (10^2-10^4 vs. 2-80). A single separation step by precipitation followed by an ACAC polishing step is likely to be the scheme of choice.

Further work in this area will include the addition of ^{103}Ru to the radioisotope studies and continued study of ACAC column separations. We are also examining the effect of substituting silicide for aluminum alloy and aluminide fuels in target processing, but results are too preliminary to report at this time.

b. Fabrication of LEU Target

Several target designs with HEU are currently used for the production of fission product ^{99}Mo. We anticipate that the curved plate and rod-type target presently used with U-Al alloy or aluminide fuel will be able to utilize the high uranium densities achievable with the new LEU silicide fuels without changing the target geometries. However, the cylindrical target design currently uses a UO_2 surface density that is close to its practical fabrication limit. A new target design and/or a much denser film material is required for use of LEU. As a result, our efforts up to this time have concentrated on a cylindrical design with a layer of uranium metal electrodeposited on the inside surface.

As a target material for ^{99}Mo production, uranium metal has several advantages over UO_2, including higher thermal conductivity, higher density, and higher plating efficiency. Disadvantages of electrodeposited uranium metal are that targets must be prepared from molten salt systems at high temperatures in inert atmospheres, and the deposit morphology tends to be dendritic. The most-promising chloride melts investigated for the electrodeposition of uranium metal appear to be the $BaCl_2$-KCl-NaCl eutectic-UCl_3 and the $BaCl_2$-$CaCl_2$, LiCl-NaCl eutectic-UCl_3 systems. Additions of small quantities of alkali metal fluorides may be helpful in improving the quality of the metal deposit. Lower current densities and pulsed currents formed uranium deposits that were denser and more evenly distributed and had smaller dendrites.

Future work will include the investigation of techniques to enhance bonding of electrodeposited uranium metal on target support and to enhance morphological characteristics of these uranium metal coatings. We will be looking at variables such as surface preparation, temperature, electrolyte composition and U^{3+} content, and plating current variations.

C. *The Integral Fast Reactor Pyrochemical Process*

The Integral Fast Reactor (IFR) is an advanced reactor concept proposed by, and under development at, Argonne National Laboratory. Its distinguishing features are that it is a sodium-cooled, pool-type reactor (i.e., all the major components, reactor core, pumps, and heat exchangers are in a large sodium-filled pot); it employs a metallic fuel (an alloy of U, Pu, and Zr clad with a stainless

steel-type alloy); and it has an integral fuel cycle (discharged core and blanket materials are reprocessed and refabricated in an on-site facility). The advantages of this concept are an exceptionally high degree of inherent safety, resulting from use of a metallic fuel with a sodium coolant, and competitive economics, resulting from low costs for reactor construction and fuel recycle.

The CMT Division has the responsibility of developing the on-site process for recovering plutonium and uranium from the core and blanket, removing fission products from them, and reenriching the core alloy with plutonium bred in the blanket.

1. Basic Flowsheets

The two basic steps of the reference flowsheet for the pyrochemical process (see Fig. VI-8) are electrorefining, which removes fission products from the core and blanket materials, and halide slagging, which increases the plutonium/uranium ratio in a product salt extract sufficiently for reenrichment of the core alloy.

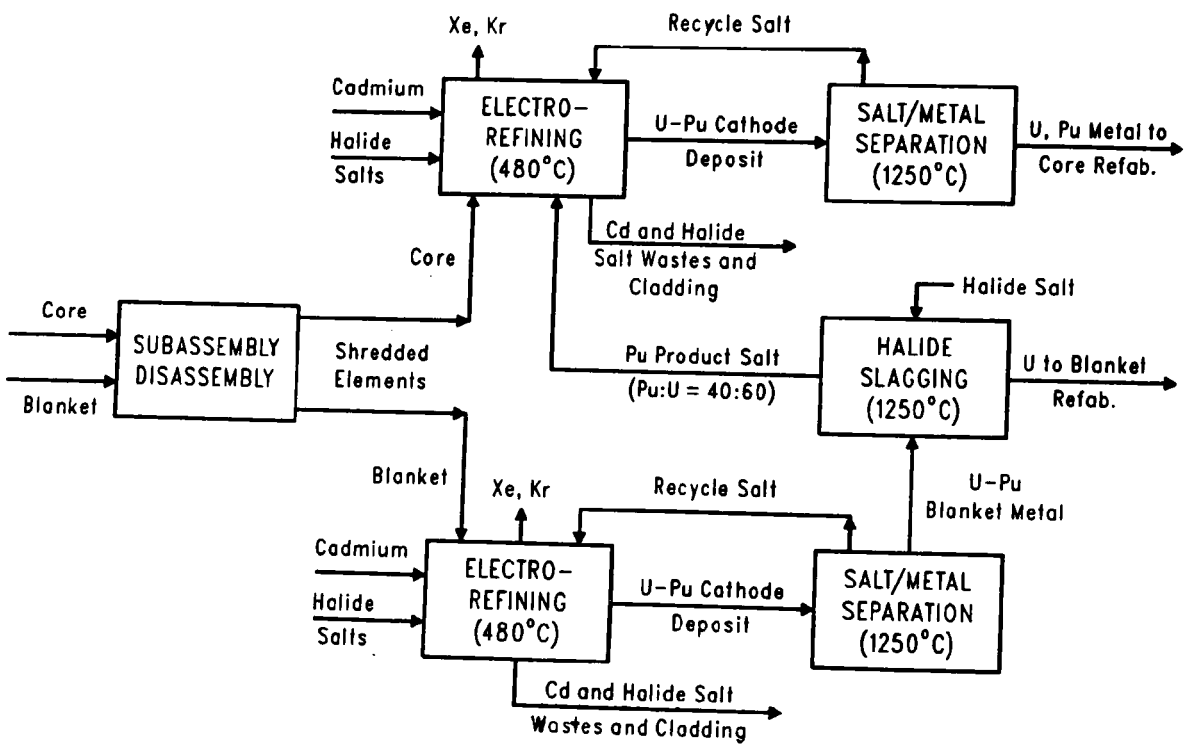

Fig. VI-8. Pyrochemical Process for IFR Core and Blanket

In the electrorefining step, the metallic fuel is first dissolved out of approximately 6-mm (1/4-in.) fuel pin segments by liquid cadmium at about 500°C; the cadmium solution becomes the anode for electrolytic transport of uranium and plutonium through a molten chloride electrolyte to a cathode. The cathode deposit is recovered mechanically and consolidated by melting to form

a product ingot, which is used to prepare new fuel or blanket pins by injection casting. Fission products and cladding hulls remain in the liquid metal or electrolyte, a portion of both being sent to waste after each batch of fuel is processed. In the halide slagging step, the metal product from the electrorefining of blanket material is melted in a beryllia crucible and held at 1300°C for about one hour under a chloride salt containing a UCl_3 oxidant. The plutonium is preferentially extracted into the salt phase, which is added to the electrolyte of the core electrorefining step for plutonium enrichment.

In an alternative process currently under consideration, only electrorefining is employed for recovery and purification of the fuel constituents. Thus, halide slagging is eliminated. This flowsheet, illustrated in Fig. VI-9, is feasible because uranium should, under appropriate conditions, be selectively transported to a cathode during electrorefining. Under other conditions, uranium and plutonium may be transferred together. In the case of blanket material, selective removal of most of the uranium leaves residual uranium in the cadmium anode enriched in plutonium. By alternating batches of core and blanket fuel through the same electrorefiner, the plutonium left after processing blanket material may be incorporated into the core material, thus reenriching it in plutonium.

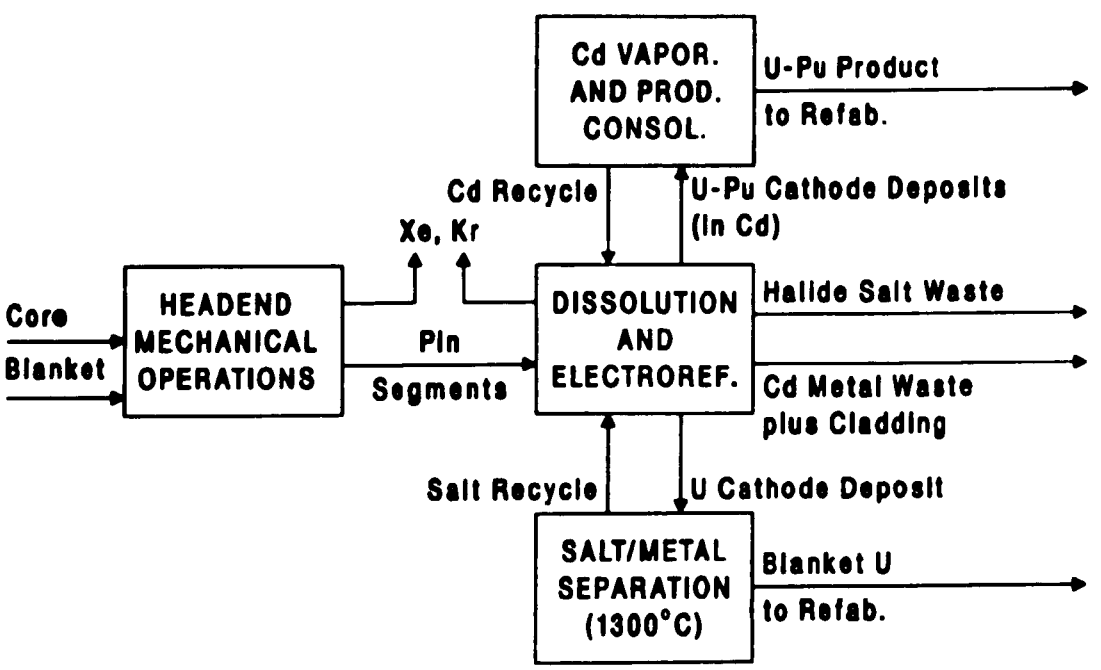

Fig. VI-9. Alternative Electrorefining Process for IFR Core and Blanket

2. Process Development Studies

Small-scale engineering studies of the electrorefining and halide-slagging steps were conducted in 1986.

a. Electrorefining

Two types of cathodes are under consideration: (1) a solid metal mandrel, e.g., steel, molybdenum, or uranium, and (2) liquid cadmium. Electrotransport of uranium onto a solid steel mandrel is straightforward, producing a dendritic deposit like that shown in Fig. VI-10 (left). This deposit may be mechanically sheared from the mandrel and consolidated by melting. When a solid cathode mandrel is used, uranium and plutonium deposit sequentially, with some overlap (see Fig. VI-11). This effect results from the lower chemical stability of UCl_3 (7 kcal/g atom of Cl^- less than $PuCl_3$), which, when present in high concentration in the electrolyte, reacts with deposited plutonium from the cathode mandrel and thereby curtails plutonium deposition until the UCl_3 is consumed. Plutonium-containing deposits are amorphous and fine-grained, as shown in Fig. VI-10 (right). When the anode and cathode both use liquid cadmium as a solvent metal, the activity coefficients of uranium and plutonium are identical in the two electrodes. Under these conditions, the thermodynamic relationships are such that only a small voltage is required for transport of uranium and plutonium, which can be transferred together from anode to cathode. The volume of cadmium in the cathode compartment can be very small, and uranium and plutonium can be "pumped" into the cadmium in amounts that far exceed their solubilities; uranium precipitates as uranium metal, plutonium as $PuCd_6$. The precipitates will settle to the bottom of the cathode compartment.

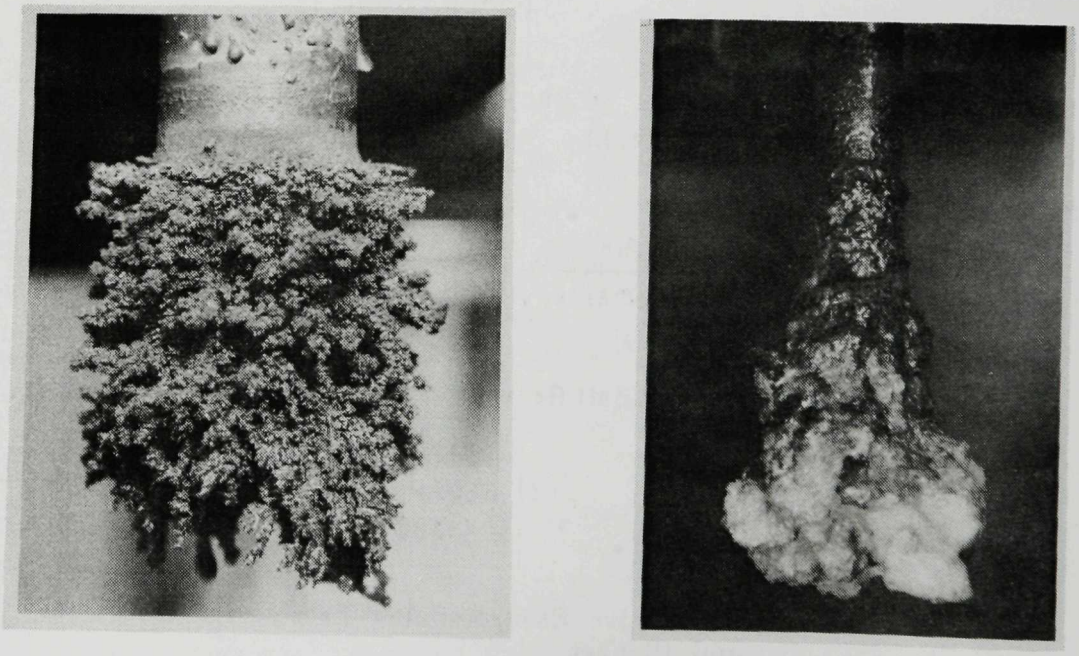

Fig. VI-10. Photographs of Electrorefining Deposits. (On left, typical dendritic deposits of uranium. On right, amorphous deposit of uranium and plutonium.)

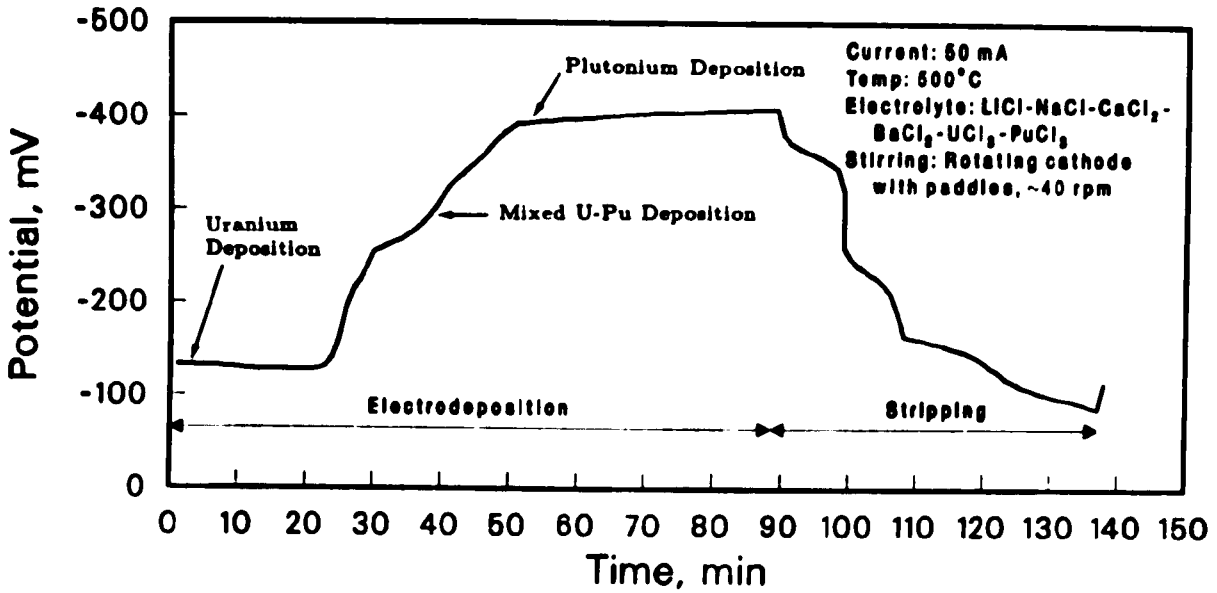

Fig. VI-11. Electrodeposition and Stripping of Uranium and Plutonium

Important results and observations of the electrorefining studies are the following:

- Fission product removals are satisfactory. Noble metals remain in the cadmium anode. Removals of electropositive fission products, which are the most difficult to separate from uranium and plutonium, are shown in Table VI-1.
- Uranium and plutonium distribute between salt and metal phases in accord with theoretical predictions, and their distribution between the phases can be easily adjusted by using $CdCl_2$ as an oxidizing agent or lithium as a reducing agent.
- The low-carbon steel vessel (used to contain molten cadmium and the halide salt electrolyte) and other low-carbon steel components show no evidence of corrosion after one year at 500°C.
- No operational difficulties were encountered with a multicomponent chloride salt electrolyte.
- Very little vaporization and deposition of cadmium and salt constituents on cold areas of the electrorefiner occurred.

In summary, the chemical basis of electrorefining has been established fairly well. Selection of the optimum method for electrodepositing uranium and plutonium requires additional work.

Table VI-1. Decontamination Factors for Electrorefining of U-Pu (inactive fission-product elements)

Fission Product	Decontamination Factor
Strontium	>2000
Barium	>1500
Yttrium	>1500
Cerium	>250
Neodymium	>1500
Zirconium	~1000

b. Halide Slagging

Two runs were made to prove the chemical feasibility of the halide-slagging process step. The experimental results of the two runs are presented along with, for comparison, calculated values in Table VI-2. The calculated values are based on the free energies of formation of UCl_3 and $PuCl_3$ and a published activity coefficient of plutonium in uranium of 0.4.[9] The experimental points for these two runs are shown in Fig. VI-12 in relation to the theoretical curves from each run. The difference in the two theoretical curves

Table VI-2. Equilibrium Data for Halide Slagging[a]

	Run A		Run B	
	Calc. Value	Exp. Result	Calc. Value	Exp. Result
Quantity, g				
Pu in Salt	25.0	24.5	18.9	18.8
Pu in Metal	4.52	4.95	3.01	3.16
U in Salt	20.5	20.9	23.3	23.5
U in Metal	779	779	781	781
Pu Recovery, %	84.7	83.2	86.3	85.6
U/Pu Wt Ratio in Prod.	0.82	0.85	1.23	1.25

[a]The reactions is UCl_3 (salt) + Pu (U) $\rightleftharpoons$ $PuCl_3$ (salt) + U. Conditions are: salt phase, $CaCl_2$-$BaCl_2$; temperature, 1250°C.

[9]P. Chiotti, V. V. Adhachinsky, I. Ansara, and M. Rand, *The Chemical Thermodynamics of Actinide Elements and Compounds*, Part 5, "The Actinide Binary Alloys," IAEA, Vienna (1981).

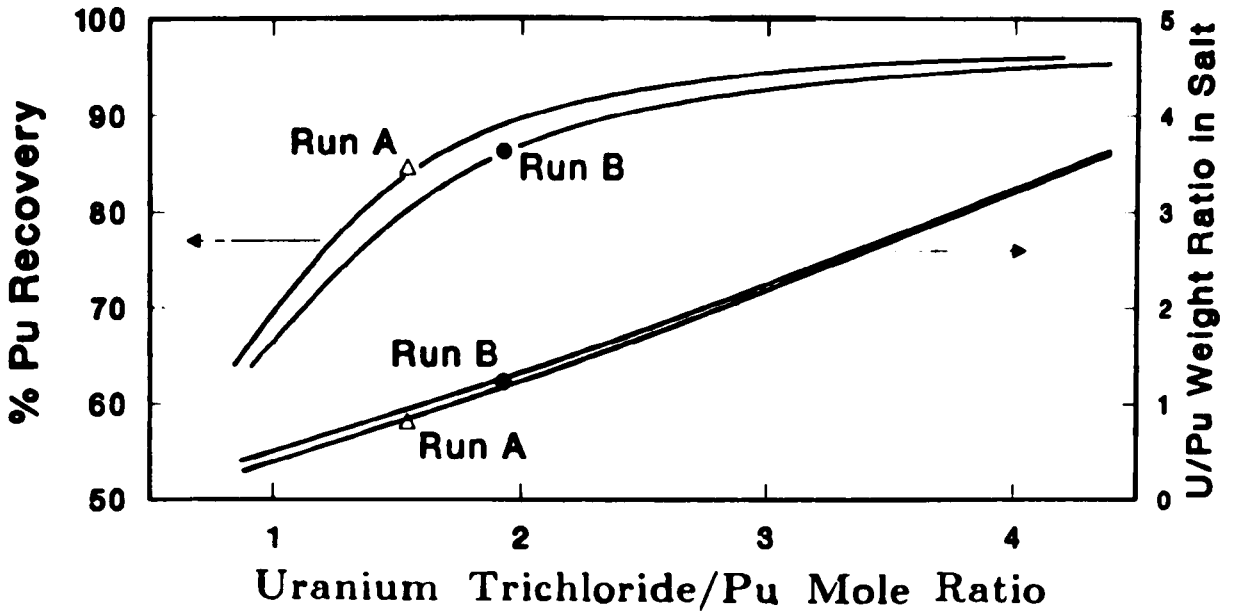

Fig. VI-12. Experimental vs. Theoretical Results for Halide Slagging

results from different uranium/plutonium ratios in the fuel. The agreement between experimental results and calculated values lends confidence to the use of theoretical calculations for predicting performance under various conditions. Figure VI-12 shows that a UCl_3-to-plutonium mole ratio of about three is required to extract over 90% of the plutonium from the blanket alloy. The resulting uranium-to-plutonium weight ratio in the salt of about two is ample reenrichment of the core.

3. Waste Management

Several methods of converting solid wastes from an IFR fuel reprocessing plant to disposable forms are being explored. The principal TRU-contaminated wastes are a cadmium alloy and a mixture of chloride salts from the electro-refining cells, stainless-steel cladding, and various ceramic materials from fuel-melting operations. Most of the fission products are contained in the waste cadmium and salt. The electropositive elements (alkali metals, alkaline earths, and rare earths) and iodine are in the salt, and the electronegative elements (zirconium and noble metals) are in the metal. Each phase is likely to contain small amounts of actinides.

Although some consideration has been given to alternative waste treatment methods, the main effort has been on the reference process shown in Fig. VI-13. The waste ceramic materials and cladding are dispersed in the cadmium wastes and then encapsulated in heavy-walled, corrosion-resistant metal containers for ultimate disposal. The extraction of actinides from the waste salts into a liquid metal is a key process step. By lowering the alpha activity below the 100 nCi/g limit permitted in low-level waste, the salt is converted to a material that may be suitable for disposal in a near-surface repository. This treatment may also extract most of the rare-earth fission products, but Cs, Sr, and I remain in the salt. The treated salt is dispersed in a portland cement mortar, which is cast into corrosion-resistant metal containers for disposal.

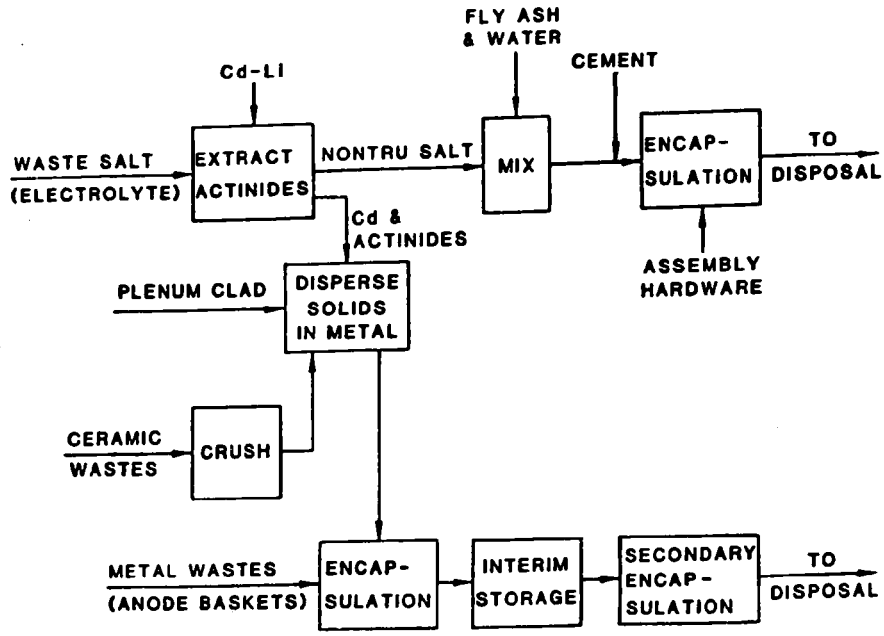

Fig. VI-13. Treatment of Solid Pyroprocess Wastes

Thermodynamic calculations supported by experimental data indicate that the actinides can be extracted from the salt by contacting it with a Cd-0.1 wt % Li alloy. In a laboratory demonstration experiment, the plutonium content of an electrolyte salt was reduced from about 3 wt % to less than 10 ppm by a single contact with a Cd-Li alloy, with the metal phase becoming about 1.5% Pu. Americium decontamination is most critical. Because it appears that all of the americium in the discharged fuel will be in the waste salt, an americium decontamination factor of about 10,000 is required to produce a nonTRU waste. Measured distribution coefficients (wt % in salt/wt % in metal) were between 0.01 and 0.02 for americium and curium and were less than 0.001 for plutonium and uranium. Calculations using these values indicated that two equilibrium contacts with fresh alloy and a total metal/salt weight ratio of 4.5 should achieve the required decontamination of the waste electrorefining salts.

An investigation of portland cement-based materials for containment of the treated salt wastes was started. The reference concept for packaging salt wastes requires that the components be mixed to produce a fluid grout that can be pumped into waste containers before the mixture begins to set. Only moderate compressive strengths would be required for the cement waste forms because the cemented waste will be cast into strong metal containers. The mortar matrix must also inhibit leaching of the chloride salts by groundwater, although the metal containers are the primary barrier against dispersal into the environment.

In initial tests, it was found that mixes of type I portland cement and a low CaO fly ash were capable of containing up to 10% salt (NaCl and $CaCl_2$) without swelling or cracking. Such mixes developed adequate compressive

strengths of about 34 MPa (5000 psi). Similar mixes containing 20% salt tended to swell excessively and were weak. The leach rate of chloride ion from cured samples of several mixes has been measured in preliminary experiments. The quantity of chloride leached was proportional to the square root of exposure time, indicating that diffusion in the solid matrix was the rate-limiting step. Mortars made from Type I or II cement and a low-CaO fly ash and then cured for seven days in saturated steam at 120°C were found to have leach rates that may be acceptable for low-level waste repositories. The addition of sand to this mix decreased the leach rate but weakened the material. A Type C fly ash (high CaO) produced strong samples that did not swell even with 20% salt, but the chloride leach rates were high even after the high-temperature curing period.

Conversion of the waste salts to glass is being considered as an alternative waste treatment method, although it appears to be much less favorable than the metal extraction method discussed above. This conversion requires the removal of chlorine (and iodine) from the salt to produce an oxide, hydroxide, or similar compound. Reacting the salt with steam directly to produce HCl is thermodynamically unfavorable. However, experiments showed that the chlorine can be removed from the salt by reaction with steam at 850°C if Pyrex glass, boric oxide, or a mixture of Pyrex and phosphoric acid is added. When chlorine had been removed, the products were glass-like materials that were insoluble in water.

4. Large-Scale Demonstration of Electrorefining

Equipment and facilities are under construction for large-scale (approximately 20 kg of uranium) demonstration of the electrorefining step. The 20-kg uranium is about half that required for a plant-scale electrorefiner serving 1300 MWe of IFR capacity. The purposes of the large-scale unit are to (1) demonstrate fuel dissolution, deposition of 10 kg of uranium per cathode, and product handling; (2) establish the duty cycle for the electrorefining unit; and (3) evaluate equipment performance. The equipment is expected to be in operation in the spring of 1987.

VII. APPLIED PHYSICAL CHEMISTRY

The program in applied physical chemistry involves studies of the thermochemical and thermophysical behavior of selected materials in environments simulating those of fission and fusion energy systems.

A. *LWR Fission Product Chemistry*

The objective of this effort is to understand the processes that control the release and transport of fission products from light water reactor (LWR) fuel so that accurate predictions can be made of the "source term." We are investigating (1) the release of fission products from a breached fuel pin, (2) their transport, condensation, and deposition within the reactor primary system, and (3) their release during the interaction of molten fuel with the concrete basemat.

1. Release of Fission Products from Breached Fuel

The objective of these studies is to determine the chemical form and the rate of release of fission products from a defected LWR fuel pin. In these experiments, a sample of irradiated fuel is inductively heated, and the gaseous species released from the sample are identified and measured with a quadrupole mass spectrometer. During 1986, we studied the effect of oxidation of UO_2 fuel on the release of fission products and determined the ratio of the release rates of cesium to xenon.

The effect of fuel oxidation on the release of xenon was studied by leaking gaseous oxygen into a platinum-lined Knudsen cell that contained a sample of irradiated fuel. When oxygen was first leaked into the cell (at 1423 K or 1150°C), reaction of the oxygen with a carbonaceous impurity in the sample occurred and the added oxygen was lost from the cell as CO and CO_2; the rate of release of xenon was not affected. With time, the rate of oxidation of the carbonaceous impurity decreased, oxidation of the fuel began, and the rate of release of the xenon increased as the O/U ratio reached about 2.003. After the O/U ratio increased above 2.01, the rate of release of xenon was found to be directly proportional to the O/U ratio. Essentially all of the xenon was released from the sample when the O/U ratio reached about 2.03. These results indicate that the urania need not be oxidized to U_4O_9 (O/U = 2.25) to release all of the xenon, and that the rate of xenon release is not proportional to the rate of oxidation of the fuel to U_4O_9.

In an attempt to discover the chemical form of the iodine released from irradiated fuel, we modified our experimental apparatus so that condensable gaseous species released from the sample were collected on a "cold" plate. A sample of irradiated fuel was slowly heated to a maximum temperature of 1187 K (914°C), and the release of fission products was monitored with the mass spectrometer while the condensable species were collected on a plate located between the mass spectrometer and the Knudsen cell. The experimental apparatus was cooled to room temperature and the plate was removed and leached with water. A drop of aqueous ammonia had been added to the water to reduce the rate of air oxidation of any iodide dissolved by the water. Additional samples were collected in which the maximum sample temperatures reached were 1668 K (1395°C) and 1563 K (1290°C). The aqueous solutions were analyzed for

cesium and iodine as iodide. Only the first sample, collected at the lowest temperature, was found to contain a significant amount of iodine as iodide. The amount of iodide found was too small to determine its isotopic composition; hence, we are uncertain whether all of the iodide found originated from the irradiated sample (there is a small possibility that some of the iodide originated from CsI that had condensed on an induction coil during CsI calibration experiments performed before the experiment with the irradiated sample). The ratio of cesium-to-xenon release was computed from the amount of cesium collected on the plate and the integration of the xenon ion-current vs. time data from the mass spectrometer. The Cs/Xe release ratio varied between about 0.01 and 0.02. Since the ratio of cesium to xenon in the sample was about 0.8, the rate of release of cesium is significantly less than what would be expected if it were equal to the rate of release of xenon. While it is highly probable that the release of cesium is related to the xenon release (i.e., the xenon acts as a carrier for the less-volatile fission products), these results indicate that the rates are not the same as had been previously assumed in nuclear accident analyses.

2. Downstream Behavior of Volatile Fission Products

During a loss-of-coolant nuclear accident, the temperature of the fuel will rise above its normal operating temperature and lead to the rupture of the cladding and the release of fission products. We are investigating the interaction of these fission products with a steam/hydrogen mixture, which could flow up from the lower regions of the reactor core. The objective of these studies is to characterize the chemical and physical processes that determine the downstream behavior of the mixture of gaseous fission products and steam as it flows from the high-temperature region of the fuel to the cooler plenum region.

In our earlier work,[1] laboratory experiments were done by injecting either CsOH, CsI, Te, or mixtures of two or more of these substances into a flowing superheated steam/hydrogen gas stream at 1273 K (1000°C). This mixture flowed down a reaction duct (3.6-m long) on which a temperature gradient [from 1273 K (1000°C) at the beginning of the duct to 473 K (200°C) at its end] had been imposed. The concentrations were chosen so that all of the fission products were gases at the highest temperature. As the temperature of the flowing gas stream decreased, condensation on the wall took place. The rate of condensation on the wall was found to be too low to reduce the concentration in the gas phase fast enough to avoid supersaturation and the resulting aerosol formation. Therefore, in the cooler regions of the reaction duct, all of the deposit on the walls was the result of aerosol deposition.

In 1986, the main research emphasis was to investigate the revaporization of material from deposition sites and to characterize movement further downstream that may play an important role in loss-of-coolant accidents. Revaporization is caused by the flow of a gas over a deposit that is undersaturated with respect to one or more of the compounds in the deposit.

---

[1] M. J. Steindler et al., *Chemical Technology Division Annual Technical Report, 1985*, Argonne National Laboratory ANL-86-14, pp. 90-91 (1986).

The rate of revaporization is determined by the vapor pressure of the deposit, which is strongly affected by its temperature. The deposit temperature is determined by a balance among the rates of heat transfer from the gas, loss of heat to surroundings, and the generation of heat owing to radioactive decay. Radioactive decay heating was experimentally simulated by forming a deposit on the wall of the duct, heating the deposit in flowing steam, and then studying its revaporization and transport.

Revaporization was studied in two stages. In the first stage, the duct was allowed to cool immediately after injection of the sample. In the second stage, the region of the duct where deposition took place was heated to about 1273 K (1000°C) and the steam flow continued for an additional half hour after the injection was completed. The sample consisted of an aqueous solution of CsI and CsOH containing a suspension of finely powdered tellurium (a mixture of Te and TeO_2). The deposit formed on each 0.3-m (1-ft) section of the duct liner was analyzed for Cs, I, and Te. The analytical data were used to compute the amount of CsI, CsOH, and Te deposited. The results for CsI are shown in Fig. VII-1. The open bars indicate the amount of CsI deposited at the end of the first stage, while the shaded bars indicate the amount deposited at the end of the second stage. The two curves indicate the temperature of the inside surface of the liner during injection (stage A) and after revaporization (stage B).

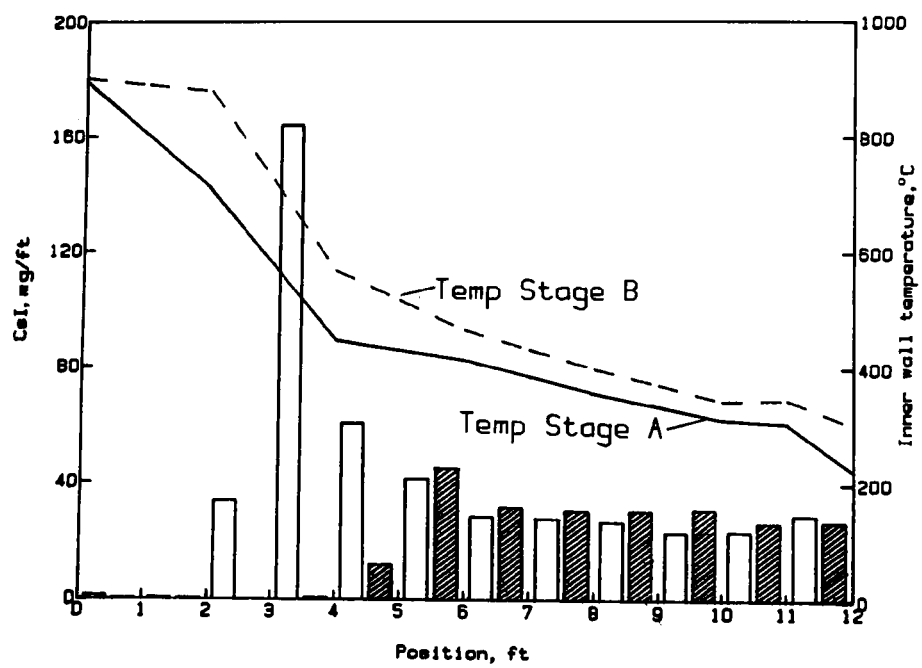

Fig. VII-1. Revaporization of CsI

Consider first the deposition at the end of the injection stage. It is seen that the deposition peaks at the fourth liner and then rapidly decreases to a nearly constant amount. The deposit on the third, fourth, and fifth liners was caused by vapor condensation, and that on the last six liners was caused by the

deposition of aerosol particles. About 18% of the CsI recovered downstream was deposited on the wall of the duct at the end of the injection stage; about 35% of this deposit was from aerosol deposition. At the end of the revaporization stage, most of the deposit that remained in the duct was from aerosol deposition. About 8% of the CsI recovered was found on the wall of the duct; about 76% of this deposit was from aerosol deposition. About 56% of the CsI deposited in the duct during the injection stage was carried out of the duct during the revaporization period. Similar results were obtained for CsOH and Te.

Our results to date strongly suggest the behavior expected in a nuclear accident. During the early stages of the accident, before the plenum has reached high temperatures, extensive deposition of the Cs, I, and Te released from the fuel is expected. The heaviest deposits would be formed where vapor condensation is possible. The amount converted to aerosol would depend on the rate of cooling of the gas: the greater the rate of cooling, the more likely that aerosols would be formed. These aerosol particles would deposit on surfaces but most would be carried downstream because of their small size. Later in the accident, the deposits formed earlier would heat up because of radioactive decay. If there is a flow of gas, they would be revaporized, converted to aerosol particles, and carried further downstream. If the piping had been breached, this could lead to release to the containment vessel.

A model is being developed to predict the downstream behavior of CsI, CsOH, and Te. This model is being tested by comparison with the results of these experiments. The algorithms developed for this model will be incorporated into the large computer programs used to estimate the consequences of various hypothetical accidents.

3. Fission Product Release from Core-Concrete Melts

The objective of this study is to experimentally examine the release of the refractory fission products La, Ba, and Sr from a core debris and concrete melt. Very little is known about the vaporization behavior of these fission products from core-concrete melts (in particular, the effect of oxygen potential on the magnitude of the release). The refractory fission products can make a significant contribution to the source term when containment failure occurs late in an accident. Predictions from various computer codes, such as the VANESA code,[2] have estimated the release of La, Ba, and Sr based on thermodynamic assessment of assumed chemical reactions involving condensed phases and gaseous species. However, very little experimental data exist to confirm these predictions. The results presented below are based on measurements made on small-scale (10-15 g) core-concrete charges.

The transpiration method was used to investigate experimentally the release of La, Ba, and Sr gaseous species from the core-concrete melt. Details of the transpiration apparatus, which was used to investigate the vaporization

[2]D. A. Powers, J. E. Brockman, and A. W. Shiver, *VANESA: A Mechanistic Model of Radionuclide Release and Aerosol Generation During Core Debris Interactions with Concrete*, NUREG/CR-4308, SAND85-1370 (July 1986).

behavior of actinide and rare earth systems, are presented elsewhere.[3,4] The core-concrete charge has a 5-g layer of concrete granules and a 5-g layer of urania fuel granules containing La_2O_3 ($X_{La_2O_3}$ =0.01), BaO (X_{BaO} =0.002), and SrO (X_{SrO} = 0.004) in solid solution with urania. Some core-concrete charges also have a metal layer consisting of a mixture of 5 g of stainless steel (Type 304) and 1 g of Zircaloy chips placed between the fuel and the concrete. The core-concrete charge is contained in refractory-oxide crucibles (thoria or stabilized zirconia) resting on the bottom of a muffle tube. The carrier gas consisted of ultra-high-purity helium saturated with water vapor at room temperature.

We completed five experimental runs (Nos. 6-10) at 2150 and 2385 K to measure the release of La, Ba, and Sr, as well as other species comprising the core-concrete charge. In runs 6-8, the charges contained fuel plus fission products, metals, and limestone or basaltic concrete; in runs 9 and 10, the core-concrete charges had no metals. The collected results, based on chemical analysis of the washings of sublimates from the condenser tube, are given in Table VII-1. From a knowledge of the composition of the core-concrete charge, one can estimate the fractional release of the species listed in Table VII-1. The estimated fractional release values are given in Table VII-2. Pertinent details of the various runs are given in forthcoming proceedings papers.[5,6]

The experimental results can be summarized as follows. For all core-concrete experiments, material loss by vaporization was by far the most important route; loss by entrainment only made a small contribution (<10%). The trend in the release of the refractory fission products followed the sequence: Ba>Sr>La. For runs 6-8, entrainment of metallic and concrete constituents was greater for melts containing limestone concrete than for melts containing basaltic concrete; release of Ba and Sr was about the same with limestone and basaltic concrete; and the transport of Sn, Mn, and Mg was very large, probably because of the strongly reducing conditions existing in the urania-metal-concrete melts. In addition, there was evidence of pyrophoric behavior of metallic Mg. For runs 9 and 10, material loss was significantly greater for limestone concrete than for basaltic concrete. For basaltic concrete containing no metals, the release of Ba, Sr, and La was negligible.

In addition to these findings, the results of our experiments to date show the following:

---

[3]M. Tetenbaum and P. D. Hunt, J. Chem. Phys. **49**, 4739 (1968).

[4]M. Tetenbaum and P. D. Hunt, J. Nucl. Mater. **34**, 86 (1970).

[5]M. Tetenbaum, J. K. Fink, C. E. Johnson, and R. Ritzman, "Fission Product Release from Core-Concrete Melts," to be published in Proc. of the Specialist Meeting on Core Debris/Concrete Interactions, Electric Power Research Institute, Palo Alto, CA, September 2-4, 1986.

[6]M. Tetenbaum, J. K. Fink, C. E. Johnson, M. Chasanov, W. H. Gunther, B. W. Spencer, R. Ritzman, and R. Sehgal, "Fission Product Release from Core-Concrete Melts," to be published in Proc. of Severe Accident Chemistry Symp., Am. Chem. Soc., Anaheim, CA, September 8-12, 1986.

Table VII-1. Measured Release Values From Core-Concrete Melts

	Amount Vaporized, μg				
	Run 6 (2150 K, Limestone + Metals)	Run 7 (2385 K, Limestone + Metals)	Run 8 (2150 K, Basaltic + Metals)	Run 9 (2150 K, Basaltic & No Metals	Run 10 (2150 K, Limestone & No Metals)
La	3	2.3	19	<1	34
Ba	130	340	80	<1	11
Sr	30	68	48	<0.5	5
U	278	118	2135	125	5875
Fe	5890	30850	54040	--	--
Cr	1360	4150	19930	--	--
Ni	340	2770	1030	--	--
Mn	51600	54850	31250	--	--
Zr	21	3	7	--	--
Sn	6090	7040	1900	--	--
Ca	3595	2130	3000	140	400
Mg	8965	125000	14100	--	1980
Si	--	--	--	--	--
Al	1045	280	830	430	1040

Table VII-2. Estimated Release Fractions From Core-Concrete Melts

	Release Fraction				
	Run 6 (2150 K, Limestone + Metals)	Run 7 (2385 K, Limestone + Metals)	Run 8 (2150 K, Basaltic + Metals)	Run 9 (2150 K, Basaltic & No Metals)	Run 10 (2150 K, Limestone & No Metals)
La	5×10^{-5}	6.6×10^{-5}	3.3×10^{-4}	--	5.9×10^{-4}
Ba	2.2×10^{-2}	9.4×10^{-2}	1×10^{-2}	--	1.8×10^{-3}
Sr	5×10^{-3}	2.0×10^{-2}	6.1×10^{-3}	--	8.6×10^{-4}
U	6.4×10^{-5}	4.5×10^{-5}	4.9×10^{-3}	2.9×10^{-5}	1.4×10^{-3}
Fe	1.6×10^{-3}	1.4×10^{-2}	1.4×10^{-2}	1.1×10^{-3}	0.27
Cr	1.5×10^{-3}	7.7×10^{-3}	2.2×10^{-2}	--	--
Ni	8.5×10^{-2}	1.2×10^{-2}	2.6×10^{-3}	--	--
Mn	0.52	0.91	0.3	--	--
Zr	2.1×10^{-5}	5.0×10^{-6}	6.8×10^{-6}	--	--
Sn	0.41	0.78	0.13	--	--
Ca	2.1×10^{-5}	2.3×10^{-3}	5.1×10^{-3}	4.4×10^{-6}	2.6×10^{-6}
Mg	4.8×10^{-2}	1.0	0.18	--	1.1×10^{-2}
Si	--	--	--	--	--
Al	1.7×10^{-2}	7.8×10^{-3}	3.1×10^{-3}	2.0×10^{-3}	1.7×10^{-2}

1. Core-concrete melts containing metals give lower oxygen potential values than do core-concrete melts containing no metals.

2. The release of stainless steel components follows the vaporization behavior of the elements in the steel.

3. The trend in the release of Ba and Sr is in accord with thermodynamic calculations.

4. Investigation of CsI-CsOH System

The objective of this effort is to obtain thermodynamic and vapor pressure data of the more-abundant species in the Cs-I-O-H system. In the duct experiments of Sec. VII.A.1, CsI and CsOH vapors were added separately and together to flowing steam at 1273 K (1000°C), and the gas mixture was subjected to a decreasing temperature gradient. Analysis of the condensate revealed that the iodine-carrying gas (i.e., CsI) condensed at a lower temperature when CsOH was present in the gas mixture.[7] It was concluded that the CsI and CsOH mixture formed a more-volatile complex, reducing the CsI molecules in the vapor. In this effort, we are investigating the mixed iodide-hydroxide (CsI•CsOH) gases over a mixture or solution of CsI and CsOH. For these studies, baseline data for CsI and CsOH are established separately and then the CsI-CsOH mixture is studied. Review of the literature showed fairly good agreement for the thermodynamic properties of CsI, a moderate uncertainty for those of the CsOH monomer, and a large uncertainty for those of the $(CsOH)_2$ dimer. Because CsOH is likely to be the principal vapor species released in an accident, the properties of $(CsOH)_2$ as well as CsOH need to be established.

We measured the total CsI pressures over CsI by transpiration between 725 and 962 K. In the transpiration measurements, the CsI sample was held in a silver crucible suspended from a vacuum balance and heated by a resistance furnace. The crucible was surrounded by a silver condenser tube through which a helium carrier gas was passed. Good agreement was found between three sets of literature data[8–10] and our measurements for CsI vaporization. A third-law calculation of the heat of sublimation of 45.9 $\pm$ 0.7 kcal/mol at 298 K was found for CsI solid sublimating to CsI(g).

We also completed transpiration measurements to determine the total CsOH pressures over liquid CsOH. There was reasonable agreement between another transpiration study[10] and ours, but our pressures were about a tenth of that calculated from the JANAF tables. The JANAF values are based on atomic spectroscopy for the monomer and mass spectrometry for the dimer.

---

[7]M. J. Steindler et al., *Chemical Technology Division Annual Technical Report, 1985*, Argonne National Laboratory Report ANL-86-14, p. 91 (1986).

[8]V. Venugol, R. Prasad, and D. D. Sood, J. Nucl. Mater. **130**, 115 (1985).

[9]I. Barin and O. Knacke, *Thermochemical Properties of Inorganic Substances*, Springer-Verlag, Berlin (1977).

[10]J. C. Cummings, R. M. Elrick, and R. A. Sallach, *Status Report on the Fission-Product Research Program*, NUREG/CR-1820, SAND80-2662 R3 (March 1982).

Next, we used a mass spectrometer to measure the partial pressures of vapor species over liquid CsOH held in a silver Knudsen cell. The ion current for each of the positive ions was measured, multiplied by the absolute temperature, and plotted in Fig. VII-2. The top curve is for Cs^+, which is believed to be a fragment of CsOH monomer; the second curve is for $CsOH^+$; and the third curve is for Cs_2OH^+, a fragment of $(CsOH)_2$. The Cs^+ data were used to calculate the total pressure as CsOH monomer.

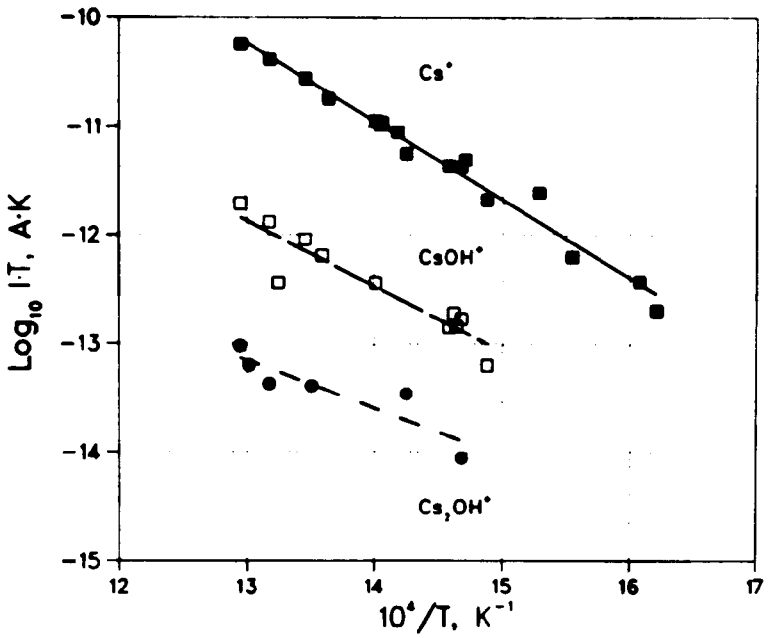

Fig. VII-2. Product of CsOH Vapor Ion Currents and Temperatures Measured with a Mass Spectrometer

Pressure can be calculated from the ion current and temperature by

$$P = K\ I\ T \tag{1}$$

where P is pressure (atm), I is ion current (A), T is the temperature (K), and K is a constant for the instrument and geometry of the system. Pressure may also be calculated by substituting the effusion rate from the Knudsen cell into the Langmuir equation,

$$P = \frac{wt}{44.33\ At}\left(\frac{T}{M}\right)^{1/2} \tag{2}$$

where wt is weight loss (g), A is area (cm^2), t is time (s), T is temperature (K), and M is molecular weight (g). The total weight loss was determined by weighing the Knudsen cell before and after the mass spectrometric measurements. Next, Eqs. 1 and 2 were combined and integrated over time to solve for the

constant K. Pressures were then calculated from Eq. 1. Figure VII-3 plots, as a function of temperature, the pressures for the CsOH vapor species (monomer and dimer) determined from the JANAF tables and our spectrometric work. The JANAF tables predict that the dimer will be more abundant than the monomer below 800 K, and that the monomer will be the dominant species above 800 K. Our data show monomer pressures about four-fold lower than those calculated with JANAF values. The largest difference was found for the dimer, where the values are 100-fold lower than the JANAF values at 800 K. When both sets of CsOH species (monomer and dimer) are added, our pressure data are a factor of ten lower than the JANAF data but are in general agreement with our transpiration results. This means that calculated release rates in an accident should be decreased by as much as a factor of ten also.

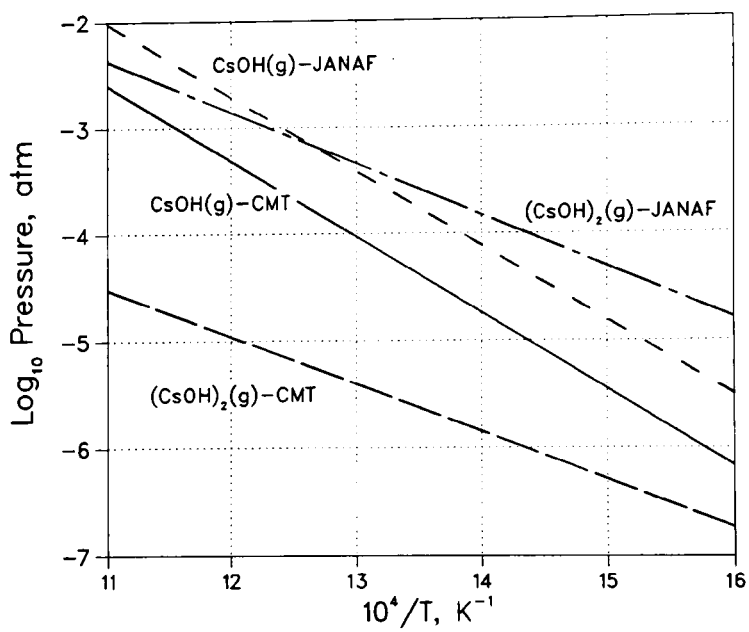

Fig. VII-3. CsOH Vapor Species Measured at CMT and Calculated from JANAF

We also used a transpiration system to measure the pressures of the CsI-CsOH complex. Both CsI and CsOH vaporize as monomers and dimers, i.e., CsOH, $(CsOH)_2$, CsI, and $(CsI)_2$. Besides these four gases, we also expect to find the CsI•CsOH complex when the vapor is in equilibrium with a solution of CsI and CsOH liquid. The partial pressures of CsI and CsOH (monomer and dimer) can be calculated from the activities of CsOH and CsI and thermodynamic data for the condensed and vapor species. If the CsI•CsOH complex is significantly larger than the iodides or the hydroxides, more iodine or hydroxide should be found in the condensate than that calculated for the monomer and dimer species. Activities for the CsOH and CsI solutions were estimated from phase diagrams for the KOH and KI system.

Our transpiration measurements on CsI-CsOH mixtures consisting of 0.885 mol CsOH and 0.115 mol CsI are shown in Fig. VII-4. The top curve is the total CsI pressure [CsI(g) + $(CsI)_2$(g)] in equilibrium with CsI liquid and solid; the lower curve is that calculated for the activity of 0.115 mol CsI dissolved in 0.885 mol CsOH; and the middle curve is the measured total pressure of CsI(g), $(CsI)_2$(g), and CsI•CsOH(g). The difference between the middle and lower curves is equal to the CsI•CsOH complex pressure. Using the estimated activity coefficients for the CsI-CsOH system, we calculated that the CsI•CsOH complex pressure is four times the CsI pressure. The data in Fig. VII-4 clearly indicate a large increase in iodine content in the vapor when CsOH is mixed with CsI, suggesting a stable CsI•CsOH complex molecule.

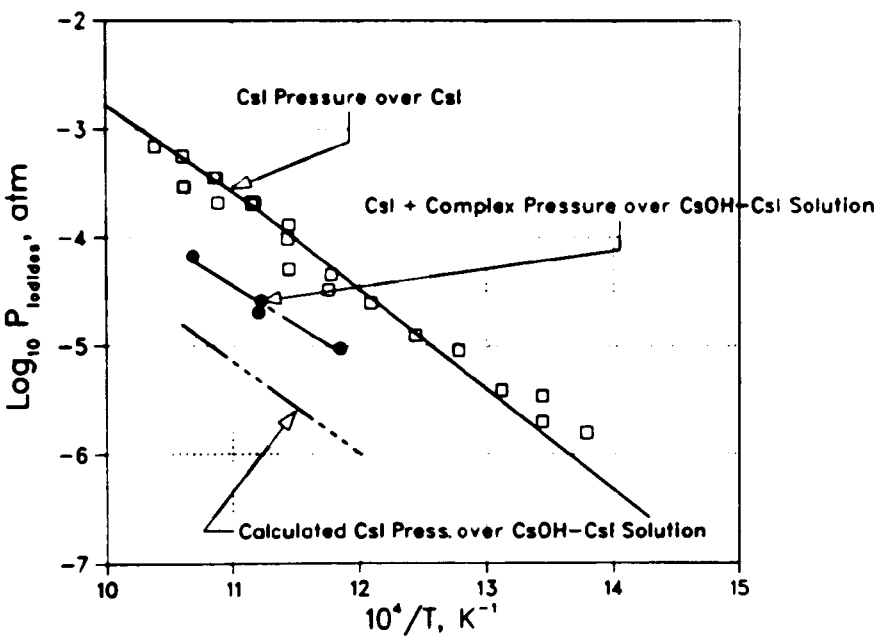

Fig. VII-4. CsI and Iodide Complex Pressures over CsI and 0.885 CsOH-0.115 CsI Solution

Since the activities of CsI and CsOH in CsI-CsOH solution are estimated, we plan to measure them. The concentration of the CsI•CsOH complex was based on CsI mass balance measurements. A mass balance of CsOH will also be used to confirm the CsI•CsOH concentration. After concluding this phase of the work, we plan to measure the thermodynamic properties of Cs_2TeO_3 gas.

5. Fission Product Chemistry in Source Term Experiments

The Source Term Experiments Program (STEP) consisted of four different reactor-accident simulations run in the Transient Reactor Test (TREAT) facility during the period June 1984 to March 1985. The behavior of fission

products released from irradiated UO_2 fuel rods (3-4.5 at.% burnup) when overheated in flowing steam to the point of catastrophic degradation of their Zircaloy cladding (temperatures of up to 2500 K in a half-hour period) was investigated in these in-pile simulations. The materials released from the failed fuel rods were carried downstream by flowing steam and hydrogen (from cladding oxidation) and were collected on various coupons and wires in three types of aerosol-characterization device: a sample cage, a sample tree, and two canisters.[11,12]

The 1986 effort focused on clarification of the chemistry involved in STEP by identifying the compounds in various deposits and developing plausible mechanisms for their formation. The compounds investigated were Cs-I, Ni-I, Ag-Cs-I, Sn-O, Cs-Mo-O, and Cs-Te.

We were unable to identify CsI in the deposits from STEP-1. X-ray diffraction (XRD) analyses were conducted on six STEP-1 samples and CsI was not found in any of these. In cooperation with J. Sanecki (Materials Science Division), electron channeling studies detected large crystals (about 1 mm) in a pure CsI sample prepared by us but did not show a CsI pattern from the small Cs- and I-containing crystals (10-50 μm) in the STEP samples.

Droplet-shaped Ni-I deposits were found on nickel wires in three different locations in a sampling canister in STEP-1. X-ray diffraction was unsuccessful because the deposits were amorphous. Electron-probe microanalysis (EPM) indicated an oxygen-to-iodine ratio of three to one. Two nickel compounds, $NiI_2 \cdot 6H_2O$ and $Ni(IO_3)_2$, have this ratio. The former compound was made by exposing nickel wires to HI-steam vapors, but the compound had two characteristics that differed from the STEP-1 deposits. First, it was extremely hygroscopic; the STEP wires were handled in air with no evidence of water pickup or other change in the deposits. Second, it lost its waters of hydration in vacuum; EPM indicated oxygen was present under high-vacuum conditions in the STEP deposits. The $Ni(IO_3)_2$ compound was generated on nickel wires exposed to HIO_3-steam vapors. These deposits were usually droplet shaped and amorphous. However, under dry ambient conditions, droplet-shaped, crystalline deposits of $Ni(IO_3)_2$ (yellow) and $Ni(IO_3)_2 \cdot 2H_2O$ (blue) were formed and were identified by XRD. Thus, the deposits formed in STEP-1 may have been an amorphous form of nickel iodate.

---

[11]B. Schlenger, P. F. Dunn, J. E. Herzeg, R. Simms, E. L. Horton, L. Baker, and R. L. Ritzman, "Chemical Characteristics of Material Released During Source Term Experiments Project (STEP) In-Pile Tests: Part I," to be published in Proc. of ACS Symp. on Chemical Phenomena Associated with Radioactivity Releases During Severe Nuclear Plant Accidents, Anaheim, CA, September 8-12, 1986.

[12]J. K. Fink, M. F. Roche, C. A. Seils, D. V. Steidl, C. E. Johnson, and R. L. Ritzman, "Chemical Characteristics of Material Released During Source Term Experiments Project (STEP) In-Pile Tests: Part II," to be published in Proc. of ACS Symposium on Chemical Phenomena Associated with Radioactivity Releases During Severe Nuclear Plant Accidents, Anaheim, CA, September 8-12, 1986.

Long needles containing collocated Ag, Cs, and I were seen on many STEP-1 coupons. X-ray diffraction analysis identified metallic silver in the scrapings from a coupon that had a large number of these needles. This result was unexpected; we had anticipated finding one or more of the $Cs_{1-x}Ag_xI$ compounds. Secondary ion mass spectroscopy (SIMS) indicated that the silver in the deposits was of natural abundance (i.e., not a fission product); the probable source was a silver coupon located in a sample cage which reached a temperature of about 1050 K. Iodine was found collocated with silver on this cage sample. A possible transport mechanism, supported by the collocation of the elements, is transport as an Ag-Cs-I vapor complex; gaseous alkali-silver halides are known to exist.[13] Assuming such a complex is formed, we are still left with the problem of understanding the reactions causing oxidation of the silver metal in the cage area and reduction to metallic silver in the canister. Further study is needed to explain this unusual behavior.

X-ray diffraction analysis of STEP-1 samples identified SnO_2. The probable transport mechanism, based on our thermodynamic calculations,[12] is steam oxidation of the Zircaloy cladding (1.5 wt% Sn) to form ZrO_2 and the gas-phase species $Sn(OH)_2$ and SnO. Below about 900 K, SnO_2 (cassiterite) becomes the stable species in the steam-hydrogen environment of STEP-1 (about 80 mol% H_2). Thus, the presence of cassiterite in the canisters at about 650 K is in accord with thermodynamic calculations.

We are investigating molybdenum release and its effect on the chemistry of Cs and I. Molybdenum was found collocated with Cs and Sn. Since tin is present as SnO_2, we can think of the molybdenum as being collocated with cesium and ignore the tin. The collocation of molybdenum and cesium suggests transport and deposition as a cesium molybdate species. The compound Cs_2MoO_4 (mp, 1215 K)[14,15] is known to be a stable gas-phase molecule,[16] and its pressure over the fuel is significant.[14] Our thermodynamic calculations[12] also suggest that steam, molybdenum, and cesia can react to form cesium molybdate. X-ray diffraction studies of selected STEP-1 samples are in progress to identify the molybdenum-containing species.

Tellurium, generally collocated with cesium, was detected on only a few isolated samples, even though tellurium was present in the fuel at a concentration more than twice that of iodine. This observation is not surprising when results of laboratory experiments on the deposition of tellurium and cesium in steam are

---

[13]A. Buchler and J. B. Berkowitz-Mattuck, "Gaseous Ternary Compounds of the Alkali Metals," in *Advances in High Temperature Chemistry, Vol. 1*, L. Eyring, ed., Academic Press, New York (1967).

[14]T. B. Lindemer, T. M. Besmann, and C. E. Johnson, J. Nucl. Mater. **100**, 178 (1981).

[15]H. Kleykamp, J. Nucl. Mater. **131**, 221 (1985).

[16]I. Johnson, J. Phys. Chem. **79**, 722 (1975).

considered.[17,18] These laboratory experiments indicated that tellurium deposition peaks in the temperature range 1000-1100 K. Thus, significant deposition of tellurium in the canisters (~650 K) is not expected. Electron-probe micro-analysis on a sponge-like deposit found in one canister indicated a Cs-to-Te ratio of 1.8 to 3.5 (mean of 2.5), and both EPM and SIMS indicated a low oxygen content. These data suggest that Cs_2Te is deposited in this case, but others have suggested CsTe,[17] Cs_2TeO_3,[17] and Cs_2TeO_4[18]. Additional work is needed in this area.

The initial flow velocities in STEP-3 and -4 were a factor of thirty lower than those in STEP-1 and -2.[11] Peak temperatures also were hundreds of degrees lower. These thermal-hydraulic differences, no doubt, account for the differences in aerosol deposits: the predominant constituents were Fe in STEP-3 and Si in STEP-4, while in STEP-1 and -2, the predominant constituents were Cs, Mo, and Sn. Because STEP-2 had deposits much like those in STEP-1, our research to date has been focused on STEP-1. Additional study of STEP-2 deposits may be of interest to resolve issues that have been raised in the STEP-1 work, particularly in the areas of iodine and tellurium chemistry.

6. Fission Product Revaporization

The rate of vaporization of selected fission products, control-rod materials, cladding, and structural components is being determined in this study. The compounds and elements under investigation are CsI, CsOH, TeO_2, SrO, Ag, In, Cd, and Sn. The objective is to provide data to model the revaporization of such materials during a reactor accident. The materials are placed in a Type 304 stainless steel boat within a heated stainless steel tube at 773 and 1023 K. Steam is passed through the tube at a controlled rate, and the vaporized materials are collected in cooler areas downstream, removed, and characterized.

In experiments with metals, 1 g Ag, 1 g Cd, 0.14 g In, and 0.035 g Sn were placed in the boat, and the transported material at 773 K (steam flow: 5 g/min for 45 min) and 1023 K (steam flow: 5.8 g/min for 30 min) was cadmium metal. The percent of the cadmium transported was 18.4 and 66.6% in the 773 and 1023 K run, respectively. In experiments with compounds, 1.1 g $CsOH \cdot H_2O$, 0.2 g CsI, 0.2 g TeO_2, and 0.07 g SrO were placed in the boat, and the transported materials were Cs, I, and Te. The percent material transported at 773 K (steam flow: 3.5 g/min for 45 min) was 11.0, 9.8, and 10.5%, respectively; the percent material transported at 1023 K (steam flow: 5.6 g/min for 15 min) was 60, 75, and 31%, respectively. For the 1023 K experiment, 14% of the iodide was found to be in the iodate form (no iodate was found in analyses of the samples from the 773 K experiment).

---

[17]I. Johnson, C. E. Johnson, M. Farahat, J. Settle, and R. Ritzman, "Downstream Behavior of Fission Products," to be published in Proc. of ACS Symp. on Chemical Phenomena Associated with Radioactivity Releases During Severe Nuclear Plant Accidents, Anaheim, CA, September 8-12, 1986.

[18]Y. Norihiro, "JAERI Analysis of Marviken Samples," presented at Marviken Code Comparison Meeting, Argonne National Laboratory, July 15-17, 1986.

Computer programs have been written to describe the transport in the above experiments so that revaporization effects in reactor accidents can be calculated. These programs employ mass-transfer correlations of the general form[19]

$$Nu = a(Re)^x(Sc)^y \tag{3}$$

where Nu, Re, and Sc are the Nusselt, Reynolds, and Schmidt numbers, respectively. To derive the transport coefficients in this equation, we conducted a series of mass-transport experiments in which the boat (containing water, ethanol, or 1-butanol) was placed in a glass tube of the same diameter as that of the experimental apparatus. Nitrogen gas at room temperature and flow rates ranging from 5.3 to 17.7 L/min was passed over the boat, and the transport rates of vapors of water, ethanol, or 1-butanol were determined from the weight loss. Correction factors were applied to these experiments, the most important being that all transport-rate data were corrected to a fill fraction of 1.0 using calibration runs. Once corrections had been made, the data were reasonably well represented by a standard correlation for mass transfer in laminar flow from a flat plate of length equal to that of the boat[19]:

$$Nu = 0.66(Re)^{1/2}(Sc)^{1/3} \tag{4}$$

The water data were fit by the equation

$$Nu = 0.75(Re)^{1/2}\ (Sc)^{1/3} \tag{5}$$

with an acceptable correlation coefficient (0.952). The constant, 0.75 $\pm$ 0.03, does not reflect any correction for meniscus effects (geometric areas were used, i.e., a contact angle of 90°). If wetting occurs, the area for mass transport will be increased because the liquid surface will be curved (this correction depends on liquid surface tension). Use of the liquid area for a contact angle of 0° (complete wetting) leads to a new constant of 0.56 $\pm$ 0.03. Our visual examinations indicated the actual wetting angle was between 0 and 90°, thus suggesting that a value between 0.75 and 0.56 is appropriate. The two values bracket the theoretical value of 0.66.

The 1-butanol data were fit by

$$Nu = 1.32(Re)^{1/2}\ (Sc)^{1/3} \tag{6}$$

but with a somewhat poorer correlation coefficient (0.90). In this case, the constant, 1.32 $\pm$ 0.06, must be altered because butanol spreads on Type 304 stainless steel. The correction for the meniscus leads to a constant of 1.23 $\pm$ 0.06. This is higher than the theoretical value (0.66), and we continue to search for an explanation of this puzzling result.

The ethanol data were fit by

$$Nu = 0.90(Re)^{1/2}\ (Sc)^{1/3} \tag{7}$$

---

[19]C. O. Bennett and J. E. Myers, *Momentum, Heat, and Mass Transfer*, Third Ed., McGraw-Hill Book Co., New York (1982).

with a correlation coefficient of 0.92. The derived constant, 0.90 ± 0.04, requires the "meniscus" correction since ethanol also spreads on the steel. The corrected value is 0.84 ± 0.04, which is not very far from the theoretical value of 0.66.

The data from the steam experiments are currently being analyzed using the above transport model. If they also agree reasonably well with the standard mass transport equation, it will be possible to calculate revaporization effects in a relatively simple manner.

B. *Metal Fuels Properties*

A recent literature survey revealed serious shortcomings in the data available on the thermophysical properties of fuel and blanket materials for the Integral Fast Reactor (IFR). Our ongoing program is designed to correct the most important of these deficiencies by performing selected experiments. In addition, study of other physicochemical areas of importance to the project has been undertaken. This report summarizes the progress made on determining thermal expansion, thermal conductivity, phase diagrams, and fuel-cladding interactions for IFR materials.

1. Thermal Expansion

We are conducting linear expansion measurements on IFR fuel alloys, using a Netzsch pushrod dilatometer installed in a helium-atmosphere glove box. After extensive calibration procedures, we investigated two alloys: U-8.4 wt% Zr and U-20 wt% Pu-1.3 wt% Zr.

Our expansion results for the first alloy agree reasonably well with literature values,[20–26] but our data show the phase transitions in greater detail. The most pronounced transitions occur at 940-950 K and 960-985 K. Transitions at 870 and 920 K are less obvious.

---

[20]Y. S. Touloukian, R. K. Kirby, R. E. Taylor, and P. D. Desai, *Thermophysical Properties Matter*, Plenum Press, New York (1965).

[21]H. A. Saller, R. F. Dickerson, and W. F. Murr, *Uranium Alloys for High-Temperature Application*, Battelle Memorial Inst. (Columbia, Ohio) Report BMI-1098 (1956).

[22]F. A. Rough, *An Evaluation of Data on Zirconium-Uranium Alloys*, Battelle Memorial Inst. (Columbus, Ohio) Report BMI-1030 (1955).

[23]R. Boucher and P. Barthelemy, *Comparison of the Alloys U-Pu-Mo, U-Pu-Nb, U-Pu, Ti, U-Pu-Zr*, ANL-Trans-138 (1964), translation by B. Blumenthal, CEA-R-2531 (1964).

[24]*Argonne National Laboratory, Metallurgy Division, Annual Progress Report for 1965*, ANL-7155, pp. 14-25 (1965).

[25]L. R. Kelman, H. Savage, C. M. Walter, B. Blumenthal, R. J. Dunworth, and H. V. Rhude, "Status of Metallic Plutonium Fast Power-Breeder Fuels," *Plutonium 1965*, A. E. Kay and M. B. Waldron, ed., Chapman and Hall, London, p. 458 (1967).

[26]D. R. Harbur, J. W. Anderson, W. J. Maraman, *Studies on the U-Pu-Zr Alloy System for Fast Breeder Reactor Applications*, Los Alamos National Laboratory Report LA-4512 (1970).

For the ternary alloy, dilatometric studies were made on two apparently identical samples. Initial measurements showed a time drift in the expansion coefficient, evidently because of sample annealing, but the readings stabilized after several heating/cooling cycles. The results are in reasonable accord with reported data.[23-26] There was a 0.4% elongation in both samples, measured at room temperature after the experiments were completed. This elongation was probably due to structural changes in the alloy. In addition, a significant difference in the thermal expansion of the two samples was found, in spite of their nearly identical overall chemical composition. Metallographic examination is planned of the heat-cycled and as-received alloys to clarify these observations.

2. Thermal Conductivity

Information on the thermophysical properties of the U-Zr system is important to the IFR project because this alloy (at a composition of ~10% Zr) is intended for initial reactor loadings. A vertical section of the available U-Zr phase diagram[27] at that composition shows the existence of $U(\alpha) + UZr_2(\delta)$ solid mixture up to a peritectoid horizontal at 890 K, another peritectoid at 935 K, a eutectoid at 966 K, and $U(\gamma),Zr(\beta)$ solid solution between 1013 K and the solidus line at ~1473 K. Previous experimental work on the thermal conductivity (λ) of the U-Zr system is limited to one study in 1954,[28] where λ was measured between 300 and 1200 K in 1.5, 5, 20, and 40 wt% Zr alloys. The present study was undertaken to verify these data and to provide additional data at an alloy composition that is nearer to IFR requirements.

The technique used in our conductivity measurements was based on a comparative method. A cylindrical alloy sample (2.54-cm dia, 2.54-cm high) was positioned in a vertical column between two identical references having a known λ and essentially the same geometry as the alloy sample. Longitudinal heat flow through the column was established by heaters placed above and below the column. The bottom heater rests on a water-cooled block and acts as a heat sink. Radial heat losses were minimized by surrounding the column with a guard furnace in which the thermal gradient was matched to that of the column and by filling the annular space with foamed-yttria granules.

Conductivity measurements were made in an inert atmosphere glove box at 50 temperatures between 600 and 1200 K on a single U-11.4 wt% Zr sample. Experience has indicated that, at these elevated temperatures, the uranium-containing alloys tend to fuse with the reference material at their contiguous surfaces, thereby making the references unfit for further use. Therefore, secondary Type 304 stainless steel references, calibrated against a primary standard from the National Bureau of Standards (NBS), were employed

---

[27]P. Chiotti, V. Akhachinkij, I. Anasara, and M. H. Rand, *The Chemical Thermodynamics of Actinide Elements and Compounds*, Part 5, "The Actinide Binary Alloys," Int. Atomic Energy Agency, Vienna (1976).

[28]H. W. Deem as reported by R. C. Westphal in *Thermal Conductivity of Reactor Fuel Elements*, Westinghouse Electric Corp., Atomic Power Division, AECD-3864 (June 1954).

in this work. Slight differences in the measured heat flux between the top and bottom references were found to be functions of the total temperature gradient (ΔT) imposed on the column. Therefore, for each temperature the column was equilibrated at two ΔT values (25 and 50 K), and a linear interpolation was then used to determine the average temperature and λ of the sample corresponding to identical heat fluxes in both references.

The data, shown in Fig. VII-5, were arbitrarily subdivided into three chronological acquisition periods, each representing a full temperature range. No

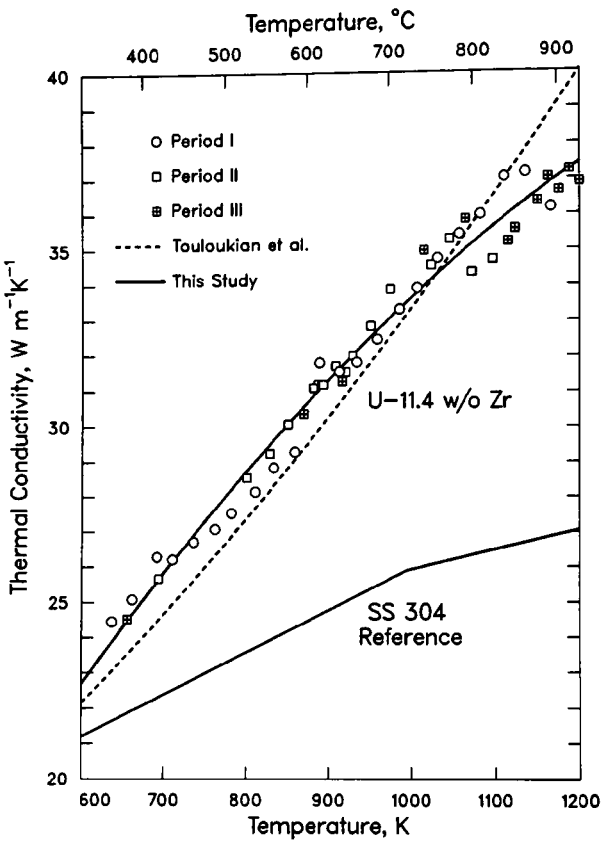

Fig. VII-5.

Thermal Conductivity of U-11.4 wt% Zr Alloy

systematic errors are apparent. The data were fitted to a second-degree polynomial:

$$\lambda = -1.763 + 4.871 \times 10^{-2}T - 1.330 \times 10^{-5}T^2 \quad (8)$$

where λ is the thermal conductivity in W m^{-1} K^{-1}, T is the Kelvin temperature, and the correlation coefficient of regression is 0.979. Because of the large scatter, no attempt was made to correlate the curve with the phase transformations. A possible source for the scatter might be the insufficiently long equilibration times allowed for the stabilization of numerous transition phases appearing in the temperature range 890-1013 K. The dashed curve represents the 1954 data calculated for 11.4 wt% Zr from a quadratic fit of those data.[28] There is a fair

agreement between the two studies, but the steadily decreasing $d\lambda/dT$ with increasing temperature of our curve is more in line with the expectation of a shorter mean free path of electrons at higher temperatures.

3. Phase Behavior

An analysis of existing data on the U-Pu-Zr system by A. D. Pelton (Ecole Polytechnique, Montreal) revealed large uncertainties in the solidus and liquidus temperatures, estimated to be about ±125 and ±75°C, respectively. We undertook differential thermal analysis (DTA) measurements to obtain more-reliable data. To ascertain that the container material does not influence the results, we performed the DTA measurements with U-20 wt% Pu-7 wt% Zr in both yttria and beryllia crucibles, since there had been indications of interaction between beryllia and a U-10 wt% Zr sample.

The experiments were performed with a Netzsch DTA apparatus located in a helium-atmosphere glove box. After completion of seven heating/cooling cycles ranging from room temperatures to 1750 K at 5 K/min, the samples were weighed and visually inspected. No obvious evidence of interaction was found. With the yttria crucible, the melt did not wet the walls of the crucible, and the sample could be removed by soft tapping; however, the melt did wet the walls of the beryllia crucible and the sample could not be removed. Good agreement was found with the two crucibles for the solid-state transitions of the U-Zr alloy, but not for its solidus and liquidus temperatures. However, the yttria crucible used was not of optimum design, and these tests will be repeated with improved yttria crucibles. Following the DTA work, the sample that had been heated in yttria was examined by microprobe techniques. No yttrium was found in the alloy. In addition, virtually all of the so-called globular phase (an α-Zr phase found in as-cast fuel) had floated to the top of the melt and had increased considerably in globule diameter. The implications of this observation for fuel fabrication and performance are being explored.

In another study of phase relations in IFR systems, we calculated ternary phase diagrams involving U, Pu, Zr, and Fe. These calculations helped clarify the role of zirconium in improving fuel-cladding performance. Although very low melting eutectic compositions are in both the U-Fe and Pu-Fe systems, the addition of Zr to either of those systems produces a very extensive Fe_2Zr phase field, which restricts the lower melting compositions to very narrow regions. These, and other, phase diagram calculations are being continued to further clarify matters related to fuel performance.

4. Fuel-Cladding Compatibility Studies

Previous studies have shown that plutonium-rich layers can segregate on the surfaces of heated U-Pu-Zr alloys when they are exposed to cladding, NaK, or helium atmosphere.[29] The phenomenon appears to be related to the availability of nitrogen at the alloy surface. To clarify these observations, we are performing tests in which selected IFR alloys are heated in nitrogen-helium mixtures that simulate the nitrogen activity estimated for the cladding.

---

[29]D. R. O'Boyle, Argonne National Laboratory, unpublished information (1967).

The tests are carried out in a sealed thermogravimetric apparatus (located in a helium-atmosphere plutonium glove box) by placing a freshly abraded cylindrical alloy sample on an alumina platform that rests upon a thermocouple connected to the TGA balance beam. After flushing the instrument with the helium-nitrogen mixture selected for the test, a slow stream of gas is continued to provide uniform nitrogen activity around the sample. A programmed heating/cooling cycle is then initiated to monitor and record the sample weight gain and temperature.

In a typical test, exposure of U-20.0 wt% Pu-1.3 wt% Zr alloy to the flowing He-50 ppm N_2 mixture for 12 h at 700°C produced a clearly distinguishable 10-μm-thick surface layer. Scanning electron microscopy/energy dispersive spectrometry (SEM/EDS) revealed that the layer underwent major compositional changes under the action of nitrogen: considerable enrichment of plutonium, some enrichment of zirconium, and large depletion of uranium. One can speculate that the reaction products of nitrogen with zirconium and plutonium are more stable than those with uranium, thereby producing activity gradients in the alloy that cause migration of Zr and Pu to the reaction site at the surface. Removal of Zr and Pu from the surface layer as unalloyed reaction products might sufficiently increase the uranium activity in the remaining alloy to cause its reverse migration. Additional nitriding tests and SEM/EDS analyses are underway to determine the degree of segregation as a function of temperature, gas-phase composition, and alloy composition.

C. *Fusion-Related Research*

A critical element in the development of the fusion reactor is the blanket for breeding tritium fuel. We are conducting several studies with the objective of determining the feasibility of using lithium-containing ceramics as breeder material. We are also conducting design studies of methods for improving fusion reactor performance and neutron dosimetry and damage analysis of fusion materials in neutron facilities.

1. Thermodynamic and Kinetic Studies of Breeder Materials

The objective of this work is to provide calculated and measured thermodynamic and kinetic data related to tritium retention and release from ceramic breeder materials. This information will enable (1) breeder materials to be compared and the most suitable one to be selected and (2) operating conditions to be established. The relevant phenomena are surface adsorption and desorption of aqueous species and the solubility of hydroxide and tritoxide in $LiAlO_2$, the breeder material under current investigation. At thermodynamic equilibrium, tritium inventory in a ceramic breeder will be composed of a portion due to dissolved tritium (tritoxide and, under some conditions, tritide) and a portion due to surface-adsorbed tritium (HTO, T_2O, HT, and T_2). Contributions from both portions must be assessed because their relative contributions depend on conditions.

a. Calculational Survey

A calculational survey, using the computer code SOLGASMIX,[30] was made of the ideal-solution equilibrium thermodynamic relationships among the gaseous and condensed phases and the breeder surface at temperatures of 700-1300 K and oxygen activities from 10^{-25} to 10^{-5}.[31] Literature values for the thermodynamic variables were used. The calculations suggested that the degree of surface adsorption at 700 K is essentially independent of oxygen activity in the range of 10^{-25} to 10^{-5}. Under these conditions, the magnitude of adsorption is substantial and accounts for 89% of the tritium in the system; 13.5% of the surface holds adsorbed material. Only 1% of the tritium in the system is in the gas phase and 10% is in solution in the $LiAlO_2$, as tritoxide. Dependence on oxygen activity becomes more significant at higher temperatures, becoming noticeable at 1000 K for oxygen activities below 10^{-20}. Substantial dependence on oxygen activity at 1300 K exists for oxygen activities lower than 10^{-15}. Above this activity, there is still independence of oxygen activity, and only about 2% of the tritium is adsorbed on the surface, but 94% is in solution as tritoxide.

From a thermodynamic perspective, the most favorable condition for tritium release is at high temperature and low oxygen activity; the reduced form of tritium (T_2) would be favored. At extremely low oxygen activity (10^{-25}) and 1300 K, 0.04% of the tritium in the system is adsorbed on the surface. Under these conditions, 94% of the tritium is in the gas as T_2 and 6% is in solid solution as tritoxide.

The relative amounts of tritium adsorbed on the surface and of tritium in solid solution remain essentially constant over the oxygen activity range for 700 and 1000 K, though the absolute quantities differ. Except for low oxygen activity (below 10^{-20}), this constancy also holds for 1300 K. The departure from constancy arises from the growing importance of tritide, T^-, as a solute species in the $LiAlO_2$. Also, under low oxygen activity, the growing importance of the reduced species, T_2, in the gas phase is augmented by the relatively poor adsorption of this species compared with T_2O.

Our calculations predict that surface adsorption can be expected to make its greatest contribution to inventory under conditions of low temperatures and high oxygen activities. Our results suggest a thermodynamic rationale for the report of enhanced tritium recovery, ascribed to "surface effects," when elemental hydrogen, which reduces oxygen activity, was in the helium sweep gas passed over the $LiAlO_2$ sample in the TRIO experiment.[32] Nominally pure helium sweep gas, which might contain 1 ppm of oxygen, would provide an oxygen activity of $>10^{-6}$, a high oxygen activity in the context of ceramic breeders. This effect is discussed further in Sec. VII.C.c.

---

[30]T. M. Besman, *SOLGASMIX-PV, A Computer Program to Calculate Equilibrium Relationships in Complex Chemical Systems*, Oak Ridge National Laboratory Report ORNL/TM-5775 (1977).

[31]A. K. Fischer, J. A. McDaniel, and C. E. Johnson, "Studies of Surface Adsorption on $LiAlO_2$," J. Nucl. Mater. **141-143**, 344-347 (1986).

[32]R. G. Clemmer et al., *The TRIO Experiment*, Argonne National Laboratory Report ANL-84-55 (1985).

b. Experimental Measurements

Frontal analysis gas chromatography (the "breakthrough technique") is being used for the measurements of adsorption. Post-adsorption uptake of water vapor by $LiAlO_2$ is being measured to determine the solubility of hydroxide in $LiAlO_2$. The data will yield adsorption isotherms to describe the thermodynamics of the adsorption of water vapor and the dissolution of hydroxide. The rates of the reverse processes, desorption and evolution of water vapor, are being measured to describe the kinetics of the release of water vapor. Determination of the dependence of these quantities on oxygen activity is included in the experimental effort. Data have been obtained for a gas of 550 ppm H_2O (by volume) in helium and in the temperature range of 486 K (213°C) to 891 K (618°C) at relatively high oxygen activity (over 10^{-6}).

Figure VII-6 plots the adsorption and dissolution of H_2O vapor at the different temperatures. The curves show the rate of water vapor flow issuing from the end of the chromatographic column as a function of time. (The ordinate is in units of "nominal ppm," which is related to mol/min by a calibration factor given in the figure caption.) The difference in the curves for 590 K (317°C) and 591 K (318°C) compared with the others is believed to reflect the appearance of a second condensed phase, a LiOH-rich one, in addition to the dominant $LiAlO_2$-rich one. This phenomenon can be understood in terms of the H_2O partial pressure in these measurements at 591 K (318°C) being greater than that over the Li_2O-LiOH system at this temperature. It follows that the maximum partial pressure of HTO, T_2O, or H_2O to avoid formation of this second condensed phase would be similar for all candidate breeder materials. Differences would be mainly attributable to the extent that different breeder materials would show different degrees of solubility in LiOH, which would lower the activity of LiOH in the second phase to different degrees.

Isothermal evolution of water vapor from the $LiAlO_2$ into a stream of pure helium was also measured. The early parts of the evolution curves in Fig. VII-7 show a short plateau before dropping off. This region reflects the process that is the converse of breakthrough and measures surface desorption, leading to information on surface desorption isotherms. The region of declining water evolution reflects the dissolved hydroxide coming out of solution.

First-order and second-order kinetics tests were applied to the water evolution data. For all temperatures considered so far, with the exception of 891 K (618°C), the evolution of water vapor during the first several hundred minutes reflects a rate-limiting process that is kinetically first order in dissolved hydroxide and suggests "hydroxide" diffusion to be the process. Since the diffusing species in solid solution (or on the surface, for that matter) is the proton, and since "hydroxide" diffusion is only the apparent result of proton diffusion, these results indicate that the evolution of water is first order in the proton concentration. Combination of hydroxides on the surface to evolve water is taken to be a second-order process. Figure VII-8 shows the excellent fit of the regression line to experimental points for a test of first-order kinetics at 591 K (318°C). However, at 891 K (618°C), the fit is better to second-order kinetics.

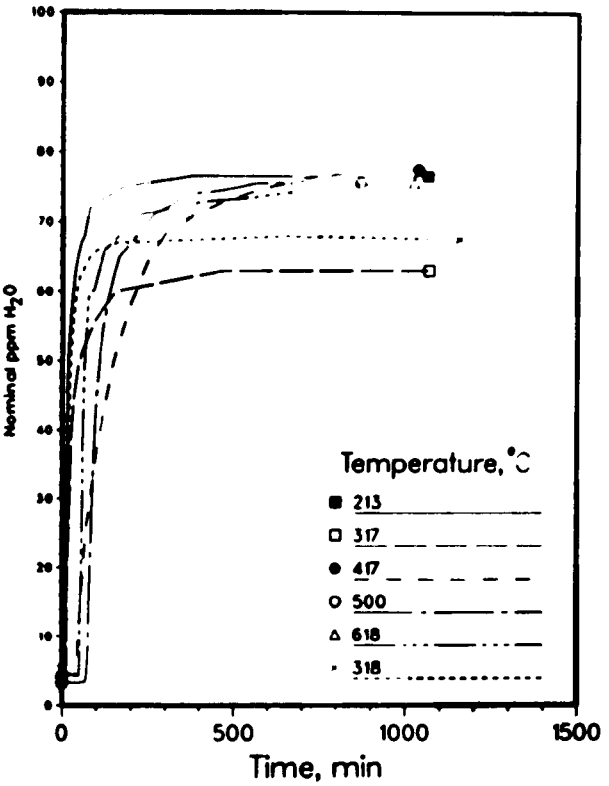

Fig. VII-6.

Adsorption and Dissolution of H_2O Vapor from Helium Stream Containing 500 ppm H_2O by volume. (Flow rate is 13.8 std. cm^3/min. "Nominal ppm" x 4.145 x 10^{-9} = mol/min.)

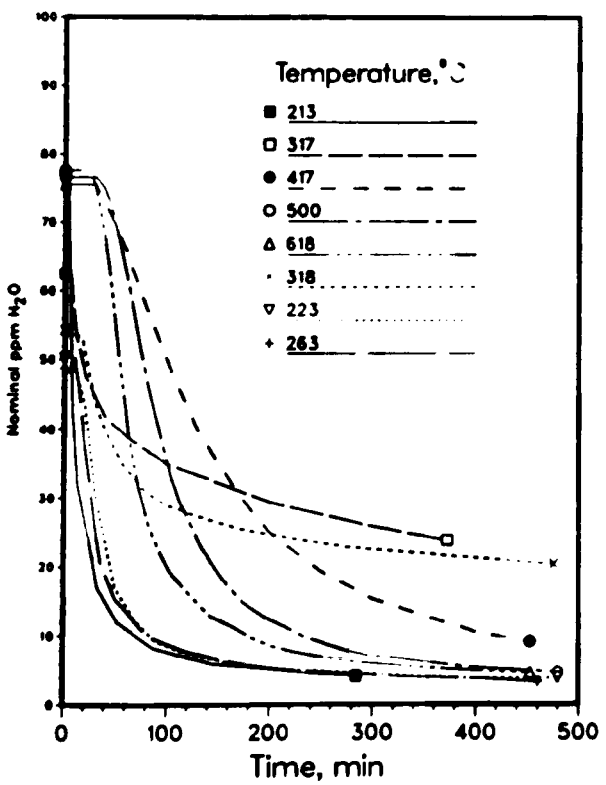

Fig. VII-7.

Desorption and Evolution of H_2O Vapor from $LiAlO_2$. (Same units as in Fig. VII-6.)

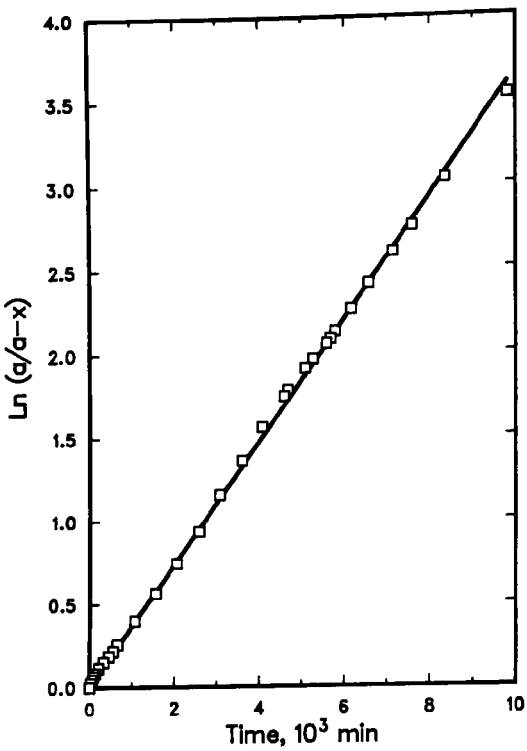

Fig. VII-8.

Test for First-Order Kinetics in Evolution of H_2O at 591 K (318°C). (On the ordinate, x is the amount of hydroxide reacted at time t, and a is the initial amount of hydroxide.)

At high temperatures, therefore, the rate-limiting process may be shifting to second order, that is, a process of proton surface diffusion and surface combination of hydroxides. Temperature alone might not be the only variable determining this: at lower temperatures, very low concentrations might also lead to release rates controlled by surface diffusion.

For some tests, the furnace set point was raised to about 888 K (615°C) after the measurements of water evolution at the temperature of the main measurement were finished. An example of these nonisothermal bakeouts is shown in Fig. VII-9, which plots both the course of water evolution and the temperature change. Two main peaks appear, and a small additional one appears on the left side of the first large one. The interpretation of these observations is that the small peak (at about 20 min) reflects desorption of water from sites of surface adsorption and the two large peaks relate to protons, localized as hydroxide groups, at two different kinds of oxide sites in the $LiAlO_2$ lattice. The crystal structure of $LiAlO_2$ is known to have significantly different interoxide ion distances for oxides in tetrahedra around a lithium ion compared with the distances in tetrahedra around aluminum ions. Such different sites are expected to allow protons to diffuse with different energetics and rate constants.

c. Discussion

By analysis of our data and the work of others, we arrived at insights into (1) the effect of oxygen or hydrogen adsorption on tritium release rates and (2) tritium diffusion in ceramic breeders.

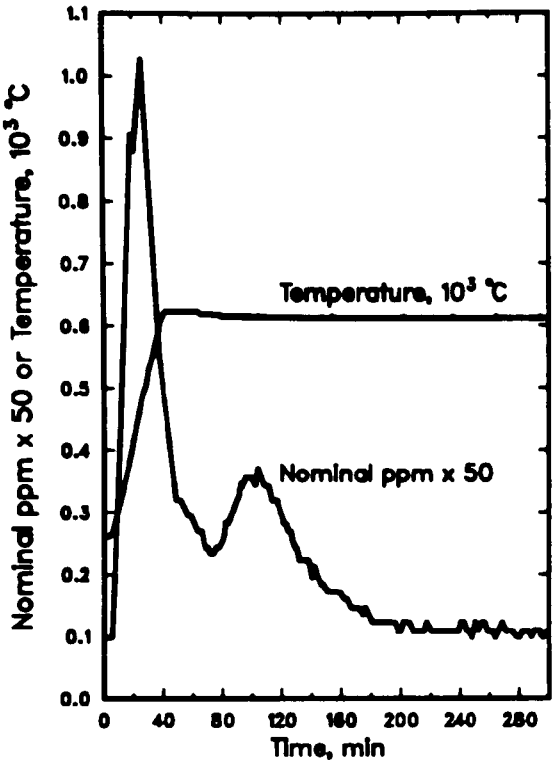

Fig. VII-9.

Evolution of H_2O Vapor During Temperature Increase from 535 to 886 K (262 to 613°C) and at 886 K (613°C)

The conductivity and charge carriers in a semiconductor can be influenced markedly by surface adsorption of either oxygen or hydrogen.[33,34] The adsorption of the molecular forms of these gases has implications for ionic transport, as well as for electronic or hole conductivity. It is now believed that adsorption of an electron-withdrawing material, such as oxygen, will induce in the solid surface region a boundary layer of positive charge.[33] Such a layer would present a repulsive barrier for penetration by protons moving to the surface so that evolution of proton-containing species would be inhibited. Conversely, adsorption of hydrogen, an electron-donating material, will enhance electron density in the near-surface oxides and present an attractive region into which proton diffusion will be enhanced. The magnitude of surface charge effects (at least the ones involving point defects) is substantial, both in depth (tenths of a micron) and in electric field gradient (thousands of volts per centimeter).[35]

These adsorptive effects can now be seen for the first time as a contributing kinetic cause for the greatly diminished release of tritium that was observed in the TRIO runs when oxygen was introduced into the sweep gas.[32] Kinetic effects related to oxygen activity also account for the common finding in release experiments that molecular hydrogen in the sweep gas enhances tritium

[33]E. G. Rochow, J. Inorg. Nucl. Chem. **29**, 65 (1967).
[34]S. E. Schwartz and E. G. Rochow, J. Inorg. Nucl. Chem. **29**, 1559 (1967).
[35]L. Slifkin, Mater. Sci. Forum **1**, 75 (1984).

release.[36,37] In addition, there is the thermodynamic contribution by which high oxygen activity favors the more strongly adsorbed species, HTO or T_2O. Thus, oxygen activity now can be expected to affect tritium release kinetically in the same direction as thermodynamically. These effects relate to any process involving proton diffusion through oxides, such as diffusion through oxide films, as well as to release from breeders.

There is a wealth of data and theory that provide strong analogical grounds for regarding "tritium" diffusion in ceramic breeders as triton diffusion. This earlier work was concerned with proton diffusion rather than triton diffusion and included both oxides and complex mixed oxides.[38] With the proton as the mobile species, diffusion involves the proton hopping from oxide ion to oxide ion. Because of the small ionic radius of the proton (about 10^{-4} Å), its high polarizing power leads to a strong tendency toward covalent bond formation with an oxide ion. As a result, it is reasonable to regard the proton or triton as remaining localized as hydroxide or tritoxide on the oxide sublattice. Considerable physical evidence attests to the presence of the O-H bond in oxides. For example, Gruen et al. report infrared spectroscopic evidence for solute OH^- in alumina bombarded with protons.[39]

The concept of proton hopping from oxide to oxide suggests that an initial understanding of tritium diffusion in ceramic breeders should center on the features of the oxide ion sublattice. Investigating the oxide sublattice would involve evaluating the diffusional pathways determined by the crystallographic O^{2-}-O^{2-} distances and by the lattice structures. Additional effects can be expected from modifications in the oxygen sublattice caused by (1) vacancies in it, (2) polarization of oxide sites by the lithium ion or other cation sublattices and by vacancies in them, (3) impurities, and (4) orbital hybridization. From this viewpoint, we have been able, on the basis of considerations of interionic oxide distance alone, to explain the differences in diffusion coefficients of tritium in $LiAlO_2$, Li_2O, and alumina.

Our future work will involve gathering sufficient additional data to construct adsorption isotherms, to determine solubility of hydroxide as a function of temperature and partial pressure of H_2O, and to determine activation energies of H_2O evolution for $LiAlO_2$. Subsequently, the breeder material Li_4SiO_4 will be the probable candidate for study in the same way as $LiAlO_2$ so that comparison of the two will be possible.

2. Thermal Conductivity of Breeder Materials

Lithium-containing ceramic breeder materials have been envisaged to be deployed within the blanket region of a fusion reactor in one of several possible

---

[36]H. Wehrle et al., J. Nucl. Mater. **141-143**, 321 (1986).

[37]J. M. Miller, S. R. Bokwa, and R. A. Verrall, J. Nucl. Mater. **141-143**, 294 (1986).

[38]R. Gonzalez, Y. Chen, and K. L. Tsang, J. Am. Ceram. Soc. **67**, 775 (1984).

[39]D. M. Gruen, R. B. Wright, R. L. McBeth, and I. Sheft, J. Chem. Phys. **62**, 1192 (1975).

configurations. One of these is the sphere-pac configuration. For this configuration an important material parameter is its thermal conductivity (K_{sp}), improvements in which would lead to enhanced mechanical and thermal performance. It is well known that K_{sp} demonstrates rather complex behavior as a function of temperature, gas pressure, gas composition, particle size, and packing fraction. The interrelationship of these parameters has been satisfactorily accounted for with a hierarchical effective media theory (HEMT).[40] For tritium self-sufficiency, most lithium ceramic breeder materials require the presence of a neutron multiplier (e.g., Be or BeO). Here, the influence of breeder configuration (i.e., how one assembles the different solid components in the sphere-pac bed) on K_{sp} becomes important. Using a generalized HEMT (i.e., a model with capability to describe systems with more than one solid material component), we have analyzed the configurational dependence of K_{sp} for sphere-pac beds composed of lithium ceramic/BeO microspheres.

Figure VII-10 shows the calculated thermal conductivity of a sphere-pac bed in the mixed-sphere (MSC) and coated-sphere (CSC) configuration. The CSC consists of a sphere-pac bed of touching spheres of $LiAlO_2$, each of which is coated with a layer of BeO of appropriate thickness, while the MSC is made up of randomly mixed similar-sized spheres of both $LiAlO_2$ and BeO. One notes immediately that the thermal conductivity of the coated-sphere configuration (K_{CSC}) is significantly above the corresponding conductivity for the mixed-sphere configuration (K_{MSC}). To indicate in a quantitative manner the comparison between the two configurations, we introduced an enhancement factor, ϵ, defined as follows:

$$\epsilon = \frac{K_{CSC} - K_{MSC}}{K_{MSC}} \times 100\% \qquad (9)$$

where ϵ is a measure of the percent enhancement achievable with CSC over that of MSC. This factor is also plotted in Fig. VII-10. For comparison, the thermal conductivity of 100%-dense sintered γ-$LiAlO_2$ is also shown.[41] Note that the packing fraction of the sphere-pac materials under consideration is only about 80%.

In powder-like systems such as the sphere-pac beds, the regions close to the points of contact between particles can have a linear dimension that is comparable or smaller than that of the mean free path of the gas (in our case, helium). In that case, there could be significant pressure dependence of the thermal conductivity. Again, the generalized HEMT was employed to estimate the pressure effect. The results are shown in Fig. VII-11, which indicates that, for very moderate changes in gas pressure at 1000 K, significant enhancement in thermal conductivity can be achieved with both bed configurations. In fact, for the CSC, almost a factor of two was gained in thermal conductivity when the gas pressure was increased from 0.1 to 0.9 MPa.

---

[40]S. W. Tam and C. E. Johnson, "The Thermal Conductivity of Materials with Multiple Characteristic Length Scales," in *Fractal Aspects of Materials II*, eds., D. W. Schaefer et al., Materials Research Society, Pittsburgh, PA (1986).

[41]C. Denuzise and N. Roux, *Data and Properties of Lithium Aluminate $LiAlO_2$*, C.E.N./Saclay, Note 84/039 (November 1984).

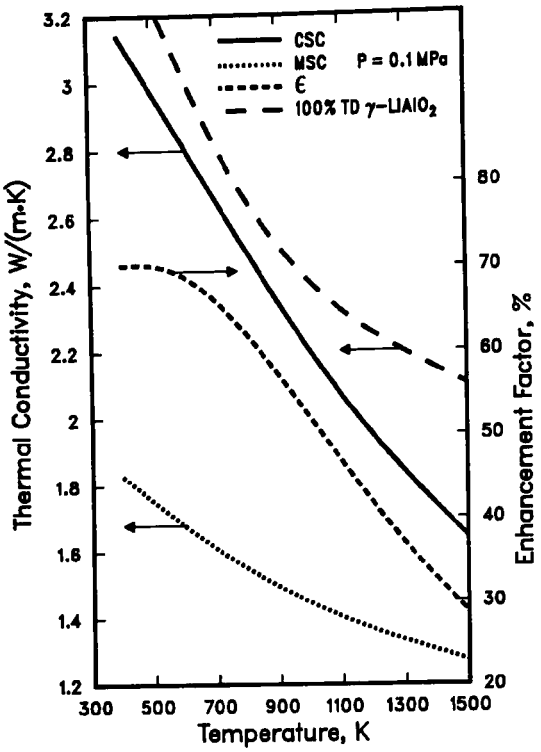

Fig. VII-10. Thermal Conductivity of $LiAlO_2$ + BeO in Different Configurations Versus Temperature

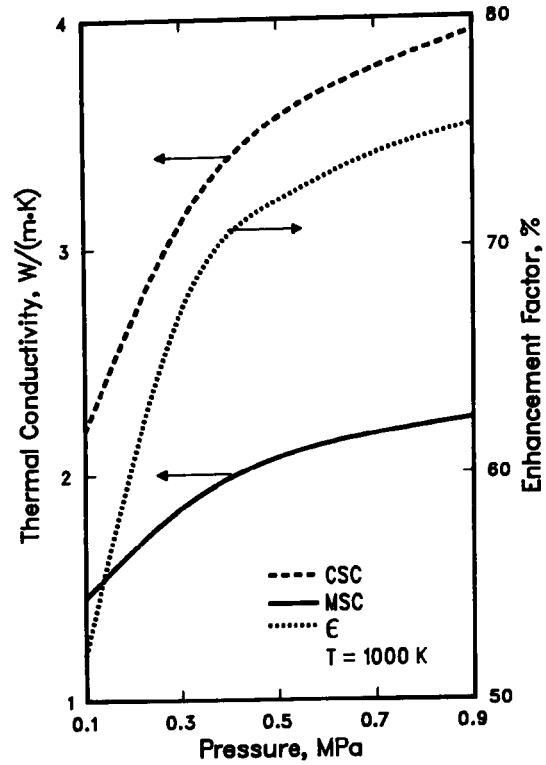

Fig. VII-11. Thermal Conductivity of $LiAlO_2$ + BeO in Different Configurations Versus Gas Pressure

The above results demonstrate the basic attractiveness of the coated-sphere concept. Although the present work concentrates on the $LiAlO_2$/BeO system, the coated-sphere concept is potentially applicable to other coating/substrate combinations (e.g., a beryllium metallic coating). The attractiveness of any specific combination can be assessed using the generalized version of HEMT.

3. Model of Tritium Transport in Breeder Materials

We are developing a computer model that depicts tritium transport and release from ceramic breeding materials. This model will include the effects of diffusion in the solid, desorption from the solid surface, and gas flow through a porous medium. In 1986, we developed a subprogram to model the solid state diffusion/surface desorption of tritium, based on the solution to a similar problem in heat conduction. The equation governing tritium transport in a spherical grain is

$$\frac{1}{D}\frac{\partial c}{\partial t} = \frac{1}{r^2}\frac{\partial}{\partial r}\left(r^2\frac{\partial c}{\partial r}\right) + \frac{G}{D} \qquad (10)$$

where D is diffusivity, r is radius, c is tritium concentration, G is tritium generation rate, and t is time.

Furthermore, at the surface,

$$\frac{dc}{dr} = K_{des}\, C_s \qquad (11)$$

where K_{des} is a surface desorption rate constant, and C_s is a surface concentration.

These equations are similar to those governing the conduction of heat in a solid sphere with constant heat generation and radiation at the surface into a medium at zero temperature, as given by Carslaw and Jaeger.[42] If a new parameter, K_d, is defined as an effective desorption rate constant so that K_d equals K_{des} times the thickness of the surface and $K_d\, C = K_d\, C_s$, Carslaw and Jaeger's equations can be used for our purpose. By substituting $\kappa = D$, $v = c$, $H = K_d$, $A_o/K = G/D$, and $K_d/D = h$ into their equation, we obtained the following equation for the tritium concentration in the grain as a function of radius and time:

$$C = \frac{G}{6hD}\,[h(a^2 - r^2)+2a] - \frac{2ha^2G}{rD} \sum_{n=1}^{\infty} \frac{\sin(r\alpha_n)\, \exp(-D\alpha_n^2 t)}{[\alpha_n^2(a^2\alpha_n^2 + ah(ah - 1))]\, \sin(a\alpha_n)} \qquad (12)$$

where a is the grain radius and α_n is the root of $a\alpha\, \cot(a\alpha)=1 - ah$. The tritium release rate will be the concentration evaluated at the surface ($r = a$) times the effective desorption rate constant, K_d.

Since both K_d and D are functions of temperature, a change in temperature from T' to T results in a change in the boundary condition from $dc/dr = K_d'C$ to $dc/dr = K_dC$. After this temperature change, Eq. 12 no longer fits the boundary conditions. We, therefore, developed an approximate solution based on Eq. 12. If before the temperature change the system reaches steady state, then the initial tritium concentration at $r = a$ will be $Ga/3K_d'$. Immediately after the temperature change the release rate will change by a factor of $(1 - K_d/K_d')$. The approximate solution is

$$C_{r=a} = \left(1 - \frac{K_d}{K_d'}\right)\left[\frac{Ga}{3K_d} - \frac{2haG}{D} \sum_{n=1}^{\infty} \frac{\exp(-D\alpha_n^2 t)}{\alpha_n^2[\alpha_n^2+ah(ah - 1)]}\right] + \frac{Ga}{3K_d'} \qquad (13)$$

This approximation was used to calculate the tritium release rate as a function of time and temperature. Our values were compared to the observed release rate profile for a Li_2SiO_3 sample in a tritium release test by another laboratory (the LISA-1 experiment). As shown in Fig. VII-12, the model provided good agreement with the observed data, although the initial release rate for the LISA-1 experiment is lower than that predicted. The effects of the activation energies of diffusion and desorption on the release rate are currently being investigated. The

[42]H. S. Carslaw and J. C. Jaeger, *Conduction of Heat in Solids*, Oxford University Press, New York (1959).

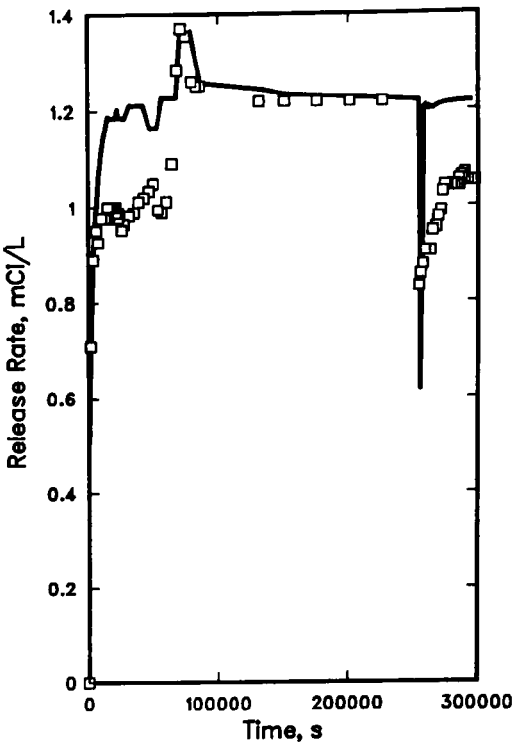

Fig. VII-12.

Calculated and Observed Tritium Release Rate as Function of Time

results so far indicate that the shape of the release rate curve is strongly dependent on both these activation energies, and that deriving a value for either activation energy would be difficult without having an accurate value for the other.

4. Reactor Design Studies

For fusion to be attractive as a commercial energy source, the direct capital cost of the reactor per kilowatt-hour and the bus-bar cost of electricity have to be significantly reduced. The goal of our present fusion design studies is to evaluate the economic impact of innovative design concepts on the direct capital cost and the operating costs of tokamak-based commercial fusion power plants. (The tokamak reactor uses toroidal magnetic fields to confine a thermonuclear plasma.)

In 1986, we completed a cost analysis of the tokamak power systems (TPSS) reactor plant.[43] This reactor design incorporates several innovative concepts: a high plasma beta value (which requires lower magnetic fields), a high-temperature lithium/vanadium breeder blanket, a high-temperature heat transport zone, a zoned reactor building, and simple maintenance scenarios. We compared the capital cost and the bus-bar cost of electricity for TPSS to costs estimated for an older fusion reactor design, STARFIRE,[44] and a design derived

[43]C. C. Baker et al., *Tokamak Power Systems Studies--FY 1985*, Argonne National Laboratory Report ANL/FPP/85-2 (December 1985).

[44]C. C. Baker et al., *STARFIRE - A Commercial Tokamak Fusion Power Plant Study*, Argonne National Laboratory Report ANL/FPP-80-1 (September 1980).

using a liquid-metal breeder blanket included in the Blanket Comparison and Selection Study (BCSS).[45] The TPSS costs were also compared with those estimated from current U.S. power plant experience. For our analysis, direct-cost algorithms were derived based on STARFIRE and BCSS costs, which were, in turn, estimated from costs for standard balance-of-plant items and the estimated costs of analogous systems for fusion reactors not yet built.

The direct capital cost, the indirect capital cost, and the total capital cost for TPSS, BCSS, and STARFIRE are listed in Table VII-3 (all costs in 1986 dollars). The TPSS reactor has the lowest direct capital cost and the lowest total capital cost. The capital cost of electricity is essentially the same for TPSS and BCSS and is about $450/kWe lower than that for STARFIRE.

Table VII-3. Costs for TPSS, BCSS, and STARFIRE (in 1986 dollars)

	Reactor Design		
	TPSS	BCSS	STARFIRE
Direct Capital Costs, $M			
Land and Land Rights	2	5	3
Structures and Site Facilities	178	346	411
Reactor Plant Equipment	624	1156	1075
Turbine Plant Equipment	147	346	294
Electric Plant Equipment	84	139	138
Miscellaneous Plant	10	12	56
Total Direct	1045	2004	1977
Indirect Capital Cost,[a] $M	627	1202	1186
Total Capital Cost, $M	1672	3206	3163
Power, MW			
Fusion	1950	3675	3510
Thermal	2518	4596	4000
Net Electric	873	1698	1200
Capital Cost of Electricity, $/kW	1197	1180	1648
Bus-bar Cost of Electricity, mill/kWh	32	31	43

[a]The indirect capital cost is assumed to be 60% of the direct capital cost and includes all contingency costs and all parts costs.

[45]D. L. Smith et al., *Blanket Comparison and Selection Study - Final Report*, Argonne National Laboratory Report ANL/FPP-84-1 (September 1984).

To put the direct capital cost for TPSS and its capital cost of electricity in perspective, we compared them to the current U.S. power plant industry experience.[46] For LWRs that have a net electrical production of 1100 MW, the direct capital cost is $1188 million for the best-managed plant; for the best-managed coal plant, the direct capital cost is $905 million. This compares with $1045 million for TPSS. In addition, the capital cost of electricity is $1080/kW for an LWR plant and $823/kW for a coal plant. These values are somewhat lower than the $1197/kW for TPSS. Since for each of the current U.S. power plants, an appreciable fraction of the cost of electricity is due to fuel costs, a true comparison between the overall cost can only be done by evaluating the total bus-bar cost of electricity for each.

An evaluation was made of the bus-bar cost of electricity expected from a fusion reactor similar to the TPSS design. The equation used to derive the cost of electricity (COE) is

$$COE = \{Cac + (Com + Cscr + Cf)(1 + e)^{P}\}/8760(Pe)(pf) \qquad (14)$$

where Com = Annual Cost of Operations and Maintenance
Cscr = Annual Cost of Component Replacement
Cf = Annual Cost of Fuel
e = Escalation Rate
p = Construction Period
Pe = Net Electrical Power
pf = Plant Availability

In addition, Cac = FCR (TCC + Int), where FCR is a fixed charge rate during operation, TCC is the total capital cost, and Int is the interest during construction.

As shown in Table VII-3, the bus-bar cost of electricity was calculated to be 32 mill/kWh for TPSS, 31 mill/kWh for BCSS, and 43 mill/kWh for STARFIRE. The cost of electricity for any of these fusion plant designs is below the current bus-bar cost of electricity in Illinois, a state with a high cost of electricity. The 1985 rate in Illinois was 51.9 mill/kWh, if calculated from actual duty factors, or 60.6 mill/kWh, if calculated assuming equal duty factors (60%) for both nuclear and coal plants.[47]

In summary, the direct capital cost and the bus-bar cost of electricity for the TPSS fusion plant are comparable to those of existing power-generating plants. Cost reductions may be expected for fusion reactors, especially in the reactor plant equipment, once fusion is a mature power industry.

5. Dosimetry and Damage Analysis

Fusion materials are being irradiated in a variety of facilities, including fission reactors, such as the High Flux Isotopes Reactor (HFIR) at Oak Ridge National Laboratory; 14 MeV d-t neutron sources, such as the Rotating Target

[46] *Nuclear Energy Cost Data Base*, Department of Energy Report DOE/NE-0044/3 (June 1985).

[47] B. Brunka, Commonwealth Edison Public Information, personal communication (December 4, 1986).

Neutron Source (RTNS) II at Lawrence Livermore National Laboratory; and higher-energy accelerator-based neutron sources. We are determining the neutron energy spectrum, flux levels, and damage parameters for each of these facilities, along with exposure parameters for each irradiation. The neutron flux and energy spectra are measured by activation analysis using a least-squares adjustment procedure. Damage parameters, including atomic displacements, gas production, and other transmutations, are then calculated using our SPECTER computer code. Nuclear data and techniques are being developed to routinely provide experimenters with these exposure data for each irradiation. The goal of this work is to correlate materials property changes between different facilities and to predict materials performance in fusion reactors.

To develop new techniques for neutron measurements, we are measuring and testing neutron cross sections. Activation cross sections have been measured over a wide range of energies. Data for 22 different activation reactions were measured in the fusion energy range of 14.5-14.8 MeV. Integral tests in Be(d,n) fields (deuteron energy, 14-40 MeV) were used to adjust the energy-dependent neutron cross sections, and spallation reaction yields were tested for dosimetry up to 800 MeV.

Recent research has focused on measuring the production rates for long-lived isotopes in fusion materials. Such data are needed for the determination of fusion waste activities, as well as for fusion reactor dosimetry. Table VII-4 lists some of the cross sections that we have measured. These measurements were performed by irradiating pure elements and separated isotopes at the RTNS II (14.8 MeV). Chemical ion-exchange separations were performed to remove undesired activities, and the long-lived activities were measured with gamma spectroscopy, liquid scintillation counting, and accelerator mass spectrometry. These data can be directly applied in fusion reactor design studies. As an example, using the STARFIRE design (22 MW y/m^2), our data for molybdenum predict 75 μCi/g of ^{94}Nb (2.0 x 10^4 y) and 12 mCi/g of ^{91}Nb (700 y), both of which are about 30% lower than previous estimates. Other measurements in progress include reactions leading to ^{14}C (5730 y), ^{93}Zr (1.5 x 10^6 y), ^{92}Nb (3.2 x 10^7 y), and ^{93}Mo (3500 y).

Table VII-4. Production of Long-Lived Isotopes at 14.8 MeV

Reaction	Half-life, y	Cross Section, mb
^{56}Fe(n,2n)^{55}Fe	2.7	454±35
^{60}Ni(n,2n)^{59}Ni	7.5 x 10^4	in progress
^{64}Ni(n,2n)^{63}Ni	100	953±67
^{63}Cu(n,p)^{63}Ni	100	54±4
^{94}Mo(n,p)^{94}Nb	2.0 x 10^4	53±5
^{92}Mo(n,x)^{91}Nb	700	~300

The intense neutron fields expected in fusion reactors will produce high rates of atomic displacements in materials. We routinely calculate the damage for materials irradiations using our SPECTER computer code. However, this code only calculates damage for pure elements. Consequently, we have developed a new code (SPECOMP) that performs damage calculations for compounds. This code integrates over the primary recoil energy distributions times the secondary displacement functions for each combination of recoil atom and matrix atom. By taking advantage of the existing recoil atom energy distributions in SPECTER, the SPECOMP code is relatively small and can be run cheaply and quickly on small computers without access to evaluated nuclear data. We have completed calculations for several tritium breeding materials, such as $LiAlO_2$ and LiO_2, as well as other insulators and alloys. For the breeder materials, this new calculation predicts significantly more damage (20-40%) than expected previously. However, there appears to be only a small effect for structural alloys such as stainless steel. Based on the compounds that we have studied, the general trend indicates that the damage calculated by SPECOMP will be significantly larger than linear combinations of elemental sums when there is a significant difference in the atomic masses involved in the compound. We intend to perform calculations for a wide range of materials and to incorporate the resultant cross sections into our SPECTER computer code. Hence, we will be able to routinely predict damage for breeders, insulators, alloys, and other compounds of interest to the fusion program.

VIII. BASIC CHEMISTRY RESEARCH

Basic chemistry research is being pursued in several different areas: new catalysis mechanisms in the fields of catalytic hydrogenation and catalytic oxidation; materials chemistry for liquids and vapors at high temperatures; interfacial processes of importance to corrosion science, surface science, and catalysis; the thermochemical properties of zeolites, related silicates, and "high-tech" materials such as chalcogenides; and the geochemical processes involved in water/rock interactions occurring in active hydrothermal systems.

A. *Fluid Catalysis*

This research is designed to determine reaction mechanisms and to explore new catalytic chemistry for converting small molecules (e.g., CO, CO_2, O_2) to desired products. Currently under investigation is a recently discovered main-group soluble oxide catalyst that promotes carbon monoxide hydrogenation and water-gas shifting. The catalysis mechanism is distinct from that of other homogeneous catalysts and seems relevant to suspected metal oxide surface mechanisms of commercial methanol synthesis catalysts. Also investigated are (1) the concept of using tertiary amines as oxygen carriers in an air separation process and (2) alternative techniques for adapting nuclear magnetic resonance (NMR) spectroscopy to high-pressure kinetic studies.

1. Soluble Oxide Catalysis

Efforts in this area during the past year focused on the identification of factors governing the reaction rate for catalysis of carbon monoxide hydrogenation by hexamethyldisiloxane. We feel that significantly improving the reaction rates for this system would strengthen the hypothesis that the oxide and formate chemistry of the type defined here is responsible for catalysis in the commercial oxide catalyst system (supported CuO/ZnO) for methanol synthesis. Although this conclusion requires substantiation from a range of differing types of evidence, we feel that the similarities already uncovered are remarkable and that demonstration of high reactivity with this chemistry would be of particular importance. The results from such a demonstration could lead to improvements in the commercial system. A synopsis describing some of our earlier results recently appeared in *Chemical and Engineering News*.[1]

The mechanism for catalysis by hexamethyldisiloxane, as we currently perceive it, is shown in Fig. VIII-1. Briefly, it involves (1) heterolytic activation of hydrogen by an oxide, $Me_3SiOSiMe_3$, (2) carbonylation of the resulting hydroxide to yield a formate, Me_3SiO_2CH, (3) hydrosilation of the formate to yield a methyleneglycoxide, $Me_3SiOCH_2OSiMe_3$, and (4) elimination of formaldehyde from the methyleneglycoxide complex. The organic products of the reaction are produced by subsequent hydrogenation of formaldehyde to yield methanol and by Tischenko dimerization of formaldehyde to yield methyl formate.

---

[1]J. Haggin, Chem. Eng. News, p. 7 (May 19, 1986).

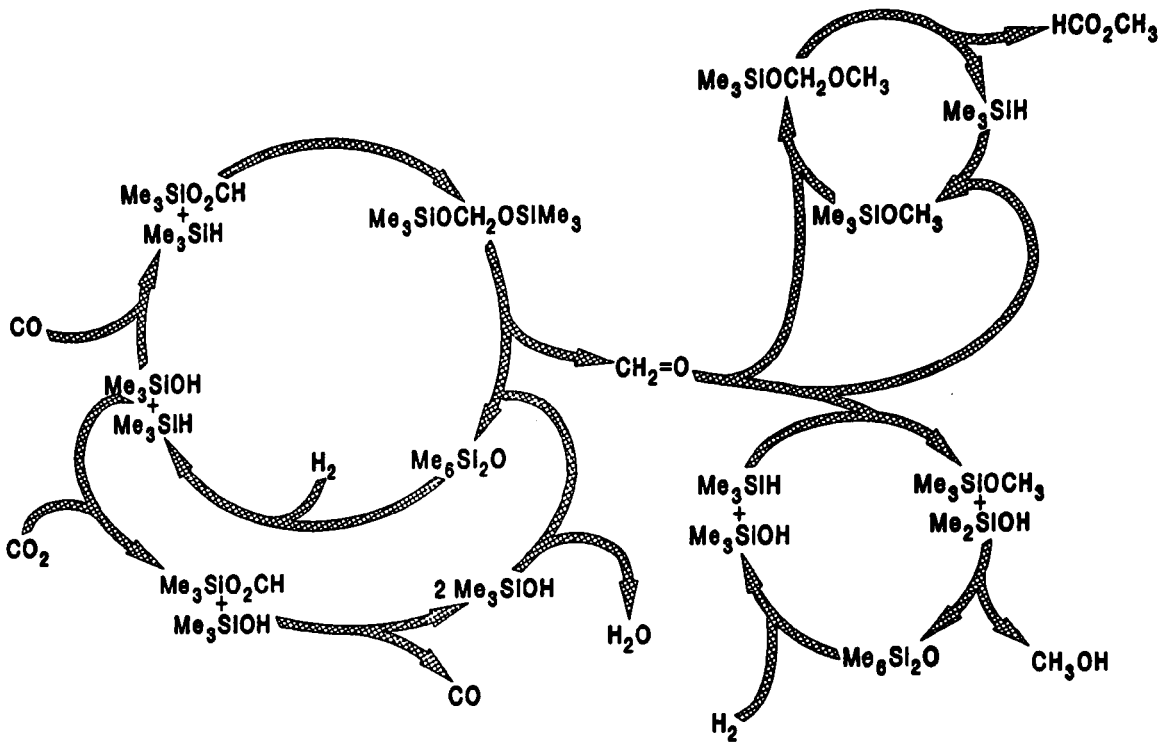

Fig. VIII-1. Proposed Mechanism for Carbon Monoxide Hydrogenation

We now know that the rate-determining step in this sequence is the heterolytic activation of hydrogen, namely,

$$Me_3Si\text{-}O\text{-}SiMe_3 + H_2 \longrightarrow Me_3Si\text{-}OH + Me_3SiH \qquad (1)$$

Thus, efforts to improve the kinetics of the overall reaction were focused on this step.

Selection of potential catalysts for Eq. 1 stems from the expectation that the reaction involves nucleophilic attack on the hydrogen molecule by the electron pairs on the oxygen atom of the siloxane. Thus, increased electron density on oxygen should facilitate the reaction. For example, the reaction below involves the nucleophilic activation of hydrogen via the highly nucleophilic hydroxide anion and occurs rapidly at 1 atm of hydrogen and 140°C:

$$H_2 + D_2O \underset{140°C,\ 1\ atm}{\overset{NaOD(0.1\ \underline{M})}{\rightleftharpoons}} HD + HOD \qquad (2)$$

A recent *ab initio* molecular orbital calculation[2] for reaction of gaseous hydroxide anion with hydrogen shows that attack occurs by donation into the empty σ^* orbital of the hydrogen molecule, with H_2 binding end-on with hydroxide in a key reactive intermediate.

This line of reasoning suggested that metal siloxides should be good candidates for catalysis of Eq. 1. For example, although sodium trimethylsiloxide, $NaOSiMe_3$, is less nucleophilic than sodium hydroxide, it is considerably more so than hexamethyldisiloxane and, thus, should react with molecular hydrogen faster than the disiloxane via

$$NaOSiMe_3 + H_2 \rightleftharpoons NaOH + HSiMe_3 \qquad (3)$$

In addition, the reaction

$$NaOH + Me_3SiOSiMe_3 \longrightarrow NaOSiMe_3 + HOSiMe_3 \qquad (4)$$

regenerates the $NaOSiMe_3$ consumed in Eq. 3 and is known to occur rapidly under mild conditions. Note that Eqs. 3 and 4 sum to Eq. 1 and thus define a potential pathway for catalysis of Eq. 1.

Unfortunately, any catalytic effect of $NaOSiMe_3$ on the rate of Eq. 1 would be very difficult to determine by direct measurement, since the thermodynamics are unfavorable (ΔH° ~+21 kcal/mol) and the equilibrium constant for the reaction is very small. However, since this reaction is rate determining in the catalytic scheme in Fig. VIII-1, added $NaOSiMe_3$ should increase the rate of carbon monoxide hydrogenation. Although a large rate increase was indeed observed, further discussion will show that the major product from carbon monoxide hydrogenation suspected in this case is not methanol, but a formaldehyde polymerization product. Under conditions where the hexamethyldisiloxane-catalyzed reaction proceeds at a barely perceptible rate, 250°C and 275 atm, the rate of carbon monoxide hydrogenation for a system containing added $NaOSiMe_3$ is very high, as shown by the rate measurement illustrated in Fig. VIII-2. The measured rate of consumption of carbon monoxide, 5 mol CO/kg(cat) per hour, compares favorably with rates for typical operating conditions of the commercial methanol synthesis catalyst from Imperial Chemical Industries. The rates for this commercial catalyst are near 16 mol CO/kg(cat) per hour at 250°C/50 atm.[3] Preliminary data obtained from ^1H NMR spectroscopy, Fourier transform-infrared spectroscopy, and chemical analysis, although not rigorously defining the major organic product of the reaction, are

$$\left[\text{-CH(OH)-}\right]_n$$

consistent with a polymer of the type $\left[\text{-CH(OH)-}\right]_n$. This formulation is also consistent with the fact that carbon monoxide and hydrogen were consumed in a 1:1 ratio and that free formaldehyde was identified in the gas phase. Our interpretation of these results is that formaldehyde is formed faster than it can be hydrogenated to methanol (as in the scheme in Fig. VIII-1) and thus can only react with itself, leading to polymerization. Polyols of the type proposed here are known to occur

---

[2]D. Cremer and E. Kraka, J. Phys. Chem. 90, 33-40 (1986).

[3]T. B. Kobylinsk, J. Catal. 56, 407 (1979).

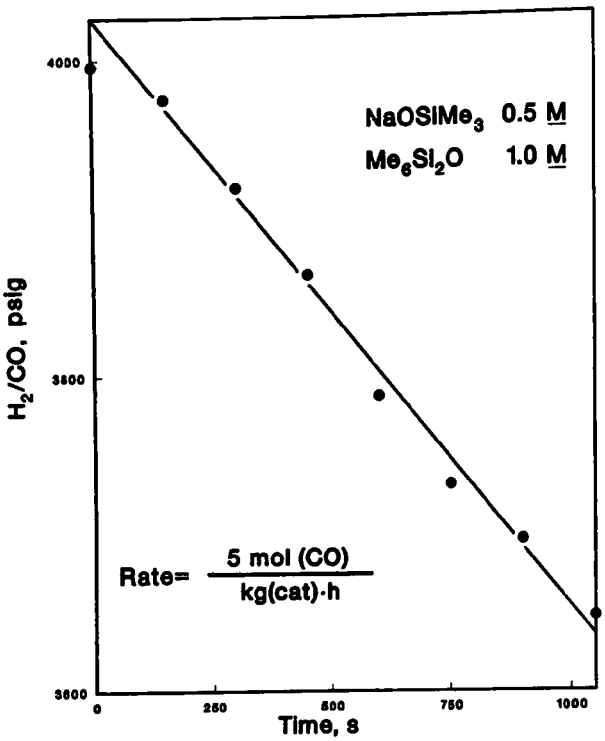

Fig. VIII-2.

Initial Rate of Syngas Consumption for Sodium Trimethylsiloxide-Catalyzed Reaction in Dioxane Solution at 250°C

when formaldehyde polymerizes under basic conditions and are distinct from the paraformaldehyde type, $[\text{-}CH_2O\text{-}]_2$, obtained under neutral or slightly acidic conditions.

We have also investigated the effect of $NaOSiMe_3$ and other siloxide bases on the formation rates of important intermediates in the carbon monoxide hydrogenation mechanism. For example, Fig. VIII-3 shows the dramatic effects of added bases on the concentration of the bis-trimethylsilylmethylene glycoxide intermediate, whose role in the catalytic sequence is identified in the scheme in Fig. VIII-1. The effects of added bases on the rates of formation of this intermediate roughly parallel the expected nucleophilic effects of the siloxide oxygen atoms in the bases. Thus, $LiOSiMe_3$ and $NaOSiMe_3$ cause the glycoxide to reach higher concentrations faster (we do not yet know whether the constant values approached in each case are steady-state or equilibrium values) than a silylated aluminate, which is, in turn, more effective than hexamethyldisiloxane alone. It is difficult to predict whether the oxygen in the lithium or sodium salt is more nucleophilic because we do not know the degree of association of the reactive species in either case. However, the lithium salt is tetrameric, with oxygen and lithium occupying the apices of a cube, in the solid state.

We have also explored a second approach to examination of catalysis of Eq. 1 by siloxide bases:

$$Ph_3SiOH + Ph_3SiH \longrightarrow Ph_3SiOSiPh_3 + H_2 \qquad (5)$$

This reaction is the reverse of Eq. 1, except that methyl groups are replaced with phenyl groups (Ph). Selection of the reverse mode of conducting the reaction avoids the problem of unfavorable thermodynamics noted for Eq. 1. We

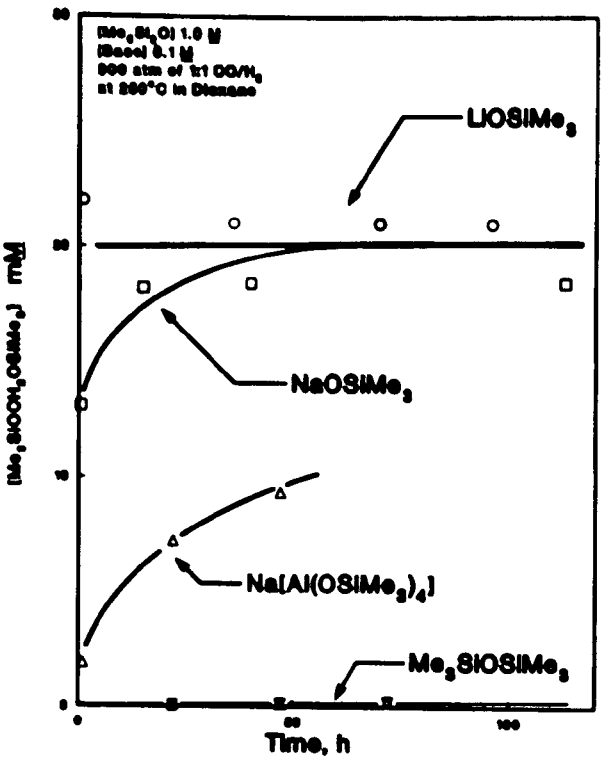

Fig. VIII-3.

Effect of Base Catalysts on Bis-trimethylsilylmethylene Glycoxide Production

determined that $NaOSiPh_3$ catalyzes Eq. 5 and that the reaction rates at 90°C in dioxane solution are first order for $[Ph_3SiH]$ and zero order for $[Ph_3SiOH]$. Preliminary results indicate that this system is amenable to accurate kinetic studies. It is hoped that we can obtain the mechanism of hydrogen activation by siloxanes with studies of this system.

Future efforts in catalysis by soluble oxides will focus on the mechanism of the reaction just discussed and on the enhanced reactivity for carbon hydrogenation occurring in the presence of added bases. The new results for carbon monoxide hydrogenation are particularly intriguing in that a system has been identified that seems to promote rapid addition of hydrogen to carbon monoxide (a molecule which is generally difficult to hydrogenate) but not to promote hydrogen addition to formaldehyde (which is generally easily hydrogenated). Although this latter fact results in a suspected formaldehyde polymer in the system studied, we are hopeful that the formaldehyde produced can be trapped. We plan to determine whether the formaldehyde can be intercepted by a hydroformylation catalyst to produce ethylene glycol from carbon monoxide and hydrogen.

2. Organic Oxygen Carriers

Research in this area is designed to test the concept of employing organic amines as oxygen carriers. This concept is based on the amines' potential reaction with molecular oxygen to yield amine-N-oxides, as in

$$2R_3N + O_2 \underset{}{\overset{K_p}{\rightleftharpoons}} 2R_3NO \qquad (6)$$

Since values of the N-O bond energies in the amine-N-oxide product should be sensitive to the electron donor properties of the substituents, one should be able to design an amine for which the equilibrium constant, K_p, is near unity. With K_p values near 1, the oxygen carrier could, in principle, store and release oxygen at low pressures by small temperature-induced changes of K_p near this value. Estimates for the degree of oxygenation at equilibrium for Eq. 6 as a function of N-O bond energy (BE) and temperature are shown in Fig. VIII-4. Note that an amine-N-oxide with an N-O bond energy of 70 kcal/mol would be 75% oxygenated at about 70°C and 75% deoxygenated at about 130°C. We feel that these characteristics could be useful in small-scale (e.g., mobile medical or aircraft oxygen systems) or large-scale (e.g., air separation) technologies. Owing to the low equivalent weight of amines (or even polyamines) for Eq. 6, the potential oxygen capacities of a system based on this concept significantly exceed those based on conventional metal coordination complexes.

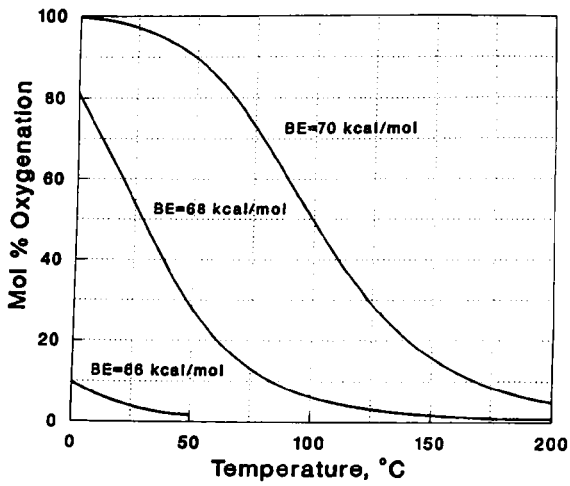

Fig. VIII-4.

Estimated Equilibrium Values for Oxidation of Amines at 1-atm Air (BE=bond energy)

Calorimetric determinations of the bond energies in pyridine-N-oxide, 70 kcal/mol, and trimethylamine-N-oxide, ~70 kcal/mol, support the feasibility of the concept. Although the favorable thermodynamics do not necessarily imply that satisfactory kinetics for the system can be achieved, we suspect that any kinetics problem, if encountered, might be resolved through catalytic studies. Even though oxidation of many types of amines has been studied, some of which even lead to the formation of amine-N-oxides, there is only one report[4] (involving trimethylamine) for the reaction proceeding cleanly with the stoichiometry of Eq. 6. Unfortunately, our own results tend to cast doubt on the accuracy of this report, and efforts described here are designed to examine the kinetics of the reaction in some detail.

[4]D. P. Riley and P. E. Correa, J. Org. Chem. **50**, 1564 (1985).

Preliminary experiments with trimethylamine and N-methylpyrrolidine indicate that the two amines are oxidized at comparable rates and selectivities in water under relatively mild conditions. Most of the research was focused on the latter amine which, because of its lower volatility, could be studied over a wider concentration range without danger of forming explosive mixtures with oxygen in the gas phase. The rate plots in Fig. VIII-5 indicate first-order dependence of [N-methylpyrrolidine] for a buffered solution of the amine under conditions where an unbuffered solution results in extensive curvature of the plot. Consistent with the pH change noted for an unbuffered solution, this curvature is attributable to lowering of the free amine concentration via protonation, which becomes more extensive as the reaction proceeds. For buffered solutions, the first-order dependence on oxygen pressure over the range of 14-68 atm was also determined and yielded a second-order rate constant of 4.1×10^{-3} atm^{-1} h^{-1} at 70°C. The second-order rate dependence is consistent with rate-determining electron transfer from amine to oxygen:

$$R_3N: + O_2 \longrightarrow R_3N^{+\cdot} + O_2^{-\cdot} \qquad (7)$$

Rate-determining electron transfer is also supported by the observation that the oxidation occurs more slowly in less-polar solvents and also more slowly with other amines having higher oxidation potentials than N-methylpyrrolidine.

The presence of the aminium radical cation, $R_3N^{+\cdot}$ in Eq. 7, may explain both the source of protons that results in curvature of the rate plot for the unbuffered amine solution in Fig. VIII-5 and the product distribution in Fig. VIII-6.

Figure VIII-6 indicates that all of the organic side products of the reaction (i.e., those other than N-methylpyrrolidine-N-oxide) result from attack at the carbon atom's α proton to the amine nitrogen. This may occur as a result of loss of an α proton from the aminium radical cation:

$$\geq N\text{-}\overset{+\cdot}{C}H\text{-} \longrightarrow \geq N\text{-}\dot{C}H + H^+ \qquad (8)$$

Since there are seven α protons in N-methylpyrrolidine and nine in trimethylamine, Eq. 8 brings up the possibility that one might obtain high yields of an amine-N-oxide through a co-oxidation process involving α-proton abstraction without any participation of Eq. 6. Although our results are not yet definitive, they tend not to support participation of Eq. 6 for oxidations involving trimethylamine or N-methylpyrrolidine. Measurements of the stoichiometry of oxidation of trimethylamine and N-methylpyrrolidine indicate that the ratio of O_2 consumed per mole of amine converted is close to 1:1, rather than the 1:2 stoichiometry expected for Eq. 6. In addition, we have not yet been able to detect molecular oxygen by heating trimethylamine-N-oxide or N-methylpyrrolidine-N-oxide to decomposition under conditions where Eq. 6 would be expected to be reversible.

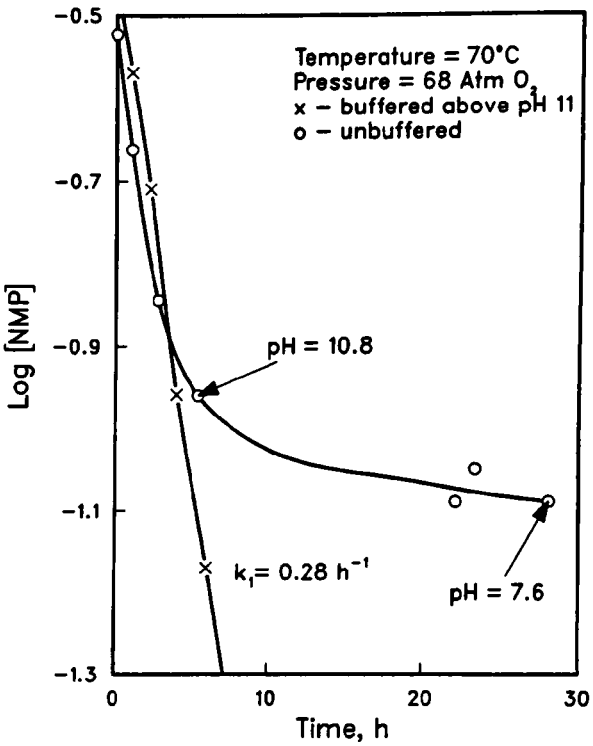

Fig. VIII-5.

First-Order Rate Plots for N-Methylpyrrolidine (NMP) Oxidation in Water

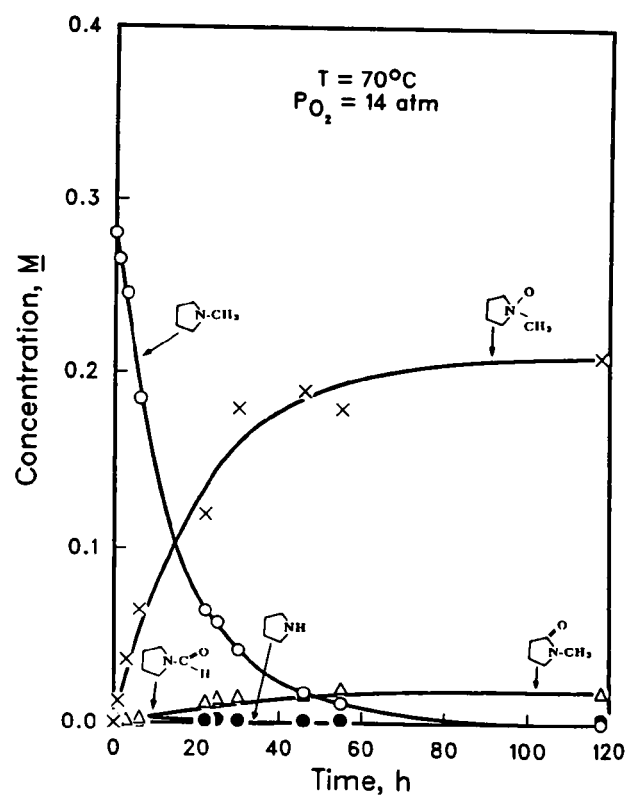

Fig. VIII-6.

Product Distribution for N-Methylpyrrolidine Oxidation in Water

Future work in this area will examine amine oxidations with amines that do not contain α protons or that contain α protons for which abstraction is known to be unfavorable.

3. High-Pressure NMR Studies

We are designing a high-pressure multinuclear NMR probe suitable for *in situ* kinetic studies that would complement or replace some of our autoclave equipment and sampling methods. The effort coincides with the planned acquisition of a high-field, 300-MHz, NMR spectrometer. The necessity for a new probe design arises because current designs do not possess gas-liquid mixing adequate for kinetic studies involving gaseous reactants and because the materials used in probe construction are not readily machinable, are reactive toward hydrogen, which is commonly used in our studies, have tensile strength too low to withstand the required pressures (300 atm) on adequate sample sizes, or have such high magnetic susceptibilities that high-resolution spectra cannot be obtained.

An alloy satisfying our material requirements, namely an aluminum-silicon bronze (CDA-642), was identified with use of a test probe that allowed rapid measurements of the effects on ^{31}P line widths and sensitivities for samples enclosed in tubes constructed of various test materials. The CDA-642 alloy did not significantly alter the line width or signal-to-noise ratio for a 5-mm OD sample containing K_2HPO_4 (33%) in D_2O. This alloy is particularly resistant to corrosion by acids and is unreactive toward hydrogen. Its tensile strength in the temperature region anticipated (-100 to +200°C) is somewhat better than 316 stainless steel, which cannot be used because of its high magnetic susceptibility.

Future efforts will involve mechanical design and pressure testing of a probe constructed from this alloy. Also to be tested is the use of a magnetically driven, thermostated centrifugal pump. This pump, which will be located remotely from the NMR magnet, will bubble gas from the probe head space through the liquid sample in the probe so that effective gas-liquid mixing can be attained.

B. *High-Temperature Materials Chemistry*

Our goal in this effort is to perform experimental and theoretical studies that lead to a basic understanding of materials chemistry at high temperature. Our focus is on molten-salt complexes and associated and ordered solutions such as chloroaluminates, silicates, and "ionic" alloys.

1. Quantum Mechanical Calculations of Molten-Salt Complexes

The stabilities of complex species involving oxygen in molten salts are of fundamental scientific interest, as well as of technological importance in such areas as magnesium and aluminum production. However, little is known of the structures, vibrational frequencies, and energetics of oxide complexes present in molten salts. In previous work, we were successful in applying *ab initio* molecular orbital methods to study the energetics of the reaction of Al^{3+} with O^{2-} to form AlO^+ in a lithium fluoride environment.[5] In the past year, we applied *ab initio*

[5]M. J. Steindler et al., *Chemical Technology Division Annual Technical Report, 1985*, Argonne National Laboratory Report ANL-86-14, pp. 114-115 (1986).

methods to determine the stabilities of MgO and Mg_2O^{2+} in four alkali halide melts (lithium fluoride, lithium chloride, sodium fluoride, and sodium chloride). The method used involves two steps. First, we obtained optimized structures of the magnesium oxide complexes with the 3-21G basis set.[6,7] Secondly, we evaluated the total energies of each complex at a higher level of calculation, using a basis set with polarization functions and inclusion of correlation effects. These calculations indicated that the complexes of dimagnesium oxide (Mg_2O^{2+}) should be stable relative to magnesium oxide (MgO) in the four melts that were considered. Our results are consistent with solubility measurements being done by T. Ostwald at the University of Trondheim in Norway. In future work, we will use similar theoretical methods to determine the relative stabilities of Al_2O^{4+} and AlO^+ complexes in alkali halide environments for comparison with the results of our proton activation measurements on similar systems, which are already underway.

We also are calculating the vibrational frequencies for a number of complex oxide anions that may be present in halide melts. The results are being used to identify and assign vibrational bands in spectroscopic studies. Our previous work on a set of XY_4^{n-} anions, for which the experimental frequencies are well established, indicated that the predicted frequencies should be within about 10% of the actual frequencies of these species in the melts.[5] Frequencies have now been predicted for four magnesium oxide complexes (F_2MgO^{2-}, Cl_2MgO^{2-}, $F_4Mg_2O^{2-}$, and F_3MgO^{3-}) and two aluminum oxide complexes (F_3AlO^{2-} and Cl_3AlO^{2-}).

In addition to the oxides, vibrational frequencies were calculated for the five- and six-coordinated Al^{3+} ions in a fluoride melt (AlF_5^{2-} and AlF_6^{3-}). Gilbert et al.[8] observed three of the six vibrational frequencies of AlF_6^{3-} at 550, 390, and 345 cm^{-1}. Our calculated vibrational frequencies are $\omega(A_{1g})$ = 559 cm^{-1}, $\omega(E_g)$ = 446 cm^{-1}, and $\omega(F_{2g})$ = 330 cm^{-1}, in good agreement with the observed values. Our calculations indicate that the three remaining frequencies are 410 cm^{-1} (F_{1u}), 727 cm^{-1} (F_{1u}), and 202 cm^{-1} (F_{2u}). The AlF_5^{2-} anion has been postulated to be present in fluoride melts but has not yet been detected.

Finally, one sulfide ion complex was studied: the radical ion S_3^-. This ion was found to have a C_{2v} structure and its frequencies were predicted to be 252 cm^{-1} (A_1), 583 cm^{-1} (A_1), and 524 cm^{-1} (B_1). Berg et al.[9] have determined that the A_1 frequencies are 244 and 529 cm^{-1} from Raman spectra, in agreement with our calculated values.

---

[6]J. S. Binkley, J. A. Pople, and W. J. Hehre, J. Am. Chem. Soc. **102**, 939 (1980).

[7]M. S. Gordon, J. S. Binkley, J. A. Pople, W. J. Pietro, and W. J. Hehre, J. Am. Chem. Soc. **104**, 2797 (1982).

[8]B. Gilbert, G. Mamantov, and G. M. Begun, J. Chem. Phys. **62**, 950 (1975).

[9]R. W. Berg, N. J. Bjerrum, G. N. Papatheodorou, and S. Von Winbush, Inorg. Nucl. Chem. Lett. **16**, 201 (1980).

2. Studies of Associated and Ordered Liquids

Recent electrical conductivity[10] and thermodynamic[11] measurements with molten K-Pb alloys have indicated unusual behavior: ordering at the equiatomic composition rather than the expected composition at 20 mol % Pb, which corresponds to the valence ratio of the metals. In our work this past year, we investigated this phenomenon by electromotive force (emf) and calorimetric measurements of molten K-Pb alloy.

The emf measurements were performed using a coulometric titration technique and a potassium β-Al_2O_3 solid electrolyte. A unique seal between the β-Al_2O_3 electrolyte and an α-Al_2O_3 insulator hermetically contained the volatile potassium in the emf cell at moderately high pressures ($\lesssim$ 2 atm). The emf measurements were performed as a function of temperature (523-873 K) at constant compositions and were accurate enough to produce reliable values of the second derivatives of the emf (i.e, the average partial molar heat capacities). The concentration dependence of the heat capacities (ΔC_p) of the molten mixtures calculated from these measurements is exhibited in Fig. VIII-7. As can be seen, a large anomalous peak occurs in the heat capacities at about the equiatomic K-Pb (X_K~0.52) composition.

The calorimetric measurements yielded enthalpies ($H_T - H_{298}$) at temperatures of 751-1124 K for the equiatomic alloy ($X_K = 0.5029$). For these measurements, we employed a copper block drop calorimeter with the sample sealed into a tantalum capsule. Heat capacities for the liquid at temperatures ranging from the melting point, 862 K, to 1124 K were deduced from the measurements and are exhibited in Fig. VIII-8. The heat capacity is very large at lower temperatures and decreases with temperature to approach values of "normal" liquids. For reference, values for pure K and pure Pb are also plotted. This type of temperature dependence is consistent with that found for order-disorder transitions and could be related to long-range ordering or to the formation of ordered clusters of, for example, Pb_4. Preliminary analyses of the results are consistent with such models. Investigations of several other alloy systems where such phenomena are possible were negative so that equiatomic K-Pb appears to be unusual in exhibiting this striking anomaly. However, further measurements are underway to search for other systems where this phenomenon is observed.

We are also calculating the sulfide capacity of slags, which is a measure of the ability of a slag to extract sulfur. Knowledge of these values is important in pyrometallurgy and in steelmaking. Current methods of predicting sulfide capacities are based on the empirical concepts of basicity and optical basicity,[12] which we have shown to be inaccurate for many cases, despite the fact that the parameters in the equations used are empirically fitted to available data. We have developed a method that leads to accurate predictions of sulfide capacities for binary slags.

---

[10]J. A. Meijer, W. Geertsma, and W. Van der Lugt, J. Phys. F: Met. Phys. **15**, 899 (1985).

[11]M.-L. Saboungi, S. R. Leonard, and J. Ellefson, J. Chem. Phys. **85**(10), 6072 (1986).

[12]D. J. Sosinksy and I. D. Sommerville, Metall. Trans. **17B**, 331 (1986).

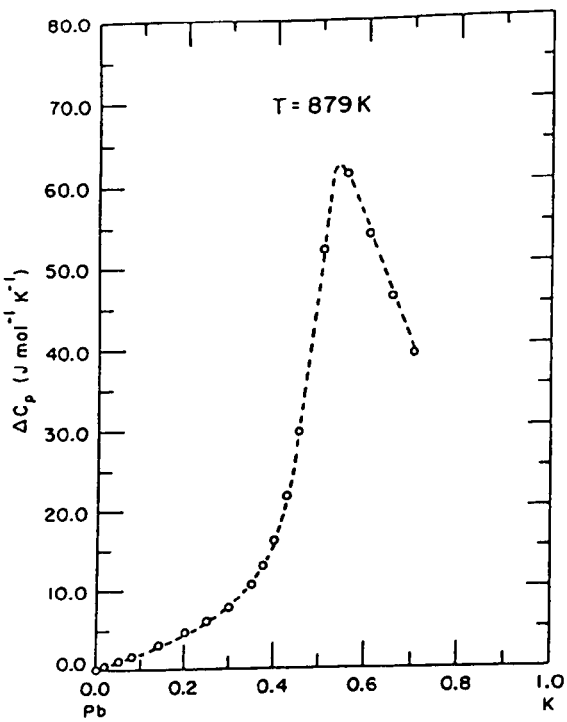

Fig. VIII-7.

Measured Differences Between Heat Capacities of K-Pb Solutions and the Pure Components as Function of Composition

Fig. VIII-8.

Variations with Temperature of Heat Capacity of Equiatomic Liquid K-Pb and Pure K and Pb

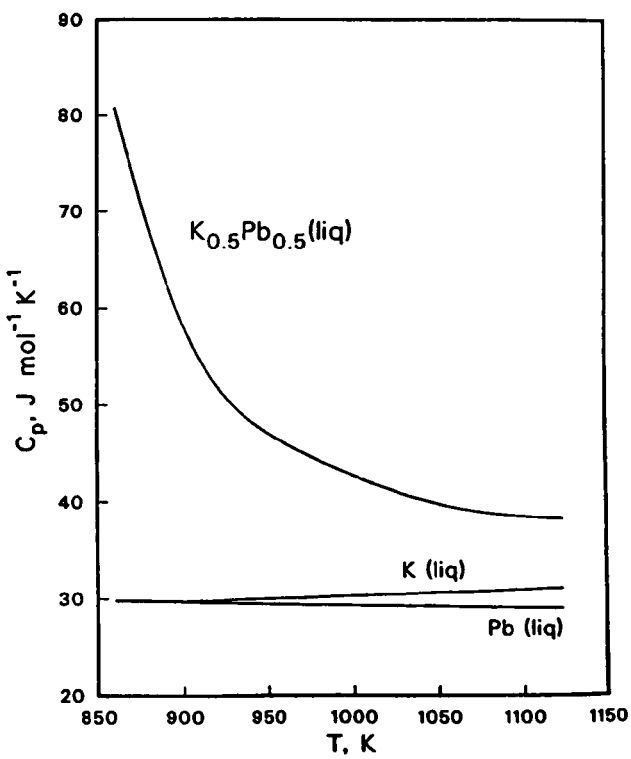

For a binary slag, such as $CaO\text{-}SiO_2$, our method starts with a calculation of the equilibrium constants for the reaction. In this case,

$$CaO(l) + \tfrac{1}{2} S_2(g) \rightleftharpoons CaS(l) + \tfrac{1}{2} O_2(g) \qquad (9)$$

For a given slag composition, temperature, and ratio of the fugacities of S_2 and O_2, we can calculate the activity of CaS in solution from the known activity of CaO. The activity coefficient of the sulfide in acid slags ($X_{SiO_2} > 0.33$) is calculated from polymer theory adapted to silicates.[13] These calculations are performed for two different polymer chain lengths--one and infinity. The value one is valid at the Ca_2SiO_4 composition and infinity, at the $CaSiO_3$ composition. In basic slags ($X_{SiO_2} < 0.33$), the activity coefficient is calculated based on the assumption that the slag is an ideal mixture of $CaO\text{-}Ca_2SiO_4$ and CaS. This assumption is based on a wealth of data on ionic systems in which mixtures of two substances with a common cation deviate little from ideality. We have completed calculations of sulfide capacities for $CaO\text{-}SiO_2$, $MgO\text{-}SiO_2$, $FeO\text{-}SiO_2$, and $MnO\text{-}SiO_2$ binary slags and achieved very good agreement between measurements and predictions. For comparison, predictions based on optical basicity differ from measurements in the $MnO\text{-}SiO_2$ system by more than two orders of magnitude. Figure VIII-9 shows the results of our calculations and those based on optical basicity for the $CaO\text{-}SiO_2$ system at 1773 and 1923 K. Our model calculations were made for two extremes of polymer chain lengths (m): 1 and ∞. As expected, the two calculations with our model bracket the measurements, which are closer to the line for infinite chain length in the more-acid melts. The precision of our predictions is far better than that from other methods. Extension of our calculational method to more complex slags will be based on concepts we have developed for reciprocal systems.[14]

Our methods, when fully developed, should prove to be useful for making predictions that are important in many technologies, including steelmaking and those involving coal combustion and conversion.

3. Calculation of Complex Gas-Condensed Phase Equilibria in Coal Combustion

We have developed a general computer program for the calculation of gas/condensed-phase equilibria in multicomponent-multiphase systems. The novelty of the program lies in its use of geometric programming for the free energy minimization and the conversion of a dual (thermodynamic) equation to a primal that can be converted to a linear equation. This program is linked to a critically analyzed data base consisting of thermodynamic properties of about 1800 species. At present, the calculational algorithm is robust enough to handle 300 species and several condensed phases, including solution phases. The concentration ratio of species with highest and lowest concentration is limited by the computer

---

[13]J. H. Hildebrand and R. L. Scott, *The Solubility of Non-Electrolytes*, 3rd Ed., Reinhold Publishing Corp., New York, pp. 347-351 (1950).

[14]M.-L. Saboungi and M. Blander, J. Am. Ceram. Soc. 58, 1-7 (1975).

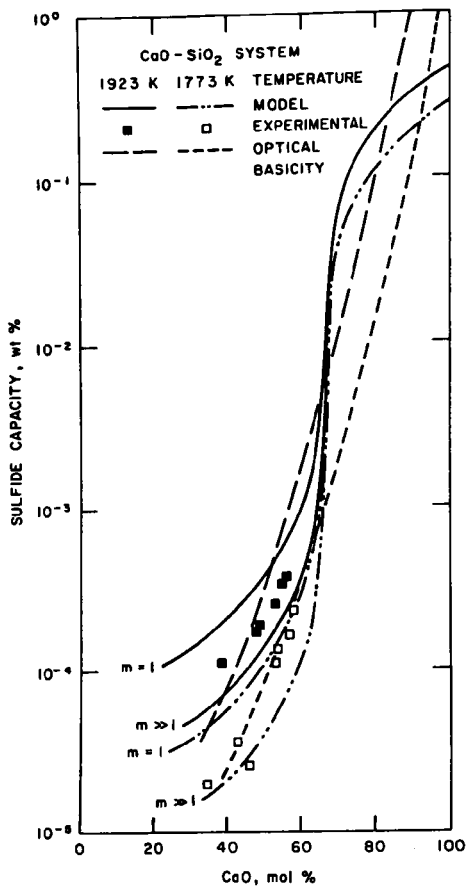

Fig. VIII-9.

Calculated and Measured Sulfide Capacities in $CaO-SiO_2$ System at 1773 and 1923 K. Calculations are shown for the two extreme values of m (the length of a silica polymer chain) of 1 and ∞ (designated as $m>>1$).

capability (e.g., $10^{\pm 303}$ in our MicroVAX II). The program has been tested on a number of problems concerned with the combustion of coal. Our preliminary calculations show that the deposits from the combustion of Illinois No. 6 high-sulfur coal are much more complex than had been believed. For example, we have shown that the first liquid condensate is a potentially corrosive silicate containing some sulfate. At equilibrium, no liquid sulfate-rich liquid forms. However, with a reasonable kinetic constraint on reactions of the liquid, a corrosive liquid sulfate phase can form. The results of such analysis should provide a basic understanding of the detailed chemistry of combustion and gasification environments of coal. Our plans are to extend our capabilities to perform calculations concerned with corrosion, energy conversion, pyrometallurgy, chemical vapor deposition, geochemistry, and other fields. Our current capabilities include a program with which we can realistically calculate equilibria among a complex silicate liquid, a multicomponent gas phase, and a number of other solid and liquid phases, including solutions.

C. *Interfacial Materials Chemistry*

The research into interfacial materials chemistry embodies a family of experimental and theoretical studies that focus on interfacial processes of importance to corrosion science, surface science, and catalysis. The experimental

work has two thrusts: (1) investigations of aqueous corrosion over a wide range of temperatures and pressures, using novel procedures based largely on the integration of spectroscopic and electrochemical techniques, and (2) coupled infrared and gas chromatographic studies of the chemistry of species adsorbed on materials with high surface area, such as zeolites. Paralleling *ab initio* theoretical research (e.g., on adsorbate/substrate interactions) and vibrational dynamics analyses are employed to support and extend the experimental findings.

1. Aqueous Corrosion Research

The corrosion of metals and alloys in aqueous media is a phenomenon that has been studied extensively. While interest in the mechanisms of aqueous corrosion has been long-standing, concerns about corrosion problems with both austenitic and nickel-base alloys in light water reactors have given a renewed impetus to research in this field. Although progress has been made in alleviating the conditions leading to stress corrosion cracking and pitting corrosion, a fundamental understanding of the factors involved in such corrosion is lacking, and the effect of metal impurities on crack tip propagation and pit growth in high-purity water at high temperatures and pressures is virtually unknown. The overall goal of this research is to provide an experimental data base against which theoretical models of aqueous corrosion can be tested over a wide range of temperatures and pressures. To reach this goal, we are undertaking studies that employ transient electrochemical techniques, coupled spectroscopic and electrochemical measurements, and modeling and theoretical calculations. Results during the past year in each aspect of this research are summarized below.

a. Electrode Kinetics Studies of Aqueous Corrosion

This effort addresses the kinetic and mechanistic aspects of corrosion reactions for metals in aqueous media at temperatures and pressures ranging from ambient to about ~300°C and 10 MPa. Aqueous corrosion processes are almost exclusively electrochemical and involve reduction of a component of the solution together with the anodic dissolution of the metal. Our research has two purposes: to determine the key factors that influence the active anodic dissolution of metals, with special emphasis on the charge transfer step, and to elucidate the kinetics and mechanisms of incipient passivation of metallic surfaces. Our experiments are closely coordinated with the theoretical effort described in Sec. VIII.C.1.c. Because of limitations in present modeling capability, we have focused the electrochemical measurements on simple electron transfer reactions that are not complicated by the making/breaking or rearranging of chemical bonds. The oxidation/reduction of hydrated transition metal ions (e.g., ferrous-ferric and chromous-chromic) exemplifies one type of simple electron transfer reaction when carried out in a noncomplexing environment. Accordingly, the ferrous-ferric perchlorate redox reaction at an inert electrode was selected for the initial measurements.

We completed a cyclic voltammetry investigation of the Fe^{2+}/Fe^{3+} system from room temperature to 150°C. The overall rate of the reaction was found to increase fourfold between 25 and 150°C--a level of increase with temperature that is typical of diffusion-controlled reactions. The increase of the charge transfer rate will have to be separated from the effect of diffusion by

future transient measurements. The temperature range of the measurements was limited to 150°C owing to the onset of incipient hydrolysis of the ferric ions. We anticipate that this limitation can be overcome through the use of fast transient techniques, provided the rate of hydrolysis is lower than that of charge transfer.

To avoid interferences from impurities, the kinetic measurements must be performed with ultra-pure media, free of perturbing species. Specifically, chloride ions, even in minute concentrations, are known to accelerate charge transfer. This year we carried out quantitative measurements at room temperature to test *in situ* methods for removal of chloride from electrodes. Two methods were developed in this work. In the first method, the measuring electrode was held at sufficiently negative potentials to desorb the chloride from the surface. This was followed by a potential step to the equilibrium potential and a pulse measurement of the kinetics. In the second method, chloride ions were removed from the surface before and during the kinetic measurement by continuous oxidation of chromous ions added in small concentration to the solution. The rate constant free of the chloride effect was found to be 2.2×10^{-5} cm s^{-1}, which is two to three orders of magnitude lower than the rates normally reported for this reaction when the chloride content of the solution is not scrupulously controlled. Good agreement was found between the rate constants determined by our methods and one previously reported rate constant determined with ultra-clean media.[15]

We developed a computer model for estimating the effect of the structure of the interfacial solution layer on the transient electrode kinetic measurements. The main purpose of the transient measurements is to separate the diffusional effects from the surface reaction kinetics. In prior studies of this type, the double-layer structure at the electrode/electrolyte interface was neglected. The justification for this has been the assumption that the thickness of the double layer is much smaller than that of the diffusion layer developing during the measurements. We have shown, in our initial model calculations, that for fast reactions (short-time measurements) this assumption is not justifiable; therefore, our kinetic data will have to be corrected accordingly to permit a meaningful comparison of measured rate constants with those predicted by the theoretical calculations described in Sec. VIII.C.1.c.

An improved high-temperature/high-pressure reference electrode is being developed. The type of reference electrode employed previously in our work had a useful lifetime of around one week because of gradual contamination of its electrolyte by the solution in the high-temperature/high-pressure cell--a common problem with virtually all high-temperature/high-pressure reference electrodes. The new electrode design eliminates the contamination problem by providing a continuous, slow flow of the electrolyte into the external solution. The lifetime of the electrode is limited only by the size of the electrolyte reservoir; a minimum lifetime of one month can be achieved with the presently used reservoir capacity.

---

[15]J. Weber, Z. Samec, and V. Marecek, J. Electroanal. Chem. Interfacial Electrochem. 89, 271 (1978).

b. Spectroelectrochemical Studies of Aqueous Corrosion

This effort addresses the relationship between the composition of metal/water interfaces and the mechanisms of corrosion and passivation reactions in aqueous media. The approach contrasts with conventional research in corrosion in that emphasis is placed on determining composition/property correlations under *in situ* conditions. The experimental methods involve a combination of spectroscopic and electrochemical techniques. Typically, laser Raman spectroscopy is employed to make *in situ* determinations of the molecular species present in anodic corrosion films on metal surfaces. Concurrently, DC polarization and AC impedance techniques are used to monitor the corrosion processes occurring in the interfacial zone. The results provide information on the mechanisms and kinetics of interfacial processes that take place during the corrosion of metals, including passivation and corrosion inhibition under steady-state conditions.

In situ laser Raman spectroscopic and electrochemical studies with very dilute aqueous sulfate solution were undertaken to demonstrate the operation of our high-temperature/high-pressure spectroelectrochemical facility.[16] Cyclic voltammograms of lead in 100 ppm (7×10^{-4} M) Na_2SO_4 solution from 25 to 280°C showed typical anodic dissolution/passivation behavior up to the highest temperature of measurement. The corrosion rate, as exemplified by the polarization resistance, increased steadily with increasing temperature. Using Raman spectroscopy, we identified the passive film on lead at low and high temperatures as $PbSO_4$; at intermediate temperatures (100 to 200°C), the passivating film was $PbO \cdot PbSO_4$. The surface film formed on open circuit below 150°C was determined to be the phase $3PbO \cdot PbSO_4 \cdot H_2O$; at higher temperatures, the monobasic form $PbO \cdot PbSO_4$ was identified. The Raman data were used in combination with values of thermodynamic quantities to construct a temperature-dependent Pourbaix diagram for the $Pb/H_2O/H_2SO_4$ system.

Alternating-current impedance methods were used to study the corrosion and passivation behavior of nickel in very dilute acid and near-neutral sulfate solutions. The nickel appears to be covered by a corrosion film at all times, with charge transfer processes occurring through the porous structure of the film. Somewhat different behavior is observed in 100 ppm H_2SO_4 solution, where the nickel actively corrodes even at open circuit. Passivation occurs with the formation of a surface film that is more coherent and apparently non-porous.

Laser Raman spectroscopy (LRS) and X-ray diffraction (XRD) studies were undertaken to characterize the types of compounds that could conceivably form as products of nickel corrosion in aqueous media. Various forms of nickel hydroxides and nickel oxides were synthesized and their structures were determined by LRS and XRD. The α and β forms of $Ni(OH)_2$ were clearly distinguished by their Raman spectra. There was evidence for the presence of intercalated H_2O, OH^-, and NO_3^- ions in the interlayer zone of α-$Ni(OH)_2$, but no such evidence for the β form. All the higher-valence oxide forms of nickel produced the same Raman spectrum, which consisted of two bands, one at 470 cm^{-1} and the other at 550 cm^{-1}. These nickel oxides appear, therefore, to possess the same structure--a layered network of NiO_2 units having D_{3d} symmetry.

---

[16] M. J. Steindler et al., *Chemical Technology Division Annual Technical Report, 1985*, Argonne National Laboratory Report ANL-86-14 p. 125 (April 1986).

The various forms (e.g., β- and γ-NiOOH, $Ni_2O_3 \cdot 2H_2O$, $Ni_3O_4 \cdot xH_2O$, and NiO_2) probably differ only in the degree of structural disorder and the nature of intercalated molecules, ions, etc. The XRD results tend to support this contention. The long-standing question concerning the valence of nickel in its higher oxide forms appears to be resolved by our results.

c. Theoretical Studies of Corrosion in Aqueous Media

The purpose of this effort is to develop microscopic models of (1) electron transfer processes suitable for the study of reaction kinetics at electrode surfaces and (2) the mechanism of metallic corrosion in aqueous solutions over a range of temperatures. Present charge transfer theories cannot explain the temperature dependence of many heterogeneous charge transfer reactions. The reasons for this include the fact that fundamental aspects of electron transfer associated with thermal activation and solvation changes are not well understood. With the aid of recent advances in computer technology, molecular dynamics, and molecular orbital theory, we are studying the kinetics of charge transfer from the metal surface to a solution species and the molecular structure in the interfacial layer. The work is being done in collaboration with J. W. Halley, a member of the Corrosion Institute at the University of Minnesota, who is carrying out molecular dynamics simulations. Molecular orbital calculations at ANL are being used to obtain potentials for the molecular dynamics calculations and to gain an understanding of the mechanistic aspects of the electron transfer process. The results of a theoretical study to determine the temperature and electrode-potential dependence of electron transfer rates will be compared with the experimental findings described in Sec. VIII.C.1.a. The ferrous-ferric electron transfer process at a gold electrode was chosen as the base case for initial development of the theoretical model.

Using a series of basis sets, we carried out *ab initio* calculations on $Fe^{2+}...OH_2$ and $Fe^{3+}...OH_2$ to determine the dependence of the potential well depth on the basis set size. Inclusion of polarization functions on oxygen and a sufficient number of p- and d-functions on iron was found to be very important. From this basis-set study, an appropriate level of calculation was chosen for the derivation of pair potentials for Fe^{2+} and Fe^{3+} interacting with water. By fitting gradients calculated at a number of carefully chosen points on the potential energy (vs. internuclear distance) surface, we accurately represented the potential energy surfaces in terms of Fe-O and Fe-H pair interactions. The existence of charge-transfer valence states such as $Fe^{2+}...(H_2O)^+$ and $Fe^{3+}...(H_2O)^+$ was also considered. The results indicate that, in the case of Fe^{3+}, such a charge transfer state may be significant in the liquid and may have to be taken into account in electron transfer simulations.

Molecular dynamics simulations of Fe^{2+} and Fe^{3+} in water were carried out using the *ab initio* pair potentials. For both cations, the simulations gave a structure for the first solvation shell that had eight water molecules in it. Experimentally, the first solvation shells of Fe^{2+} and Fe^{3+} have only six water molecules.[17] There have only been a few other molecular dynamics studies[18] of transition metal cations in water, and they also gave coordination numbers of

[17]Y. Marcus, *Ionic Solvation*, Wiley & Sons, New York (1985).

[18]A. Gonzalez-Lafont, J. M. Lluch, A. Oliva, and J. Bertian, Int. J. Quant. Chem. **29**, 1373 (1986); D. G. Bounds, Mol. Phys. **54**, 1335 (1985).

eight rather than six for the cations. No explanation had heretofore been set forth for the discrepancy. By computing three-body interaction energies from the interaction of two water molecules with the cations, we found that the origin of the problem is in the assumption of the additivity of the *ab initio* pair potentials, i.e., the neglect of the many-body forces in the simulation of the liquid. Inclusion of three-body forces dramatically stabilizes clusters with six relative to eight water molecules. On the basis of the insight provided by the *ab initio* pair potentials, we derived empirical potentials that take approximate account of the many-body forces and yield a reasonable account of the physical properties of Fe^{2+} and Fe^{3+} in an aqueous solution. These potentials are currently being used to determine the temperature dependence of the electron transfer rate for the Fe^{2+}/Fe^{3+} reaction at a gold electrode.

2. Studies of the Chemistry of Zeolite Catalysis

The purpose of this research is to develop new understanding of the reactivity and catalytic activity of zeolite cage networks through detailed study of their vibrational spectroscopic properties and by application of advanced theoretical methods. The key unknowns we seek to resolve in this research are (1) the mechanism(s) by which carbon-carbon bond formation, olefin cyclization (to produce cyclohexanes and substituted benzenes), and aromatic ring fusions (leading to coke formation) occur within the zeolite framework, and (2) the dynamics of reactant and product molecule movement within the zeolite structure. The results of this basic research could have broad fundamental application, particularly in the design of zeolite catalysts for specific product synthesis. Concurrent with the investigations of the vibrational frequencies of molecular species adsorbed on zeolites, detailed *ab initio* molecular orbital and normal mode calculations are being performed to provide information on the internal potential energy and vibrational kinematics of zeolite framework structures and zeolite-adsorbate interactions. The new knowledge and insight gained from this research are expected to contribute to an understanding of (1) acid-site chemistry in synthetic zeolites and its effect on product composition during shape-selective catalysis, (2) adsorbate conformations in zeolite pores and channels, and (3) the synthesis of new shape-selective zeolite catalysts.

a. Molecular Spectroscopy of Interactions in Zeolites

The previous annual report[19] described the considerable success achieved using Fourier transform infrared (FTIR) diffuse reflectance spectroscopy to study the reactivity of synthetic zeolite catalysts toward light hydrocarbons. During the past year, these studies were augmented by attaching a gas chromatograph (GC) to the controlled-environment diffuse reflectance (DR) cell so that on-line analyses of reaction products being formed in the DR cell could be performed at the same time that FTIR spectra of the zeolite/reactant system were being recorded. With this arrangement, we are now able to correlate product species and reaction rates with (1) the characteristic organic fragments

[19]M. J. Steindler et al., *Chemical Technology Division Annual Technical Report, 1985*, Argonne National Laboratory Report ANL-86-14, p. 126 (1986).

migrating through the zeolite channel network and (2) the labile proton occupancy of the catalytically active "acid" (Al-O-H) site of the zeolite. The combined DR/GC experimental assembly has been used to study the reactions of a series of alcohols, $CH_3(CH_2)_nOH$ (n = 0, 1, 2, 3, and 4), on the classic "Mobil" catalyst H-ZSM-5. The objective of this work is to explore the temperature sensitivity of the carbon-carbon bond-forming reaction and the relationship of that sensitivity to the chain length of the reactant alcohol.

Comparative studies of methanol (CH_3OH) and ethanol (CH_3CH_2OH) on H-ZSM-5 at 15, 250, and 350°C revealed the following reactivity scenario. At 15°C reactivity is nil but the alcohol is interactive with the acid site, producing a fully saturated (nonolefinic, nonaromatic) organic fragment, which appears to be CH_3 in the case of methanol and CH_3CH_2 in the case of ethanol. At 250°C, ethanol/H-ZSM-5 is much more reactive than methanol/H-ZSM-5, indicating that the carbon-carbon bond-forming step wherein a C_2 fragment is formed (critical for CH_3OH reactivity but not for CH_3CH_2OH reactivity) is rate controlling. At 400°C, both alcohols react at about the same rate, which is approximately five times the CH_3CH_2OH/H-ZSM-5 rate at 250°C. The product mix at 250°C for CH_3CH_2OH and at 400°C for both alcohols is dominated by substituted benzenes and cyclohexanes having from seven to nine carbon atoms in total.

Other highlights of the alcohol/H-ZSM-5 series of investigations may be summarized as follows. Using CD_3CH_2OH we have shown that the rate of C-H (C-D) bond cleavage (a key reaction step) increases steadily with temperature, and that deuterium atoms from the β-carbon (CD_3 group) populate both the aluminol and silanol hydroxyl positions. Although we know (from the work of the prior year) that the silanol proton site is not catalytic, it may serve the purpose of a proton storage register during catalysis. For the longer chain alcohols (n-propanol, n-butanol, and n-pentanol), we find reactivity and fragmentation behavior similar to that of ethanol on H-ZSM-5. Isopropanol appears to be more reactive, but additional experiments are needed to confirm this.

Investigations of the vibrational dynamics of zeolite framework structures have also continued. Factor group determinations of the correct vibrational representations for the normal modes of three additional zeolite systems were completed, bringing to 12 the number of different structures that have been fully analyzed by group theory. Included in this set of analyzed framework structures are zeolite A, zeolite X, faujasite, zeolite ZK5, zeolite rho, and offretite, i.e., those zeolite systems that are among the most important from the standpoint of practical applications. Conclusions from the previous year's work[20] concerning the importance of symmetry in determining the number of expected Raman and infrared active modes and the high expectation level for extensive accidental degeneracy of modes have been further substantiated. Most important, however, is the fact that the theoretical groundwork for detailed lattice dynamics calculations on crystalline zeolite structures has been laid.

---

[20]M. J. Steindler et al., *Chemical Technology Division Annual Technical Report, 1985*, Argonne National Laboratory Report ANL-86-14, p. 127 (1986).

Following the factor group calculations, the next step toward lattice dynamics analysis of zeolites is the development and testing of a suitable potential energy function. To proceed with such a task in an orderly fashion, we began by selecting a well-studied model system that emulated as much as possible the bonding characteristics of zeolitic structures. The model system chosen was the rutile structure, examples of which are TiO_2, PbO_2, SnO_2, and GeO_2. The rutile lattice is a network structure comprised of metal-oxygen-metal bridges (much like those in zeolites). The $(Si,Al)_xO_{2x}$ repeat character of zeolites is common to oxides of the rutile class. The structures are dissimilar in that the rutile oxides are built on "MO_6" distorted octahedra while zeolites are composed of "MO_4" tetrahedra, but this dissimilarity should not seriously affect the commonality of the bonding character in these two types of oxygen-bridged network structures. Accordingly, three types of classical potential energy functions (the simple valence force field model, the rigid ion model, and the shell model) were evaluated for the rutile structure. The extensive, well-characterized Raman spectroscopic data base for rutile-type crystals was used for this evaluation. A simple three-parameter valence force field model was found to give very good fits to observed vibrational data for four metal dioxides and five metal difluorides all having the rutile structure. (During the course of this work, numerous errors and inconsistencies were found in the published dynamical equations for the rutile structure.) The valence force field model is being used to complete a dynamical analysis of sodalite, one of the simplest and most symmetrical of all zeolites.

b. Theoretical Studies of Surface Interactions in Zeolites

This research involves quantum chemical studies of zeolite-substrate interactions. One area of study is the dynamics of molecules important as templates in zeolite crystallization. The role of organic bases in the formation of zeolites continues to be a topic of considerable debate and is of fundamental interest. Theoretical studies using *ab initio* molecular orbital theory can provide useful information on the rotational barriers and vibrational frequencies of organic bases, which will shed light on the way in which these template molecules direct the crystallization of the zeolite framework about it. Quantum chemical calculations are also used to study adsorbate-substrate interactions as they relate to catalytic and structural properties of zeolites and the energetics of metal atom clusters.

Using the STO-3G basis set,[21] we determined the vibrational frequencies of the tetramethylammonium ion (TMA) from its harmonic force field, which was calculated by analytical evaluation of the second derivatives of the Hartree-Fock energy with respect to nuclear coordinates. The STO-3G equilibrium structure of the TMA ion with tetrahedral symmetry was used in the calculation. The STO-3G predictions for the two torsional frequencies (one A_2 mode and a triply degenerate T_1 mode) of TMA are expected to be reasonably accurate, based on comparison of experimental vibrational frequencies[22] for a related molecule, trimethylamine, with vibrational frequencies which we calculated for it using the STO-3G basis set. The theoretical results were used to help interpret the

---

[21]W. I. Hehre, R. F. Stewart, J. A. Pople, J. Chem. Phys. 51, 2657 (1969).

[22]S. J. Cyvin and O. Gebhardt, J. Mol. Struct. 12, 215 (1972).

torsional vibrational frequencies of TMA occluded in ZK-4 (LTA) and omega (MAZ) zeolites as measured by inelastic neutron scattering. The experimental work was carried out by T. Brun and L. Iton (ANL Materials Science Division) in collaboration with a group at Exxon led by J. Newsam. The splitting between the two torsional modes is fairly constant in the different cages and in good agreement with our calculation. The general positions of the torsional modes are clearly very sensitive to the nature of the TMA environment, and as the cage size increases, these frequencies approach the calculated frequencies of the free ion. This work shows that the torsional modes of occluded templates are a sensitive indicator of their interaction with the zeolite cage.

In other related work, the natural bond orbital (NBO) method for analysis of wave functions from quantum chemical calculations has been tested (in collaboration with F. Weinhold, University of Wisconsin, and A. Reed, Erlangen-Nurnberg University) on the interaction of CO and NH_3 with clusters of Al atoms. For Al_4 interacting with CO, the traditional σ-donor picture of CO and metal-π back-donation, which had recently been questioned, was confirmed by the quantum chemical analysis. The bonding in the Al_4-CO system is fascinating in that very large changes in the electronic structure occur even though the binding energy of the complex (i.e., the driving force for these changes) is only around 5 kcal/mol. The NBO computational method of analysis will be extended to the study of adsorbate interactions in zeolites and to more-extensive investigations of the catalytic and structural properties of zeolites.

D. *Thermochemistry*

This effort is concentrated on determining the thermochemical properties of zeolites and related silicates and "high-tech" materials such as chalcogenides.

1. Minerals

Modeling studies of rock-water interactions depend greatly for their success on the accuracy and precision of the thermodynamic information available for the mineral assemblages involved. One example of such a study is the application of geochemical models to high-level nuclear waste repositories. In that connection and others, thermodynamic data for zeolites play an important role since those minerals comprise a major portion of the secondary phases found in volcanogenic rocks.

One of the recurrent difficulties in the application of thermodynamic information to practical geochemical problems has to do with variations in composition of the zeolites. The zeolite compositions that have been studied do not exist or are not representative of those found in nature. As a consequence, there are no thermodynamic values for those zeolites that are predominant in geological assemblages. Two examples of composition variability in zeolites are differences in the Si-to-Al ratios and differences in the substituted cations (i.e., Ca^{2+} for $2Na^{+}$). We have decided to address the first problem and its concomitant question: what effect does the variation of the Si-to-Al ratio have on basic thermodynamic properties of zeolites such as the standard molar enthalpy of formation ($\Delta_f H_m^\circ$) and the standard entropy (S_m°)?

Three specimens of the zeolite faujasite with the following compositions were synthesized by W. S. Wise (University of California at Santa Barbara): $Na_{2.083}Al_{2.083}Si_{5.917}O_{16}\cdot 5.835H_2O$ (Y-20), $Na_{3.583}Al_{3.583}Si_{4.417}O_{16}\cdot 9.202H_2O$ (13-X), and $Na_{2.375}Al_{2.375}Si_{5.625}O_{16}\cdot 9.921H_2O$ (Y-52). The Si-to-Al ratio of these materials varies between 1.23 and 2.84. These faujasites can be dehydrated completely without disruption of the aluminosilicate framework, a property possessed by relatively few zeolites. Analysis of the anhydrous faujasites will yield the Si-to-Al ratio contribution without interference from the variable H_2O content.

Standard molar enthalpies of formation of the faujasites are being determined by reaction with 24.4 mass % HF:

$$Na_xAl_xSi_yO_{16}\cdot zH_2O + (4x + 6y)HF(aq) = xNaF\cdot xAlF_3\cdot yH_2SiF_6\cdot(z + 16)H_2O(aq) \quad (10)$$

The calorimetric samples, equilibrated with an atmosphere of 50 % relative humidity and encapsulated in Teflon, are introduced into the gold reaction vessel of our LKB-8700 calorimeter and are then reacted with the HF. Auxiliary measurements of the enthalpies of reaction with HF of SiO_2 (silicalite), NaF, and $Al(OH)_3$, needed to complete the Hess cycle, are also performed.

Preliminary values for $\Delta_fH^\circ_m$ of two faujasites and their anhydrides have been determined. They are: $\Delta_fH^\circ_m$ ($Na_{2.375}Al_{2.375}Si_{5.625}O_{16}\cdot 9.921H_2O$, cr, 298.15 K) = -(10861.4±5.9) kJ mol^{-1}, $\Delta_fH^\circ_m$($Na_{2.375}Al_{2.375}Si_{5.625}O_{16}$, cr, 298.15 K) = -(7841.0±6.0) kJ mol^{-1}; $\Delta_fH^\circ_m$($Na_{3.583}Al_{3.583}Si_{4.417}O_{16}\cdot 9.202H_2O$, cr, 298.15 K) = -(10991.0±6.3) kJ mol^{-1}, and $\Delta_fH^\circ_m$($Na_{3.583}Al_{3.583}Si_{4.417}O_{16}$, cr, 298.15 K) = -(8136.3±6.4) kJ mol^{-1}. Measurements on the third faujasite are in progress. Upon completion of this work, a quantitative measure of the effect on $\Delta_fH^\circ_m$ of the Si-to-Al ratio in zeolites will be available.

The average binding energy of water is 18.6 kJ mol^{-1} for the Y-52 zeolite and 24.4 kJ mol^{-1} for the 13-X zeolite. These energies are smaller than our values for mordenite, 29.7 kJ mol^{-1}, and analcime, 40.9 kJ mol^{-1}.[23] This variability of the binding energy of the water in zeolites is significant, for example, in modeling studies. A method[24] for estimating the Gibbs free energy of formation of zeolites, based on the assumption that this value can be written as the sum of the standard Gibbs free energies of formation of the component oxides, <u>including water</u>, clearly cannot give realistic results because there is no unique value for the contribution of zeolitic water that can be applied to all zeolites.

Heat-capacity measurements from 5 to 350 K have been carried out on the dehydrated faujasites in our low-temperature adiabatic calorimeter. The molar heat capacities at 298.15 K ($C^\circ_{p,m}$) and the derived standard molar entropies (S°_m) for the dehydrated faujasites are as follows:

---

[23]G. K. Johnson, H. E. Flotow, P. A. G. O'Hare, and W. S. Wise, Am. Mineral. 67, 736 (1982).

[24]A. La Iglesia and A. Aznar, J. Zeolites 6, 26 (1986).

	$C^{\circ}_{p,m}$ (298.15 K) / (J K^{-1} mol^{-1})	S°_{m}(298.15 K) / (J K^{-1} mol^{-1})
$Na_{3.583}Al_{3.583}Si_{4.417}O_{16}$	429.14±1.54	440.43±1.59
$Na_{2.375}Al_{2.375}Si_{5.625}O_{16}$	470.23±1.97	492.94±2.07
$Na_{2.083}Al_{2.083}Si_{5.917}O_{16}$	425.22±1.02	425.82±1.02

In addition to the enthalpy of solution and low-temperature calorimetric techniques mentioned earlier, we have also used high-temperature drop calorimetry in our measurements on stilbite, a vein-forming, Ca-rich zeolite. Our results for stilbite, $Ca_{1.019}Na_{0.136}K_{0.006}Al_{2.180}Si_{6.820}O_{18}{\cdot}7.33H_2O$, at T = 298.15 K are summarized as follows: $\Delta_f H^{\circ}_m(T)$ = -(11034.6±6.6) kJ mol^{-1}, $C^{\circ}_{p,m}(T)$ = (808.73±1.62) J K^{-1} mol^{-1}, $S^{\circ}_m(T) - S^{\circ}_m(0)$ = (805.54±1.61) J K^{-1} mol^{-1}, $\Delta_f G^{\circ}_m(T)$ = -(10143.0±6.6) kJ mol^{-1}.

Retrieval of a $\Delta_f G^{\circ}_m$ value for laumontite from hydrothermal phase equilibrium experiments involving the zeolites (stilbite + laumontite)[25] and (heulandite + laumontite)[26] failed to yield concordant results. The disparity, more than 100 kJ mol^{-1}, between the two retrieved values may be attributed to differences between the compositions (e.g., Si-to-Al ratio) of the heulandite[27] and stilbite[28] used in the calorimetric studies and those involved in the hydrothermal experiments.[24] Another contributing factor to the discrepancy could be Si-Al disorder in the zeolites. A characterization of the Al and Si site occupancies in the heulandite and stilbite samples would allow a calculation of the configurational entropy contribution to the third-law entropy derived from our calorimetric measurements.

The enthalpy of formation of gibbsite, $Al(OH)_3$, is an important auxiliary datum in deriving the enthalpies of formation of zeolites and other aluminum-containing minerals. Therefore, we felt that it was necessary to confirm this quantity. The enthalpies of reaction at 298.15 K of Al and $Al(OH)_3$ in hydrofluoric acid according to the reactions

$$Al(cr) + 3HF(aq) = AlF_3(aq) + 3/2H_2(g) \quad (11)$$

and

$$Al(OH)_3(cr) + 3HF(aq) = AlF_3(aq) + 3H_2O(aq) \quad (12)$$

---

[25]J. G. Liou, Contr. Mineral. Petrol. **31**, 171 (1971).

[26]M. Cho, S. Maruyama, J. G. Liou, Int. Mineral. Assoc. Mtg. Abstracts, July 13-18, 1986, Stanford University, p. 76 (1986).

[27]G. K. Johnson, H. E. Flotow, P. A. G. O'Hare, W. S. Wise, Am. Mineral. **70**, 1065 (1985).

[28]D. A. Howell, M.S. Thesis, Western Michigan University (1987).

were measured with the LKB-8700 calorimeter. The measured quantities were combined with the enthalpy of formation of water to derive $\Delta_f H_m^\circ\{Al(OH)_3, cr, 298.15\ K\} = -(1294.9\pm1.2)$ kJ mol^{-1}. This value is in agreement with the results of Hemingway and Robie,[29] -(1293.1±1.2) kJ mol^{-1}, and Gross et al.,[30] -(1294.2±2.9) kJ mol^{-1}, all of which are significantly more negative than that obtained by Barany and Kelley,[31] -(1281.9±1.3) kJ mol^{-1}.

A new calorimetric effort has been initiated in support of the NNWSIP (Nevada Nuclear Waste Storage Investigations Project) EQ3/6 data base, with emphasis on thermodynamic properties of minerals related to nuclear-waste storage. The following properties are of interest: standard molar entropies at 298.15 K, low- and high-temperature heat capacities, standard molar enthalpies of solution, and standard molar enthalpies of formation at 298.15 K. The materials to be studied in the first phase of the investigation are tobermorite, soddyite, schoepite, uranophane, clinoptilolite, Wyoming bentonite, and sodium boltwoodite.

2. "High-tech" Materials

At a three-day symposium of the American Chemical Society held in Chicago in late 1985, speakers told of a large number of newly synthesized inorganic materials. An entire recent issue of *Scientific American* (October, 1986) was devoted to advanced materials, with emphasis on their application in new technologies and their impact on the economy of the United States. These two examples illustrate the importance that has now been assumed in science and industry by the so-called "high-tech" materials. The thermodynamic properties of such compounds, both new and well known, are largely ignored or unappreciated to date. These properties can be used advantageously, for example, to predict chemical behavior at extremes of temperature and pressure or in aggressive surroundings or to design efficient methods of synthesis.

For a number of years, we have been using fluorine-combustion calorimetry to determine standard molar enthalpies of formation of high-temperature and refractory materials. In the past few years, our studies have been concentrated on chalcogenides--compounds of metals and nonmetals with S, Se, or Te, many of which are important in the new technologies. It is therefore not surprising that our interests have intersected with the field of "high-tech" materials. The chalcogenides among those materials have many applications, including the following: tribology (high-temperature lubricants); semiconductors, thin films, glasses, photoresists, photomicrography (electronics); intercalation of alkali and other metals (battery technology); catalysis (dehydrosulfurization); solar energy conversion; manufacture of ceramics (Si_3N_4, for example); extractive metallurgy (desulfurization as practiced in the steel industry); and corrosion in sulfur-containing atmospheres (e.g., H_2S).

---

[29]B. S. Hemingway and R. A. Robie, J. Res. U.S. Geol. Survey 5, 413 (1977).

[30]P. Gross, J. Christie, and C. Hayman, Fulmer Research Institute (U.K.) Report 6, PG/JMN/R (1970).

[31]R. Barany and K. K. Kelley, U.S. Bureau of Mines Report RI-5825 (1961).

In a recent publication[32] from this laboratory, an up-to-date list was given of those chalcogenides studied by fluorine-combustion calorimetry. Perusal of the corresponding papers shows that this technique is uniquely suited to the determination of $\Delta_f H_m^\circ$ for chalcogenides and, in general, yields results superior to other methods.

Some time ago, in collaboration with scientists from Bell Communications Research, we used fluorine-bomb combustion calorimetry to study a polycrystalline specimen of $GeSe_2$; that work has since been published.[33] Although our determination of $\Delta_f H_m^\circ(GeSe_2, cr)$ had been undertaken because of the importance of $GeSe_2$ in electronic devices and in solid-state science in general, it subsequently turned out that there is even greater interest in the amorphous diselenide, $GeSe_2$(vit). Because of that interest, we measured,[34] in a collaborative effort with K. Volin and S. Susman (ANL's Materials Science Division), the energies of combustion in fluorine of vitreous $GeSe_2$ and a specimen recrystallized from the vitreous material. The enthalpy of transition between the two forms was found to be $-(12.1\pm4.2)$ kJ mol^{-1}. In addition, $\Delta_f H_m^\circ(GeSe_2, cr) = -(103.7\pm3.1)$ kJ mol^{-1} was also determined and agreed well with our published value, $-(102.2\pm2.6)$ kJ mol^{-1}.[33]

Molybdenum selenides, the best known of which is the diselenide (nominally $MoSe_2$), are increasingly being used in a number of advanced technologies, for example, as solid lubricants,[35] electrode materials,[36,37] and materials for solar-energy conversion.[38,39] The (molybdenum + selenium) phase behavior was explored by Spiesser et al.[40] who reported that, up to 1473 K, only the diselenide was formed by heating the elements together in various proportions; the lower compositional limit of this phase was found to be $MoSe_{1.9}$. However, at 1523 K, a second phase was observed with limiting compositions of $MoSe_{1.45}$ and $MoSe_{1.27}$. Since that work was published, other molybdenum selenides, e.g., Mo_6Se_6 and $Mo_{15}Se_{19}$, have been synthesized, but not by direct combination of just molybdenum and selenium. These Chevrel phases are being explored[37,41] as electrodes for secondary lithium batteries.

---

[32]W. T. Murray and P. A. G. O'Hare, J. Chem. Thermodyn. **16**, 335 (1984).

[33]P. A. G. O'Hare, J. Chem. Thermodyn. **18**, 555 (1986).

[34]P. A. G. O'Hare, K. J. Volin, and S. Susman, J. Non-Cryst. Solids, in press.

[35]L. F. Kolesnichenko, Z. T. Il'ina, Poroshk. Metall. **12**, 27 (1984).

[36]D. Ilic, K. Wiesener, W. Scheider, H. Oppermann, and G. Krabbes, J. Power Sources **14**, 223 (1985).

[37]J. M. Tarascon, J. Electrochem. Soc. **132**, 2089 (1985).

[38]H. Tributsch, J. Electrochem. Soc. **125**, 1086 (1978).

[39]H. Gerischer, D. Roβ, M. Lübke, Z. Phys. Chem. Neue Folge **139**, 1 (1984).

[40]M. Spiesser, J. Rouxel, M. Kerriou, and M. G. Goureaux, Bull. Soc. Chim. France, p. 1427 (1969).

[41]J. M. Tarascon, G. W. Hull, and J. V. Waszczak, Mater. Res. Bull. **20**, 935 (1985).

Few thermodynamic studies of (molybdenum + selenium) have been described. The molar heat capacities of Mo_6Se_8 below 30 K[42,43] and $MoSe_2$ to 350 K[44] have been reported. Studies of the vaporization of the molybdenum diselenide phase have been described by Glazunov et al.[45] and by Viksman and Gordienko.[46]

As an additional step toward firmly establishing the thermodynamic properties of the molybdenum selenides, the present research was undertaken to determine $\Delta_f H_m^\circ$ of $MoSe_2$ and Mo_6Se_6 at 298.15 K. Combustion calorimetry in fluorine yielded the following results: $\Delta_f H_m^\circ(MoSe_2, cr, 298.15\ K) = -(234.2\pm3.3)$ kJ mol^{-1} and $\Delta_f H_m^\circ(Mo_6Se_6, cr, 298.15\ K) = -(477.8\pm10.0)$ kJ mol^{-1}.

The high-temperature dissociation of $MoSe_2$ has been investigated by Glazunov et al.[45] and, more recently, by Viksman and Gordienko.[46] The former authors studied the evaporation of $MoSe_2$ from an effusion cell and deduced $\Delta_{vap}H_m^\circ = 213$ kJ mol^{-1}, which they attributed to the reaction:

$$MoSe_2(cr) = Mo(cr) + Se_2(g) \qquad (13)$$

Viksman and Gordienko observed, using mass spectrometry, the dissociation of hypostoichiometric diselenide:

$$MoSe_{1.91}(cr) = Mo(cr) + 0.955Se_2(g) \qquad (14)$$

and reported $\Delta_r H_m^\circ = (404.4\pm30)$ kJ mol^{-1} at 298.15 K. Our result for $\Delta_f H_m^\circ(MoSe_2)$, combined with $\Delta_f H_m^\circ(Se_2, g) = (144.1\pm0.6)$ kJ mol^{-1},[47] gives $\Delta_r H_m^\circ = (378.3\pm3.4)$ kJ mol^{-1} for reaction 13. This enthalpy of vaporization is very different from that given by Glazunov et al. but probably agrees with Viksman and Gordienko's determination, since the effect of nonstoichiometry on their value is likely to lie within the quoted ±25 kJ mol^{-1} uncertainty.

The fluorine bomb result is clearly superior to the previous determinations of $\Delta_f H_m^\circ$. To date ours is the first thermodynamic property to be reported for the Chevrel phase Mo_6Se_6.

---

[42]N. E. Alekseevski, N. M. Dobrovol'skii, G. Wolf, C. Hohlfeld, Zh. Eksp. Teor. Fiz. 83, 1500 (1982).

[43]C. Hohlfeld, B. Pietrass, J. Low-Temp. Phys. 48, 503 (1982).

[44]H. L. Kiwia, E. F. Westrum, Jr., J. Chem. Thermodyn. 7, 683 (1975).

[45]M. P. Glazunov, E. S. Mikhailov, N. V. Piskarev, M. S. Chupakhin, Poroshk. Metall. 11, 59 (1976).

[46]G. Sh. Viksman, S. P. Gordienko, A. A. Yanaki, L. A. Klochkov, Poroshk. Metall. 1, 75 (1986).

[47]F. Grønvold, J. Drowart, E. F. Westrum, Jr., *The Chemical Thermodynamics of Actinide Elements and Compounds. Part 4. The Actinide Chalcogenides (excluding Oxides)*, International Atomic Energy Agency, Vienna (1984).

E. *Geochemistry of Natural Hydrothermal Systems*

The objective of this project is to gain a better understanding of the geochemical processes involved in water/rock interactions that occur in active hydrothermal systems in the Earth's crust. The approach being taken is to investigate specific problems through detailed chemical and isotopic analyses of rock, mineral, water, and gas sampled from active hydrothermal systems. These data are interpreted in terms of the processes governing rock alteration and element redistribution in hydrothermal systems. We are investigating the rates and mechanisms of element redistribution, the time scale of rock alteration and element redistribution, water/rock ratios, and the relations between hydrothermal activity and local tectonomagmatic events. Potential applications of this work are in nuclear waste isolation, geothermal energy exploration and development, and mineral exploration. Highlights of the progress during 1986 are described in the following paragraphs.

1. Uranium-Series Disequilibrium Studies

The extent of radioactive disequilibrium among members of the ^{238}U decay series can be exploited for many applications in the earth and environmental sciences. We have been determining the time scale of hydrothermal activity with U-series methods in several active systems that are under study as part of the Continental Scientific Drilling Program (CSDP). These systems are located at Yellowstone (Wyoming), Valles (New Mexico), and Long Valley (California).

During 1986, we collected new samples from old sinter deposits in the Yellowstone and Long Valley calderas and then completed chemical separations of U and Th from these samples. In addition, alpha spectrometric measurements were partially completed. When the alpha spectrometric measurements are completed, we will attempt to calculate the ages of the deposits and relate these to the local geologic history.

Samples from a drill core in the Valles caldera (designated VC-1) were also obtained. Calcite veins from the VC-1 core were analyzed and age determinations were made where possible. Most of the veins for which ages could be estimated were older than the resolution of the technique (>300,000 years). Some of the veins did not have sufficient uranium concentrations for age determination.

We received representative samples of thermal water from the Valles caldera from colleagues at Los Alamos and measured uranium concentrations and $^{234}U/^{238}U$ activity ratios in these samples. In the high-temperature (above 270°C) reservoir within the caldera, uranium concentrations were found to be 0.03-0.04 $\mu g/L$. Unfortunately, $^{234}U/^{238}U$ activity ratios could not be determined with available sample amounts. In the hydrothermal outflow plume, uranium concentrations reached 0.99 $\mu g/L$, $^{234}U/^{238}U$ activity ratios ranged from 1.27 to 2.32, and uranium appeared to behave as a conservative species (i.e., did not react with the rocks through which it flows).

Analyses of ^{226}Ra in a set of samples from a Yellowstone drill core (Y-7) showed unsupported ^{226}Ra in clinoptilolite-rich samples. The amount of "excess ^{226}Ra" (i.e., activity of ^{226}Ra greater than that produced by decay of ^{230}Th in same sample) correlated 1:1 with the amount of barium in the samples and with their clinoptilolite content. The *in situ* distribution coefficient for barium is close to that measured in the laboratory. These data suggest active redistribution of radium and barium, probably by an ion-exchange reaction with the clinoptilolite.

2. Oxygen and Carbon Isotopic Studies: Drill Cores

Analysis of oxygen and carbon isotope ratios in minerals from drill core samples can provide information that is useful for investigating past temperature conditions, water/rock ratios, and sources of dissolved components.

To date, we have analyzed approximately 50 samples of hydrothermal silica and carbonate minerals from Yellowstone drill cores. This work is being done in collaboration with K. Muehlenbachs at the University of Alberta. The $^{18}O/^{16}O$ ratio of the hydrothermal minerals generally decreased with depth, reflecting the thermal gradient. Isotopic data for thermal water samples, provided by the U.S. Geological Survey, facilitated the interpretation of our drill-core data. Most of the silica minerals have $^{18}O/^{16}O$ ratios that are higher than the equilibrium ratios predicted for present temperatures and thermal water composition. This observation indicates that the minerals were deposited at higher temperatures and/or from water having a higher $^{18}O/^{16}O$ ratio than present thermal water. Complex silica veins, having two or more deposits of silica minerals, showed a consistent decrease in $^{18}O/^{16}O$ ratio from the earliest to the latest mineral. The earliest mineral is chalcedony (probably deposited as amorphous silica), and the latest mineral is quartz. This leads us to speculate that initial deposition of amorphous silica occurs relatively rapidly when a new fracture opens and allows flow of silica-supersaturated water. At this time the water is not in thermal, chemical, or isotopic equilibrium with the rock. The flow of water then decreases or stops, the water reaches local thermal and isotopic equilibrium with the rock, and silica concentration decreases to the level of quartz saturation.

Hydrothermal calcite has relatively high $^{13}C/^{12}C$ ratios, indicating that a large component of the dissolved carbon has a sedimentary marine carbonate source. Oxygen isotopic ratios are consistent with isotopic equilibrium between the calcite and the present thermal water at temperatures measured during drilling (100-200°C).

3. Relation between Hydrothermal Activity and Volcanism

The hydrothermal system of the Nevado del Ruiz volcano (Colombia) has been under investigation since its catastrophic eruption in November 1985. The continuing activity of the volcano provides an excellent opportunity to examine its effects upon its complex hydrothermal system. Our study of the hydrothermal activity for this volcano is being conducted in collaboration with colleagues from Louisiana State University and from several Colombian organizations. The increased understanding of this hydrothermal system resulting from our study may have applications for local geothermal energy development and for evaluation of volcanic hazards.

To date, we have collected a wide variety of data from chemical and isotopic analyses of thermal waters and gases, cold surface waters, and the lava ejected during the eruption. These data are consistent with two separate hydrothermal reservoirs within the volcano. The water being discharged from boiling springs at low elevations (<3000 m) is dilute, alkali-chloride-bicarbonate water having near-neutral pH. This water comes from a reservoir that is being evaluated for its geothermal energy potential by the Colombian government. The water being discharged at elevations >3000 m is near 65°C, has about 15,000 mg/L dissolved solids (mostly sulfate), and has a pH near 1.5. These acid springs are interpreted to come from a separate reservoir that derives its high acidity and sulfate concentration from magmatic volatiles. This hypothesis is consistent with the location of the acid-sulfate springs around the volcanic crater. These springs occur over an area of several hundred square kilometers, suggesting a fairly extensive reservoir.

We are monitoring one of the more accessible acid-sulfate springs on a regular (approximately every two months) basis to see if anything is changing because of the recent volcanic activity. Thirteen months after the 1985 eruption, significant changes in water temperature and composition were detected. Tritium analyses indicated a water residence time on the order of tens of years; therefore, changes in spring temperature and composition may continue to be detected for some time following the eruption. These changes will give us insight into the relation of the hydrothermal system to the underlying magma chamber.

4. New Facilities

During 1986, we obtained and tested an apparatus for phase equilibrium studies of the minute (micron scale) fluid inclusions in minerals. The apparatus consists of a heating/freezing stage that can attain sample temperatures of -196 to +700°C under controlled cooling or heating rates, and a special microscope adapted for viewing phase changes within the inclusions during their analysis. The data provided by the analysis of the inclusions relates directly to their composition and to the temperature and pressure under which the host mineral formed.

IX. ANALYTICAL CHEMISTRY LABORATORY

The Analytical Chemistry Laboratory (ACL) is a full-cost-recovery service center, with the primary mission of providing a broad range of technical support services to the scientific and engineering programs at ANL. In addition, the ACL conducts a research program in analytical chemistry, works on instrumental and methods development, and provides analytical services for governmental, educational, and industrial organizations.

The ACL functions administratively within CMT, the principal user (about 58% in FY 1986), but provides analytical support for all of the technical divisions and programs at ANL. The ACL has three groups--Chemical Analysis, Instrumental Analysis, and Organic Analysis--which together include 35 to 40 technical staff members.

The Chemical Analysis Group performs wet-chemical, instrumental, spectrochemical, and coal analyses and provides specialized analytical services. The Instrumental Analysis Group uses nuclear decay counting techniques, analyzes gases with mass spectrometry (MS) and gas chromatography (GC), analyzes solids by X-ray techniques, performs remote analysis of radioactive samples, and does work in dosimetry, neutron activation, inert gas fusion, and isotope analysis. The Organic Analysis Group uses a number of complementary techniques to separate and analyze complex organic mixtures and compounds, including synthetic fuels, toxic substances, fossil fuel residues and emissions, pollutants, biologically active compounds, pesticides, and drugs.

The majority of the technical accomplishments of the ACL staff are contained in technical summaries given in the previous sections of this report and in similar reports of other ANL divisions. Selected accomplishments are also summarized here.

In the electrorefining of uranium and plutonium fuels for the Integral Fast Reactor (IFR), metallic fuel pins (U, Pu, Zr) are dissolved in a molten cadmium anode, and the actinide elements are electrochemically transported through a halide-salt electrolyte to the cell cathode, where they are collected as a metallic deposit (see Sec. VI. C). The ACL has contributed to bench-scale studies of this electrorefining process by determining each element of interest in samples of the cadmium anode, the halide-salt electrolyte, and the cathode product. During FY 1986, ACL completed approximately 250 analyses for U and Pu on assay samples and measured the elements Ba, Ca, Sr, Ce, Nd, Na, Li, Y, Cd, and Zr in approximately 50 samples. Special dissolution procedures were developed for each sample matrix type, and separation schemes based on solvent extraction and ion exchange were established to isolate the sought-for elements from matrix components and from each other. Both U and Pu were determined by mass spectrometric isotope dilution after spiking with ^{235}U and ^{244}Pu and extracting into hexone. The fission-product and matrix elements were measured by inductively coupled plasma/atomic emission spectrometry (ICP/AES), following removal of alpha-emitting nuclides (U, Pu, Am) by ion exchange. Results of the electrorefining studies proved to be quite satisfying and showed good agreement between the experimentally determined distribution of the elements among the various phases and that calculated from the themodynamics of the multicomponent system. The results are shown in Table IX-1.

Table IX-1. Equilibrium Data for Electrorefining Bench-Scale Run

Element in Specified Phase	Amount, g	
	Calculated Value	Experimental Result
Pu (salt)	16.25	16.29
U (salt)	51.17	51.14
Pu (Cd)	25.50	25.46
U (Cd)	111.3	111.3

The Department of Energy has initiated a program designed to identify current and/or potential environmental problems and areas of environmental risk at DOE facilities. Over 40 sites nationwide will be surveyed in the next three years. Argonne is providing field survey teams for about eight of these sites, and the ACL is providing analytical chemistry support for these teams with organic, inorganic, and radiological analyses. Oak Ridge National Laboratory (ORNL), Oak Ridge Gaseous Diffusion Plant, Idaho National Engineering Laboratory (INEL), and Battelle Columbus are also involved in this DOE Site Survey Program. The principal effort in FY 1986 was devoted to the development of strategies for analysis that are consistent with the program objectives and to the preparation of facilities, instrumentation, and analytical methodologies for handling the anticipated large volume of field samples. Analysis began on samples from the first DOE site in this program, the Feed Materials Production Center in Fernald, Ohio.

In another effort, existing equipment was combined to form a laser Raman microprobe that is capable of resolving areas on solids approximately 1 μm^2. Raman spectroscopy measures vibrational frequencies and, thus, allows the determination of molecular information. The assembled system is being tested to determine its potential applications.

Through an interagency agreement with the Region V office of the U.S. Environmental Protection Agency (EPA), the ACL has completed several projects, including one to identify and quantify the pollutant loading in precipitation samples, and another to analyze priority pollutants in samples taken under the Resource Conservation and Recovery Act (RCRA). In the former, data collection and analysis were completed, and the final report for the pollutant loading was issued in FY 1986. In the latter, the RCRA samples were from two groundwater surveys that were sampled in August 1986 and analyzed by established EPA methods for organic priority pollutants. These pollutants included volatile organic and extractable organic compounds, PCBs, and organochlorine pesticides. An ongoing project for the EPA entails method development and analysis of air samples taken from a Midwest rubber reclamation plant. Both quantitative and qualitative information was obtained for the extremely odiferous compounds in the plant's emissions and was then reported to EPA.

The EPA Region VII methodology, which is used for the analysis of most soil samples for 2,3,7,8-tetrachlorodibenzo-p-dioxin, provides several alternative cleanup techniques to remove unwanted coextractives that interfere with measurements of targeted compounds from a soil extract and also allow GC/MS quantitation. These cleanup techniques, even if implemented sequentially, sometimes do not completely remove all coextractives that interfere with the quantitation. An alternative cleanup technique using size-exclusion liquid chromatography was developed by ACL and appears to aid in the analysis scheme by removing the bulk of some coextracted material. The dioxin cleanup is done with an SX-3 resin which, under low pressure, separates species by molecular size. By selecting the optimum solvent mixture and collection period, the analyst can recover the dioxin free from the large organic components typically coextracted from soils. This method of size-exclusion liquid chromatography has been found to facilitate other cleanup steps when their implementation is necessary. Dioxin recoveries from various soil extracts were generally in the 90% range. The recoveries are particulary good considering that interferences were eliminated.

Monitoring of emissions from municipal waste incinerators has shown that dioxins and furans are present. To determine the extent of contamination of the emissions and their variation as a function of operating parameters, a cooperative study with the National Bureau of Standards (NBS) is underway. A small-scale incinerator will be fitted with a sampling train that will collect the organic components emitted during controlled runs. The sampling train components will be sent to ACL for analysis of the dioxin and furan content. The objective of this study is to find the operating conditions that minimize the formation of these compounds.

The ACL provided analytical support for an ANL High-Sulfur Dry-Scrubber Test conducted for DOE by ANL's Energy and Environmental Systems Division. Feed materials and products from combustion of high-sulfur coal were subjected to a variety of analyses, including available lime, total alkalinity, total sulfur and sulfite, nitrite, nitrate, carbonate, sodium, calcium and silica, and moisture. Approximately 1400 determinations were made in support of the test.

Analytical support for the National Acid Precipitation Assessment Program was continued this year. The objectives of this program are to gain a better understanding of degradation mechanisms and to find ways of maintaining historical monuments and buildings. Test briquettes, exposed to a variety of atmospheric conditions at a number of sites throughout the country, are being brought to ACL quarterly for sampling and analysis. To date, hundreds of specimens have been analyzed for anions (fluoride, chloride, nitrate, and sulfate) by ion chromatography and for metals by ICP/AES. These results will be used in an effort to quantify the individual effects of the important damage parameters, which should lead to improved strategies for environmental protection of stone.

Studies were carried out to investigate some of the problems associated with the commercial production and separation of ^{99}Mo from irradiated uranium when low-enriched uranium is substituted for highly enriched uranium in the process that is presently in use. Studies were made of the effectiveness of the separation of ^{99}Mo from U, Np, Pu, and fission products (^{110}Ag, ^{131}I, and ^{137}Cs) by precipitation with α-benzoin-oxime, as well as the separation and purification of ^{99}Mo using columns containing silver-coated activated charcoal. Although the technique appeared promising, further studies of promising alternatives are underway.

Organics in solid and sludge wastes from new energy technologies (such as coal gasification and liquefaction and the extraction of oil from shale) were studied to (1) characterize, by narrow-bore capillary column GC/MS, the organics in solid and sludge wastes from these energy technologies and (2) determine the potential of organics leaching from these wastes after disposal. With this knowledge, strategies for treatment of the waste before disposal can be formulated. Thirteen waste samples were analyzed, including feed coals, pulverized feed coal, equalization tank sludge, pitch, tar, and heavy distillates. Each sample was extracted, typically with methylene chloride, and then analyzed by GC/MS. In addition, the samples were leached according to the extraction procedure developed by the EPA, and the leachates were extracted with methylene chloride and analyzed by GC/MS. The types of compounds found in the wastes included alkanes, benzenes, naphthalenes, polynuclear aromatic hydrocarbons, and phenols.

Advanced separation and instrumental techniques were applied to characterize those organics in solid-waste mixtures that cannot be analyzed by GC/MS. Even with a high-resolution capillary column coupled to a mass spectrometer, full identification is often difficult owing to the incomplete resolution of many of the peaks in the complex mixtures typically found in these wastes. A second problem that arises in GC/MS analysis is that the mass spectrum of a GC peak does not always lead to a positive identification of the peak (e.g., phenanthrene and anthracene have indistinguishable spectra, as do the eight isomeric dimethyl naphthalenes and the three isomeric xylenes). For cases in which the mass spectrum does not contain a molecular ion, identification is more difficult (e.g., alcohols, carboxylic acids, and esters). High-performance liquid chromatography (HPLC) was used to separate the very complex mixtures into four simpler mixtures for which there was sufficient resolution of peaks for GC/MS analysis. To analyze those compounds whose mass spectra do not lead to positive identification, the technique of gas chromatography/matrix-isolation/infrared spectroscopy (GC/MI/IR) was investigated. The GC/MI/IR technique was found to have sufficient sensitivity, of the order of GC/MS, and was useful for differentiating between the eight isomeric dimethyl naphthalenes, the three isomeric xylenes, and phenanthrene and anthracene. Each of these compounds gave unique infrared spectra, and the sharpness of the peaks in the fingerprint region (as is characteristic of MI/IR spectra) was paramount to obtaining accurate identification of the compounds.

Four coals, including one Illinois #6 high-sulfur coal, have been processed through the Premium Coal Sample Preparation Facility during this past year. This ANL facility was established to provide the coal community with well-characterized and stabilized samples of coal as an aid in research. Efficacy of mixing to form a homogeneous sample was monitored by the neutron activation technique and high-resolution gamma-ray spectroscopy. Approximately 160 coal samples were irradiated and counted for isotopes of Na, K, As, La, and Sc.

The ACL's inert-gas fusion apparatus for determining hydrogen, oxygen, and nitrogen in metals was adapted to measure these elements in several sulfides and selenides that showed anomalous or variable properties when their structure and formation thermodynamics were studied. Measurements on a series of silicon-sulfide glasses showed a strong correlation between oxygen content of each glass and intensity of an extraneous line in its neutron-diffraction pattern. This extraneous line had tentatively been identified as belonging to SiO_2; the oxygen

results helped confirm this assignment. Because oxygen was absent in the silicon and sulfur starting materials from which the glasses were prepared, the researchers were prompted to reassess their procedure for preparing these compounds. Impurities in the materials being studied were suspected to be the cause of the variability in heats of formation that had been determined by fluorine-bomb calorimetry for sulfides, selenides, and tellurides of such elements as Ge, Mo, W, and Si. Measurements on samples of the compounds and starting materials used in their preparation again showed oxygen, introduced during or after the compounds were made, to be the culprit. These compounds are now routinely screened by the ACL to avoid having to perform calorimetry on samples for which the oxygen content is high, and the analytical results are used in applying corrections to the thermodynamic data. The oxygen content of chalcogenide samples such as analyzed by ACL can affect the apparent enthalpy of formation by 5 to 10 kJ/mol--a significant error in itself and even more significant when the measured enthalpies are used in equilibrium calculations.

The Source Term Experiments Project (STEP) is a series of four experiments that focus on characterizing the source term associated with a postulated light water reactor accident. The experiments are conducted at the ANL Transient Reactor Test (TREAT) Facility in Idaho and are designed to capture representative fission products from fuel pins that have degraded in a steam environment. The experimental sample system is designed such that aerosol and volatile fission products can be determined through detailed post-test examination and analysis. Primary fission products of interest are Cs and I, with Mo, Sn, and Zr being secondary. Several samples obtained from the first set of experiments, STEP-1, have been analyzed for cesium and iodine. Cesium was determined by analyzing a sample for its isotopic content and normalizing this value to a known quantity of either ^{134}Cs or ^{137}Cs. The isotopic composition of the samples was determined by thermal ionization mass spectrometry (TIMS), and the ^{134}Cs and ^{137}Cs disintegration rates were determined by absolute gamma-ray spectrometry. Iodine was determined by ion chromatography. Results showed that iodine is often, but not always, associated with cesium in these samples.

A study of the degradation of toluene in an organic Rankine cycle engine has been completed. Toluene is the first fluid for which the degradation at temperatures of 316, 343, and 358°C has been studied. The results are important in selecting the appropriate fluids for use in industrial cogeneration of energy by utilizing "waste" heat. Identification of degradation products was based upon GC/MS and GC/Fourier transform infrared (FTIR) spectrometry. Quantitative analysis was done by capillary GC using new rapid-analysis software designed at Argonne. Degradation appeared to occur by a free-radical mechanism. At the low temperature (316°C), the major degradation product was bibenzyl, which formed from a methyl radical on the toluene molecule. At the higher temperatures, the toluene ring was activated, and C2-biphenyls and C1-diphenylmethanes were formed.

The Light Water Breeder Reactor Proof-of-Breeding (LWBR-POB) Analytical Support Project is part of a national program to establish the breeding gain of the $^{233}UO_2$-$^{232}ThO_2$ core in the LWBR, which operated at Shippingport, PA, from 1977 to 1982. Argonne's role in the program was to carry out precise, destructive analyses on 17 end-of-life fuel rods from the LWBR. This work was completed early in FY 1986, following an intensive 15-month campaign in which

the ACL provided chemical and radiometric measurements on dissolver solutions and gas samples obtained during processing of 152 segments sheared from the rods. On completion of ANL's measurements on these fuel rods, the ACL assumed the lead role in preparing a comprehensive final report describing the facilities and operations involved in their processing and in evaluating the performance of the ANL systems and procedures. Through detailed statistical consideration of quality assurance measurements (e.g., hundreds of duplicate analyses, measurements on standards, etc.), the precision and accuracy of the ANL measurements were shown to have met the demanding requirements of the parent LWBR-POB program. The LWBR-POB project at ANL was thus brought to a satisfying conclusion.

A laser photoacoustic spectrometer has been developed for the trace level detection and speciation of aqueous actinide ions under conditions relevant to nuclear waste disposal for the Basalt Waste Isolation Program (BWIP) of Rockwell Hanford Operations. Synthetic groundwater solutions of Am^{3+}, UO_2^{2+}, U^{4+}, Pu^{4+}, and PuO_2^{2+} are currently under investigation. Methods that allow measurements to be taken at temperatures in excess of 90°C have also been established. Detection limits at this time are 10^{-5} absorbance units per centimeter--a 10^3 increase in sensitivity over conventional optical absorption methods.

The objective of the Plastic Pipe Program for the Gas Research Institute is to analyze and characterize the chemical and molecular properties of polyethylene (PE) resins and to determine the effect of these properties on the mechanical strength of commercial PE pipe presently used for gas distribution. Achieving the program objective will be extremely challenging because PE pipe is a mixture of amorphous and crystalline regions, polymers of a range of molecular weights, antioxidants, ultraviolet absorbents, lubricants, opacifiers, dyes, other additives, ethylene oligomers, other unsaturated hydrocarbons, oxidized polyethylene, oxidized antioxidant, catalyst, and compounds in the free-radical state. To date, PE pipe has been analyzed by several techniques, including ^{13}C nuclear magnetic resonance, X-ray diffraction, gel permeation chromatography, and GC/MS. The information from this work will ultimately be used to control and optimize the mechanical properties and long-term performance of PE pipe for use in gas distribution systems.

The ACL was responsible for the analytical portion of a program to assess the environmental implications of neutralizing spills of hydrazine fuels with hypochlorite. Hydrazine and substituted hydrazines were reacted with a hypochlorite solution under various conditions, and the extracts of the reaction mixtures were analyzed by GC/MS. Most of the hydrazines were found to react with hypochlorite to form numerous by-products, some of which have been identified. From an environmental point of view, an important class of compounds identified in the reaction mixtures is N-nitrosoamines, because some N-nitrosoamines are carcinogenic. A calibration curve was prepared for N-nitrosodimethylamine that had been detected in reaction mixtures of dimethylhydrazine.

The New Brunswick Laboratory (NBL), which is responsible for preparing, certifying, and distributing reference materials related to nuclear safeguards measurements in the United States, is working toward producing a ^{243}Am certified

reference material (CRM) and a $^{241}Am/^{243}Am$ isotopic CRM. These standards will be prepared from chemically and isotopically pure metals provided by Oak Ridge National Laboratory early in FY 1987. The ACL has been contracted by NBL to carry out the hot-cell dissolution of the ^{241}Am and ^{243}Am metals, to perform precise assays of the americium in each solution, and to prepare accurately weighed aliquots of the solution for subsequent dilution and dispensing into CRM ampuls. During FY 1986, the ACL effort in this area was directed toward establishing a precise, complexometric titration procedure for the americium assays and adapting the procedure for use in a glove-box facility in CMT. This procedure uses a Hg^{2+}/Hg^{0} indicating electrode to determine the end point for titration of Am with ethylenediaminetetraacetic acid (EDTA) after the EDTA is standardized with NBS standards containing Pb and Zn. The standard deviation for a single determination is estimated to be 0.06% (relative) for a sample containing 10 to 15 mg Am.

A synthetic form of the rare mineral djerfisherite, of the general formula $(Li,Na,K)_7(Fe,Cu,Ni)_{24+x}S_{26}Cl$ (J phase), was produced in an electrochemical cell of the type LiAl/LiCl-KCl/FeS, which was operated at 450°C in a molten-salt electrolyte LiCl-KCl. The synthetic form was isolated in a relatively pure state (less than 5% impurities) and in sufficient quantity (4 g) to allow neutron diffraction examination. Neutron powder diffraction provided more structural detail than X-ray powder diffraction data because of the greater difference in the scattering factors for the transition elements and the ions K^{+}, S^{2-}, and Cl^{2-}. The ANL Intense Pulsed Neutron Source (IPNS) was used to collect a much larger number of Bragg reflections than were collected for the J phase by the X-ray powder technique. As a consequence, a better refinement of crystallographic parameters was obtained. The data, 682 reflections, were collected on the time-of-flight neutron diffractometer at the IPNS. A crystallographic refinement of the neutron diffraction data by the Rietveld analysis technique showed an improvement in the atom coordinate positions by a factor of ten over prior X-ray powder diffraction data. This refinement indicates 23 iron atoms randomly distributed about 24 available sites such that the formula of the synthetic form of djerfisherite can be expressed as $K_6LiFe_{23}S_{26}Cl$.

Other analytical work included the following items:

- Application of GC/FTIR/MS to the study of degradation of flavors used in chewing gums.
- Carbon, hydrogen, nitrogen, and sulfur analyses and chemical characterization of ashes for the Premium Coal Sample Program and other basic coal programs.
- Determination of moisture, ash, and gross calorific value of chars and tars for a program on municipal waste utilization.
- Determination of distribution coefficients for numerous samples of fission-product metals in immiscible phases by the ICP/AES technique for a program on separations chemistry.

- Complete chemical analysis of slag and chromite samples for a program in corrosion of refractories in synthetic coal ash slag with application to slagging coal gasifiers.

- Analysis of leached metals by ICP/AES, determination of leached anions by ion chromatography, determination of low levels of uranium by fluorescence analysis, and determination of alkali metals by atomic absorption or ICP/AES for a study of high-level waste repository interactions.

- Analysis of deposits of Pb, $PbSO_4$, and PbO_2 mixtures for a battery research program.

- Characterization of lithium metal-trace metals, nitrogen determination, and lithium assay for a study of fusion-power materials.

- Technology transfer to Morgantown Energy Technology Center of software that allows rapid computerized analysis of complex organic mixtures.

- Assay of a variety of fuel materials--uranium silicides, $U_6Mn_{1.3}$, and U-Ni--using a combination of gravimetric and ICP/AES determinations for a fuel materials program for the Reduced Enrichment Research Test Reactor (RERTR).

- Measurement of arsine and stibine generated in a test battery using methods developed at ANL.

Additional improvements in ACL facilities and capabilities were made in FY 1986. Work was completed on construction of a containment room located in CMT. This room will allow the safe handling of potentially hazardous samples from field studies. Samples prepared in the containment room can then be safely analyzed by existing GC and GC/MS systems. Work was completed on a room for handling and analyzing samples in the IFR Program; this room has an ICP/AES unit dedicated to radioactive samples. A sample-receiving facility was constructed for the DOE Site Survey Program. In this room, sample coolers will be received, unpacked, and logged in; the samples are then stored in refrigerators until distribution to appropriate laboratories.

New equipment installed in FY 1986 includes a liquid scintillation analyzer, a high-resolution monochromator for a general-purpose ICP/AES system, and a supercritical fluid chromatograph (SFC). The SFC has been installed and tested. As a test, a paraffin wax sample was separated into individual alkanes up to C40. The peaks were symmetric, and the peak widths at half-height were approximately 10 to 15 s, which is comparable with capillary GC peaks. Samples to be analyzed with the SFC are coal and coal-derived liquids.

The Scintrex uranium UA-3 analyzer, which is used for uranium analyses in solution by laser-induced fluorescence, has been upgraded so that the measured fluorescence is read directly by the computer. Reading or recording errors by the operator are eliminated with this improvement.

The ACL has updated its gas analysis capabilities with the acquisition of a Tracor 540 trace gas analyzer. This "state-of-the-art" gas chromatograph uses an ultrasonic detector, which measures variations in the speed of sound traveling through a gas, to quantify levels of components in a sample. The Tracor is coupled to a Spectra Physics SP4290 computing integrator that is capable of providing, among other things, hard copy of peak areas and relative retention times directly onto the chromatogram. Currently, a small-volume evacuated sampling system is being designed for the Tracor to allow direct analysis of gas sampling loops and compressed gas cylinders.

A high-precision isotope ratio mass spectrometer (Consolidated Nier, CEC 21-201) has been dedicated to measuring $^{13}C/^{12}C$ and $^{18}O/^{16}O$ ratios in carbon dioxide. Most recent determinations have been of ^{13}C in atmospheric methane worldwide. The method involves simultaneous measurement of the mass 45 (or 46) peak on one collector and the mass 44 peak on a second collector, alternatively for a reference CO_2 and the unknown CO_2, from dual inlets. The ACL data acquisition system (described by Stevens and Krout[1]) is now controlled by an IBM personal computer, and older components of the system (preset counter, digital printer, Vidar voltage-to-frequency converters) have been replaced. A new display provides for continuous monitoring of instrument and analysis status. The printout identifies sample and reference gases, along with the date and time, and also provides intensity and ratio data, including the calculated ratio of the unknown to the reference.

Finally, data communication between analytical instruments and various computer systems was improved to allow for the manipulation and transfer of raw or calculated data used in the production of reports and to establish data communication between laboratory personal computers, the mainframe IBM computer at ANL, and the VAX computers in various ANL divisions.

[1]C. M. Stevens and L. Krout, J. Mass Spect. Ion Phys. 8(4), 265 (1972).

X. COMPUTER APPLICATIONS

The Computer Applications Group provides assistance to CMT staff in many aspects of computer-related activities, including (1) laboratory data acquisition and control, (2) computer modeling and simulation studies, (3) post-analysis of experimental results, (4) graphics applications, (5) information management systems and data-base development, (6) computer operating-system maintenance, (7) small and large computer networking, (8) procurement of equipment for automatic data processing, and (9) advisory, educational, and consulting services.

The Computer Applications Group has responsibility for (1) software maintenance and development of nearly 20 minicomputer data acquisition systems and the Division's VAX central computing facility and (2) hardware maintenance of various small systems and peripherals, including the Division's terminal communications system.

Improvements to data acquisition systems during 1986 have included upgrading of the interface hardware and computer systems for the FEUL coal combustor (Sec. III.D) and their integration into CMT's network environment. Updating the computer hardware for the FEUL oil combustor is planned for 1987. This year has also seen considerable growth in the use of personal computers in the Division as part of both instrumentation packages and data-acquisition systems. Incorporation of many of these personal computers into the Division's local area network (Ethernet) has routinely provided users with convenient, high-speed access to the many software aids available on the VAX.

During 1986, the VAX 11/780 was upgraded to a VAX 11/785 (which offers a 50-70% increase in throughput), and its disk storage capacity was expanded to approximately 2.5 gigabytes (Gb). Memory has been increased from 16 to 32 Mb and supports up to 60 simultaneous users.

The Computer Applications Group continues to be involved in working with Computer Services, the Electronics Division, and Laboratory committees to develop plans for Laboratory-wide computer networking. This year has seen the installation of a site-wide DECnet, which allows VAXs and other smaller computers to communicate with one another. This network extends far beyond the Laboratory through its connection to HEPnet, an international high-energy physics network. Additional connections to BITNET and the Energy Research/Fusion Energy (NMFECC) networks allow CMT users to communicate electronically with several thousand research institutions located around the world. Installation of a Private Branch Exchange (PBX) at ANL is scheduled to be completed by August 1987. This will further enhance data communications at the Laboratory by providing the capability for high-speed terminal-to-host and host-to-host data links, including Laboratory-wide Ethernet capability.

The VAX 11/785 is being used for a wide variety of applications, including post-analysis of experimental data, theoretical calculations in basic energy science, graphics applications, electronic mail, and other office automation and management functions. The use of sophisticated laser printers has increased sharply and has almost completely replaced other printing systems in the Division. Access to a soon-to-be-installed Laboratory typesetting system through existing network

channels will permit CMT users to obtain extremely high-resolution output when needed. At present, the VAX is being utilized by over 250 members of the division and other related ANL personnel.

The High-Temperature Materials Group in CMT continues to run large, CPU-intensive theoretical calculations on its MicroVAX-II. This system, which provides approximately 90% of the computational power of a VAX 11/780, is connected to CMT's Ethernet to provide access to various peripherals and computer networks.

A block diagram of the Divisional computing configuration is shown in Fig. X-1.

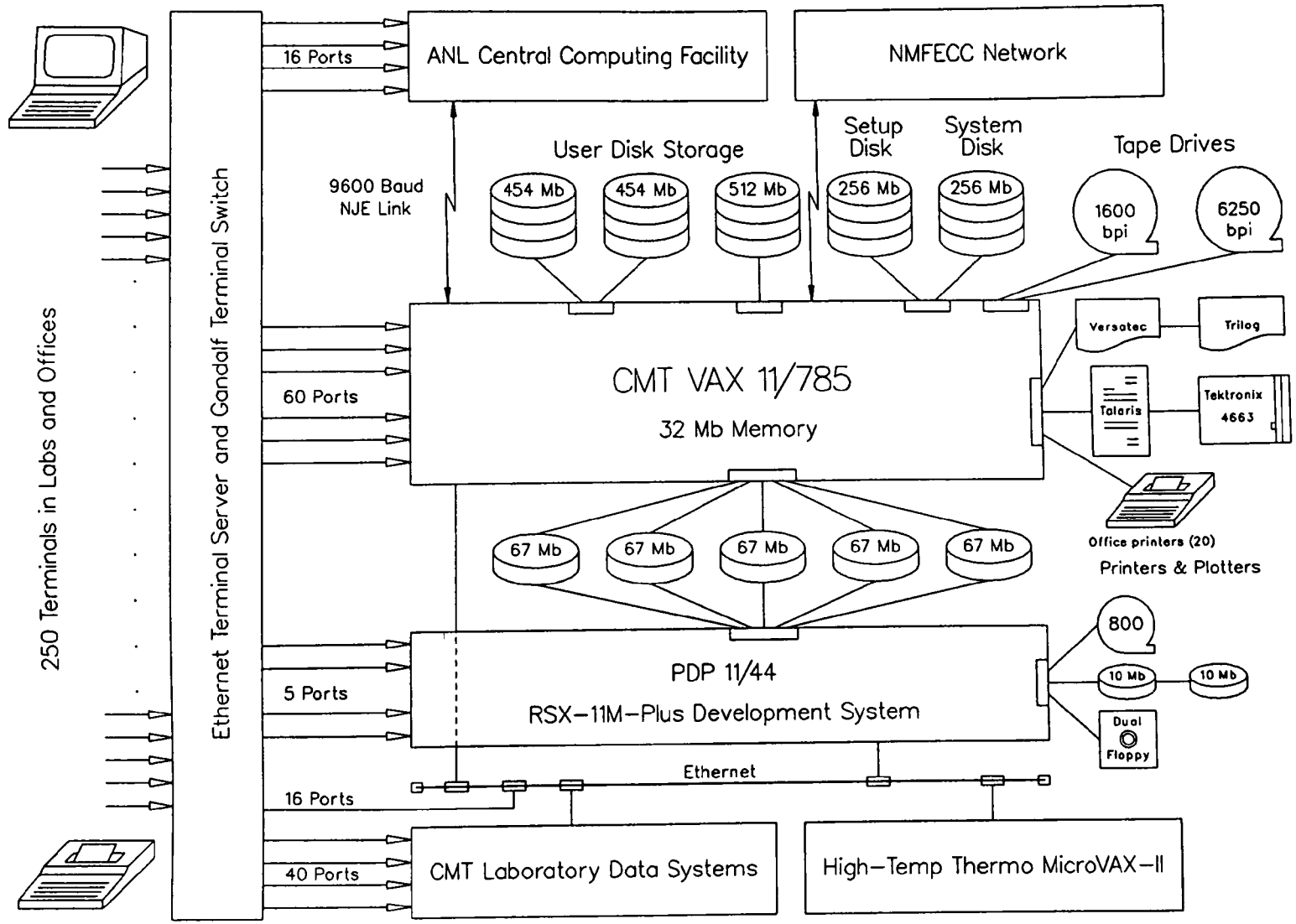

Fig. X-1. Block Diagram of CMT Computing Facilities

XI. ADDENDUM.

CHEMICAL TECHNOLOGY DIVISION PUBLICATIONS--1986

The Division's publications and oral presentations for 1986 were entered into a bibliographic data base on the VAX-11/785 computer. The pages that follow are a printout of this information sorted into six categories: (1) journal articles and book chapters, (2) patents, (3) ANL progress and topical reports, as well as contributions to reports published by organizations other than ANL, (4) abstracts and papers published in proceedings of conferences, symposiums, workshops, etc., (5) oral presentations at scientific meetings and seminars not referenced in the fourth category, and (6) papers accepted for publication but not yet published.

CHEMICAL TECHNOLOGY DIVISION PUBLICATIONS — 1986

A. Journal Articles & Book Chapters

Technical Requirements of Experiments and Facilities for Fusion Nuclear Technology
M. A. Abdou, P. Gierszewski, M. Tillack, J. Grover, R. Puigh, D. K. Sze, and D. Berwald
Fusion Technol. **10**(3), 1065 (November 1986)

Blanket Material and Engineering Issues, and Requirements for Experiments and Facilities
M. A. Abdou, P. Gierszewski, M. A. Tillack, A. R. Raffray, D. K. Sze, and R. Puigh
J. Nucl. Mater. **141–143**, 10–18 (1986)

Aqueous Corrosion of Natural and Nuclear Waste Glasses. I: Comparative Rates of Hydration in Liquid and Vapor Environments at Elevated Temperatures
T. A. Abrajano, Jr., J. K. Bates, and C. D. Byers
J. Non-Cryst. Solids **84**, 251–257 (1986)

Materials for High-Temperature Fuel Cells
J. P. Ackerman and T. D. Claar
J. Mater. Energy Syst. **8**(3), 284–290 (December 1986)

Post-Test Analyses of Sodium-Sulfur Cells and Aqueous Batteries
J. E. Battles, J. A. Smaga, and J. J. Marr
J. Power Sources **17**(1-3), 221–225 (January–April 1986)

Photoionization Mass Spectrometric Study and *Ab Initio* Calculations of the Ionization and Bonding in P-H Compounds; Heats of Formation, Bond Energies and the $^3B_1$-$^1A_1$ Separation in PH_2^+
J. Berkowitz, L. A. Curtiss, S. T. Gibson, J. P. Greene, G. L. Hillhouse, and J. A. Pople
J. Chem. Phys. **84**(1), 375–384 (January 1, 1986)

Analyses of Thermodynamic Properties of Molten Slags
M. Blander and A. D. Pelton
Mineral Matter and Ash in Coal, ed. K. S. Vorres, Am. Chem. Soc. Symp. Ser. **301**, 186–194 (1986)

Molecular Dynamics Studies of Complexing in Binary Molten Salts. II. Molten M_3AX_6 and MA_3X_{10}
M. Blander, M.-L. Saboungi, and A. Rahman
J. Chem. Phys. **85**(7), 3995–4004 (October 1, 1986)

Corrosion of Nickel-200 and AISI-1008 Steel in Sodium Polysulfides and Sulfur at 350°C
A. P. Brown and J. E. Battles
J. Electrochem. Soc. **133**(7), 1321–1325 (1986)

Rekindled Interest in Pyrometallurgical Processing (The 1984 Robert E. Wilson Memorial Lecture)
L. Burris
Chem. Eng. Prog. **82**(2), 35–39 (February 1986)

On the Composition of Anodic Corrosion Films on Nickel in Near-Neutral and Acid Solutions
K. Carr, S. Baer, and C. A. Melendres
Corrosion **42**, 307 (1986)

Three Super-Batteries Move Closer to Practical Applications
A. A. Chilenskas, T. D. Kaun, and I. Bloom
Logos 4(2), 6–11 (Summer 1986)

The LISA1 Experiment: In-Situ Tritium Release Investigations
R. G. Clemmer, H. Werle, and M. Briec
J. Nucl. Mater. 141–143, 321–326 (1986)

Swelling of Spinel after Low-Dose Neutron Irradiation
W. A. Coghlan, F. W. Clinard, Jr., N. Itoh, and L. R. Greenwood
J. Nucl. Mater. 141–143, 382–386 (1986)

Ab Initio Molecular Orbital Calculation and Semiempirical Analysis of the Vibrational Frequencies and Force Constants of ONF and FON
L. A. Curtiss and V. A. Maroni
J. Phys. Chem. 90(1), 56–61 (1986)

Theoretical Studies of O_2^-: $(H_2O)_n$ Clusters
L. A. Curtiss, C. A. Melendres, A. E. Reed, and F. Weinhold
J. Comput. Chem. 7(3), 294–305 (1986)

Theoretical Studies of the Interaction of H_2O with Small Clusters of Beryllium Atoms
L. A. Curtiss and J. A. Pople
Int. J. Quantum Chem. 19, 613–628 (1986)

Computerised Rapid Analysis for Specialised Applications—A Simplified Method to Produce Customised Gas Chromatrographic Software
J. C. Demirgian
J. Chromatogr. Sci. 24, 189–197 (May 1986)

Differential Thermal Analysis of U_3Si-Al and U_3Si_2-Al Reactions
R. F. Domagala, T. C. Wiencek, J. L. Snelgrove, M. I. Homa, and R. R. Heinrich
Am. Ceram. Soc. Bull. 65(8), 1164–1170 (1986)

Preparation of a ^7Be Target Via the Molecular Plating Method
B. W. Fillipone and M. A. Wahlgren
Nucl. Instrum. Methods Phys. Res. A243, 41–44 (1986)

An Evaluation of Polarised Fuels in a Commercial Deuterium/Tritium Tokamak Reactor
P. A. Finn, J. N. Brooks, D. A. Ehst, M. Y. Gohar, R. F. Mattas, and C. C. Baker
Fusion Technol. 10, 902 (1986)

A Process to Recover Tritium from High Pressure Helium
P. A. Finn and D. K. Sze
Fusion Technol. 10, 1362 (1986)

Studies of Surface Adsorption on $LiAlO_2$
A. K. Fischer, J. A. McDaniel, and C. E. Johnson
J. Nucl. Mater. 141–143, 344–347 (1986)

New Ideas in Dosimetry and Damage Calculations for Fusion Materials Irradiations
L. R. Greenwood
J. Nucl. Mater. **141–143**, 654–657 (1986)

Production of ^{91}Nb, ^{94}Nb, and ^{95}Nb from Mo by 14.5–14.8 MeV Neutrons
L. R. Greenwood, D. G. Doran, and H. L. Heinisch
Phys. Rev. **34C**, 986–994 (1986)

New Neutron Cross Sections for Fusion Materials Studies
L. R. Greenwood and R. K. Smither
Radiat. Eff. **92–96**, 163–166 (1986)

Neutron Irradiation of Superconductors and Damage Energy Scaling of Different Neutron Spectra
P. A. Hahn, H. W. Weber, M. W. Guinan, R. C. Birtcher, B. S. Brown, and L. R. Greenwood
Adv. Cryog. Eng. Mater. **32**, 865–872 (1986)

The Tritium System for a Tokamak with a Self-Pumped Limiter
A. M. Hassanein and D. K. Sze
Fusion Technol. **10(3)**, 1355 (November 1986)

Isolation of a Highly Mutagenic Aminophenanthrene from a Coal Gasification Process Tar
D. A. Haugen, V. C. Stamoudis, M. J. Peak, and A. S. Boparai
Environ. Res. **39**, 60–73 (1986)

The FUBR-1B Experiment—Irradiation of Lithium Ceramics to High Burnups under Large Temperature Gradients
G. W. Hollenberg, R. C. Knight, P. J. Densley, L. A. Pember, C. E. Johnson, R. B. Poeppel, and L. Yang
J. Nucl. Mater. **141–143**, 271–274 (1986)

Oxygen Isotopic Study of the Oxidation of SO_2 by H_2O_2 in the Atmosphere
B. D. Holt and R. Kumar
Fossil Fuels Utilization: Environmental Concerns ACS Symp. Ser. No. **319**, pp. 277–283 (June 1986)

Oxygen-18 Study of the Atmospheric-Aquatic Linkage in Adirondack Watersheds
B. D. Holt and R. Kumar
Water, Air, Soil Pollut. **31**, 175–186 (1986)

Autonormalization of Battery Test Data to Significantly Reduce Impact of Battery Aging on Test Results
F. Hornstra
J. Power Sources **17(1-3)**, 107–113 (January/April 1986)

A Simple Methodology for Obtaining Battery Discharge Times (and Vehicle Ranges) for Arbitrarily Structured Load Profiles
F. Hornstra
J. Power Sources **17(1-3)**, 284–294 (January/April 1986)

Test Programs at the National Battery Test Laboratory
F. Hornstra
J. Power Sources **17(1–3)**, 81–87 (January/April 1986)

Journal of Power Sources
F. Hornstra and R. Knödler, eds.
Special Issue of J. Power Sources, F. Hornstra and R. Knödler, guest eds., 17(1-3), 1-304 (January/April 1986)

The Standard Molar Enthalpy of Formation of $SiF_4(g)$ at 298.15 K by Fluorine Bomb Calorimetry
G. K. Johnson
J. Chem. Thermodyn. 18, 801-802 (1986)

The Costs and Benefits of Utilising Beryllium as an Energy Multiplier
A. C. Klein and D. K. Sze
J. Nucl. Mater. 141-143, 61-64 (1986)

Flibe-Vanadium Alloy System Corrosion Product Radiation Hazards Analysis
A. C. Klein and D. K. Sze
Fusion Technol. 10(3), 747 (November 1986)

Exploring Catalytic Methanol Synthesis Using Soluble Metal Oxide Complexes
R. J. Klingler, I. Bloom, and J. W. Rathke
Am. Chem. Soc. Div. Petr. Chem. Prepr. 31, 61 (1986)

Formates in Methanol Synthesis? The Reversible Production of Methyl Formate from Coordinated Formate
R. J. Klingler and J. W. Rathke
Organometallics 5, 2568 (1986)

High Resolution Monochromator Systems Using Thermal Gradient Induced Variable Bragg Spacing
G. S. Knapp and R. K. Smither
Nucl. Instrum. Methods Phys. Res. A246, 365-367 (1986)

Helium Production in HFIR-Irradiated Pure Elements
D. W. Kneff, L. R. Greenwood, B. M. Oliver, and R. P. Skowronski
J. Nucl. Mater. 141-143, 824-828 (1986)

Helium Production in Copper by a Thermal Three-Stage Reaction
D. W. Kneff, L. R. Greenwood, B. M. Oliver, R. P. Skowronski, and E. L. Callis
Radiat. Eff. 92-96, 553-556 (1986)

Helium Production in Pure Elements, Isotopes, and Alloy Steels by 14.8 MeV Neutrons
D. W. Kneff, B. M. Oliver, H. Farrar, and L. R. Greenwood
Nucl. Sci. Eng. 92, 491-524 (1986)

Ionic Conductivities and Glass Transition Temperatures of Na_2O-ZrO_2-Al_2O_3-SiO_2 Glasses
G. H. Kucera, I. Bloom, and M. F. Roche
J. Electrochem. Soc. 133(10), 1996-2002 (October 1986)

Three-Dimensional Thermal Modeling of Electric Vehicle Batteries
J. Lee, K. W. Choi, N. P. Yao, and C. C. Christianson
J. Electrochem. Soc. 133(7), 1286-1291 (1986)

Factors Influencing Major, Minor, and Trace Element Variations in U.S. Coals
P. C. Lindahl and R. B. Finkelman
Chapter 5 in *Mineral Matter and Ash in Coal*, ed. K. S. Vorres, Am. Chem. Soc. Symp. Ser. **301** (1986)

Thermal Conductivity of Fusion Solid Breeder Materials
Y. Y. Liu and S. W. Tam
Mater. Chem. Phys. **15**, 315 (1986)

Three-Dimensional Analysis of a Radiant Furnace—Application to Nitric Oxide Decomposition
R. W. Lyczkowski, C. S. Wang, L. S. H. Chow, T. R. Johnson, and G. F. Berry
J. Propul. Power **2**(5), 457–464 (September–October 1986)

Surface Raman Scattering and Electrochemistry of Iron Protoporphyrin IX at a Polycrystalline Silver Electrode
J. J. McMahon, S. Baer, and C. A. Melendres
J. Phys. Chem. **90**(8), 1572–1577 (1986)

High-Temperature "In-Situ" Surface Raman Spectroelectrochemistry in Aqueous Solutions
C. A. Melendres, J. J. McMahon, and W. E. Ruther
J. Electroanal. Chem. **208**, 175–178 (1986)

Evidence for the Presence of Sulfate in the Passive Film on Nickel in Concentrated Sulfuric Acid Solution
C. A. Melendres and B. S. Tani
J. Electrochem. Soc. **133**, 1059 (1986)

Effect of Mass Transport on the Determination of Corrosion Rates from Polarization Measurements
Z. Nagy and D. A. Thomas
J. Electrochem. Soc. **133**(10), 2013–2017 (1986)

Palladium/Hydrogen Membrane Electrode for High-Temperature/High-Pressure Aqueous Solutions
Z. Nagy and R. M. Yonco
J. Electrochem. Soc. **133**(11), 2232–2235 (1986)

Physical and Chemical Behavior of Welding Fluxes
C. A. Natalie, D. L. Olson, and M. Blander
Ann. Rev. Mater. Sci. **16**, 389–413 (1986)

The Standard Molar Enthalpy of Formation at 298.15 K of Crystalline Germanium Diselenide ($GeSe_2$). Thermochemical Ge-Se Bond-Dissociation Enthalpies. Revised Values for the Standard Molar Enthalpies of Formation of $GeF_4(g)$ and $SeFe_6(g)$
P. A. G. O'Hare
J. Chem. Thermodyn. **18**, 555–562 (1986)

Thermochemistry of Inorganic Sulfur Compounds. VIII. Na_2SO_3 and K_2SO_3: Standard Molar Enthalpies of Solution and Formation at 298.15 K, High-Temperature Enthalpy Increments and Heat Capacities, and Temperatures and Enthalpies of Transition
P. A. G. O'Hare, K. J. Jensen, and G. K. Johnson
J. Chem. Thermodyn. **18**, 765–786 (1986)

Thermochemistry of Inorganic Sulfur Compounds. VII. Standard Molar Enthalpy of Formation at 298.15 K, High-Temperature Enthalpy Increments, and Other Thermodynamic Properties to 1100 K of Titanium Disulfide, TiS_2

P. A. G. O'Hare and G. K. Johnson

J. Chem. Thermodyn. **18**, 189–199 (1986)

Thermodynamic Analysis of Ordered Liquid Solutions by a Modified Quasichemical Approach—Application to Silicate Slags

A. D. Pelton and M. Blander

Metall. Trans. **17B**(4), 805–815 (December 1986)

Theoretical Thermochemistry 2. Ionisation Energies and Proton Affinities of AH_n Species (A=C to F and Si to Cl); Heats of Formation of their Cations

J. A. Pople and L. A. Curtiss

J. Phys. Chem. **91**, 155–162 (1987)

Thermochemistry of Inorganic Sulfur Compounds. IX. Molar Heat Capacity of $KHSO_5$(cr) from 5 to 300 K, and the Partial Molar Entropy of HSO_5^-(aq)

J. S. Price, I. R. Tasker, E. H. Appelman, and P. A. G. O'Hare

J. Chem. Thermodyn. **18**, 923–930 (1986)

Gas Chromatography/Mass Spectrometry

L. A. Raphaelian

Metals Handbook (Materials Characterisation), Ninth Edition, Volume 10, R. E. Wahn, Coordinator, American Society for Metals, Metals Park, OH, pp. 639–648 (June 1986)

Natural Bond Orbital Analysis of Molecular Interactions: Theoretical Studies of Binary Complexes of HF, H_2O, NH_3, N_2, O_2, F_2, CO, and CO_2, with HF, H_2O, and NH_3

A. E. Reed, F. Weinhold, L. A. Curtiss, and D. J. Pochatko

J. Chem. Phys. **84**(10), 5688–5705 (May 1986)

Tritium Recovery from a Breeder Material: Gamma Lithium Aluminate

E. Roth, F. Botter, M. Briec, M. Rostaing, H. Werle, and R. G. Clemmer

J. Nucl. Mater. **141–143**, 275–281 (1986)

Anomalous Behavior of Liquid K-Pb Alloys: Excess Stability, Entropy, and Heat Capacity

M.-L. Saboungi, S. R. Leonard, and J. Ellefson

J. Chem. Phys. **85**(10), 6072–6081 (November 15, 1986)

Electrostatically Augmented Particulate Removal Devices for High Temperature and High Pressure Applications

S. C. Saxena, R. F. Henry, and W. F. Podolski

Advances in Transport Processes, eds. A. S. Mujomdar and R. A. Mashelkar, Wiley Eastern Limited, New Delhi, India, pp. 465–505 (1986)

A Comparison of GC/IR Interfaces: The Light Pipe Versus Matrix Isolation

J. F. Schneider, J. C. Demirgian, and J. C. Stickler

J. Chromatogr. Sci. **24**, 330–335 (August 1986)

Ocean Floor Sediment as a Repository Barrier: Comparative Diffusion Data for Selected Radionuclides in Sediments from the Atlantic and Pacific Oceans

F. Schreiner, C. S. Sabau, A. M. Friedman, and S. M. Fried

Scientific Basis for Nuclear Waste Management IX, ed. L. O'Werme, Materials Research Society, pp. 771–778 (1986)

Comments on Aircraft Observations of Extreme Ozone Concentrations near Thunderstorms

D. Sisterson and R. Kumar

Atmos. Environ. **20**(7), 1508–1509 (1986)

Statutes of Fusion Reactor Blanket Design

D. L. Smith and D. K. Sze

Fusion Technol. **10**(3), 599 (November 1986)

Element Redistribution during Hydrothermal Alteration of Rhyolite in an Active Geothermal System: Yellowstone Drill Cores Y-7 and Y-8

N. C. Sturchio, K. Muehlenbachs, and M. G. Seitz

Geochim. Cosmochim. Acta **50**(8), 1619–1631 (1986)

Mapping of Serpentinites in the Eastern Desert of Egypt by Using Landsat Thermatic Mapper Data

M. Sultan, R. E. Arvidson, and N. C. Sturchio

Geology **14**(12), 995–999 (1986)

IPFR, Integrated Pool Fusion Reactor Concept

D. K. Sze

Fusion Technol. **10**(3), 875 (November 1986)

Fusion Blanket Inherent Safety Assessment

D. K. Sze, J. Jung, and E. T. Cheng

Fusion Technol. **10**(3), 1197 (November 1986)

Conceptual Design of a Self-Cooled Flibe Blanket

D. K. Sze, J. Jung, E. T. Cheng, S. Piet, and A. Klein

Fusion Technol. **10**(3), 624 (November 1986)

The Thermal Conductivity of Mixed Beryllia/Li Ceramic in Sphere-Pac Forms

S. W. Tam and C. E. Johnson

J. Nucl. Mater. **141–143**, 348–352 (1986)

Investigations of the Empire Creek Stock, Montana, as an Analogue to a Nuclear Waste Repository

H. Y. Tammemagi, B. Haverslew, and N. C. Sturchio

Chem. Geol. **55**, 375–385 (1986)

Neutron Diffraction Study of Electrochemically Synthesized Djerfisherite

B. S. Tani, F. C. Mrazek, J. Faber, and R. Hitterman

J. Electrochem. Soc. **133**(12), 2644–2649 (1986)

Required Momentum, Heat and Mass Transfer Experiments for Liquid Metal Blankets

M. S. Tillack, D. K. Sze, and M. A. Abdou

Fusion Technol. **10**(3), 1088 (November 1986)

Emf Measurements on Select Transitions of the Li-Al/FeS_2 System
Z. Tomcsuk and D. R. Vissers
J. Electrochem. Soc. 133, 2505-2508 (1986)

The Solubility of Carbon in Low-Nitrogen Liquid Lithium
R. M. Yonco and M. I. Homa
J. Nucl. Mater. 138, 117-122 (1986)

B. Patents

Can-Out Hatch Assembly and Positioning System
P. J. Basner, R. C. Frank, and J. C. Hoh
Statutory Invention Registration No. H11, issued January 7, 1986

Can-Out Hatch Assembly with Magnetic Retention Means
R. C. Frank and J. C. Hoh
Statutory Invention Registration No. H10, issued January 7, 1986

Flue Gas Desulfurization/Denitrification Using Metal-Chelate Additives
J. B. L. Harkness, R. D. Doctor, and R. J. Wingender
Patent No. 4,612,175, issued September 16, 1986

Accordian-Folded Boot Shield for Flexible Swivel Connection
J. C. Hoh
Patent No. 4,607,852, issued August 26, 1986

Fuel Cell Electrode and Method of Preparation
T. D. Kaun
Statutory Invention Registration No. H16, issued January 7, 1986

Electronically Conductive Ceramics for High Temperature Oxidizing Environments
G. H. Kucera, J. L. Smith, and J. W. Sim
Patent No. 4,564,567, issued January 14, 1986

Electrolysis Cell for Reprocessing Plutonium Reactor Fuel
W. E. Miller, M. J. Steindler, and L. Burris
Patent No. 4,596,647, issued June 24, 1986

C. Reports

The Effect of Gamma Radiation on Groundwater Chemistry and Glass Leaching as Related to the NNWSI Repository Site

T. A. Abrajano, J. K. Bates, W. L. Ebert, and T. J. Gerding

UCRL-15825 (1986)

The Reaction of Glass During Gamma Irradiation in a Saturated Tuff Environment. Part 1: SRL 165 Glass

J. K. Bates, D. F. Fischer, and T. J. Gerding

ANL-85-62 (March 1986)

One-Year Results of the NNWSI Unsaturated Test Procedure: SRL 165 Glass Application

J. K. Bates and T. J. Gerding

ANL-85-41 (August 1986)

NNWSI Waste Form Testing at Argonne National Laboratory, Semiannual Report, July-December 1985

J. K. Bates, T. J. Gerding, T. A. Abrajano, Jr., and W. L. Ebert

UCRL-15801 (March 1986)

Continued Swelling of Spinel after Neutron Irradiation

W. A. Coghlan, F. W. Clinard, N. Itoh, and L. R. Greenwood

Eighth Annual Progress Report on Special Purpose Materials, DOE/ER-0113/5, pp. 17-19 (March 1986)

Effects of Operating Temperature on the Characteristics of Nickel/Iron Traction Batteries

W. H. DeLuca, R. L. Biwer, and A. F. Tummillo

ANL-86-6 (July 1986)

Effect of Depth of Discharge on Lead-Acid Battery Overcharge Requirements

W. H. DeLuca and A. F. Tummillo

ANL-85-68 (March 1986)

Analysis of External Combustion of Municipal Solid Waste

C. B. Dennis, G. F. Berry, G. N. Reddy, and J. E. Helt

ANL/CNSV-53 (March 1986)

Analytical Chemistry Laboratory Progress Report for FY 1986

D. W. Green, R. R. Heinrich, K. J. Jensen, et al.

ANL/ACL-86-2 (November 1986)

Dosimetry and Damage Analysis for the Hafnium Full-Power Test, JP1 and JP3 Experiments in HFIR

L. R. Greenwood

Damage Analysis and Fundamental Studies Quarterly Progress Report, DOE/ER-0046/24, pp. 5-9 (February 1986)

Neutron Dosimetry and Damage Calculations

L. R. Greenwood

Alloy Development for Irradiation Performance Semiannual Progress Report, DOE/ER-0045/16, pp. 17-24 (March 1986)

Pyrolysis of Municipal Solid Waste—Annual Report, July 1984–June 1985
J. E. Helt, R. K. Agrawal, and K. M. Myles
ANL/CNSV-54 (July 1986)

Alkali Metal Vapor Removal from Pressurized Fluidized-Bed Combustor Flue Gas, Annual Report, October 1984–September 1985
S. H. D. Lee, R. F. Henry, S. D. Smith, W. I. Wilson, and K. M. Myles
ANL/FE-86-7 (November 1986)

Proceedings of the International Workshop on High-Temperature Molten Salt Batteries, April 16–18, 1986
F. McLarnon, R. Weaver, and D. R. Vissers, eds.
ANL-86-40 (December 1986)

Cost Analysis of Particulate Emission Control Technology for Heavy-Duty Diesel Vehicles
J. B. Rajan and M. K. Singh
ANL-EES-TM-310 (May 1986)

Chemical Technology Division Annual Technical Report, 1985
M. J. Steindler, P. A. Nelson, J. P. Ackerman, C. E. Johnson, et al.
ANL-86-14 (May 1986)

Construction of an Automated, Sequential Air Sampler for Remote Monitoring of Organic Atmospheric Pollutants
R. J. Wingender, R. M. Williams, R. V. White, and R. S. Ely
ANL/ACL-86-1 (July 1986)

Characterization and Optimization of Polyethylene Resins and Gas Pipe, Annual Report, January–December 1985
J. E. Young, D. G. Ettinger, L. A. Raphaelian, and D. T. Raske
Gas Research Institute Report (June 1986)

D. Abstracts and Proceedings Papers

Redox Equilibria during Peridotite Hydration and the Abiogenic Production of Hydrogen and Methane
T. A. Abrajano
EOS (Trans. Am. Geophys. Union) 67(44), Abs. Suppl. (1986)

Electrodeposition of Cadmium from a Low-Melting Molten Salt
R. R. Agarwal, R. Varma, and J. R. Selman
Extended Abstracts, 170th Electrochem. Soc. Meeting, San Diego, CA, October 19–24, 1986, Vol. 86-2, p. 693 (1986)

Production of Oxygenated Fuels from Municipal Solid Waste Components
R. K. Agrawal and J. E. Helt
Proc. of the Energy from Biomass and Wastes X Conf., Washington, DC, April 7–10, 1986 (1986)

Failure Analysis of Lithium-Alloy/Iron Sulfide Cells
J. E. Battles
Proc. of the Int. Workshop on High-Temperature Molten Salt Batteries, Argonne, IL, April 16–18, 1986, ANL-86-40, pp. B-59 to B-66 (1986)

Materials Corrosion in Sulfur and Sodium Polysulfides
J. E. Battles and A. P. Brown
Proc. of the Beta Battery Workshop VI, Snowbird, UT, May 19–23, 1985, Ceramatec SPEC-8601, pp. 7-1 to 7-7 (September 1986)

The Structure of Equimolar LiCl-$AlCl_3$ Melt by Neutron Scattering
S. Biggin, S. Cummings, J. E. Enderby, and M. Blander
Proc. of the Fifth Int. Symp. on Molten Salts, Las Vegas, NV, October 13–18, 1985, Vol. 86-1, The Electrochemical Society, Inc., Pennington, NJ, pp. 81–96 (1986)

Electrochemical Effects on Weld Pool Chemistry in Submerged Arc and D.C. Electroslag Welding
M. Blander and D. Olson
Proc. of the Int. Conf. on Trends in Welding Research, Gatlinburg, TN, May 18–22, 1986, 363–366 (1986)

High-Conductivity Glass Electrolytes for Sodium/Sulfur Cells
I. Bloom, J. Bradley, G. H. Kucera, and M. F. Roche
Proc. of the Beta Battery Workshop VI, Snowbird, UT, May 19–23, 1985, Ceramatec SPEC 8601, pp. 9–28 to 9–35 (September 1986)

Low-Resistivity Glass Electrolytes for Sodium-Sulfur Cells
I. Bloom, J. A. Smaga, P. A. Nelson, and M. F. Roche
Extended Abstracts, 170th Electrochem. Soc. Meeting, San Diego, CA, October 19–24, 1986, Vol. 86-2, p. 110 (1986)

The Corrosion of Metals and Alloys with Sodium Polysulfide Melts at 350°C
A. P. Brown and J. E. Battles
Extended Abstracts, 170th Electrochem. Soc. Meeting, San Diego, CA, October 19–24, 1986, Vol. 86-2, pp. 123–124 (1986)

Monolithic Fuel Cell Based Power Source for Sprint Power Generation

D. C. Fee, S. Bhattacharyya, D. E. Busch, L. Carlson, T. D. Claar, D. W. Dees, J. T. Dusek, T. E. Easler, W. A. Ellingson, B. K. Flandermeyer, R. J. Fousek, H. Geyer, J. J. Heiberger, K. Kuczen, S. Majumdar, C. C. McPheeters, F. C. Mrazek, J. J. Picciolo, and R. B. Poeppel

Program and Abstracts, Third Symp. on Space Nuclear Power Systems, Albuquerque, NM, January 13–16, 1986 (1986)

Monolithic Fuel Cell Development

D. C. Fee, P. E. Blackburn, D. E. Busch, T. D. Claar, D. W. Dees, J. T. Dusek, T. E. Easler, W. A. Ellingson, B. K. Flandermeyer, R. J. Fousek, J. J. Heiberger, T. E. Kraft, S. Majumdar, C. C. McPheeters, F. C. Mrazek, J. J. Picciolo, R. B. Poeppel, and S. A. Zwick

Program and Abstracts, 1986 Fuel Cell Seminar, National Fuel Cell Coordinating Group, Tucson, AZ, October 26–29, 1986, pp. 40–43 (1986)

Monolithic Fuel Cells

D. C. Fee, D. W. Dees, P. E. Blackburn, J. J. Heiberger, C. C. McPheeters, F. C. Mrazek, D. E. Busch, T. D. Claar, J. T. Dusek, T. E. Easler, W. A. Ellingson, B. K. Flandermeyer, R. J. Fousek, S. Majumdar, J. J. Picciolo, and R. B. Poeppel

Abstracts, 21st Intersoc. Energy Conversion Eng. Conf., Am. Chem. Soc., San Diego, CA, August 25–29, 1986, Vol. 3, pp. 1634–1637 (1986)

Interconnection Development for Monolithic Solid Oxide Fuel Cells

B. K. Flandermeyer, J. T. Dusek, P. E. Blackburn, D. W. Dees, C. C. McPheeters, and R. B. Poeppel

Program and Abstracts, 1986 Fuel Cell Seminar, National Fuel Cell Coordinating Group, Tucson, AZ, October 26–29, 1986, pp. 68–71 (1986)

DOE Molten Carbonate Fuel Cell Program Technology Issues and Plans

F. D. Gmeindl and V. M. Kolba

Proc. of the 21st Intersoc. Energy Conversion Eng. Conf., San Diego, CA, August 25–29, 1986, Vol. 2, pp. 1128–1132 (1986)

Hot Gas Alkali Determination

W. J. Haas, Jr., D. E. Eckels, S. H. D. Lee, and K. M. Myles

Proc. of the Sixth Annual Contractors' Meeting on Contaminant Control in Coal-Derived Gas Streams, Morgantown Energy Technology Center, Morgantown, WV, June 4–5, 1986, DOE/METC-86/6042, pp. 343–353 (July 1986)

Recent Developments and Observations Pertinent to Real-Time Monitoring of Alkali Concentrations in Hot Gas Streams from Fluidized-Bed Combustion of Coal

W. J. Haas, Jr., D. E. Eckels, S. H. D. Lee, and R. F. Henry

Proc. of the Fifth Annual Contractors' Meeting on Containment Control in Coal-Derived Gas Streams, Morgantown, WV, May 7–9, 1985, DOE/METC-85/6025, pp. 493–512 (January 1986)

Chromium Composite Coatings

G. A. Hope and R. Varma

Extended Abstracts, 170th Electrochem. Soc. Meeting, San Diego, CA, October 19–24, 1986, Vol. 86-2, p. 754 (1986)

The Thermodynamic Properties of the Zeolite Stilbite

D. A. Howell, G. K. Johnson, I. R. Tasker, and W. S. Wise

Abstracts, 41st Calorimetry Conf., Clinton, NJ, August 17–22, 1986, p. 123 (1986)

Inelastic Neutron Scattering Study of Tetraalkylammonium Ions in Salts and Pores of Molecular Sieve Materials

L. E. Iton, T. O. Brun, and L. A. Curtiss

Abstracts, Am. Phys. Soc. Meeting, Las Vegas, NV, March 31-April 4, 1986, in Bull. Am. Phys. Soc. 31(3), 508 (March 1986)

The Enthalpies of Formation of Low Albite and Gibbsite

G. K. Johnson

Abstracts, 41st Calorimetry Conf., Clinton, NJ, August 17-22, 1986, p. 125 (1986)

Thermodynamic Studies of Zeolites: Mordenite and Dehydrated Mordenite

G. K. Johnson, I. R. Tasker, H. E. Flotow, and W. S. Wise

Abstracts, Zeolite Symp., 23rd Annual Clay Mineral Soc. Meeting, Jackson, MS, October 12-15, 1986, p. 18 (1986)

Development of the Lithium-Limited FeS Cell

T. D. Kaun

Proc. of the Int. Workshop on High-Temperature Molten Salt Batteries, Argonne, IL, April 16-18, 1986, ANL-86-40, pp. B-101 to B-114 (1986)

A Stable Iron Disulfide Secondary Cell with LiCl-LiBr-KBr Electrolyte

T. D. Kaun

Proc. of the Int. Workshop on High-Temperature Molten Salt Batteries, Argonne, IL, April 16-18, 1986, ANL-86-40, pp. B-138 to B-144 (1986)

A Stable, High-Performance Lithium/Iron Disulfide Cell with LiCl-LiBr-KBr Molten Electrolyte

T. D. Kaun

Proc. of the 21st Intersoc. Energy Conversion Eng. Conf., Am. Chem. Soc., San Diego, CA, August 25-29, 1986, pp. 1048-1051 (1986)

Assessment of Molten Carbonate and Phosphoric Acid Fuel Cells for Utility Central Station Applications

M. Krumpelt, V. Minkov, E. J. Daniels, and C. B. Dennis

Program and Abstracts, 1986 Fuel Cell Seminar, National Fuel Cell Coordinating Group, Tucson, AZ, October 26-29, 1986, pp. 308-312 (1986)

The Effect of Manganese Doping on the Resistivity of $LiFeO_2$ for Carbonate Fuel Cell Cathodes

G. H. Kucera, J. L. Smith, N. Q. Minh, and J. R. Stapay

Extended Abstracts, 170th Electrochem. Soc. Meeting, San Diego, CA, October 19-24, 1986, Vol. 86-2, pp. 131-132 (October 1986)

Battery Thermal Modeling—Its Methodology and Applications

J. Lee

Extended Abstracts, 170th Electrochem. Soc. Meeting, San Diego, CA, October 19-24, 1986, Vol. 86-2, pp. 182-183 (1986)

Capacity and Peak Power Degradation of Lead-Acid Battery under Simulated Electric Vehicle Operations

J. Lee, A. F. Tummillo, J. F. Miller, F. Hornstra, and C. C. Christianson

Proc. of the Eighth Int. Electric Vehicle Symp., Washington, DC, October 20-23, 1986, pp. 151-156 (November 1986)

Measurement of Alkali Vapors in PFBC Flue Gas and Their Control by a Granular-Bed Sorber

S. H. D. Lee, R. F. Henry, W. I. Wilson, K. M. Myles, W. J. Haas, Jr., and D. E. Eckels

Proc. of the Fifth Annual Contractors' Meeting on Contaminant Control in Coal-Derived Gas Streams, Morgantown, WV, May 7–9, 1985, DOE/METC-85/6025, pp. 513–528 (January 1986)

An Abstract Report on Alkali Vapor Removal Activities

S. H. D. Lee and K. M. Myles

Proc. of the 1986 Int. Gas Turbine Conf., ASME, Atlanta, GA, p. 17 (1986)

Measurement of Alkali Vapor in PFBC Flue Gas and Its Control by a Fixed Granular Bed of Activated Bauxite

S. H. D. Lee and K. M. Myles

Proc. of the Institution of Chemical Engineers Symp. (IChemE) Series No. 99 on Gas Cleaning at High Temperatures, University of Surrey, Guildford, England, September 16–18, 1986, pp. 149–166 (1986)

Measurement of Alkali Vapors in PFBC Flue Gas and Their Removal with a Fixed Granular-Bed Sorber

S. H. D. Lee, K. M. Myles, W. J. Haas, Jr., and D. E. Eckels

Proc. of the Sixth Annual Contractors' Meeting on Contaminant Control in Coal-Derived Gas Streams, Morgantown, WV, June 4–5, 1986, DOE/METC-86/6042, pp. 58–77 (July 1986)

Correlation of Potential Dependent SERS with Electrochemistry of Special Adsorbate Sites for Iron Protoporphyrin IX at a Silver Electrode

J. J. McMahon, S. Baer, and C. A. Melendres

Extended Abstracts, 169th Meeting of the Electrochem. Soc., Boston, MA, May 4–9, 1986, Vol. 86-1, pp. 792–793 (1986)

Tape Casting High-Density Electrolyte for Solid Oxide Fuel Cells

C. C. McPheeters and T. D. Claar

Program and Abstracts, 1986 Fuel Cell Seminar, National Fuel Cell Coordinating Group, Tucson, AZ, October 26–29, 1986, pp. 64–67 (1986)

Fabrication of a Solid Oxide Fuel Cell Monolithic Structure

C. C. McPheeters, D. C. Fee, R. B. Poeppel, T. D. Claar, D. E. Busch, B. K. Flandermeyer, T. E. Easler, J. T. Dusek, and J. J. Picciolo

Program and Abstracts, 1986 Fuel Cell Seminar, National Fuel Cell Coordinating Group, Tucson, AZ, October 26–29, 1986, pp. 44–47 (1986)

AC Impedance and Raman Spectroscopy Studies on the Corrosion/Passivation Behavior of Nickel in Dilute Sulfate Solutions

C. A. Melendres and S. Baer

Extended Abstracts, 169th Meeting of the Electrochem. Soc., Boston, MA, May 4–9, 1986, Vol. 86-1, pp. 6–7 (1986)

High-Temperature "In-Situ" Raman Spectroscopy of Surface Films in Aqueous Environments

C. A. Melendres, J. J. McMahon, and W. Ruther

Proc. of the Tenth Int. Conf. on Raman Spectroscopy, Eugene, OR, August 31–September 6, 1986 (1986)

Batteries for Hybrid Vehicles or Other High-Power Applications

J. F. Miller, J. Lee, and C. C. Christianson

Proc. of the Eighth Int. Electric Vehicle Symp., Washington, DC, October 20–23, 1986, pp. 172–178 (November 1986)

The Influence of Preparation Conditions on Electronic Resistivity of $LiFeO_2$ Synthesised in Molten Carbonates

N. Q. Minh, G. H. Kucera, and J. L. Smith

Proc. of the Fifth Int. Symp. on Molten Salts, Las Vegas, NV, October 13–18, 1985, Vol. 86-1, The Electrochemical Society, Inc., pp. 597–603 (1986)

Design and Economics of Large Fuel Cell Power Plants

V. Minkov, E. J. Daniels, C. B. Dennis, and M. Krumpelt

Program and Abstracts, 1986 Fuel Cell Seminar, National Fuel Cell Coordinating Group, Tucson, AZ, October 26–29, 1986, pp. 255–262 (1986)

Applicability of the Potential Step Relaxation Technique in the Non-Linear Current Density-Overpotential Range

Z. Nagy

Extended Abstracts, 170th Electrochem. Soc. Meeting, San Diego, CA, October 19–24, 1986, Vol. 86-2, pp. 1075–1076 (1986)

Electrode Kinetic Measurements of Very Fast Reactions: Metal Deposition-Dissolution in Molten Halides

Z. Nagy and J. L. Settle

Proc. of the Int. Workshop on High-Temperature Molten Salt Batteries, Argonne, IL, April 16–18, 1986, ANL-86-40, pp. C-2 to C-11 (1986)

Palladium/Hydrogen Membrane Electrode for High-Temperature/High-Pressure Aqueous Solutions

Z. Nagy and R. M. Yonco

Extended Abstracts, 169th Electrochem. Soc. Meeting, Boston, MA, May 4–9, 1986, Vol. 86-1, pp. 20–21 (1986)

Inorganic Chalcogenides: High-Tech Materials, Low-Tech Thermodynamics (Huffman Memorial Lecture)

P. A. G. O'Hare

Abstracts, 41st Calorimetry Conf., Clinton, NJ, August 17–22, 1986, p. 51 (1986)

Thermochemistry of Crystalline Sodium and Potassium Sulfites and Aqueous Sulfite Ion

P. A. G. O'Hare and G. K. Johnson

Abstracts, Ninth IUPAC Conf. on Chemical Thermodynamics, Lisbon, Portugal, July 14–18, 1986, Paper 9.1 (1986)

Worldwide Ni/Fe Battery Development for Electric Vehicle Applications

P. G. Patil, W. J. Walsh, and J. F. Miller

Proc. of the Eighth Int. Electric Vehicle Symp., Washington, DC, October 20–23, 1986, pp. 48–52 (1986)

Investigation of Alternative MCFC Cathode Materials at Argonne National Laboratory

R. D. Pierce and J. L. Smith

Extended Abstracts, Int. Symp. on Fuel Cell and Advanced Battery, Institute of Applied Energy, Tokyo, Japan, January 21–22, 1986, pp. 99–103 (1986)

Cyclic Voltammetric Study of the Reduction of U(III) to Uranium Metal in Molten LiCl-NaCl-$CaCl_2$-$BaCl_2$

D. S. Poa, Z. Tomczuk, and R. K. Steunenberg

Extended Abstracts, 170th Electrochem. Soc. Meeting, San Diego, CA, October 19–24, 1986, Vol. 86-2, pp. 985–986 (1986)

Modeling of Sulfide Capacities of Silicate Melts

R. G. Reddy and M. Blander

Abstracts, Ann. Meeting of the Metallurgical Society—American Institute of Mechanical Engineers, New Orleans, LA, March 2–6, 1986, in J. Met. 38(1), 96 (January 1986)

Power Performance of LiAlSi/(FeNi)S_2 Cells

L. Redey

Proc. of the Int. Workshop on High-Temperature Molten Salt Batteries, Argonne, IL, April 16–18, 1986, ANL-86-40, pp. B-131 to B-137 (1986)

Reference-Electrode Systems and Their Application in Li/MS_x Battery Research

L. Redey

Proc. of the Int. Workshop on High-Temperature Molten Salt Batteries, Argonne, IL, April 16–18, 1986, ANL-86-40, pp. B-92 to B-100 (1986)

Apparatus for High Temperature *In Situ* Laser Raman Spectroelectrochemical Studies of Metal Corrosion and Passivation in Aqueous Environments

W. E. Ruther, J. J. McMahon, and C. A. Melendres

Extended Abstracts, 170th Electrochem. Soc. Meeting, San Diego, CA, October 19–24, 1986, Vol. 86-2, pp. 297–298 (1986)

Prediction of Thermodynamic Properties of Molten Salt Solutions

M.-L. Saboungi and M. Blander

Proc. of the Int. Workshop on High-Temperature Molten Salt Batteries, Argonne, IL, April 16–18, 1986, ANL-86-40, p. A-2 (1986)

Investigation of Liquid Alloys and Intermetallics Using Beta Alumina as Solid Electrolytes

M.-L. Saboungi, J. Ellefson, S. Leonard, and W. Freyland

Extended Abstracts, 170th Electrochem. Soc. Meeting, San Diego, CA, October 19–24, 1986, Vol. 86-2, pp. 1119–1120 (1986)

Proceedings of the Fifth International Symposium on Molten Salts

M.-L. Saboungi, D. S. Neuman, K. Johnson, and D. Inman, eds.

From 168th Electrochem. Soc. Meeting, Las Vegas, NV, October 13–18, 1985, Vol. 86-1, The Electrochemical Society, Inc., Pennington, NJ (1986)

A Molecular Dynamics Study of the Composition Dependence of Ordering in Molten Salt Complexing Solutions

M.-L. Saboungi, A. Rahman, and M. Blander

Proc. of the Fifth Int. Symp. on Molten Salts, ed. M.-L. Saboungi et al., 168th Electrochem. Soc. Meeting, Las Vegas, NV, October 13–18, 1985, Vol. 86-1, The Electrochemical Society, Inc., Pennington, NJ, pp. 97–108 (1986)

Matrix Isolation Versus the Light Pipe as an Interface for Gas Chromatography/Fourier Transform Infrared Spectrometry

J. F. Schneider, J. C. Demirgian, and J. C. Stickler

Proc. of the 28th Conf. on Analytical Chemistry in Energy Technology, Oak Ridge National Laboratory/Department of Energy, Oak Ridge, TN, September 30–October 3, 1985, p. 159 (1986)

Key Fuel Cell Technology Issues in the United States

J. E. Sholes and R. D. Pierce

Extended Abstracts, Int. Symp. on Fuel Cell and Advanced Battery, Institute of Applied Energy, Tokyo, Japan, January 21-22, 1986, pp. 62-65 (1986)

Materials Selection for Molten Salt Battery Components

J. A. Smaga

Proc. of the Int. Workshop on High-Temperature Molten Salt Batteries, Argonne, IL, April 16-18, 1986, ANL-86-40, pp. B-72 to B-87 (1986)

Morphological Changes in the Sulfur Electrode of Lifecycle-Tested Na/S Cells

J. A. Smaga and J. E. Battles

Extended Abstracts, 170th Electrochem. Soc. Meeting, San Diego, CA, October 19–24, 1986, Vol. 86-2, pp. 125–126 (1986)

Post-Test Examinations of FACC Sodium/Sulfur Cells

J. A. Smaga and J. E. Battles

Proc. of the Beta Battery Workshop VI, Snowbird, UT, May 19–23, 1985, Ceramatec SPEC-8601, pp. 7-21 to 7-26 (September 1986)

Progress on Molten Carbonate Fuel Cell Alternative Cathodes

J. L. Smith, G. H. Kucera, and N. Q. Minh

Program and Abstracts, 1986 Fuel Cell Seminar, National Fuel Cell Coordinating Group, Tucson, AZ, October 26–29, 1986, pp. 163–167 (1986)

Electronic Defects in $LiFeO_2$

J. L. Smith, G. H. Kucera, N. Q. Minh, and J. R. Moreschi

Program and Abstracts, 1986 National Fuel Cell Seminar, National Fuel Cell Coordinating Group, Tucson, AZ, October 26–29, 1986, pp. 234–239 (1986)

Cyclic Amine Complexes as O_2 Reduction Catalysts: Electrochemical and Laser Raman Spectroscopy Studies

J. Stinson and C. A. Melendres

Extended Abstracts, 170th Electrochem. Soc. Meeting, San Diego, CA, October 19–24, 1986, Vol. 86-2, pp. 213–214 (1986)

The Hydrothermal System of the Nevado Del Ruis Volcano

N. C. Sturchio, K. Muehlenbachs, and S. N. Williams

Eos (Trans. Am. Geophys. Union) **67**(16), 404 (1986)

Digital Mapping of Ophiolite Melange Zones from Landsat Thematic Mapper (TM) Data in Arid Areas: Meatiq Dome, Egypt

M. Sultan, R. E. Arvidson, and N. C. Sturchio

Program and Abstracts, Geological Society of America, Vol. 18, No. 6, p. 766 (1986)

The Thermal Conductivity of Materials with Multiple Characteristics Length Scales
S. W. Tam and C. E. Johnson
Proc. of the Symp. on Fractal Aspects of Materials, Materials Research Society, ed. D. Schriffer, S. Liu, and B. Mandelbrot (1986)

Molar Heat Capacity of $KHSO_5$(cr) from 5 to 300 K, and the Partial Molar Entropy of HSO_5^-(aq)
I. R. Tasker, J. S. Price, E. H. Appelman, and P. A. G. O'Hare
Abstracts, 41st Calorimetry Conf., Clinton, NJ, August 17–22, 1986, p. 151 (1986)

Testing and Evaluation of an Industrial Lead-Acid Battery for Utility Load-Leveling
R. Varma, E. S. Folke, D. S. Corp, and T. G. Tillary
Extended Abstracts, 169th Electrochem. Soc. Meeting, Boston, MA, May 4–9, 1986, Vol. 86-1, pp. 595–596 (1986)

Microstructure Control in Chromium Electrodeposition from KCl-LiCl Eutectic
R. Varma and T. Vargas
Extended Abstracts, 169th Electrochem. Soc. Meeting, Boston, MA, May 4–9, 1986, Vol. 86-1, pp. 584–585 (1986)

Electrocrystallization of Cadmium from Cadmium Fluoborate Solutions
R. Varma, T. Vargas, T. Hoeller, and V. S. Agarwala
Extended Abstracts, 169th Electrochem. Soc. Meeting, Boston, MA, May 4–9, 1986, Vol. 86-1, pp. 794–795 (1986)

Techniques for Electrodeposition of Metals from Molten Salt Systems
R. Varma, T. Vargas, H. Shimotake, K. Koyama, and G. Hope
Proc. of the Int. Workshop on High-Temperature Molten Salt Batteries, Argonne, IL, April 16–18, 1986, ANL-86-40, p. C-33 (1986)

Review of Cell Development for Molten-Salt Battery
D. R. Vissers
Proc. of the Int. Workshop on High-Temperature Molten Salt Batteries, Argonne, IL, April 16–18, 1986, ANL-86-40, pp. B-2 to B-17 (1986)

Neutron Flux Density Distribution in the Central Irradiation Thimble of the TRIGA Mark II Reactor in Vienna
H. W. Weber, H. Bock, E. Unfried, and L. R. Greenwood
Proc. of the TRIGA Users Conf., College Station, TX (April 1986)

Development and Test Evaluation of Advanced Lead-Acid Batteries for Load-Leveling Applications
N. P. Yao and J. F. Miller
Extended Abstracts, Int. Symp. on Fuel Cell and Advanced Battery, Institute of Applied Energy, Tokyo, Japan, January 21–23, 1986, pp. 186–190 (1986)

E. Papers Presented at Scientific Meetings

Blanket Material and Engineering Issues, and Requirements for Experiments and Facilities
M. A. Abdou, P. Gierszewski, M. A. Tillack, A. R. Raffray, D. K. Sze, and R. Puigh
Presented at the Int. Conf. on Fusion Reactor Materials, Chicago, IL, April 13-17, 1986

Metallogenesis of the Zambales Ophiolite
T. A. Abrajano
Presented at the Int. Ophiolite Conf., Manila, Phillipines, February 14-21, 1986

Unresolved Issues on the Origin of Phillipine Ophiolites
T. A. Abrajano
Presented at the Int. Ophiolite Conf., Manila, Phillipines, February 14-21, 1986

Transport and Reaction Kinetics at the Gel:Glass Solution Interface Region: Results of Repository-Oriented Leaching Experiments
T. A. Abrajano and J. K. Bates
Presented at the Fall Meeting of the Materials Research Soc., Boston, MA, December 1-6, 1986

The Effect of Gamma Radiation on Groundwater Chemistry and Glass Leaching as Related to the NNWSI Repository Site
T. A. Abrajano, J. K. Bates, W. L. Ebert, and T. J. Gerding
Presented at the Third Annual Nuclear Waste Symp., Am. Ceram. Soc., Chicago, IL, April 27-May 1, 1986

Advanced Electrochemical Power Systems
J. P. Ackerman
Presented at General Motors Research Laboratories, Warren, MI, June 16, 1986

Applications of Thermogravimetry in Energy from Solid Waste Research
R. K. Agrawal and J. E. Helt
Presented at the Applications of Thermal Analysis in Energy Research Symp., 15th Annual NATAS Conf., Cincinnati, OH, September 1986

Hydrogen Speciation in Hydrated Layers on Nuclear Waste Glass
R. D. Aines, H. C. Weed, and J. K. Bates
Presented at the Fall Meeting of the Materials Research Soc., Boston, MA, December 1-6, 1986

Electrochemical Research at Argonne National Laboratory
J. E. Battles
Presented at Monthly Regional Meeting of the local Electrochem. Soc. Chapter, Willowbrook, IL, March 6, 1986

Meteorites as Nonequilibrium Nebular Condensates
M. Blander
Presented at the Ninth IUPAC Conf. on Chemical Thermodynamics, Lisbon, Portugal, July 14-18, 1986

Thermodynamic Properties of Molten Salt Solutions

M. Blander

Presented at the Advanced Study Institute on Molten Salt Chemistry, NATO and the Univ. of Camerino, Camerino, Italy, August 3–15, 1986

High-Conductivity Glass Electrolytes for Sodium-Sulfur Batteries

I. Bloom, P. A. Nelson, and M. F. Roche

Presented at the 32nd Int. Power Sources Conf., Cherry Hill, NJ, June 9–12, 1986

Liquid and Supercritical Fluid Chromatographic Mobile Phases as Potential Matrices in Matrix-Isolation Infrared Spectrometry

A. S. Boparai

Presented at the Sixth ACL Technical Meeting, Argonne National Laboratory, Argonne, IL, April 10, 1986

Liquid and Supercritical Fluid Chromatographic Mobile Phases as Potential Matrices in Matrix-Isolation Infrared Spectrometry

A. S. Boparai, D. G. Ettinger, and J. F. Schneider

Presented at the 37th Pittsburgh Conf. and Exposition on Analytical Chemistry and Applied Spectroscopy, Atlantic City, NJ, March 10–14, 1986

Analytical Support of Pyrometallurgical Processes at ANL

D. L. Bowers, E. G. Rauh, F. L. Williams, and E. A. Huff

Presented at the Sixth Annual Pyrochemical Workshop, Los Alamos National Laboratory, Los Alamos, NM, October 7–8, 1986

Inelastic Neutron Scattering Study of Tetraalkylammonium Ions in Salts and in Pores of Molecular Sieve Materials

T. O. Brun, L. A. Curtiss, L. E. Iton, and D. Le Poire

Presented at the Seventh Int. Conf. on Zeolites, Tokyo, Japan, August 17–22, 1986

The Application of Electrorefining for Recovery and Purification of Fuel Discharged from the Integral Fast Reactor

L. Burris, R. K. Steunenberg, and W. E. Miller

Presented at the Annual AIChE Meeting, Miami, FL, November 2–7, 1986

Experimental Alteration of Basalt Glass Applied to the Alteration of Nuclear Waste Glass

C. D. Byers, R. C. Ewing, and M. J. Jercinovic

Presented at the Third Int. Symp. on Nuclear Waste Management, Am. Ceram. Soc., Chicago, IL, April 27–May 1, 1986

Recent ANL Data on MHD Fouling

L. S. H. Chow, C. S. Wang, and W. M. Swift

Presented at the 24th Symp. on the Engineering Aspects of MHD, USDOE, Butte, MT, June 24–27, 1986

The LISA-1 and TRIO In-Pile Tests

R. G. Clemmer, H. Werle, and M. Briec

Presented at the Int. Symp. on Fusion Reactor Blanket and Fuel Cycle Technology, University of Tokyo, Japan, October 27–29, 1986

The LISA1 Experiment: In-Situ Tritium Release Investigations

R. G. Clemmer, H. Werle, and M. Briec

Presented at the Int. Conf. on Fusion Reactor Materials, Chicago, IL, April 13–17, 1986

Swelling of Spinel after Low-Dose Neutron Irradiation

W. A. Coghlan, F. W. Clinard, Jr., N. Itoh, and L. R. Greenwood

Presented at the Int. Conf. on Fusion Reactor Materials, Chicago, IL, April 13–17, 1986

Ab Initio Molecular Orbital Calculations of Reaction Energies in Molten Salts

L. Curtiss

Presented at the Euchem Conf. on Molten Salts 1986, Geiranger, Norway, August 24–29, 1986

Computerised Rapid Analysis for Specialised Applications—A Simplified Method to Produce Customised Gas Chromatographic Software

J. C. Demirgian

Presented at the 37th Pittsburgh Conf. and Exposition on Analytical Chemistry and Applied Spectroscopy, Atlantic City, NJ, March 10–14, 1986

Data Transmission Between Analytical Instrumentation, Lab Computer, and Mainframe—A Method to Improve the Efficiency of Data Management

J. C. Demirgian

Presented at the 29th Conf. on Analytical Chemistry in Energy Technology, Oak Ridge National Laboratory/Department of Energy, Knoxville, TN, September 30–October 2, 1986

Applications of GC/FTIR to Environmental and Degradation Studies

J. C. Demirgian, V. Stamoudis, J. Stetter, K. Brubaker, and R. Cole

Presented at the 37th Pittsburgh Conf. and Exposition on Analytical Chemistry and Applied Spectroscopy, Atlantic City, NJ, March 10–14, 1986

Glass–Water Vapor Interaction

F. E. Diebold and J. K. Bates

Presented at the Third Int. Symp. on Nuclear Waste Management, Am. Ceram. Soc., Chicago, IL, April 27-May 1, 1986

Laser Photoacoustic Spectroscopy for Trace Level Detection of Actinides in Groundwater

M. M. Doxtader, V. A. Maroni, J. V. Beitz, and M. Heaven

Presented at the Fall Meeting of the Materials Research Soc., Boston, MA, December 1–6, 1986

The Effects of Gamma Radiation on Groundwater Chemistry and Glass Reaction in a Saturated Tuff Environment

W. L. Ebert, J. K. Bates, T. J. Gerding, and R. A. Van Konynenburg

Presented at the Fall Meeting of the Materials Research Soc., Boston, MA, December 1–6, 1986

Solid Oxide Fuel Cells

D. C. Fee, D. E. Busch, T. D. Claar, D. W. Dees, J. T. Dusek, T. E. Easler, W. A. Ellingson, B. K. Flandermeyer, R. Fousek, J. J. Heiberger, S. Majumdar, C. C. McPheeters, F. C. Mrasek, J. J. Picciolo, and R. B. Poeppel

Presented at the First National Aerospace Plane Technical Symp., Langley Research Center, Hampton, VA, May 20–22, 1986

Solid Oxide Fuel Cells

D. C. Fee, D. E. Busch, T. D. Claar, D. W. Dees, J. T. Dusek, T. E. Easler, W. A. Ellingson, B. K. Flandermeyer, R. J. Fousek, J. J. Heiberger, S. Majumdar, C. C. McPheeters, F. C. Mrazek, J. J. Picciolo, and R. B. Poeppel

Presented at the Hydrogen Technology Conf., NASA Lewis Research Center, Cleveland, OH, June 4–5, 1986

Chemical Characteristics of Material Released during Source Term Experiments Project (STEP) In-Pile Tests: Part II

J. K. Fink, M. F. Roche, C. A. Seils, D. V. Steidl, C. E. Johnson, and R. L. Ritzman

Presented at the Severe Accident Chemistry Symp., Am. Chem. Soc., Anaheim, CA, September 8–12, 1986

An Evaluation of Polarized Fuels in a Commercial Deuterium/Tritium Tokamak Reactor

P. A. Finn, J. N. Brooks, D. A. Ehst, M. Y. Gohar, R. F. Mattas, and C. C. Baker

Presented at the Seventh Topical Meeting on the Technology of Fusion Energy, Reno, NV, June 15–19, 1986

A Process to Recover Tritium from High Pressure Helium

P. A. Finn and D. K. Sze

Presented at the Seventh Topical Meeting on the Technology of Fusion Energy, Reno, NV, June 15–19, 1986

Oxidation of Tritium Atoms at a Stainless Steel Surface

P. A. Finn and E. H. Van Deventer

Presented at the Int. Symp. on Fusion Reactor Blanket and Fuel Cycle Technology, University of Tokyo, Japan, October 27–29, 1986

Studies of Surface Adsorption on $LiAlO_2$

A. K. Fischer, J. A. McDaniel, and C. E. Johnson

Presented at the Int. Conf. on Fusion Reactor Materials, Chicago, IL, April 13–17, 1986

The Discipline of Analytical Chemistry: Routine or Research?

D. W. Green

Presented at the Chemistry Department Seminar, Illinois Institute of Technology, Chicago, IL, April 17, 1986

Quality Assurance Controls for the Analytical Chemistry Laboratory

D. W. Green

Presented at the Tenth Annual Quality Assurance Day, Argonne, IL, April 3, 1986

Dosimetry and Radiation Damage

L. R. Greenwood

Presented at the Fifth Coordination Meeting of Participants in the Office of Basic Energy Science Program, Argonne National Laboratory, Argonne, IL, September 17–19, 1986

New Ideas in Dosimetry and Damage Calculations for Fusion Materials Irradiations

L. R. Greenwood

Presented at the Int. Conf. on Fusion Reactor Materials, Chicago, IL, April 13–17, 1986

Recent Research in Neutron Dosimetry and Damage Analysis for Materials Irradiations

L. R. Greenwood

Presented at the Symp. on Effects of Radiation on Materials, American Society for Testing of Materials, Seattle, WA, June 23–25, 1986

Nuclear Data Requirements for Dosimetry and Radiation Damage Estimates

L. R. Greenwood and F. M. Mann

Presented at the IAEA Advisory Group Meeting on Nuclear Data for Fusion Reactors, Gausig, German Democratic Republic, December 1–5, 1986

First Principles and Molecular Dynamics Studies of Fe^{+3}/Fe^{+2} in Water

J. W. Halley, J. Hautman, A. Rahman, and L. A. Curtiss

Presented at the Int. Conf. on Structure and Dynamics of Solid/Electrolyte Interfaces, West Berlin, West Germany, September 2–5, 1986

Thermochemical Processing of Solid Waste

J. E. Helt

Presented at the Workshop on Biomass Energy, Tallahassee, FL, November 19, 1986

The FUBR-1B Experiment—Irradiation of Lithium Ceramics to High Burnups under Large Temperature Gradients

G. W. Hollenberg, R. C. Knight, P. J. Densley, L. A. Pember, C. E. Johnson, R. B. Poeppel, and L. Yang

Presented at the Int. Conf. on Fusion Reactor Materials, Chicago, IL, April 13–17, 1986

Oxygen-18 Studies of Atmospheric Sulfate Formation

B. Holt and R. Kumar

Presented at the Fifth Symp. on Environmental Analytical Chemistry, Brigham University, Provo, UT, June 18–20, 1986

A Methodology to Assess the Impact of Driving Schedules and Drive Train Characteristics on Electric Vehicle Range

F. Hornstra, T. P. Mulcahey, R. L. Biwer, C. C. Christianson, E. T. Carothers, R. L. Hogrefe, J. E. Kulaga, and C. E. Webster

Presented at the Eighth Int. Electric Vehicle Symp., Washington, DC, October 20–23, 1986

The Characterization of Selected Nuclear Fuel Cycle Materials by ICP-AES

E. A. Huff

Presented at the 1986 Winter Conf. on Plasma Spectrochemistry, Kailua-Kona, HI, January 2–8, 1986

Separation of Actinide Elements by Column Extraction Chromatography prior to ICP-AES Analysis

E. A. Huff and D. L. Bowers

Presented at the 29th Conf. on Analytical Chemistry in Energy Technology, Oak Ridge National Laboratory/Department of Energy, Knoxville, TN, September 30–October 2, 1986

Methods of Chemical Analysis for Selected Species in the Marble and Limestone Surfaces Exposed to the Acidic Outdoor Environment

K. J. Jensen, F. L. Williams, E. A. Huff, and C. A. Youngdahl

Presented at the Materials Effects Task Group VII Peer Review Meeting, Durham, NC, April 6–11, 1986

Thermodynamic Performance of Tritium Breeding Ceramic Blanket Materials

C. E. Johnson and A. K. Fischer

Presented at Seventh Topical Meeting on the Technology of Fusion Energy, Am. Nucl. Soc., Reno, NV, June 15–19, 1986

Ceramic Tritium Breeder Materials—Promise and Performance

C. E. Johnson and G. W. Hollenberg

Presented at the 14th Symp. on Fusion Technology in the European Community, Avignon, France, September 8–12, 1986

The Role of Chemistry in Nuclear Accidents

C. E. Johnson and I. Johnson

Presented at the Severe Accident Chemistry Symp., Am. Chem. Soc., Anaheim, CA, September 8–12, 1986

BEATRIX—The International Breeder Materials Exchange

C. E. Johnson, T. C. Reuther, and J. DuPuoy

Presented at the 14th Symp. on Fusion Technology in the European Community, Avignon, France, September 8–12, 1986

Behavior of Volatile Fission Products in Primary Reactor System

I. Johnson, M. M. Farahat, J. L. Settle, J. D. Arntzen, and C. E. Johnson

Presented at the Third Int. Symp. on Ceramics Nuclear Waste Management, Am. Ceram. Soc., Chicago, IL, April 27–May 1, 1986

Downstream Behavior of Fission Products

I. Johnson and C. E. Johnson

Presented at Severe Accident Chemistry Symp., Am. Chem. Soc., Anaheim, CA, September 8–12, 1986

Diffuse Reflectance Infrared Studies of the Formation and Reactivity of Protonated Sites in Synthetic Zeolite Catalysts

S. A. Johnson, R.-M. Rinkus, T. C. Diebold, L. E. Iton, and V. A. Maroni

Presented at the 60th Colloid and Surface Science Symp., Atlanta, GA, June 15–18, 1986

Development of IFR Fuel Cycle

T. R. Johnson

Presented at the Sixth Annual Pyrochemical Workshop, Los Alamos National Laboratory, Los Alamos, NM, October 7–8, 1986

IFR Pyroprocess Waste Treatment

T. R. Johnson and D. F. Fischer

Presented at the Sixth Annual Pyrochemical Workshop, Los Alamos National Laboratory, Los Alamos, NM, October 7–9, 1986

An Advanced Lithium-Aluminum/Iron Disulfide Secondary Cell

T. D. Kaun

Presented at the 32nd Int. Power Sources Symp., Cherry Hill, NJ, June 9–12, 1986

Molten Salt Battery Research for a Lithium-Alloy/Iron Disulfide Cell

T. D. Kaun, L. Redey, T. Hashman, M. Dupont, and E. Wolski

Presented at the Technology Base Research Review Meeting, Washington, DC, December 16-17, 1986

The Costs and Benefits of Utilising Beryllium as an Energy Multiplier

A. C. Klein and D. K. Sze

Presented at the Int. Conf. on Fusion Reactor Materials, Chicago, IL, April 13-17, 1986

Exploring Catalytic Methanol Synthesis Using Soluble Metal Oxide Complexes

R. J. Klingler, I. Bloom, and J. W. Rathke

Presented at the 191st National Meeting of the Am. Chem. Soc., New York, NY, April 13-18, 1986

Helium Production in HFIR-Irradiated Pure Elements

D. W. Kneff, L. R. Greenwood, B. M. Oliver, and R. P. Skowronski

Presented at the Int. Conf. on Fusion Reactor Materials, Chicago, IL, April 13-17, 1986

Modeling of Nickel/Iron Batteries for Vehicle Propulsion Applications

J. Lee, J. F. Miller, and C. C. Christianson

Presented at AIChE Annual Meeting, Miami, FL, November 2-7, 1986

Thermophysical Properties of Metallic Fuels and Blankets in Liquid-Metal Reactors

L. Leibowits and E. Veleckis

Presented at the Third Int. Symp. on Ceramics Nuclear Waste Management, Am. Ceram. Soc., Chicago, IL, April 27-May 1, 1986

Recent Advances in Centrifugal Contactors for Solvent Extraction

R. A. Leonard

Presented at the Tenth Actinide Workshop, Los Alamos National Laboratory, Los Alamos, NM, May 12-15, 1986

Separation of Am and Pu from Nuclear Wastes by the TRUEX Process

R. A. Leonard, G. F. Vandegrift, and C. W. Manry

Presented at the AIChE National Meeting, Am. Inst. of Chem. Eng., Boston, MA, August 24-27, 1986

Effects of Gamma Radiolysis on Waste Package Components

M. A. Lewis and D. T. Reed

Presented at the Fall Meeting of the Materials Research Soc., Boston, MA, December 1-6, 1986

Determining Major and Minor Elements in Coal Ash—AA or ICP?

P. C. Lindahl, E. A. Huff, and I. M. Fox

Presented at the FACSS XIII Meeting, Federation of Analytical Chemistry and Spectroscopy Soc., St. Louis, MO, September 28-October 3, 1986

Factor Group Analysis of the Vibrational Representations of High Symmetry Zeolites

V. A. Maroni

Presented at the 60th Colloid and Surface Science Symp., Atlanta, GA, June 15-18, 1986

Lithium-Alloy/Iron Sulfide Batteries

P. A. Nelson and H. Shimotake

Presented at the Institute of Applied Energy Fuel Cell and Advanced Battery Int. Symp., Tokyo, Japan, January 21–23, 1986

Integrated Testing of the SRL-165 Glass Waste Form

D. L. Phinney, F. J. Ryerson, V. M. Oversby, W. A. Lanford, R. D. Aines, and J. K. Bates

Presented at the Fall Meeting of the Materials Research Soc., Boston, MA, December 1–6, 1986

High-Temperature Fuel Cells

R. D. Pierce

Presented at the Conf. on Electrochemistry as an Emerging High-Technology Area, Case Western Reserve University, Cleveland, OH, September 15–17, 1986

Materials Research for High-Temperature Fuel Cells

R. D. Pierce

Presented at the Metallurgical and Mineral Engineering Dept., University of Wisconsin, Madison, WI, September 25, 1986

Status of Molten Carbonate Fuel Cell Technology

R. D. Pierce

Presented at the 40th Meeting of the Fuel Cell Users Group, Government Industrial Research Institute at Osaka, Japan; and Kobe Steel, Kobe, Japan; and Mitsubishi Metals, Central Research Institute, Tokyo, Japan, January 27, 29, and 30, 1986

Pressurized Fluidized-Bed Combustion

W. F. Podolski

Presented at Fluidized-Bed Combustion Technology Workshop, Washington, DC, March 20–21, 1986

Cost Analysis of Particulate Emission Control Technology for Heavy-Duty Diesel Vehicles

J. B. Rajan and M. K. Singh

Presented at the 79th Annual Meeting and Exposition of the Am. Pollution Control Assn., Minneapolis, MN, June 23–27, 1986

Reference Electrodes for Pyrochemical Applications

L. Redey

Presented at the Sixth Annual Pyrochemical Workshop, Los Alamos, NM, October 7–8, 1986

Separation and Recovery of Metal Ions by Supported Liquid Membranes: Science and Applications

L. Reichley-Yinger

Presented at the Int. Symp. on Metal Speciation, Separation, and Recovery, Industrial Waste Elimination Research Center, IIT Center, Chicago, IL, July 27–August 1, 1986

PUREX-TRUEX Recovery of Plutonium and Americium from Chloride Salt Wastes

L. Reichley-Yinger and G. F. Vandegrift

Presented at the Tenth Annual Actinide Workshop, Los Alamos National Laboratory, Los Alamos, NM, May 12–15, 1986

The Chemical Desulfurisation of Coal

V. M. Rickert, K. S. Vorres, J. E. Young, and Ravi Varma

Presented at Am. Chem. Soc. Great Lakes Meeting, June 2–4, 1986

A Waste Treatment Process for a Pyrochemical Fuel Processing Facility

R. H. Rigg, T. R. Johnson, and L. Burris

Presented at the Waste Management and Decontamination Conf., Am. Nucl. Soc., Niagara Falls, NY, September 14–18, 1986

Tritium Recovery from a Breeder Material: Gamma Lithium Aluminate

E. Roth, F. Botter, M. Briec, M. Rostaing, H. Werle, and R. G. Clemmer

Presented at the Int. Conf. on Fusion Reactor Materials, Chicago, IL, April 13–17, 1986

Radioactive Waste: A Problem of the Energy of the Future?

C. S. Sabau

Presented at the 12th Convention of the American Romanian Academy of Science and Arts, Boulder, CO, May 8–10, 1986

Anomalous Behavior of Liquid Ordered Alloys

M.-L. Saboungi

Seminar presented at the Dept. of Metallurgy and Materials Sciences, University of Toronto, Canada, May 5, 1986

On the Conformal Ionic Solution Theory—Principles and Applications

M.-L. Saboungi

Presented at the Advanced Study Institute on Molten Salt Chemistry, NATO and the University of Camerino, Italy, August 3–15, 1986

Transitions in Liquid Alkali Lead Alloys

M.-L. Saboungi

Presented at the Chaos, Disordered Systems, and Phase Transition Conf., Trieste, Italy, August 11–29, 1986

The Coordination Cluster Theory: Extension to Multicomponent Solvents

M.-L. Saboungi, D. Caveny, I. Bloom, and M. Blander

Presented at the Ninth IUPAC Conf. on Chemical Thermodynamics, Lisbon, Portugal, July 14–18, 1986

Advanced Instrumental Methods for Analysing Organics in Solid Waste

J. Schneider and L. Raphaelian

Presented at the Joint PETC/METC Solid Flows, Direct Utilisation, AR&TD Contractor Review Meeting, Warrendale, PA, September 22–25, 1986

GC/Fourier Transform IR Detectors

J. F. Schneider

Presented at the Joint Am. Soc. for Testing Mater. Committee E-19 Meeting and Chicago Chromatography Forum, Chicago, IL, October 1986

GC/MI/FTIR Applications: Analysis of Fossil Fuels

J. F. Schneider, A. S. Boparai, and L. A. Raphaelian

Presented at the Fall Am. Chem. Soc. Meeting, Anaheim, CA, September 7–12, 1986

Equilibrium Calculations for Complex Multicomponent Systems Using Geometric Programming

S. Sinha, R. Land, and M. Blander

Presented at the CALPHAD XV Meeting, Fulmer Grange, England, July 7–11, 1986

The Science, Technology, and Regeneration of Nuclear Waste Disposal

M. J. Steindler

Presented at Kent Law School, Kent, OH, April 7, 1986

Fluoride Volatility Reprocessing of Reactor Fuels

R. K. Steunenberg

Presented at Tenth Annual Actinide Workshop, Los Alamos National Laboratory, Los Alamos, NM, May 12–15, 1986

Pyrochemistry

R. K. Steunenberg

Presented at the R. D. Baker Memorial Symp., Los Alamos National Laboratory, Los Alamos, NM, May 12, 1986

U/Th Geochronology of Hydrothermal Activity in Long Valley Caldera: Little Hot Creek and the Blue Chert

N. C. Sturchio, C. Binz, and M. Sorey

Presented at the Second Workshop on Hydrologic and Geochemical Monitoring of Long Valley Caldera, U.S. Geological Survey and Earth Science Div. of Lawrence Berkeley Lab., Mammoth Lakes, CA, July 15–16, 1986

An Assessment of Tritium Issues and Data Requirements for Liquid Breeders

D. K. Sze

Presented at the Tritium Technology Workshop, Japan-U.S. Agreement on Fusion Energy, Naka, Japan, October 1986

Technical Requirements of Experiments and Facilities for Fusion Blanket Development

D. K. Sze, M. A. Abdou, M. Tillack, P. Gierszewski, and R. Puigh

Presented at the Int. Symp. on Fusion Reactor Blanket and Fuel Cycle Technology, University of Tokyo, Japan, October 1986

ASPIRE-Advanced Safe Pool Immersed Reactor

D. K. Sze, Y. Cha, J. D. Gordon, J. K. Garner, S. Piet, E. T. Chenf, J. DeVan, and A. Klein

Presented at the Int. Symp. on Fusion Reactor Blanket and Fuel Cycle Technology, University of Tokyo, Japan, October 1986

Quantum Percolation from the Perspective of Fractal Random Walk

S. W. Tam

Presented at University of Illinois at Chicago, February 19, 1986

A Dimension Invariant Relationship between Quantum Percolation and Fractal Random Walk

S. W. Tam and C. E. Johnson

Presented at the Second University of California Conf. on Statistical Mechanics, Univ. of Calif.-Davis, Davis, CA, March 26–29, 1986

The Thermal Conductivity of Mixed Beryllia/Li Ceramic in Sphere-Pac Forms

S. W. Tam and C. E. Johnson

Presented at the Int. Conf. on Fusion Reactor Materials, Chicago, IL, April 13–17, 1986

Fission Product Release from Core-Concrete Melts

M. Tetenbaum, J. K. Fink, C. E. Johnson, M. G. Chasanov, W. H. Gunther, B. W. Spencer, R. Ritsman, and R. Sehgal

Presented at the Severe Accident Chemistry Symp., Am. Chem. Soc., Anaheim, CA, September 8–12, 1986

Fission Product Release from Core-Concrete Melts

M. Tetenbaum, J. K. Fink, C. E. Johnson, and R. Ritsman

Presented at the Committee on Safety of Nuclear Installations Specialist Meeting on Core Debris/Concrete Interactions, Electric Power Research Institute, Palo Alto, CA, September 2–4, 1986

IFR Pyroprocessing Support

Z. Tomczuk, R. D. Wolson, R. K. Steunenberg, and W. E. Miller

Presented at the Sixth Annual Pyrochemical Workshop, Los Alamos National Laboratory, Los Alamos, NM, October 7–8, 1986

Generic Data-Base Generation for TRUEX Processing

G. F. Vandegrift, D. J. Chaiko, D. R. Fredrickson, and R. A. Leonard

Presented at the Tenth Annual Actinide Workshop, Los Alamos National Laboratory, Los Alamos, NM, May 12–15, 1986

Preliminary Investigations for Technology Assessment of ^{99}Mo Production from LEU Targets

G. F. Vandegrift, D. J. Chaiko, R. R. Heinrich, E. T. Kucera, K. J. Jensen, D. S. Poa, R. Varma, and D. R. Vissers

Presented at the 1986 Int. Meeting on Reduced Enrichment for Research and Test Reactors, Gatlinburg, TN, November 3–6, 1986

A Close-Coupled PUREX/TRUEX Process for Processing Nuclear Fuel

G. F. Vandegrift, R. A. Leonard, L. Burris, and N. M. Levitz

Presented at the First Int. Conf. on Separations Science and Technology, Am. Chem. Soc., Nuclear Division, New York, NY, April 16–18, 1986

High-Speed Cadmium Review

R. Varma

Presented at the Corrosion Technology Review, Naval Air Development Center, Warmister, PA, November 19–20, 1986

Phase Relations for Reactions of Hydrogen with Sodium Oxide between 500 and 900°C

E. Veleckis and L. Leibowitz

Presented at the Symp. on Experimental Techniques in High Temperature Science held during the TMS-AIME Annual Meeting, New Orleans, LA, March 2–6, 1986

Thermodynamic and Heat Management Studies on High Temperature Alloy LiAl/FeS_2 Battery Cells

D. R. Vissers and Z. Tomczuk

Presented at the Physical Electrochemistry Session of the Gordon Research Conf., New London, NH, August 13, 1986

Priority Pollutants in Wet Deposition Samples

R. J. Wingender

Presented at the 1986 Johnson Conf. on Measurement Challenges of the 80's: Indoor Air, Acid Rain, and Asbestos, ASTM Committee D-22 on Sampling and Analysis of Atmospheres, Johnson State College, Johnson, VT, July 17, 1986

The Integral Fast Reactor Fuels Reprocessing Laboratory at Argonne National Laboratory—Illinois

R. D. Wolson, Z. Tomczuk, D. F. Fischer, M. A. Slawecki, and W. E. Miller

Presented at the 1986 Plutonium/Uranium Chemical Recovery Operations Conf.,
E. I. du Pont de Nemours and Co., Savannah River Plant, Aiken, SC, October 14–16, 1986

F. Papers Accepted for Publication

Fusion Nuclear Technology Testing Requirements

M. A. Abdou, D. K. Sze, et al.

To be published in the Proc. of the IAEA Fourth Technical Committee Meeting and Workshop on Fusion Reactor Design and Technology, Yalta, USSR, May 26–June 6, 1986

Transport and Reaction Kinetics at the Gel:Glass Solution Interface Region: Results of Repository-Oriented Leaching Experiments

T. A. Abrajano and J. K. Bates

To be published in *Scientific Basis for Nuclear Waste Management X*

The Effect of Gamma Radiation on Groundwater Chemistry and Glass Leaching as Related to NNWSI Repository Site

T. A. Abrajano, J. K. Bates, W. L. Ebert, and T. J. Gerding

To be published in Ceramics Advances

The Zambales Ophiolite. I. Geology and Petrology of the Critical Zone of the Acoje Massif

T. A. Abrajano, G. C. Baxter, and J. D. Pasteris

To be published in Tectonophysics

Wastage of In-Bed Heat Transfer Surfaces in the Pressurised Fluidised-Bed Combustor at Grimethorpe

J. S. Anderson, E. L. Carls, P. J. Mainhardt, W. M. Swift, J. M. Wheeldon, S. Brooks, A. J. Minchener, and J. Stringer

To be published in the J. Eng. Gas Turbines Power

The Reaction of Reference Commercial Nuclear Waste Glasses during Gamma Irradiation in a Saturated Tuff Environment

J. K. Bates, W. L. Ebert, T. J. Gerding, and D. Fischer

To be published in J. Mater. Res.

Scientific Basis for Nuclear Waste Management X

J. K. Bates and W. B. Seefeldt, eds.

To be published by the Mater. Res. Soc.

Thermodynamic Analysis of Binary Liquid Silicates and Prediction of Ternary Solution Properties by Modified Quasichemical Equations

M. Blander and A. D. Pelton

To be published in Geochim. Cosmochim. Acta

EDTGRAF—An Easy Way to Use DISSPLA

I. Bloom

To be published in The DEC Professional

Low-Resistivity Glass Electrolytes for Sodium-Sulfur Cells

I. Bloom, J. Bradley, G. H. Kucera, P. A. Nelson, and M. F. Roche

To be published in Proc. of the 170th Electrochem. Soc. Meeting, San Diego, CA, October 19–24, 1986

Raman and ^{67}Zn NMR Studies of the Structure of Zinc(II) Solutions in Concentrated Aqueous Potassium Hydroxide

K. J. Cain, C. A. Melendres, and V. A. Maroni

To be published in J. Electrochem. Soc.

Nonadditivity of *Ab Initio* Pair Potentials for Molecular Dynamics of Multivalent Transition Metal Ions in Water

L. A. Curtiss, J. W. Halley, J. Hautman, and A. Rahman

To be published in J. Chem. Phys.

Theoretical Investigation of Na and Mg Atom Complexes with H_2O

L. A. Curtiss, E. Kraka, J. Gauss, and D. Cremer

To be published in J. Phys. Chem.

Additional Measurements of the Radiation Environment at the Los Alamos Spallation Radiation Effects Facility at LAMPF

D. R. Davidson, R. C. Reedy, L. R. Greenwood, W. F. Sommer, and M. S. Wechsler

To be published in J. Nucl. Mater.

Laser Photoacoustic Spectroscopy for Trace Level Detection of Actinides in Groundwater

M. M. Doxtader, V. A. Maroni, J. V. Beitz, and M. Heaven

To be published in *Scientific Basis for Nuclear Waste Management X*

The Effects of Gamma Radiation on Groundwater Chemistry and Glass Reaction in a Saturated Tuff Environment

W. L. Ebert, J. K. Bates, T. J. Gerding, and R. A. Van Konynenburg

To be published in *Scientific Basis for Nuclear Waste Management X*

Recent Research in Neutron Dosimetry and Damage Analysis for Materials Irradiations

L. R. Greenwood

To be published in J. Nucl. Mater.

Method for Determination of $S^{18}O$ of Hydrogen Peroxide in Rainwater

B. D. Holt and R. Kumar

To be published in Anal. Chem.

Thermodynamic Properties of Silicalite (SiO_2)

G. K. Johnson, I. R. Tasker, D. A. Howell, and J. V. Smith

To be published in J. Chem. Thermodyn.

Adiabatic Diesel Engines

L. Johnson, R. Rajan, and S. LaBelle

To be published in *Energy Technologies and the Environment: 1987 Update*

An Advanced Lithium-Aluminum/Iron Disulfide Secondary Cell

T. D. Kaun

To be published in Proc. of the 32nd Int. Power Sources Symp.

Use of Electronic Worksheets for Calculation of Stagewise Solvent Extraction Processes

R. A. Leonard

To be published in Sep. Sci. Technol.

Effects of Gamma Radiolysis on Waste Package Components
M. A. Lewis
To be published in *Scientific Basis for Nuclear Waste Management X*

Reference Electrodes for Molten Electrolytes
N. Q. Minh and L. Redey
To be published in *Molten Salt Techniques*, eds. R. L. Lovering and D. G. Lovering, Plenum Press, Vol. 3

Calorimetric Measurements on High-Purity ScI_3
P. A. G. O'Hare, G. K. Johnson, I. R. Tasker, H. E. Flotow, and C. E. Struck
To be published in J. Chem. Thermodyn.

Investigation of Alternative MCFC Cathode Materials at Argonne National Laboratory
R. D. Pierce, J. L. Smith, and G. H. Kucera
To be published in *Progress in Batteries and Solar Cells*, Vol. 6 (1987)

The Coordination Cluster Theory. Extension to Multicomponent Systems
M.-L. Saboungi, D. Caveny, I. Bloom, and M. Blander
To be published in Metall. Trans.

Serpentinisation of the Acoje Massif, Zambales Ophiolite Phillipines: Oxygen and Hydrogen Isotope Geochemistry
N. C. Sturchio, T. A. Abrajano, J. Murowchick, and K. Muelenbach
To be published in Tectonophysics

Fission Product Release from Core-Concrete Melts
M. Tetenbaum, J. K. Fink, C. E. Johnson, M. G. Chasanov, W. H. Gunther, B. W. Spencer, R. Ritzman, and R. Sehgal
To be published in the ACS Symp. Ser. and in the Proc. of the Committee on Safety of Nuclear Installations Specialist Meeting on Core Debris/Concrete Interactions, Palo Alto, CA, September 2–4, 1986

Techniques for Characterisation of Electrodes and Electrochemical Processes
R. Varma and J. R. Selman, eds.
To be published by John Wiley and Sons, New York, NY, and the Electrochemical Society, Pennington, NJ

Pyrochemical Extraction of Transition Metals from Pacific Ocean Deep Sea Nodules
S. von Winbush and V. A. Maroni
To be published in Sep. Sci. Technol.

Determination of Oxygen in Molten Alkali Halide Salts by Proton Activation Analysis
C. M. Wai and M. E. Dysart
To be published in J. Anal. Chem.

Advanced Batteries for Electric Vehicles
W. J. Walsh and J. B. Rajan
To be published in *Transportation Research Record*

Distribution for ANL-87-19

Internal:

J. P. Ackerman
C. C. Baker
J. K. Bates
J. E. Battles
T. M. Beasley
M. Blander
I. D. Bloom
R. L. Breyne
H. L. Brown
L. Burris
F. A. Cafasso
E. L. Carls
Y. Chang
A. A. Chilenskas
C. C. Christianson
L. F. Coleman
E. J. Croke
W. H. DeLuca
H. Drucker
M. D. Erickson
D. C. Fee
F. Y. Fradin
S. D. Gabelnick
D. W. Green
D. M. Gruen
J. E. Harmon (4)
R. R. Heinrich
J. E. Helt
K. J. Jensen
C. E. Johnson
T. R. Johnson
V. M. Kolba
A. B. Krisciunas
J. R. LaFevers
S. H. D. Lee
L. Leibowitz
V. A. Maroni
J. F. Miller
W. E. Miller
T. P. Mulcahey
K. M. Myles
P. A. Nelson
N. J. O'Fallon
P. A. G. O'Hare
M. Petrick
R. D. Pierce
W. F. Podolski
R. B. Poeppel
J. W. Rathke
A. Schriesheim
W. B. Seefeldt
M. A. Slawecki
J. A. Smaga
J. L. Smith
M. J. Steindler (75)
N. C. Sturchio
W. M. Swift
C. E. Till
G. F. Vandegrift
D. R. Vissers
R. W. Weeks
ANL Patent Dept.
ANL Contract File
ANL Libraries (2)
TIS Files (5)

External:

DOE-TIC, for distribution per UC-2 and -13 (134)
Manager, Chicago Operations Office, DOE
R. J. Gariboldi, DOE-CH
D. T. Goldman, DOE-CH
F. Herbaty, DOE-CH
V. H. Hummel, DOE-CH
S. A. Mann, DOE-CH
Chemical Technology Division Review Committee Members:
  S. Baron, Brookhaven National Lab., Upton, NY
  T. L. Brown, U. of Illinois, Urbana, IL
  L. Newman, Brookhaven National Lab., Upton, NY
  J. B. Wagner, Jr., Arizona State U., Tempe, AZ
  R. G. Wymer, Oak Ridge National Lab., Oak Ridge, TN
R. D. Alkire, U. of Illinois, Urbana, IL
B. S. Baker, Energy Research Corp., Danbury, CT
K. F. Barber, Div. of Electric and Hybrid Propulsion, USDOE, Washington, DC
J. Batchelor, Office of Fossil Energy, USDOE, Germantown, MD
D. L. Bauer, Office of Coal Processing/FE, USDOE, Washington, DC
T. Bechtel, Morgantown Energy Technology Center, USDOE, Morgantown, WV
J. T. Bell, Oak Ridge National Lab., Oak Ridge, TN
D. N. Bennion, Brigham Young U., Provo, UT
S. E. Berk, Office of Fusion Energy, USDOE, Washington, DC

J. Birk, Electric Power Research Inst., Palo Alto, CA
W. S. Bishop, Aero Propulsion Lab., Wright-Patterson AFB, OH
D. F. Bowersox, Los Alamos National Lab., Los Alamos, NM
J. Braunstein, Oak Ridge National Lab., Oak Ridge, TN
M. Breiter, General Electric Research and Development Center, Schenectady, NY
L. Brewer, U. of California, Berkeley, CA
J. J. Brogan, Div. of Energy Utilization Research, USDOE, Washington, DC
P. J. Brown, Div. of Electric and Hybrid Propulsion, USDOE, Washington, DC
E. J. Cairns, Lawrence Berkeley Lab., Berkeley, CA
D. Christensen, Los Alamos National Lab., Los Alamos, NM
S. W. Chun, Pittsburgh Energy Technology Center, USDOE, Pittsburgh, PA
R. P. Clark, Sandia National Laboratories, Albuquerque, NM
A. L. Conn, Arthur L. Conn & Associates, Chicago, IL
M. Coops, Lawrence Livermore National Lab., Livermore, CA
J. Cuttica, Gas Research Inst., Chicago, IL
H. T. Davis, U. of Minnesota, Minneapolis, MN
J. H. DeVan, Oak Ridge National Lab., Oak Ridge, TN
W. J. Dippold, Div. of Electric and Hybrid Propulsion, USDOE, Washington, DC
E. Dowgiallo, Div. of Electric and Hybrid Propulsion, USDOE, Washington, DC
J. Dunning, General Motors Research Lab., Warren, MI
S. Ehrlich, Electric Power Research Inst., Palo Alto, CA
H. Feibus, Office of Fossil Energy, USDOE, Germantown, MD
L. M. Ferris, Oak Ridge National Lab., Oak Ridge, TN
A. P. Fickett, Electric Power Research Inst., Palo Alto, CA
V. Fiore, Gas Research Inst., Chicago, IL
E. Gillis, Electric Power Research Inst., Palo Alto, CA
F. Gmeindl, Morgantown Energy Technology Center, USDOE, Morgantown, WV
S. Goldsmith, Battelle-Columbus Labs., Columbus OH
K. P. Grothaus, Sandia National Laboratories, Albuquerque, NM
R. Guidotti, Sandia National Laboratories, Albuquerque, NM
G. M. Haas, Office of Fusion Energy, USDOE, Washington, DC
G. L. Hagey, Div. of Advanced Energy Conv. Syst., USDOE, Washington, DC
R. A. Harlow, Ford Aerospace and Communications Corp., Newport Beach, CA
R. G. Hickman, Lawrence Livermore National Lab., Livermore, CA
W. Huber, Morgantown Energy Technology Center, USDOE, Morgantown, WV
L. C. Ianniello, Office of Basic Energy Sciences, USDOE, Germantown, MD
G. J. Janz, Rensselaer Polytechnic Inst., Troy, NY
D. Jewell, Morgantown Energy Technology Center, USDOE, Morgantown, WV
E. F. Johnson, Princeton U., Princeton, NJ
R. S. Kirk, Div. of Electric and Hybrid Propulsion, USDOE, Washington, DC
K. W. Klein, Electric Energy Systems Div., USDOE, Washington, DC
A. R. Landgrebe, Energy Storage and Distribution Div., USDOE, Washington, DC
B. Lee, Inst. of Gas Technology, Chicago, IL
M. Levenson, Bechtel National, Inc., San Francisco, CA
G. G. Libowitz, Allied Chemical Co., Morristown, NJ
W. Lueckel, United Technologies Corp., South Windsor, CT
N. J. Magnani, Sandia National Laboratories, Albuquerque, NM
A. Malinauskis, Oak Ridge National Lab., Oak Ridge, TN
W. H. McVey, Div. of LMFBR Fuel Cycle Projects, USDOE, Washington, DC
L. Nelson, Sandia Corp., Albuquerque, NM

J. S. Newman, U. of California, Berkeley, CA
J. E. Notestein, Morgantown Energy Tech. Center, USDOE, Morgantown, WV
L. G. O'Connell, Electric Power Research Inst., Palo Alto, CA
R. A. Osteryoung, State U. of New York, Buffalo, NY
P. G. Patil, Office of Vehicle & Engine R&D, USDOE, Washington, DC
C. E. Pax, Office of Coal Utilization, USDOE, Washington, DC
A. A. Pitrolo, Morgantown Energy Technology Center, USDOE, Morgantown, WV
J. E. Quinn, Div. of Energy Utilization Research, USDOE, Washington, DC
T. C. Reuther, Jr., Office of Fusion Energy, USDOE, Washington, DC
R. L. Ritzman, Electric Power Research Inst., Palo Alto, CA
G. Rudins, Office of Fossil Energy, USDOE, Germantown, MD
R. L. San Martin, Renewable Energy, USDOE, Washington, DC
A. W. Searcy, Lawrence Berkeley Lab., Berkeley, CA
J. R. Selman, Illinois Inst. of Technology, Chicago, IL
R. W. Shivers, Div. of Energy Utilization Research, USDOE, Washington, DC
J. Sholes, Morgantown Energy Technology Center, USDOE, Morgantown, WV
D. Shores, U. of Minnesota, Minneapolis, MN
J. S. Siegel, Office of Fossil Energy, USDOE, Washington, DC
M. Singer, Office of Fossil Energy, USDOE, Germantown, MD
F. D. Stevenson, Office of Basic Energy Sciences, USDOE, Germantown, MD
J. P. Strakey, Pittsburgh Energy Technology Center, USDOE, Pittsburgh, PA
J. Stringer, Electric Power Research Inst., Palo Alto, CA
G. E. Voelker, Office of Fossil Energy, USDOE, Germantown, MD
R. C. Vogel, Electric Power Research Inst., Palo Alto, CA
D. K. Walter, Office of Con. and Renewable Tech., USDOE, Washington, DC
G. Weiner, Westinghouse Research Labs., Pittsburgh, PA
B. Wilcox, Defense Advanced Research Projects Agency, Arlington, VA
F. Will, General Electric Co., Schenectady, NY
R. Williams, Defense Advanced Research Projects Agency, Arlington, VA
M. C. Wittels, Div. of Materials Sciences, USDOE, Washington, DC
R. R. Woods, Gas Research Inst., Chicago, IL
W. L. Worrell, U. of Pennsylvania, Philadelphia, PA
K. Yeager, Electric Power Research Inst., Palo Alto, CA
C. Zeh, Morgantown Energy Technology Center, USDOE, Morgantown, WV
L. Kittridge, Library, Ontario Ministry of Energy, Toronto, Ontario, CANADA